

Enhancing the Stability of Biologically Active Peptides Apelin and Lactocin S

by

Shaun Mitchell Kirk McKinnie

A thesis submitted in partial fulfillment of the requirements for the degree of

Doctor of Philosophy

Department of Chemistry
University of Alberta

© Shaun Mitchell Kirk McKinnie, 2015

Abstract

Peptides have a host of beneficial physiological effects and are often considered for therapeutic application to treat disease. However, poor bioavailabilities, problems with administration, sensitivity to environmental factors, and susceptibility to proteases limit them. The work presented in this thesis highlights efforts towards the chemical synthesis of analogues of two biologically active peptides that have improved stability to their respective limiting factors. An investigation of their improved stability through biological assays will also be used to assess the success of their synthetic modifications.

Chapter 2 will discuss antimicrobial lantibiotic lactocin S (**26**), which rapidly loses its biological activity upon exposure to atmospheric oxygen. The synthesis of a double sulfur-substituted analogue, NleDAP lactocin S (**47**) will be highlighted along with the antimicrobial testing of this peptide. An assessment of the oxidative stabilities of additional synthetic sulfur-substituted analogues will be done to qualitatively examine the effect of these substitutions on the retention of antimicrobial activity.

Chapter 3 will discuss the synthesis of analogues of pyr-1-apelin-13 (**71**) and apelin-17 (**70**), peptides with many physiologically significant roles, particularly in the cardiovascular system. However, these peptides are rapidly degraded by plasma proteases *in vivo* and *in vitro*. Biochemical evidence to support the significance of angiotensin-converting enzyme 2 (ACE2) in the *in vitro* degradation of apelin peptides in mouse and human plasma was initially investigated. The synthesis of two unique pyr-1-apelin-13 analogues (**103**, **104**) that showed complete stability to ACE2 and were not inhibitors of this critical regulatory enzyme will be described. Physiological assessments performed by collaborators confirmed that analogue **104** retained full biological activity,

and further application of these synthetic modifications to the apelin-17 isoform have resulted in apelin analogues with improved pharmacodynamic properties.

The application of ACE2 resistant analogues has enabled the investigation into additional areas of proteolysis of native apelin peptides. Three novel sites of degradation have been identified, along with the proposal of two putative protease candidates believed to be responsible. Lastly, six unique synthetic modifications have been incorporated at one of these cleavage positions, of which Arg4-substituted pyr-1-apelin-13 analogues show dramatically improved pharmacokinetic stabilities to plasma *in vitro*. Future physiological testing and structural characterization of these Arg-Leu analogues will give some insight into the proteolysis of this region, as well as the structure-activity relationship of this critical region of the peptide.

Preface

Section 2.2.1 has been published as: Ross, A. C.; McKinnie, S. M. K.; Vederas J. C., The synthesis of active and stable diaminopimelate analogues of the lantibiotic peptide lactocin S. *J. Am. Chem. Soc.*, **2012**, *134*, 2008-2011. I was responsible for developing an oxidative stability assay for DAP-substituted peptide analogues and performing antimicrobial assays to determine their activities. The other authors synthesized and purified the DAP-substituted peptides, and wrote the majority of the manuscript. For this manuscript, I performed approximately 10% of the work and assisted in the writing of relevant sections.

Sections 2.2.2, and 2.2.3 have been published as: McKinnie, S. M. K.; Ross, A. C.; Little M. J.; Vederas J. C., The solid phase supported peptide synthesis of analogues of the lantibiotic lactocin S. *Med. Chem. Commun.*, **2012**, *3*, 971-974. I was responsible for synthesizing orthogonally-protected amino acids and small peptides through solution-phase chemistry, synthesizing a double-sulfur substituted peptide analogue through solid-phase peptide synthesis, purifying peptide analogues, assessing the antimicrobial activity of all reported analogues, and performing oxidative stability assays on all reported peptide analogues. The other authors synthesized and purified single sulfur substituted peptide analogues. I performed approximately 55% of the work, and wrote the manuscript.

Sections 3.3.2, 3.3.3, and 3.3.4 have been published as: Wang, W.; McKinnie, S. M. K.; Patel, V. B.; Haddad, G.; Wang, Z.; Zhabyeyev, P.; Das, S. K.; Basu, R.; McLean, B.; Kandalam, V.; Penninger, J. M.; Kassiri, Z.; Vederas, J. C.; Murray, A. G.; Oudit, G. Y., Loss of apelin exacerbates myocardial infarction adverse remodeling and ischemia-

reperfusion injury: therapeutic potential of synthetic apelin analogues. *J. Am. Heart Assoc.*, **2013**, *2*, e000249. I was responsible for synthesizing, purifying and characterizing two novel peptide analogues, performing *in vitro* assays to determine their proteolytic stability, and assessing their ability to act as protease inhibitors. The other authors on this paper performed extensive physiological experiments and statistical analyses. All physiological experiments performed by collaborators were done according to the Canadian Council on Animal Care Guidelines, and protocols were reviewed and approved by the Animal Care and Use Committee at the University of Alberta. I performed approximately 20% of the work in this manuscript, and assisted in the writing of relevant sections.

At the time of distribution of this thesis, sections 3.2.2, 3.2.3, 3.2.4 and parts of 3.3.6 have been submitted for publication as: Wang, W.; McKinnie S. M. K.; Farhan, M.; Paul, M.; McDonald T.; McLean, B.; Hazra, S.; Murray, A. G.; Vederas, J. C.; Oudit, G. Y., Angiotensin converting enzyme 2 metabolizes and partially inactivates pyr-angiotensin-13 and angiotensin-17: Physiological effects in the cardiovascular system. *J. Biol. Chem.* (September 29, 2015). I was responsible for performing *in vitro* enzyme assays on apelin substrates, determining enzyme kinetic parameters, synthesizing and purifying apelin analogues, and assessing the *in vitro* stability of apelin peptides and analogues to mouse and human plasma. The other authors on this paper performed extensive physiological experiments and statistical analyses. All physiological experiments performed by collaborators were done according to the Canadian Council on Animal Care Guidelines, and protocols were reviewed and approved by the Animal Care and Use Committee at the

University of Alberta. I performed approximately 35% of the work in this manuscript, and assisted in the writing of relevant sections and editing the manuscript.

Acknowledgements

Attempting to contain my appreciation for everyone who has supported me throughout my doctoral studies into a few paragraphs is undoubtedly the hardest part of writing this thesis. First and foremost, I am extremely grateful to Dr. John Vederas for the incredible opportunity to work in his lab, initially as an undergraduate researcher for two separate summer studentships (2006 and 2007), and then to return as a graduate student in 2010. I have thoroughly benefitted from his continued mentorship, guidance and wisdom throughout all stages of my education and appreciate the additional trust and responsibilities that have been placed upon me throughout my lab tenure.

I am also extremely thankful for the involvement of my initial undergraduate research supervisor, Dr. Vijay Pattabiraman. His guidance, training, and enthusiasm helped to foster a naïve undergraduate curiosity about organic chemistry into a source of great interest and future career path. He has been the model supervisor that I've done my best to attempt to emulate.

The environment of learning and support instilled within our lab has been extremely beneficial for my growth and development over the past few years. It has been a pleasure to work with Vederas lab members past and present, as they have truly made coming to the lab each day an enjoyable experience. I do have to give a 'shout out' to a few people in particular though, especially to the W2-62 crew. Dr. Justin Thuss has been like the brother I've never had over the past 5 years. Randy Sanichar is such a solid guy in the lab and is the personification of work ethic and determination. Stephen Cochrane has been a continuous source of knowledge and advice that I'm incredibly appreciative of, and I've thoroughly enjoyed getting to know Eva Rodriguez-Lopez and working

together with her on a collaborative project that was not included in this thesis. I'd also like to thank Dr. Avena Ross, Dr. Clarissa Sit, Dr. Chris Lohans, Dr. Dave Dietrich, Dr. Brandon Findlay, Kaitlyn Towle and many others for all of their assistance over the years. A huge thank you goes out to Dr. Conrad Fischer and Dr. Marco van Belkum, Jeella Acedo, Randy and Justin for their assistance with the editing and organization of this thesis.

Collaboration is a critical component to interdisciplinary projects, and I have thoroughly benefitted from the opportunity and privilege to collaborate with Dr. Gavin Oudit and Wang Wang. They have been instrumental in the development of our apelin project and have been exceptional mentors and collaborators. I have also had the privilege to work with a large number of young undergraduate and high school researchers, who have all been so enthusiastically helpful. A special thank you goes out to Kelvin Tran (summer 2013), Isaac Jones (Chem 403 student, winter 2014), Kevin Kalin (summer 2014), Andrea Werny (HYRS, summer 2014) and Tyler McDonald (summer 2015) for all of their efforts.

The support staff within the Department of Chemistry is truly second to none, and a lot of the work included within this thesis would remain incomplete without their efforts. I would particularly like to thank Jing Zheng, Bela Reiz, Dr. Angie Morales-Izquierdo, and Dr. Randy Whittal in the mass spectrometry lab, Wayne Moffat and Jennifer Jones in the analytical lab, and Dr. Ryan McKay and Mark Miskolzie for all their NMR assistance. Thank you to the Natural Sciences and Engineering Research Council, Alberta Innovates Health Solutions, and the University of Alberta for the financial support to allow me to focus more heavily on my studies.

Lastly, a heartfelt thanks goes out to my family and friends for all of their emotional support throughout these past five years; I could not have done this alone. I am thoroughly grateful in particular to Marc de Bellefeuille and Mikhaila Skehor for their unwavering friendship over the years. Finally, my backbone throughout this process has been my parents, Bob and Carol, and my sister, Leah. Love you guys.

Table of Contents

1	Introduction	1
1.1	Introduction to biologically active peptides.....	1
1.2	Peptide synthesis methodology	3
1.3	Peptide stability	7
1.4	Thesis overview	10
2	Lactocin S.....	12
2.1	Introduction.....	12
2.1.1	Lantibiotics background	12
2.1.2	Lactocin S structure and biology	16
2.1.3	Syntheses of lantibiotic peptides by solid-phase peptide synthesis.....	17
2.1.4	Substitution of lanthionine residues in lantibiotics nisin and lactocin 3147 A2	19
2.1.5	Substitution of lanthionine and methionine sulfur atoms in lactocin S.....	24
2.2	Results	27
2.2.1	Oxygen-stability assays of DAP-substituted lactocin S analogues ⁶⁶	27
2.2.2	Synthesis of NleDAP-lactocin S (47), a doubly sulfur-substituted lactocin S analogue ⁶⁸	29
2.2.3	Activity testing of NleDAP lactocin S (47) ⁶⁸	36
2.2.4	Oxygen-stability testing of Met12-substituted lactocin S analogues ⁶⁸	38
2.3	Conclusions and future directions	40
3	Apelin 41	
3.1	Introduction.....	41
3.1.1	Apelin structure and processing.....	41

3.1.2	Apelin receptor interactions.....	43
3.1.3	Physiological effects of the apelinergic system.....	47
3.1.4	Structure-activity relationship of apelin	49
3.2	Role of angiotensin converting enzyme 2.....	54
3.2.1	Introduction to angiotensin converting enzyme 2	54
3.2.2	Results - <i>In vitro</i> ACE2 experiments with pyr-1-apelin-13 and apelin-17 ¹³⁰	58
3.2.3	Quantification of pyr-1-apelin-13 and apelin-17 in wildtype and ACE2- knockout plasma ¹³⁰	60
3.2.4	Quantification of pyr-1-apelin-13 and apelin-17 in human plasma ¹³⁰	62
3.2.5	Attempted synthesis of ACE2 inhibitor MLN-4760 and ACE2 inhibition in human plasma.....	63
3.3	Synthesis of ACE2 resistant apelin analogues.....	72
3.3.1	Previous SAR work surrounding ACE2 cleavage site	72
3.3.2	Synthesis of substituted Pro12-Phe13 pyr-1-apelin-13 analogues ¹¹⁵	74
3.3.3	Assessment of ACE2 stability of Pro12-Phe13 pyr-1-apelin-13 analogues ¹¹⁵	75
3.3.4	Physiological testing of Pro12-Phe13 substituted pyr-1-apelin-13 analogues ¹¹⁵	79
3.3.5	Synthesis and physiological testing of elongated and internally substituted apelin A2 analogues	81
3.3.6	<i>In vitro</i> human plasma stability of ACE2 resistant analogues.....	84
3.3.7	Synthetic efforts towards Pro12-Phe13 pyr-1-apelin-13 isosteres	85
3.4	Further protease degradation of ACE2 resistant apelin analogues	90
3.4.1	Identification of additional sites of protease cleavage in ACE2 resistant analogue 104.....	90

3.4.2	Additional literature sites of degradation	92
3.4.3	The synthesis of a fluorescent probe to aid in the activity-guided fractionation of human plasma	95
3.4.4	Activity-guided fractionation of human plasma	100
3.4.5	Kallikrein experiments identifying degradation	106
3.4.6	Quantification of <i>in vitro</i> human plasma degradation products of ACE2- resistant apelin analogues	113
3.5	Synthesis of Arg-Leu analogues	120
3.5.1	Introduction and synthetic targets	120
3.5.2	D-Leu analogues	124
3.5.3	N-MeLeu analogues	125
3.5.4	α -Methyl analogues	127
3.5.5	aza-Analogues	143
3.5.6	Pharmacokinetics of Arg4-Leu5 apelin analogues in human plasma	158
3.5.7	Physiological testing of Arg4-Leu5 apelin analogues	161
3.6	Conclusions and future directions	163
4	Experimental Procedures	165
4.1	General information	165
4.1.1	Reagents, solvents and purification	165
4.1.2	Characterization	166
4.2	Lactocin S synthesis	167
4.2.1	General procedure for elongation using Fmoc SPPS ⁶⁸	167
4.2.2	General procedure for cleavage and purification of lactocin S analogues ⁶⁸	168
4.2.3	Orthogonally-protected DAP synthesis ⁶⁶	169
4.2.4	Synthesis of N-terminal dipeptide 68	177

4.2.5	Synthesis of NleDAP lactocin S (47) ⁶⁸	181
4.2.6	Characterization of NleDAP lactocin S (47) ⁶⁸	186
4.2.7	Biological testing	187
4.3	Apelin analogue syntheses	190
4.3.1	MLN' inhibitor synthesis.....	190
4.3.2	General apelin analogue synthesis information.....	198
4.3.3	Apelin analogue SPPS	203
4.3.4	Pro12-Phe13 isostere syntheses.....	210
4.3.5	Fluorescent probe SPPS.....	221
4.3.6	D-Leu analogues.....	224
4.3.7	N-Methyl leucine analogues	225
4.3.8	α -Methyl arginine analogues	230
4.3.9	α -Methyl leucine analogues.....	249
4.3.10	aza-Arginine analogues	255
4.3.11	aza-Leucine analogues.....	263
4.3.12	Apelin biological experiments.....	278
5	References	291

List of Tables

Table 2.1 – Loss of antimicrobial activity based on zones of clearing after serial dilutions of lactocin S (26) and sulfur-substituted analogues (42-47). ^{66,68}	38
Table 3.1 – <i>In vitro</i> ACE2 hydrolysis of pyr-1-apelin-13 and apelin-17 peptides to pyr-1-apelin-3 and apelin-16, respectively. ¹³⁰	58
Table 3.2 – ACE2 kinetic parameters for apelin-13, ¹²⁴ pyr-1-apelin-13 and apelin-17. ¹³⁰	59
Table 3.3 – Quantification of pyr-1-apelin-13 and apelin-17 after incubation with wild-type (WT) and ACE2-knockout (KO) plasma. ¹³⁰	61
Table 3.4 – Incubation of pyr-1-apelin-13 and apelin-17 in human plasma. ¹³⁰	63
Table 3.5 – Literature pyr-1-apelin-13 analogues incorporating C-terminal substitutions and corresponding apelin receptor binding and % peptide remaining after 3 h. ¹¹⁸ ...	73
Table 3.6 – Remaining percentage of ACE2 resistant apelin analogues in human plasma comparison to native apelin. ¹³⁰	84
Table 3.7 – <i>In vitro</i> KLKB1 (left) and KLK1 (right) experiments with apelin substrates.	111
Table 3.8 – Apelin receptor binding affinity of D-Scan analogues. ¹¹⁸	124
Table 3.9 – Reaction conditions for the optimization of 204	145
Table 3.10 – Test alkylation conditions for semicarbazone 223	152
Table 3.11 – Remaining percentage of Arg4-Leu5 apelin analogues after incubation in human plasma and C ₁₈ RP-HPLC analysis.....	159
Table 4.1 – Organisms used for activity testing	187
Table 4.2 – ¹ H-NMR chemical shifts of pyr-1-apelin-13 A1 analogue 103 . ¹¹⁵	204

Table 4.3 – ^1H -NMR chemical shifts of pyr-1-apelin-13 A2 analogue 104 . ¹¹⁵	205
Table 4.4 – Ion exchange binding experiments of pH adjusted 40% ASP fractions.....	285
Table 4.5 – Inhibition experiments of 40% ASP fractions.....	286

List of Figures

Figure 1.1 – Structures of biologically active peptides represented through equivalent depictions..	2
Figure 1.2 – Simplified cycle of one round of Fmoc-SPPS coupling.	5
Figure 1.3 – SPPS elongation and resin cleavage with concomitant side-chain deprotection.	5
Figure 1.4 – Native chemical (left) ⁶ and α -ketoacid hydroxylamine (right) ⁹ ligation strategies to facilitate the chemoselective combination of individually synthesized peptide monomers.	7
Figure 1.5 – Stabilization of the site of proteolytic degradation of OXM ₁₋₃₇ (6) by alanine substitution, generating prOXM ₁₋₃₇ (7). ¹⁵	8
Figure 1.6 – Structures of GLP-1(7-37)-NH ₂ (8) and unnatural amino-acid substituted analogue (9). ¹⁹	9
Figure 1.7 – Structures of biologically active <i>cis</i> -alkene oxytocin (10) ²⁰ and [CF ₃] ₂ -(<i>E</i>)-alkene gramicidin S (11) ²³ peptides.	10
Figure 2.1 – Examples of key post-translational modifications found in lantibiotic systems.	15
Figure 2.2 – Structure of lactocin S (26).	17
Figure 2.3 – Bubble structure of nisin A (27)	18
Figure 2.4 - Bubble structures of two component lantibiotics lactacin 3147 A1 (28) and A2 (29).	19
Figure 2.5 – Lanthionine substituted analogues of lactacin 3147 A2 (29). ^{56,57,58}	20

Figure 2.6 – Nisin Z structure (33) and various lanthionine ring substituted products (34-39) accessed by RCM. ^{59,60,61,62}	22
Figure 2.7 – Semi-synthetic conjugates of native nisin Z ABC rings with synthetic RCM-prepared DE rings (40, 41). ⁶³	23
Figure 2.8 – Structure of DAP-substituted lactocin S analogues: A-DAP (42), B-DAP (43), and D-DAP (44) lactocin S. ⁶⁶	24
Figure 2.9 - Structure of Met12-substituted lactocin S analogues: Leu12 (45), and Nle12 (46) lactocin S. ^{67,68}	25
Figure 2.10 – Spot-on-lawn activity testing of 100 µM lactocin S (26) and lanthionine-substituted A-DAP (42), B-DAP (43) or D-DAP (44) lactocin S analogues against <i>Pediococcus acidilactici</i> PAC1.0 after exposure to oxygen gas for up to 6 h. ⁶⁶	27
Figure 2.11 – Spot-on-lawn activity testing of 100 µM lactocin S (26) and lanthionine-substituted A-DAP (42), B-DAP (43) or D-DAP (44) lactocin S analogues against <i>Pediococcus acidilactici</i> PAC1.0 after exposure to oxygen gas for 24 h.	28
Figure 2.12 - Spot on lawn activity testing of 100 µM lactocin S (26) and dilutions of NleDAP lactocin S analogue (47) against <i>Pediococcus acidilactici</i> PAC1.0 (left) and <i>Lactobacillus delbrueckii</i> subsp. <i>bulgaricus</i> 11842 (right). ⁶⁸	37
Figure 2.13 –Spot-on-lawn activity testing of 100 µM lactocin S (26), methionine-substituted Leu12 (45), and Nle12 (46) lactocin S, and double substituted NleDAP lactocin S (47) against <i>Pediococcus acidilactici</i> PAC1.0 (left) and <i>Lactobacillus delbrueckii</i> subsp. <i>bulgaricus</i> 11842 (right) after exposure to oxygen gas for 6 h (top) or 24 h (bottom). ⁶⁸	39
Figure 3.1 – Structures of native isoforms of apelin.	42

Figure 3.2 – Key signaling pathways activated by apelin-APJ interactions. Figure modified from Chapman <i>et al.</i> ⁸⁹ and Kalea <i>et al.</i> ⁸⁵	45
Figure 3.3 – Alanine-scan data for pyr-1-apelin-13 (71) based on decreased binding to the apelin receptor (APJ). ^{98,109}	50
Figure 3.4 – D-amino acid scan data for pyr-1-apelin-13 (71) based on decreased binding to the apelin receptor (APJ). ¹¹⁸	51
Figure 3.5 – (PEG) ₄ -substituted pyr-1-apelin-13 analogue 72 . ¹¹⁸	52
Figure 3.6 – Phe13-substituted pyr-1-apelin-13 analogues 73 -75 . ¹²³	53
Figure 3.7 – Hydrolysis of angiotensin II and apelin-13 by ACE2 and the relative effect on blood pressure in the cardiovascular system.	55
Figure 3.8 – Physiological experiments highlighting the significance of ACE2. ¹³⁰	57
Figure 3.9 – Structure of internal standard dansyl-YVG (81) used for the standardization of apelin in human plasma samples.....	62
Figure 3.10 – Selected ACE2 inhibitors MLN-4760 (82) ¹²⁷ and DX-600 (83). ¹³¹	63
Figure 3.11 – Differences in ACE2 inhibition for MLN-4760 (82) diastereomers 95-97 . ¹²⁷	67
Figure 3.12 – ¹ H-NMR comparison of commercial MLN-4760 (82) with 102	70
Figure 3.13 – Structures of Nle11Inp12BrPhe13 pyr-1-apelin-13 (pyr-1-apelin-13 A1, 103) and Nle11Aib12BrPhe13 pyr-1-apelin-13 (pyr-1-apelin-13 A2, 104) analogues. ¹¹⁵	75
Figure 3.14 - Analytical C ₁₈ RP-HPLC traces of <i>in vitro</i> ACE2 incubation of pyr-1-apelin-13 A1 (103 , top) and pyr-1-apelin-13 A2 (104 , bottom). ¹¹⁵	76
Figure 3.15 – Analytical C ₁₈ RP-HPLC traces of <i>in vitro</i> ACE2 inhibition assay.....	77

Figure 3.16 – Pyr-1-apelin-13 analogues 105 – 107 and their <i>in vitro</i> ACE2 stability....	78
Figure 3.17 – Physiological testing performed on pyr-1-apelin-13 analogue 1 (103) and analogue 2 (104). ¹¹⁵	80
Figure 3.18 – Structures of apelin-17 A2 (108) and internally substituted analogues 109 and 110	82
Figure 3.19 – Physiological testing performed on extended apelin A2 analogue 108 , and internally substituted analogues 109 and 110	83
Figure 3.20 – Initial amide bond isostere targets for Pro12-Phe13.	86
Figure 3.21 – Proposed sites of proteolytic degradation of pyr-1-apelin-13 analogue 104 in mouse and human plasma after LC-MS/MS analyses.	91
Figure 3.22 – Proposed pyr-1-apelin-13 pattern of fragmentation based on HPLC-MS analyses. ¹⁴⁸	93
Figure 3.23 – General approach of FRET assay with fluorescent Abz moiety and intermolecular quencher 3-nitrotyrosine.	96
Figure 3.24 – Initial FRET assays with fluorescent probe 141	98
Figure 3.25 – Chemical structures of synthetic fluorescent probes 141 , 142 and 143 (left), and their increased fluorescence after incubation in human plasma (right)....	99
Figure 3.26 – ExPASy predicted degradation sites of pyr-1-apelin-13.	100
Figure 3.27 – Activity-guided fractionation of human plasma using FRET-based assay with fluorescent probe 141	102
Figure 3.28 – Isoelectric point approximation of unknown plasma protease in 40% ASP fraction.	103
Figure 3.29 – Inhibition experiments performed on 40% ASP fraction.	105

Figure 3.30 – Analytical C ₁₈ RP-HPLC traces of pyr-1-apelin-13 analogue 106 with mouse Arg-C endoproteinase at 37 °C.....	108
Figure 3.31 – Kallikrein activation assay.....	109
Figure 3.32 – Quantification of major peptide fragments of pyr-1-apelin-13 A2 (104) by LC-MS and EIC following the incubation in human plasma for 0 – 30 minutes. ..	115
Figure 3.33 – Quantification of major peptide fragments of apelin-17 A2 (108) by LC-MS and EIC following the incubation in human plasma for 0 – 30 minutes.....	117
Figure 3.34 – Proposed degradation pathway of apelin-17 A2 analogue 108 for <i>in vitro</i> human plasma.....	118
Figure 3.35 – Proposed sites of endopeptidase degradation of pyr-1-apelin-13 A2 analogue 104 and apelin-17 A2 analogue 108	119
Figure 3.36 – Synthetic modifications surrounding the proposed Arg-Leu cut site.	120
Figure 3.37 – Structures of D-Leu5 pyr-1-apelin-13 A2 (154) and D-Leu9 apelin-17 A2 (155) analogues.	125
Figure 3.38 – Structures of NMeLeu5 pyr-1-apelin-13 A2 (162) and NMeLeu9 apelin-17 A2 (163) analogues.	127
Figure 3.39 – Williams (164), ¹⁵⁷ Schollkopf (165) ¹⁵⁸ and Ni-Schiff base (166) ¹⁵⁹ chiral glycine auxiliaries for the stereoselective syntheses of amino acids.	128
Figure 3.40 – Crystal structure of 184 confirming the (<i>S</i>) absolute stereochemistry at amino acid α -carbon C2.....	135
Figure 3.41 – Proposed side product formation from activated 175	137
Figure 3.42 – Structures of α MeArg4 pyr-1-apelin-13 A2 (193) and α MeArg8 apelin-17 A2 (194) analogues.	139

Figure 3.43 – Crystal structure of 195 confirming the (<i>S</i>) absolute stereochemistry at amino acid α -carbon C2.....	141
Figure 3.44 – Structures of α MeLeu5 pyr-1-apelin-13 A2 (199) and α MeLeu9 apelin-17 A2 (200) analogues.	142
Figure 3.45 – Structures of aza-Arg4 pyr-1-apelin-13 A2 (210) and aza-Arg8 apelin-17 A2 (211) analogues.	148
Figure 3.46 – ¹ H-NMR spectra of aza-tripeptide 234 (top) and 237 (bottom).....	156
Figure 3.47 – Structures of aza-Leu5 pyr-1-apelin-13 A2 (239) and aza-Leu9 apelin-17 A2 (240) analogues.	157
Figure 3.48 – Stability of aza analogues to hydrolysis.....	160
Figure 3.49 – Hypotension assay testing for D-Leu5-pyr-1-apelin-13 analogue 154	162
Figure 4.1 – HPLC trace of NleDAP lactocin S.....	186
Figure 4.2 – MS/MS spectrum of NleDAP lactocin S.	186
Figure 4.3 – Spot-on-lawn activity testing of 100 μ M lactocin S (26) and dilutions of NleDAP lactocin S analogue (47) against producer organism <i>Lactobacillus sakei</i> L45 (top left), <i>Pediococcus pentosaceus</i> FBB63 (top right), and <i>Lactobacillus helveticus</i> 18009 (bottom). ⁶⁸	188

List of Schemes

Scheme 2.1 – Dual method of lanthionine formation for Class I and Class II lantibiotic systems.	13
Scheme 2.2 – NisB-catalyzed dehydration of serine and threonine amino acids to generate Dha (14) and Dhb (15) amino acids. ³⁵	14
Scheme 2.3 – Synthesis of lactocin S B-ring and N-terminal extension to nonapeptide 51 . ⁶⁸	30
Scheme 2.4 – Synthesis of orthogonally protected diaminopimelic acid derivative 61 . ^{66,68}	32
Scheme 2.5 – Solid-phase peptide synthesis of bicyclic 35-mer 64 . ⁶⁸	33
Scheme 2.6 – Synthesis of N-terminal dipeptide 68 . ^{45,66,68}	34
Scheme 2.7 – Synthesis of NleDAP-analogue 47 . ⁶⁸	36
Scheme 3.1 – Synthesis of N π -arylated histidine derivative 90 . ¹²⁷	65
Scheme 3.2 – Attempted reductive amination approach to di-methylester protected 94 . 66	
Scheme 3.3 – Synthesis of α -bromo leucine derivative 99 and attempted stereoselective synthesis of MLN-4760 (82).	68
Scheme 3.4 – Efforts towards the synthesis of Pro-Phe ketone isostere 111	87
Scheme 3.5 – Efforts towards the synthesis of Pro-Phe triazole isostere 112	88
Scheme 3.6 – Efforts towards the synthesis of Pro-Phe azadipeptide 113	89
Scheme 3.7 – Observed LC-MS/MS fragments and proposed protease degradation pathways of pyr-1-apelin-13 analogue 104 after incubation in mouse plasma.	90
Scheme 3.8 - Fragmentation of apelin analogue 135 <i>in vitro</i> in rat plasma. ¹⁴⁹	94
Scheme 3.9 – Solid phase peptide synthesis of FRET probe 141	97

Scheme 3.10 – General SPPS approach to the synthesis of Arg4-Leu5 apelin analogues beginning from common heptapeptide 153	123
Scheme 3.11 – Synthesis of Fmoc-Arg(diBoc)-NMeLeu dipeptide 161	126
Scheme 3.12 – Synthesis of Ala-Ni-(<i>S</i>)-BPB complex 170 . ¹⁶⁴	129
Scheme 3.13 – Syntheses of protected propylamine bromide electrophiles.....	130
Scheme 3.14 – Efforts towards dialkylation of Ala-Ni-(<i>S</i>)-BPB (170).....	131
Scheme 3.15 – Retrosynthetic approach to access 175 from Ni-complex 174	131
Scheme 3.16 – Attempted α -methylation of Orn(Boc)(Cbz)-Ni-(<i>S</i>)-BPB complex 179	133
Scheme 3.17 – Preparation of dialkylated α Me-L-azidoOrn-Ni-(<i>S</i>)-BPB 184	134
Scheme 3.18 – Synthesis of Fmoc- α Me-L-Arg(di-Boc)-OH 175	136
Scheme 3.19 – Synthesis of Fmoc- α Me-L-Arg(diBoc)-Leu-OH dipeptide 192	138
Scheme 3.20 – Synthesis of Fmoc- α Me-L-Leu-Ser(tBu)-OH dipeptide 198	141
Scheme 3.21 – Synthesis of chloropropyl-alkylated semicarbazide precursor 204	145
Scheme 3.22 – Synthesis of Fmoc-Pro-aza-Arg(diBoc)-Leu-OH aza-tripeptide 209	147
Scheme 3.23 – Attempted on-resin aza-leucine formation.....	149
Scheme 3.24 – Formation and proposed mechanism for the synthesis of dehydrated hydantoin 222	150
Scheme 3.25 – Synthesis of <i>tert</i> -butyl ester protected semicarbazone 223 and test alkylation scheme overview.....	151
Scheme 3.26 – Alternate approaches to synthesis of semicarbazide 230	153
Scheme 3.27 – Attempted coupling of semicarbazide 230 with Fmoc-Arg(Pmc)-OH and syntheses of aza-Leu-containing tripeptides 233 and 234	154

Scheme 3.28 – Test *tert*-butyl ester deprotection conditions on Fmoc-Ser(*t*Bu)-OtBu

(**235**) and aza-tripeptide **234** and completion of aza-tripeptide **238**. **155**

Scheme 3.29 – Proposed dehydration of aza-Leu-containing apelin analogues..... **158**

List of Abbreviations

$[\alpha_D]^{26}$	specific rotation at 26 °C
Abz	2-aminobenzoic acid, anthranilic acid
AC	adenylate cyclase
Ac	acetyl
ACE2	angiotensin-converting enzyme 2
Acpc	1-aminocyclopropane carboxylic acid
AESBF	4-(2-aminoethyl) benzenesulfonyl fluoride
Aib	2-aminoisobutyric acid
Akt	protein kinase B
Ala, A	alanine
All	allyl
Alloc	allyloxycarbonyl
AMC	7-amino-4-methylcoumarin
AMP	adenosine monophosphate
APJ	apelin receptor
Ar	aryl
Arg, R	arginine
Asn, N	asparagine
ASP	ammonium sulfate pellet
Asp, D	aspartic acid
AT ₁	angiotensin II receptor, type 1
ATP	adenosine triphosphate

BHT	butylated hydroxytoluene
Bn	benzyl
Boc	<i>tert</i> -butyloxycarbonyl
BPB	2-[<i>N</i> -(<i>N'</i> benzylpropyl)amino]benzophenone
br	broad
Bu	butyl
<i>c</i>	concentration
CDI	1,1'-carbonyldiimidazole
C-terminus	carboxy terminus
cAMP	cyclic adenosine monophosphate
Cbz	carboxybenzyl
CD	circular dichroism
Cha	cyclohexylalanine
CHES	<i>N</i> -cyclohexyl-2-aminoethanesulfonic acid
Cys, C	cysteine
DAP	diaminopimelic acid
DBU	1,8-diazabicyclo[5.4.0]undec-7-ene
DCC	<i>N,N'</i> -dicyclohexylcarbodiimide
DCE	1,2-dichloroethane
δ	chemical shift
Dha	dehydroalanine
Dhb	dehydrobutyrine
DIC	<i>N,N'</i> -diisopropylcarbodiimide

DIPEA	<i>N,N</i> -diisopropylethylamine
DMAP	4-dimethylaminopyridine
DMF	dimethylformamide
DMSO	dimethylsulfoxide
dP/dt	change in pressure over change in time
DSS	2,2-dimethyl-2-silapentane-5-sulfonic acid
DTT	dithiothreitol
EDTA	ethylenediaminetetraacetic acid
EI	electron ionization
EIC	extracted ion chromatogram
eNOS	endothelial nitric oxide synthase
ERK	extracellular-signal-regulated kinases
ESI, ES	electrospray ionization
Et	ethyl
Fmoc	9 <i>H</i> -fluorenylmethyloxycarbonyl
Fmoc-OSu	9 <i>H</i> -fluorenylmethylsuccinimidyl carbonate
FRET	Förstner resonance energy transfer
FTICR	Fourier-transform ion cyclotron resonance
Gln, Q	glutamine
Gln, E	glutamic acid
Gly, G	glycine
GPCR	G protein-coupled receptor
GTP	guanosine triphosphate

HATU	O-(7-Aza-1H-benzotriazol-1-yl)- <i>N,N,N',N'</i> - tetramethyluronium hexafluorophosphate
HBTU	O-(1H-benzotriazol-1-yl)- <i>N,N,N',N'</i> - tetramethyluronium hexafluorophosphate
HCCA	α -cyano-4-hydroxycinnamic acid
His, H	histidine
HIV	human immunodeficiency virus
HMWK	high molecular weight kininogen
HOAt	1-hydroxy-7-azabenzotriazole
HOBt	1-hydroxybenzotriazole
HPLC	high performance liquid chromatography
HRMS	high resolution mass spectrometry
IA	iodoacetamide
IC ₅₀	half maximal inhibitory concentration
Ile, I	isoleucine
Inp	isonipecotic acid, 4-piperidine carboxylic acid
IR	infrared
<i>J</i>	coupling constant
KAHA	α -ketoacid hydroxylamine
k _{cat}	turnover number
kDa	kilodalton
KLK1	kallikrein 1, tissue kallikrein, kidney/pancreas/salivary gland kallikrein

KLKB1	plasma kallikrein
K_m	Michaelis constant
KO	knockout
LC-MS/MS	liquid chromatography-tandem mass spectrometry
Leu, L	leucine
Lys, K	lysine
MABP	mean arterial blood pressure
MALDI-TOF	matrix-assisted laser desorption ionization time of flight
Me	methyl
MES	2-(<i>N</i> -morpholino)ethanesulfonic acid
Met, M	methionine
mmHg	millimeters of mercury
mol	mole
MQ	Milli-Q water filtration system
mRNA	messenger ribonucleic acid
MRS	de Man Rogosa and Sharpe
MRSA	methicillin-resistant <i>Staphylococcus aureus</i>
Ms	methanesulfonyl
MS	mass spectrometry
mTOR	mechanistic target of rapamycin
MWCO	molecular weight cut off
N-terminus	amino terminus
Nal	naphthyl

NCL	native chemical ligation
Nle	norleucine
NMM	<i>N</i> -methylnmorpholine
NMR	nuclear magnetic resonance
NO	nitric oxide
NO ₂ Y	3-nitrotyrosine
NOE	nuclear Overhauser effect
NOESY	nuclear Overhauser effect spectroscopy
NRPS	non-ribosomal peptide synthetase
Orn	ornithine
<i>p</i> -BrPhe, BrPhe	<i>para</i> -bromophenylalanine
<i>p</i> -NB	<i>para</i> -nitrobenzyl
<i>p</i> -NZ	<i>para</i> -nitrobenzyloxycarbonyl
<i>p</i> -Ts	<i>para</i> -toluenesulfonyl
Pbf	2,2,4,6,7-pentamethyldihydrobenzofuran-5-sulfonyl
PCSK3	proprotein convertase subtilisin/kexin 3, furin
PEG	polyethylene glycol
pGlu, pE	pyroglutamic acid
Phe, F	phenylalanine
pI	isoelectric point
PI3K	phosphoinositide 3-kinase
PKC	protein kinase C

PLC β	1-phosphatidylinositol-4,5-bisphosphate phosphodiesterase β
Pmc	2,2,5,7,8-pentamethylchroman-6-sulfonyl
PMSF	phenylmethylsulfonyl fluoride
PP _{II}	polyproline II helix
ppm	parts per million
Pr	propyl
Pro, P	proline
PyBOP	benzotriazole-1-yl-oxytrispyrrolidinophosphonium hexafluorophosphate
Q-sepharose	quaternary ammonium strong anion exchange resin
RCM	ring-closing metathesis
R _f	retention factor
rh	recombinant human
ROESY	rotating frame nuclear Overhauser effect spectroscopy
RP	reversed phase
SAR	structure activity relationship
Ser, S	serine
S _N 2	bimolecular nucleophilic substitution
SP-sepharose	sulfopropyl strong cation exchange resin
SPPS	solid phase peptide synthesis
tBu	<i>tertiary</i> -butyl
TCEP	tris(2-carboxyethyl)phosphine

TEMPO	2,2,6,6-tetramethyl-1-piperidine 1-oxyl
Tf	trifluoromethanesulfonyl
TFA	trifluoroacetic acid
THF	tetrahydrofuran
Thr, T	threonine
TIPS	triisopropylsilane
TLC	thin layer chromatography
TOCSY	total correlation spectroscopy
Tris	tris(hydroxymethyl)aminomethane
Trp, W	tryptophan
Trt	trityl
Tyr, Y	tyrosine
UV	ultraviolet
v/v	volume per volume
Val, V	valine
V_{\max}	enzyme maximum rate
VRE	vancomycin-resistant <i>Enterococci</i>
WT	wild type

1 Introduction

1.1 Introduction to biologically active peptides

Peptides and their larger counterparts, proteins, are incredibly important biomolecules, with a host of physiological roles in nature.¹ A peptide is a small polymer of amino acid monomers, connected through amide bonds to give a repeating three-atom backbone. However, this scaffold is considerably diversified through the amino acid side chain 'R' groups, which impart a differentiation of features on the molecule. Ribosomally synthesized peptides are primary metabolites, and are composed of the twenty canonical amino acids; these peptides will be the main focus of the projects discussed in this thesis. However significant post-translational modifications can occur to amino acid moieties within the peptide to further elaborate their considerable diversity. A second group of peptides, formed by non-ribosomal peptide synthetase enzymes (NRPSs), incorporate a larger variety of unusual amino acids into their scaffolds.² These non-ribosomal peptides, typically from bacterial or fungal sources, also comprise a vast array of biologically significant activities but will not be discussed further in this thesis.

Although only a tiny representation of the vast diversity of peptide structures and functions, select biologically active peptides are shown using a variety of depictions in Figure 1.1. To simplify the redundant peptide backbone, larger peptides will be shown via bubble structures, or using one or three letter amino acid codes, while still highlighting any unique side chain modifications or alterations to the native amino acid structures. All depictions are equally valid and will be used to describe peptide

structures throughout this thesis. Unless otherwise denoted, as seen with the D-phenylalanine residues in gramicidin S (5), all amino acids are L-amino acids. One can unambiguously assign an (*S*)-stereochemistry at the α -carbons of all canonical amino acids, with the exception of L-cysteine which has an (*R*)-stereocenter because of Cahn-Ingold-Prelog nomenclature.³

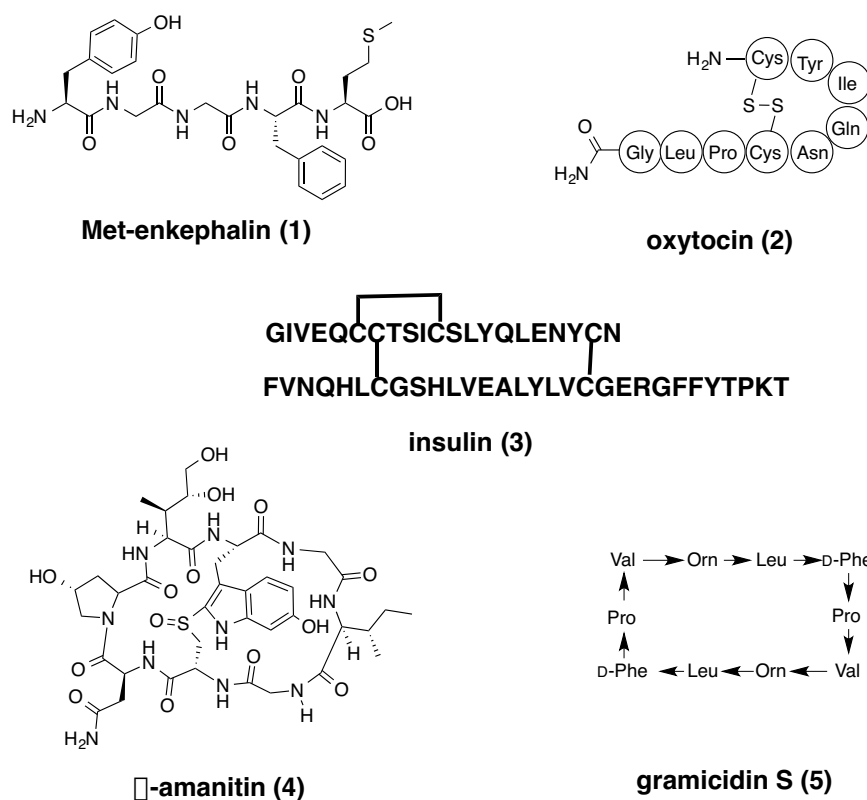


Figure 1.1 – Structures of biologically active peptides represented through equivalent depictions. Examples include: analgesic peptide Met-enkephalin (1), potent peptide hormones oxytocin (2) and insulin (3), toxic peptide α -amanitin produced from fungal sources (4) and non-ribosomal antibacterial peptide gramicidin S (5).

1.2 Peptide synthesis methodology

The exquisite control over the synthesis of peptides is due to the development of solid-phase peptide synthesis (SPPS) by Robert Bruce Merrifield,⁴ recipient of the Nobel Prize in Chemistry in 1984. The general SPPS methodology involves the initial covalent attachment of the C-terminal end of a carbamate-protected amino acid to a functionalized solid support. From there, the amine can be liberated chemoselectively, retaining the C-terminus on-resin. The introduction of a second carbamate-protected amino acid and additional ‘activating’ reagents *in situ* generates an activated ester; this can subsequently react with the deprotected amine on-resin to ‘couple’ together the amino acids, forming a new amide bond. The major advantage of SPPS is the facile removal of reaction byproducts by draining the reaction mixture through a porous filter, retaining the resin-bound material for further reaction. This minimizes chromatographic purification steps, as well as enables the use of superstoichiometric equivalents of reagents to improve yields and decrease reaction times. However, in the event of an incomplete peptide coupling, analyses such as a ninhydrin-based Kaiser test⁵ are used to qualitatively determine the presence of a free amino group. To prevent any unreacted amines from participating in subsequent amide bond formations, the resin is typically treated with acetic anhydride to ‘end-cap’ any free amines. Although ‘end-capping’ decreases overall peptide yields, this procedure is performed to minimize the formation of artificially truncated fragments. These peptide fragments may have similar chromatographic properties to the desired product, so their removal simplifies the purification process. After this treatment, the carbamate of the resin-bound dipeptide can be removed and the

cycle can be repeated. It should be noted that chemical peptide synthesis goes the reverse direction (C to N terminus) of the biological process.

Two main SPPS methodologies are currently used (Boc- and Fmoc-SPPS), varying in their carbamate protecting groups. Although the two strategies use the same processes, they differ in the reagents required to deprotect the carbamate, and to ultimately liberate the peptide from the resin. Due to ease of use and safety, Fmoc-SPPS was exclusively used for the work performed in this thesis. A simplified cycle, using piperidine to deprotect the Fmoc group from the resin-bound amino acid (red) and HATU/DIPEA to couple the second amino acid (blue), is illustrated in Figure 1.2. The highly UV-active dibenzofulvene-piperidine adduct (highlighted in yellow) can be monitored to assess the deprotection of the Fmoc moiety.

Through the continued repetition of SPPS cycles, amino acids can be incorporated at the appropriate sequence location, and the peptide is elongated to the desired length. In Fmoc-SPPS, the peptide can be selectively cleaved following acid treatment of varying strength based on the resin, often removing acid-labile side chain protecting groups concomitantly (Figure 1.3).

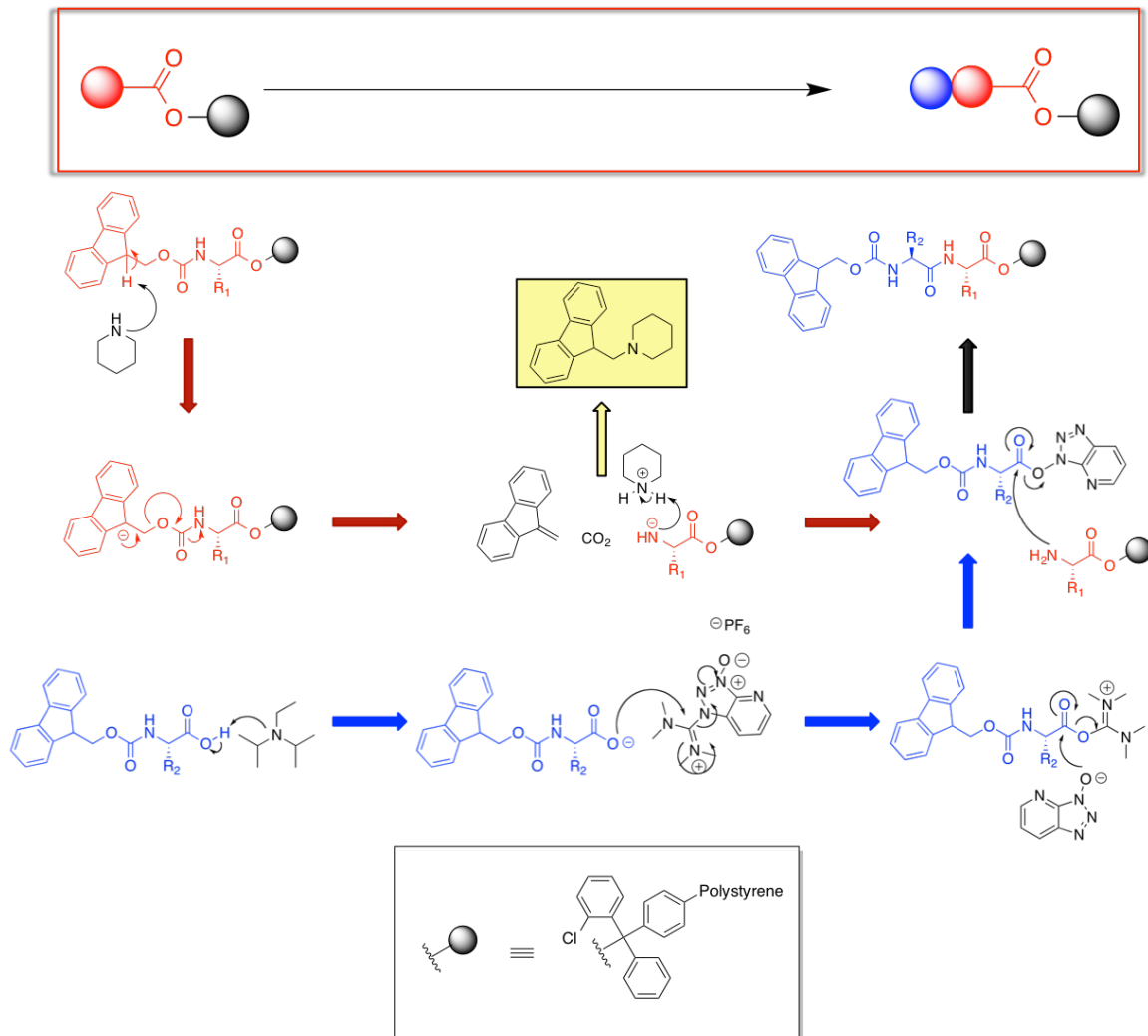


Figure 1.2 – Simplified cycle of one round of Fmoc-SPPS coupling.

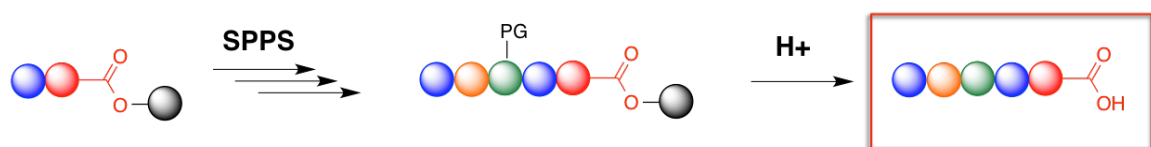


Figure 1.3 – SPPS elongation and resin cleavage with concomitant side-chain deprotection.

One of the most exciting extensions of SPPS has been the development of ligation strategies to join peptide fragments together in solution. As SPPS

methodologies gave chemists and biochemists an exquisite level of control over the synthetic manipulation of peptides, the advent of native chemical ligation has extended this control to the synthetic preparation of larger proteins (Figure 1.4).⁶ Native chemical ligation is initiated by the trans-thioesterification of a C-terminal thioester of peptide fragment 1 with a cysteine sulfhydryl moiety located at the N-terminus of peptide fragment 2. This reaction is particularly advantageous as it can be performed in the presence of unprotected amino acid side chains. A thermodynamically favorable S to N acyl transfer ligates the two fragments together via a native amide bond. Native chemical ligation however is dependent on the presence of a cysteine, one of the least common amino acids in proteins,⁷ in the primary sequence of the desired synthetic protein. However, desulfurization techniques can be used to retroactively remove the cysteine thiol post-ligation provided no other cysteine amino acids are in the structure. This methodology has been used to produce some large proteins, perhaps most notably the heavily glycosylated 166 amino-acid long hormone erythropoietin.⁸ A recently developed alternative protocol, the α -ketoacid hydroxylamine (KAHA) ligation,⁹ has a more relaxed sequence specificity, generating serine¹⁰ or its non-canonical homologue homoserine post ligation. This approach has already been applied to the synthesis of large proteins, such as the 20 kDa heme-binding protein nitrophorin 4.¹¹ Further applications of peptide ligation approaches built upon the advancements in peptide synthesis will give future generations the advanced control over the whole chemical synthesis of proteins.¹²

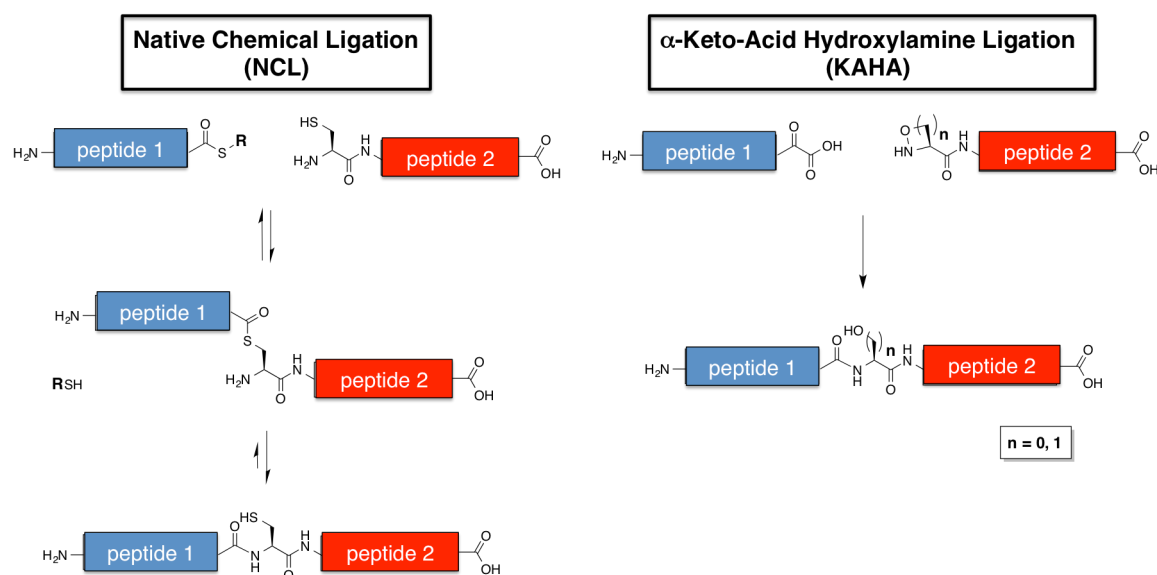


Figure 1.4 – Native chemical (left)⁶ and α -ketoacid hydroxylamine (right)⁹ ligation strategies to facilitate the chemoselective combination of individually synthesized peptide monomers.

1.3 Peptide stability

Despite their countless uses, peptide drug candidates do have some limitations for use as exogenously applied therapeutics. They have very poor bioavailability and are difficult to administer to humans, as oral administration typically results in hydrolysis and poor absorption into the bloodstream. Certain amino acid side chains are sensitive to oxidation, which can be detrimental to the activity of peptides, particularly those produced in anaerobic environments. Perhaps the most dominant factor to the application of peptides for therapeutic purposes is their susceptibility to proteases, specific enzymes that degrade peptides and proteins and limit their functions.

Despite these limitations, there have been considerable efforts at improving the stability of biologically active peptides through chemical means, and applying these peptides for therapeutic purposes.^{13,14} Common approaches to the stabilization of

bioactive peptides involve: substitution with non-canonical amino acids; epimerization to D-amino acids; macrocyclizations; *N*-methylations; β -amino acid incorporation; and isosteric replacement of the susceptible amide bond. Although there are numerous examples of improving the pharmacokinetics of peptides, a few relevant analogues will be highlighted that retain the full biological activities of the parent peptides.

The incorporation of simple amino acid substitutions was successful in imparting significant proteolytic resistance for OXM₁₋₃₇ (**6**),¹⁵ a significant peptide for the stimulation of insulin secretion and lowering of blood glucose *in vivo*.¹⁶ MS-based analysis indicated a rapid proteolytic degradation between two internal arginine residues occurring in under fifteen minutes *in vitro* in mouse plasma (red lines, Figure 1.5). Subsequent alanine replacement led to prOXM₁₋₃₇ (**7**), which showed no degradation after 30 minutes plasma incubation and a comparable EC₅₀ to native **6** (Figure 1.5).¹⁵

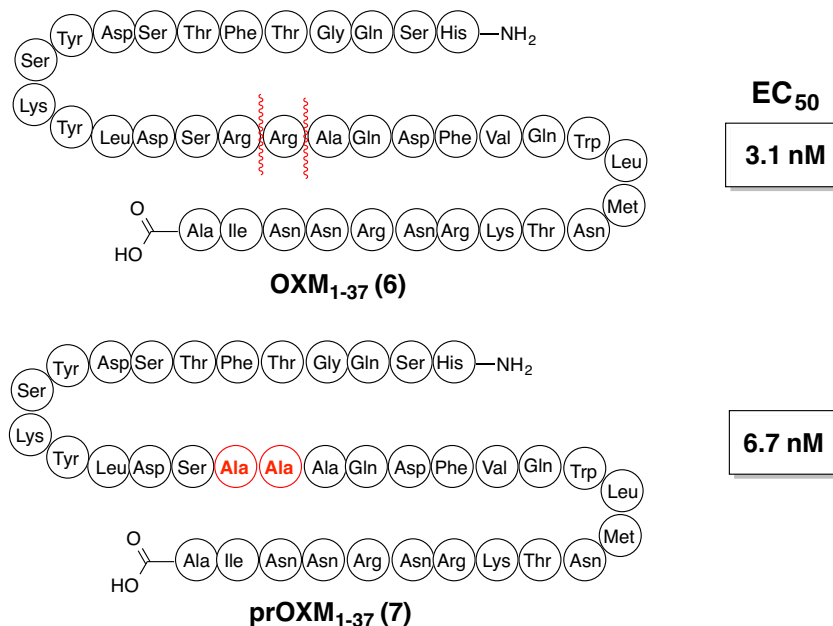


Figure 1.5 – Stabilization of the site of proteolytic degradation of OXM₁₋₃₇ (6**) by alanine substitution, generating prOXM₁₋₃₇ (**7**).¹⁵**

An analogous peptide that interacts with the same biological receptor, the glucagon-like peptide 1 receptor (GLP-1R), as **6**¹⁷ is GLP-1(7-37)-NH₂ (**8**). Peptide hormone **8** also has promising therapeutic properties for the treatment of diabetes.¹⁸ The incorporation of unnatural amino acids at key locations within this peptide hormone led to a substantial improvement of plasma stability while retaining virtually all agonistic activity (Figure 1.6).¹⁹

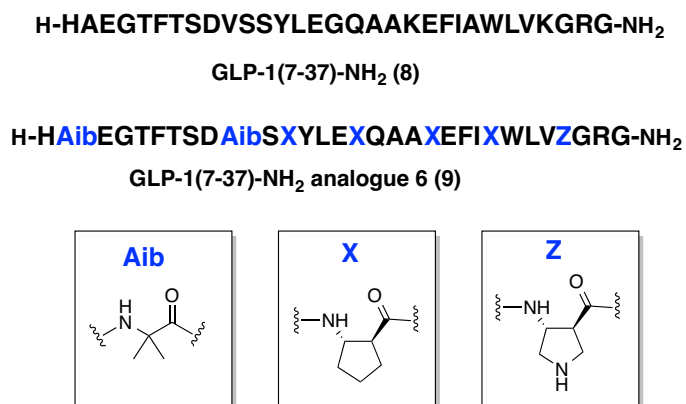


Figure 1.6 – Structures of GLP-1(7-37)-NH₂ (8) and unnatural amino acid substituted analogue (9).¹⁹

The *cis*-olefin oxytocin analogue **10**, generated from the on-resin ring-closing metathesis of two allylglycine residues, showed highly potent, albeit slightly reduced agonistic activity compared to native oxytocin (**2**).²⁰ This peptide had the added benefit of improved metabolic stability based on the non-reducible nature of the olefin moiety compared to the more labile disulfide. Amide bond isosteres can also be advantageously incorporated into peptide backbones to negate the effect of proteolysis, leading to a variety of effects on the inherent biological activity of the peptide.^{21,22} An example of a trifluoromethyl olefin-substituted amide bond mimic of gramicidin S (**11**) that retained significant antimicrobial activity against *Bacillus subtilis* is highlighted in Figure 1.7.²³

Further modifications made to relevant peptide substrates will be discussed throughout the body of this thesis.

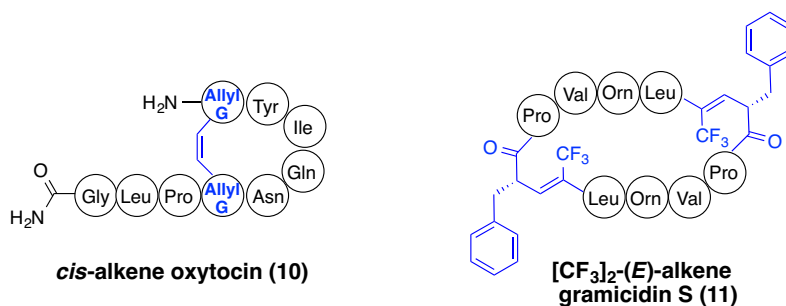


Figure 1.7 – Structures of biologically active *cis*-alkene oxytocin (10)²⁰ and [CF₃]₂-(*E*)-alkene gramicidin S (11)²³ peptides.

1.4 Thesis overview

The work presented in this thesis highlights efforts towards the chemical synthesis of analogues of two biologically active peptides that have improved stability to environmental limiting factors. An investigation of their improved stability through biological assays will also be used to assess the success of their synthetic modifications.

Chapter 2 will discuss antimicrobial lantibiotic peptide lactocin S, which rapidly loses its biological activity after exposure to atmospheric oxygen. The synthesis of a double sulfur-substituted analogue of lactocin S will be described. An assessment of the oxidative stabilities of synthetic sulfur-substituted lactocin S analogues will be highlighted to qualitatively assess the effect of their substitutions on the retention of antimicrobial activity.

Chapter 3 will discuss the synthesis of analogues of pyr-1-apelin-13 and apelin-17, cardiovascular peptides with many physiologically significant roles, which are rapidly degraded by plasma proteases *in vivo* and *in vitro*. The role of angiotensin-

converting enzyme 2 (ACE2) in the *in vitro* degradation of apelin peptides will be initially investigated, followed by the synthesis of ACE2 resistant apelin analogues that are non-hydrolyzable substrates and not inhibitors of this critical regulatory enzyme. The remainder of this chapter will use these ACE2 resistant analogues to identify additional apelin sites of degradation, suggest additional proteases responsible for the degradation, and synthesize second generation analogues at this new location of hydrolysis. An *in vitro* pharmacokinetic assessment of apelin analogue stability will be used throughout to highlight the improvement of synthetic apelin analogues to proteolytic resistance.

2 Lactocin S

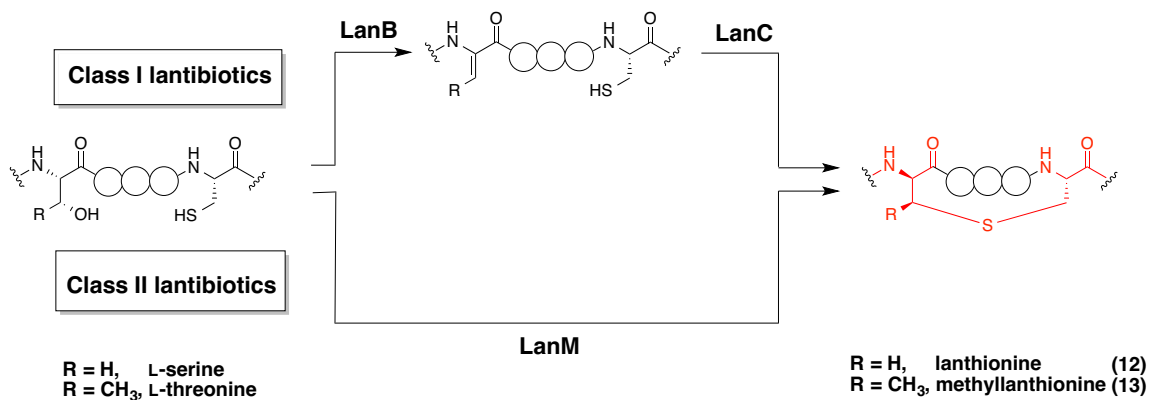
2.1 Introduction

2.1.1 Lantibiotics background

Lantibiotics are ribosomally-synthesized, post-translationally modified peptides produced by bacteria to inhibit the growth of rival species.^{24,25,26} The term ‘lantibiotic’ comes from peptides containing lanthionine amino acids that show antibacterial activity.²⁷ Not all lanthionine-containing peptides (generally termed ‘lanthipeptides’) possess antimicrobial activity, but those that do typically target lipid II or lipid II precursors, an essential component for peptidoglycan cell wall biosynthesis in bacteria. Because of the critical role of lipid II in bacterial cell viability, the opportunity for resistance development is minimized.²⁸ At higher concentrations, some lantibiotics also induce pore formation. Relevant pathogenic Gram-positive organisms sensitive to lantibiotics include methicillin-resistant *Staphylococcus aureus* (MRSA) and vancomycin-resistant enterococci (VRE) among many others.^{29,30,31,32} The prototypical lantibiotic, nisin, has been used commercially as a preservative in the dairy industry for over 50 years, with minimal resistance being developed.³³

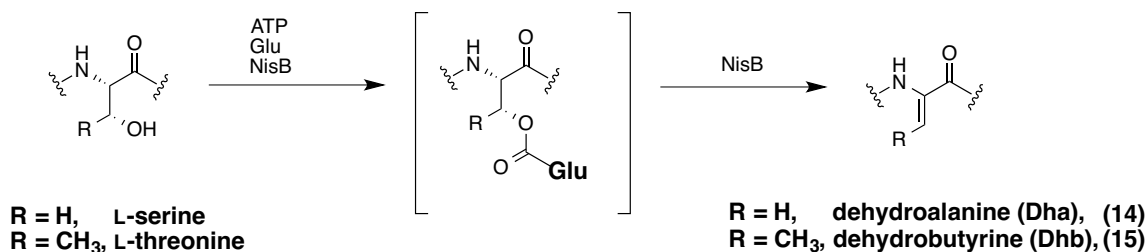
The namesake lanthionine (**12**) and methyllanthionine (**13**) amino acid residues are formed by an enzyme-catalyzed dehydration of serine and threonine amino acids to dehydroalanine (Dha, **14**) and dehydrobutyrine (Dhb, **15**), respectively, followed by a stereoselective enzyme-catalyzed Michael addition of a cysteine sulfhydryl group (Scheme 2.1). The main classes of lantibiotics are differentiable based on the mechanism of lanthionine formation. Class I lantibiotics have two enzymes, LanB and

LanC that independently perform the dehydration and thioether formation steps respectively. Class II lantibiotics have both functionalities encapsulated within one LanM enzyme. Class III and IV lanthipeptides have slightly variable modes of lanthionine formation, but will not be discussed further in this thesis.



Scheme 2.1 – Dual method of lanthionine formation for Class I and Class II lantibiotic systems.

The mechanism of lanthionine formation in class II lanthipeptides is driven by the consumption of ATP to directly phosphorylate and then eliminate the β -hydroxyl group. This was previously studied with a LtnM enzyme from lactacin 481.³⁴ However, mutational analysis of catalytic residues in NisB, the dehydratase domain of the lanthionine synthase of type I lantibiotic nisin, showed intermediates incorporating a post-translational addition of glutamate. It is now believed that class I lanthipeptide LanB enzymes catalyze their dehydrations via an ATP-dependent glutamylation intermediate prior to elimination.^{35,36}



Scheme 2.2 – NisB-catalyzed dehydration of serine and threonine amino acids to generate Dha (14) and Dhb (15) amino acids.³⁵

After formation of these dehydrated amino acids, a variety of enzyme-catalyzed post-translational modifications can occur on these unique moieties. These modifications can be grouped together into enzyme-catalyzed Michael additions (Figure 2.1 A), protease cleavage N-terminal to the dehydroamino acid (Figure 2.1 B), and enzymatic reduction (Figure 2.1 C). The presence of a leader peptide N-terminal to the lantibiotic sequence directs the relevant enzymatic machinery to facilitate these post-translational modifications.³⁷

Prior to 2013, enzyme-catalyzed stereoselective Michael addition was always observed to generate *meso*, or D,L-lanthionine residues. However, recent reports have shown that having a dehydrated amino acid immediately C-terminal to the Dha/Dhb can instead generate an L,L-lanthionine stereoisomer at this new position for both the lanthionine (**16**) and methyllanthionine (**17**) moieties.³⁸ Although this diastereomer has only been seen in two lantibiotic systems thus far,^{39,40} this substitution highlights the structural diversity present in this class of peptides. Lanthionine stereochemistry has been shown to be critically important for the lantibiotic lactacin 481, as the incorporation of the non-native lanthionine diastereomer through chemical synthesis abolished its antimicrobial activity.⁴¹ Cysteine sulfhydryl conjugate addition also generates

aminovinylcysteine (**18**) and its methyl derivative (**19**), along with ‘domino’ conjugate addition product labionine (**21**) seen in class III lanthipeptides. An analogous nucleophilic attack by the ϵ -amine of lysine can form lysinoalanine (**20**).

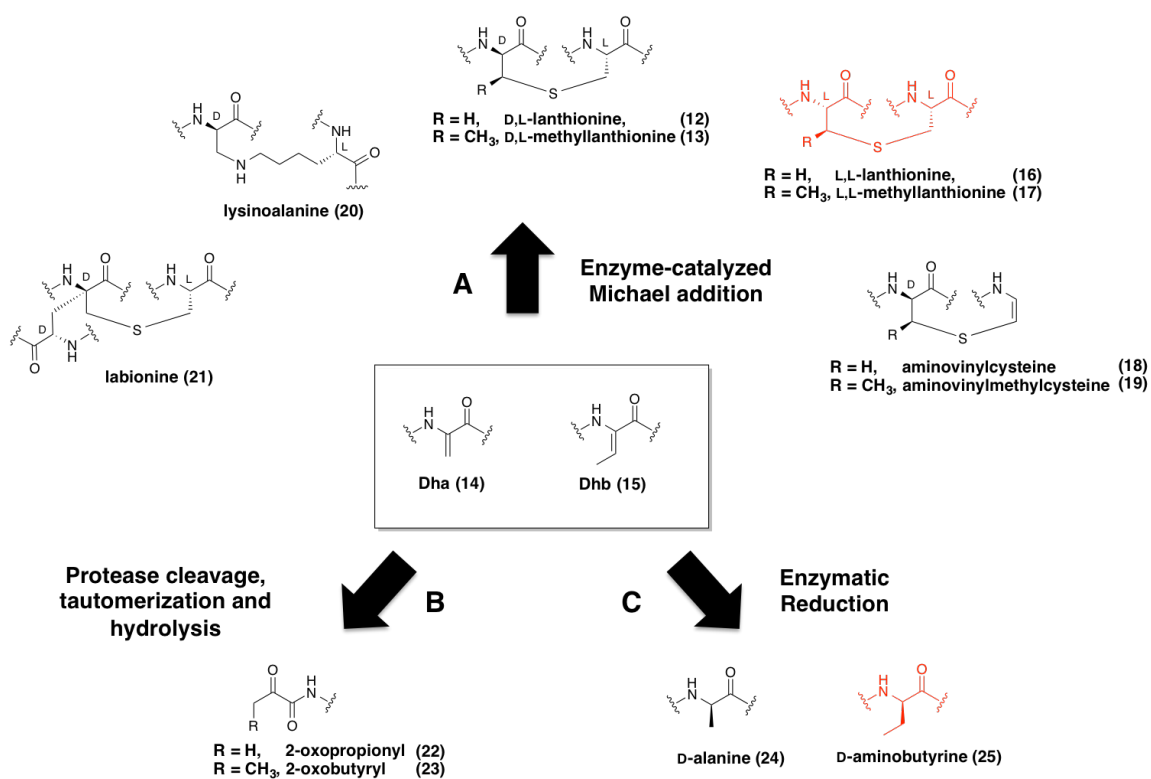


Figure 2.1 – Examples of key post-translational modifications found in lantibiotic systems. All modifications are derived from the initial dehydrated Dha (**14**) and Dhb (**15**) amino acids. Recently discovered L,L-lanthionine/methylanthionine (**16/17**)^{39,40} and D-aminobutyryne (**25**)⁴⁰ modifications are highlighted in red.

Following protease cleavage N-terminal to a dehydroamino acid, the resultant enamine will tautomerize and hydrolyze to form α -keto amide moieties **22** and **23**. In select cases, this residue can be reduced to give a lactate functionality.⁴² Lastly, enzymatic reduction to generate D-alanine (**24**) residues has been observed in a few lantibiotic systems,⁴³ notably with lactocin S and the two-component lactacin 3147 A1

and A2 peptides, both of which will be discussed in later sections. A recent discovery in our lab has highlighted the first reduction of a Dhb residue to the corresponding D-aminobutyrate (**25**) in carnolysin A2.⁴⁰ These interesting structural moieties all originate from post-translational modifications to canonical amino acids in ribosomally synthesized peptides, and play a role in the unique structures and corresponding activities of lanthipeptides.

2.1.2 Lactocin S structure and biology

Lactocin S (**26**) is a bacteriocin that was originally isolated by Nes and coworkers from *Lactobacillus sakei* L45 found in fermented sausage.⁴⁴ This bacteria showed antimicrobial activity against closely related Gram-positive strains of *Pediococcus*, *Lactobacilli* and *Leuconostoc* strains. Lactocin S (**26**) is a 37-amino acid peptide with two macrocyclic lanthionine thioether bridges at the C-terminus with the more conventional D,L-stereochemistry (Figure 2.2).⁴⁵ The formation of lanthionine residues is catalyzed by LasM, a LanM-like enzyme, implying that lactocin S should be a class II lantibiotic; however, its structure is relatively long and flexible, a trait shared amongst class I lantibiotic peptides. Due to this ambiguity, lactocin S is typically grouped independently of conventional nomenclature. All of the cationic residues are located at the C-terminus of the peptide, with three basic amino acids encapsulated within the B-ring. These are predicted to electrostatically interact with the negatively charged phospholipid head groups on the outside of bacterial cells. While the precise mode of action of the antimicrobial effects of lactocin S has yet to be elucidated, it is proposed to involve a lipid II-independent mechanism.

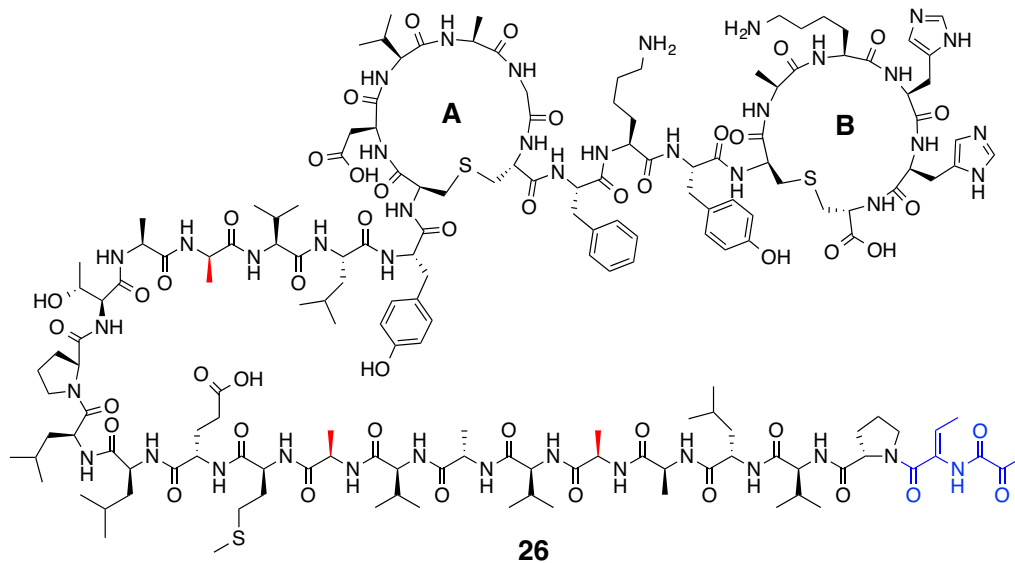


Figure 2.2 – Structure of lactocin S (26). D-alanine residues (red) and the α -ketoamide N-terminus (blue) are highlighted.

Additional structural features of lactocin S include the conversion of three genetically encoded serine residues at positions 7, 11 and 19 to D-alanines through a yet-to-be discovered reductase,^{43,46,47} and an 2-oxopropionyl moiety at the N-terminus of the peptide.

2.1.3 Syntheses of lantibiotic peptides by solid-phase peptide synthesis

Nisin (**27**) was the first lantibiotic synthesized in a monumental undertaking which took ten years to complete (Figure 2.3).⁴⁸ The high complexity of the structure, coupled with the incompatibility of dehydroalanine residues with Fmoc-SPPS forced Shiba and coworkers to complete the total synthesis in solution. To this date, no other groups have reproduced this herculean effort on solid-phase, although individual ring systems have been prepared.^{49,50}

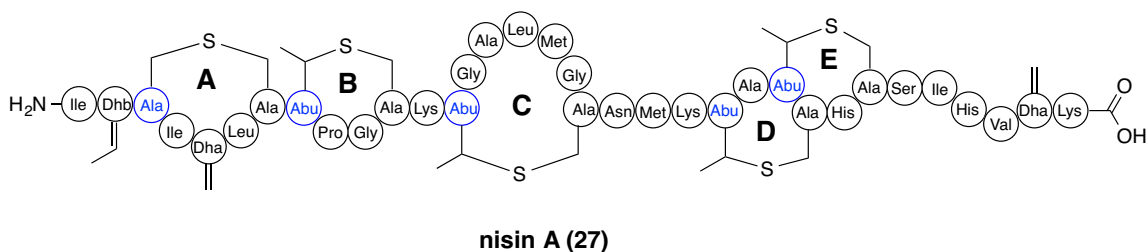
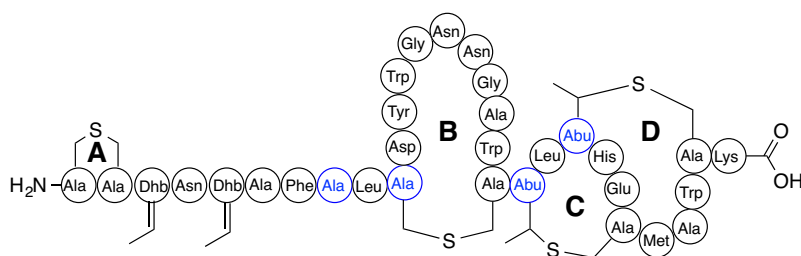
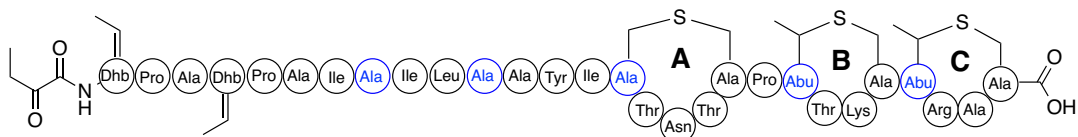


Figure 2.3 – Bubble structure of nisin A (27). The macrocyclic lanthionine ring systems are denoted A-E, along with dehydrated amino acid side chains, and positions with D-stereochemistry (blue).

To accomplish the preparation of any macrocyclic peptide rings via SPPS, the concept of orthogonal-protection is critical. Tabor and coworkers utilized an orthogonal Alloc/All protecting group strategy of the lanthionine residues in combination with Fmoc SPPS to complete the synthesis of the C-ring of nisin.⁴⁹ Following analogous methodology, lactocin S (**26**) was the first lantibiotic peptide synthesized by SPPS in 2010.⁴⁵ This was soon followed by the synthesis of the first two-component lantibiotic lactacin 3147 A1 (**28**) and A2 (**29**).⁵¹ Lactacin 3147 A1 (**28**) had the added complication of interlocking lanthionine rings in the A1 peptide, requiring two unique orthogonal protection schemes (Alloc/All and *p*-NZ/*p*-NB).⁵¹ Although a similar methodology has been employed to generate the interlocking DE rings of nisin, its total synthesis with SPPS still remains to be completed.⁵⁰ Subsequent synthetic undertakings have since generated lactacin 481⁴¹ and epilancin 15X⁵² with comparable antimicrobial activity to the native peptides.



lacticin 3147 A1 (28)



lacticin 3147 A2 (29)

Figure 2.4 - Bubble structures of two-component lantibiotics lacticin 3147 A1 (28) and A2 (29). Macrocyclic lanthionine ring systems are denoted (A-D for A1, A-C for A2), along with dehydrated amino acid side chains, and positions with D-stereochemistry (blue).

2.1.4 Substitution of lanthionine residues in lantibiotics nisin and lacticin 3147 A2

Studies have shown that the activity of lantibiotics is dramatically impaired upon lanthionine sulfoxide formation.⁵³ Only one lantibiotic peptide, actagardine, is known to retain full biological activity in the presence of an oxidized lanthionine ring.⁵⁴ Lanthionine residues would therefore be a desirable structural moiety to substitute in order to improve biological stability. The effect of amino acid substitutions on the activity of lantibiotic peptides has also been thoroughly examined.⁵⁵

Most early lanthionine-substituted lantibiotic analogues were prepared due to the synthetic methodologies available, not in an effort to improve oxidative stability. Des-methyl lacticin 3147 A2 (**30**) was the first full lantibiotic analogue with native lanthionine moieties to be synthesized,⁵⁶ although ring-expanded olefin mimic (**31**) was

prepared chronologically earlier.⁵⁷ Isosteric oxa-lactacin 3147 A2 (**32**) has also been synthesized via SPPS using orthogonally protected oxa-lanthionine ethers (Figure 2.5).⁵⁸

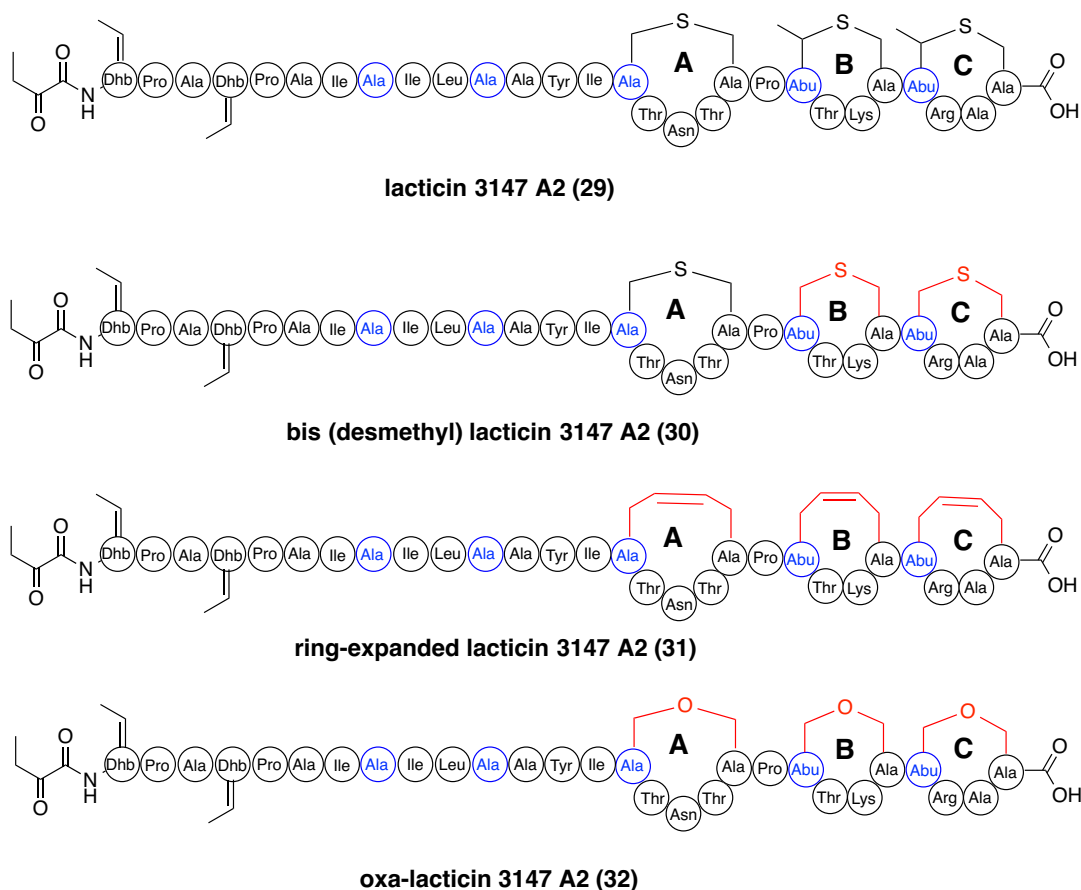


Figure 2.5 – Lanthionine substituted analogues of lactacin 3147 A2 (29). Alterations from the native **29** structure include solely lanthionine residues for rings B and C (**30**),⁵⁶ olefin moieties (**31**),⁵⁷ and oxa-lanthionine (**32**).⁵⁸

The inherent antimicrobial activities of analogues **30-32** were compared to native **29** and assessed for synergistic activity with lactacin 3147 A1 (**28**). Of the three lanthionine-substituted analogues, only oxa-analogue **32** showed independent antimicrobial activity, but no synergistic activity with **28**.⁵⁸ Conversely, synergistic activity with **28** was retained with desmethyl A2 analogue **30**, but no independent

antimicrobial activity for **30** was observed.⁵⁶ Alkene-substituted analogue **31** showed no antimicrobial activity, nor synergistic activity.⁵⁷ These results suggest that both ring size and heteroatom presence in lanthionine rings are critical for lantibiotic activity.

On-resin ring closing metathesis has allowed for the synthesis of individual ring isosteres of nisin. Using the nisin Z (**33**) scaffold, Liskamp and coworkers have prepared modified rings incorporating alkyne,⁵⁹ alkene,^{60,61,62} and alkane⁶¹ macrocyclizations (Figure 2.6).

Although nisin fragments would not individually impart antimicrobial activity, the assessment of binding of the AB(C) rings to the pyrophosphate moiety of lipid II was performed for both analogues and compared to the native nisin AB(C) ring system. Synthetic analogue **37**, possessing the native D,L-lanthionine stereochemistry, showed the greatest affinity for lipid II, but at 50 times higher concentration than the native nisin AB(C) rings. Neither **36** nor **38**, containing the analogous ‘methylanthionine’-like substitution, showed any binding interaction with vesicle-bound lipid II.⁶¹

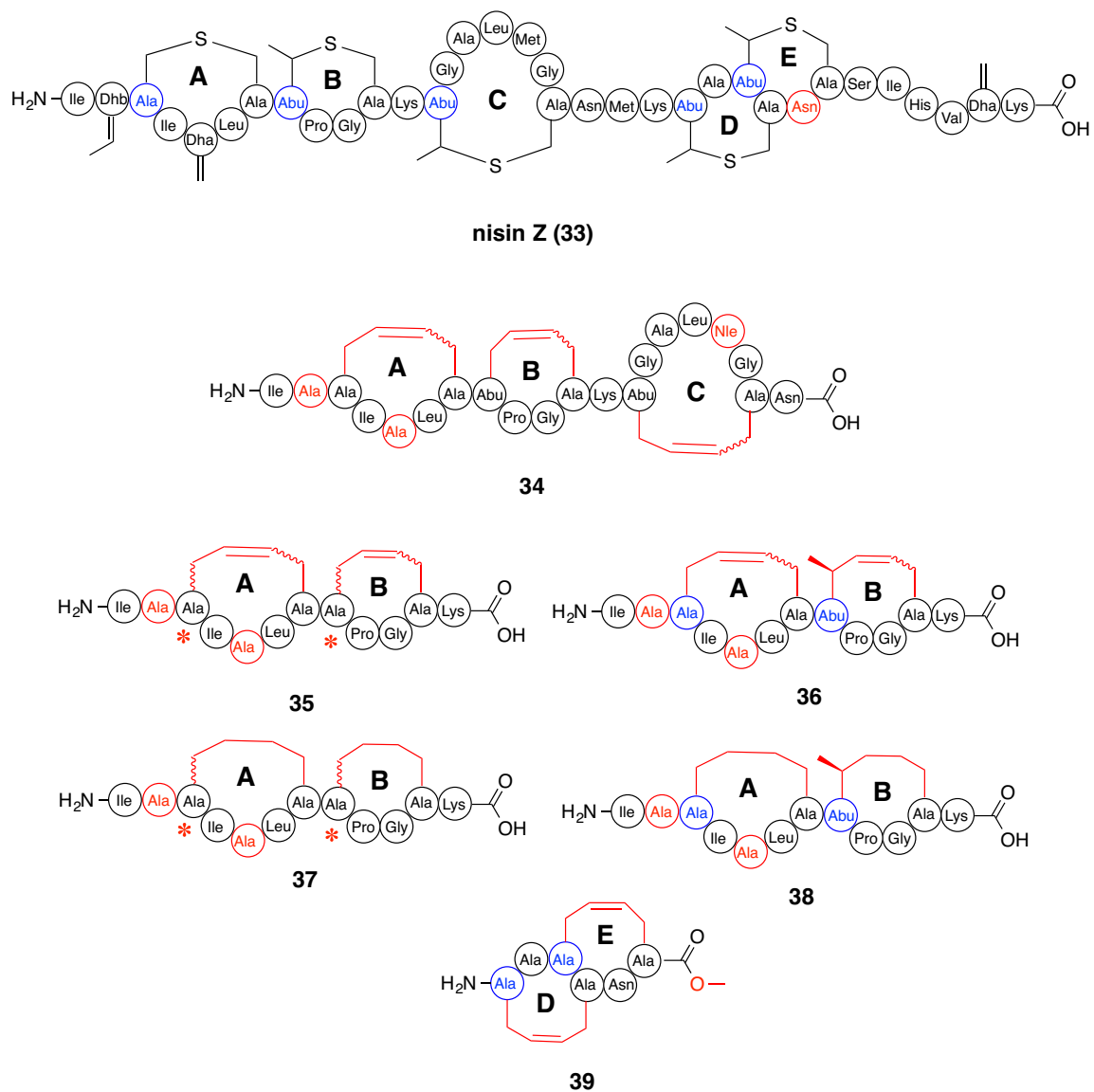


Figure 2.6 – Nisin Z structure (33) and various lanthionine ring substituted products (34-39) accessed by RCM. Alterations to native nisin Z sequence are shown in red; blue circles denote D-stereochemistry; both diastereomers were individually prepared and assessed at location of asterisks.^{59,60,61,62}

Synthetic modifications made to the DE-ring of nisin Z were conjugated to the native ABC ring system, obtained through enzymatic degradation, to assess the impact of DE-ring substitutions to induce pore-formation (Figure 2.7).⁶³ Although both **40** and **41** retained full lipid II binding capabilities, neither were capable of inducing the formation

of pores. These results further emphasize the significance of native lanthionine rings to proper lantibiotic function.

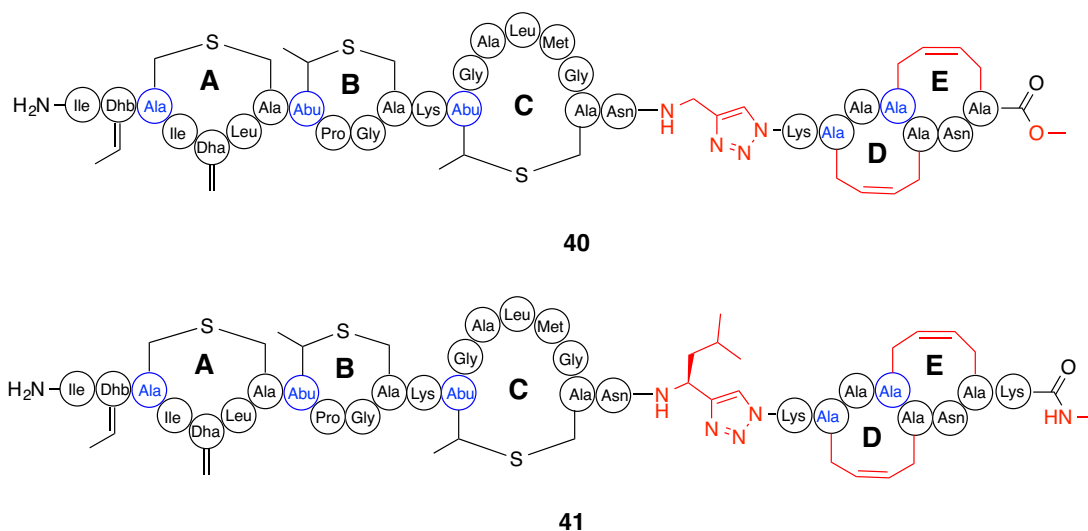


Figure 2.7 – Semi-synthetic conjugates of native nisin Z ABC rings with synthetic RCM-prepared DE rings (40, 41). D-amino acid moieties (blue), and deviations from the nisin Z scaffold (red) are highlighted.⁶³

Selenolanthionine, the selenium-isostere, has been incorporated into nisin ring C, and has seen application as a stable disulfide mimic in oxytocin.⁶⁴ Contrary to current orthogonal protection strategies, selenolanthionine residues can be cyclized stereoselectively on-resin due to the reduced pKa of selenol compared to thiol. However, the application of this model to a multiple lanthionine ring containing system would lead to an undesirable mix of regioisomers.⁶⁴ Both selenolanthionine and recently synthesized azalanthionine residues⁶⁵ have yet to be incorporated into a native lantibiotic structure and assessed for physiological activity. Differential lanthionine heteroatom substitution would slightly alter the ring geometry and could provide insight into the importance of hydrogen bond acceptor/donor capabilities of the heteroatom.

2.1.5 Substitution of lanthionine and methionine sulfur atoms in lactocin S

The initial approach to stabilize the antimicrobial activity of lactocin S in the presence of oxygen involved the incorporation of the isosteric diaminopimelic acid (DAP), instead of native lanthionine. Previous substitution of lanthionine thioether bridges with alkane moieties via RCM of allylglycine residues had not retained antimicrobial activity.⁶¹ However this could be due to the macrocyclic ring being one carbon too large which could affect the ring geometry and have a deleterious effect on antimicrobial activity. DAP residues would incorporate a similar ring size, and through an orthogonal protection and on-resin cyclization SPPS strategy, Dr. Avena Ross synthesized three DAP analogues of lactocin S, A-DAP (**42**), B-DAP (**43**) and D-DAP (**44**) differing in their substitution of lanthionine residues (Figure 2.8).

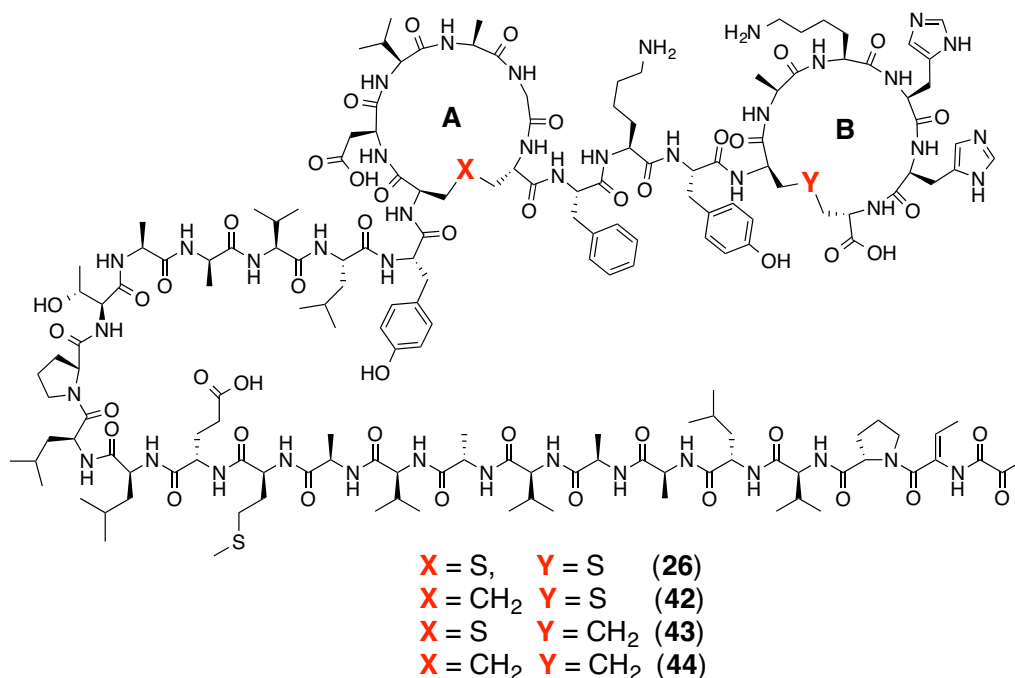


Figure 2.8 – Structure of DAP-substituted lactocin S analogues: A-DAP (42**), B-DAP (**43**), and D-DAP (**44**) lactocin S.⁶⁶**

After antimicrobial testing against sensitive organism *Pediococcus acidilactici* PAC1.0, all DAP-substituted analogues remained biologically active, and A-DAP lactocin S (**42**) showed an enhanced zone of clearing compared to the native lactocin S (**26**) via spot-on-lawn assays.⁶⁶ This represents the first successful substitution of a lanthionine residue in a lantibiotic peptide with retention of full biological activity.

Analogous to the discovery of lanthionine oxidation limiting biological activity of lantibiotic peptides,⁵³ the oxidation of methionine-12 during the initial synthesis of lactocin S was found to abolish its antimicrobial effects.⁶⁷ Dr. Avena Ross and undergraduate research summer student Mr. Michael Little synthesized two novel methionine-substituted analogues. The synthetic incorporation of canonical amino acid leucine, or isosteric homologue norleucine, at position 12, generated Leu12 lactocin S (**45**) and Nle12 lactocin S (**46**), with the native lanthionine sulfur atoms (Figure 2.9).⁶⁷ Biological testing of **45** and **46** yielded a full retention of antimicrobial activity.⁶⁸

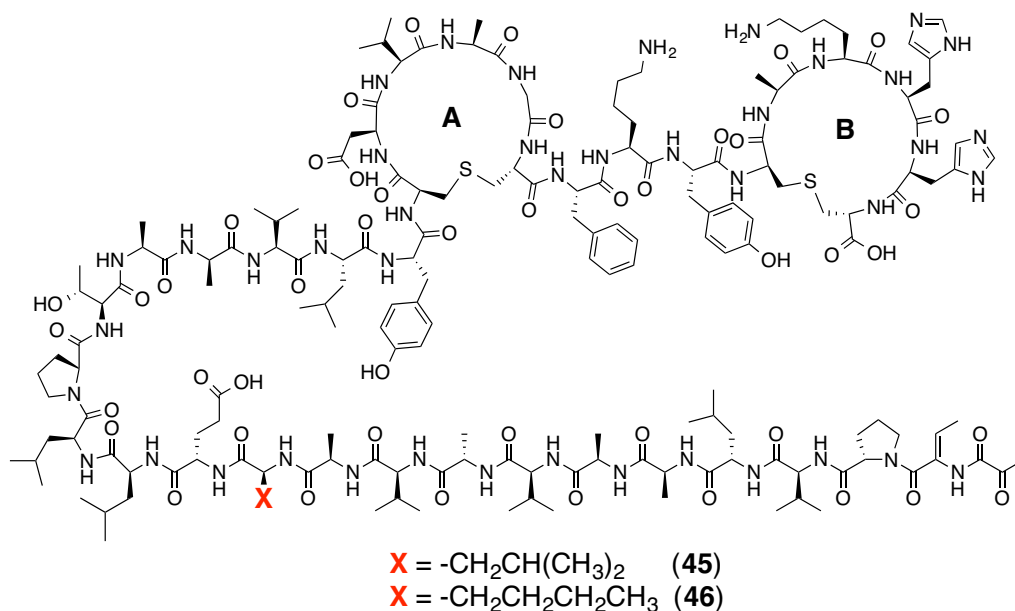


Figure 2.9 - Structure of Met12-substituted lactocin S analogues: Leu12 (45**), and Nle12 (**46**) lactocin S.**^{67,68}

To expand upon these exciting results, the extent of stability to atmospheric oxygen imparted by these sulfur-substitutions remained to be determined. We were also curious to examine the oxidative stability and antimicrobial activity of a lactocin S analogue combining two conservative sulfur atom substitutions at the methionine-12 and A-ring lanthionine positions.

2.2 Results

2.2.1 Oxygen-stability assays of DAP-substituted lactocin S analogues⁶⁶

To assess the stability of previously synthesized lanthionine sulfur-substituted lactocin S analogues, a qualitative assay was developed to assess the *in vitro* stability of these peptides under accelerated oxidation conditions. DAP analogues **42-44** were exposed to a contained environment of pure oxygen gas for increasing time increments up to 6 h and compared to that of native lactocin S (**26**). The remaining antimicrobial activity following oxygen exposure was qualitatively assessed via spot-on-lawn assays against sensitive organism *Pediococcus acidilactici* PAC1.0 (Figure 2.10).

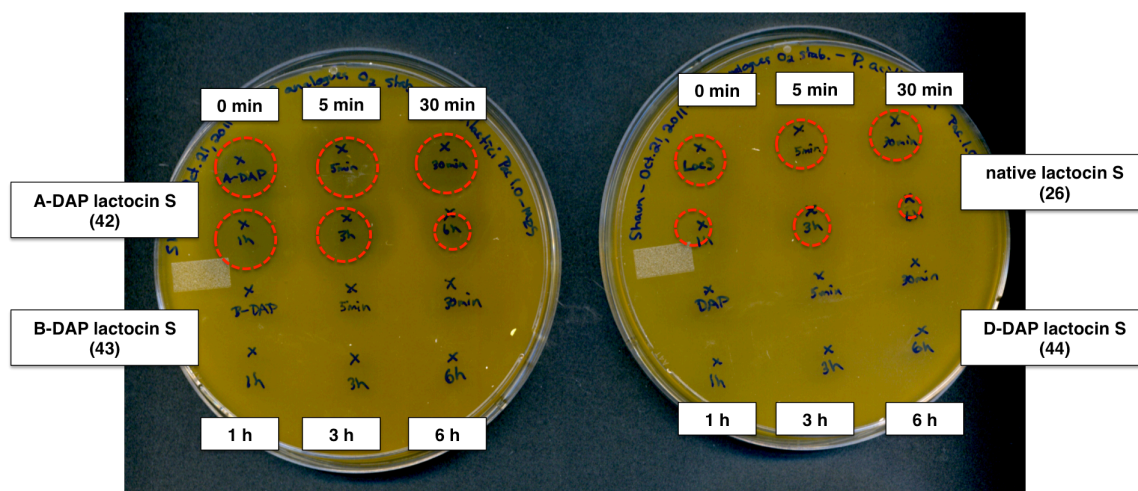


Figure 2.10 – Spot-on-lawn activity testing of 100 μ M lactocin S (26**) and lanthionine-substituted A-DAP (**42**), B-DAP (**43**) or D-DAP (**44**) lactocin S analogues against *Pediococcus acidilactici* PAC1.0 after exposure to oxygen gas for up to 6 h.⁶⁶**

While native lactocin S (**26**) lost virtually all of its antimicrobial activity after 6 h of oxygen exposure, the more potent A-DAP substituted analogue **42** retained its

antimicrobial activity over a longer duration of time. For this assay, the B-ring and D-DAP analogues (**43** and **44**, respectively) showed minimal antimicrobial activity even without exposure to oxygen gas. This was likely due to oxidation at remaining sulfur atoms based on the relative age of peptide solutions. Attempts were made to assess the extent of oxidation by MALDI-TOF analyses but were unfortunately inconclusive. Oxygen exposure times were extended to 24 h, and a small zone of inhibition was still observed for A-DAP lactocin S (**42**). All other DAP analogues and native lactocin S showed no activity against *P. acidilactici* (Figure 2.11).

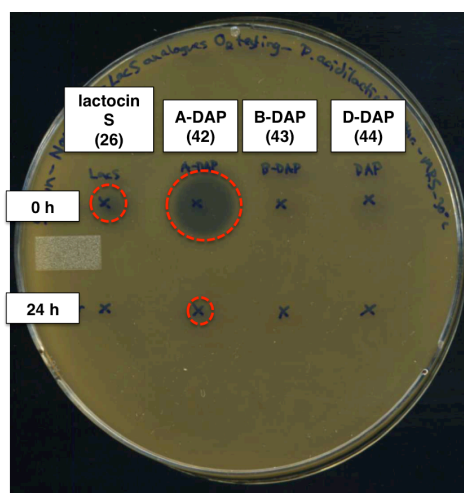


Figure 2.11 – Spot-on-lawn activity testing of 100 μ M lactocin S (26**) and lanthionine-substituted A-DAP (**42**), B-DAP (**43**) or D-DAP (**44**) lactocin S analogues against *Pediococcus acidilactici* PAC1.0 after exposure to oxygen gas for 24 h.**

These oxygen-stability experiments led us to hypothesize that the isosteric replacement of lanthionine in lactocin S ring A was advantageous from a stability perspective. The greater zone of inhibition of **42** compared to native lactocin S (**26**) could be a result of an improved geometric arrangement of the A-ring, but a more likely

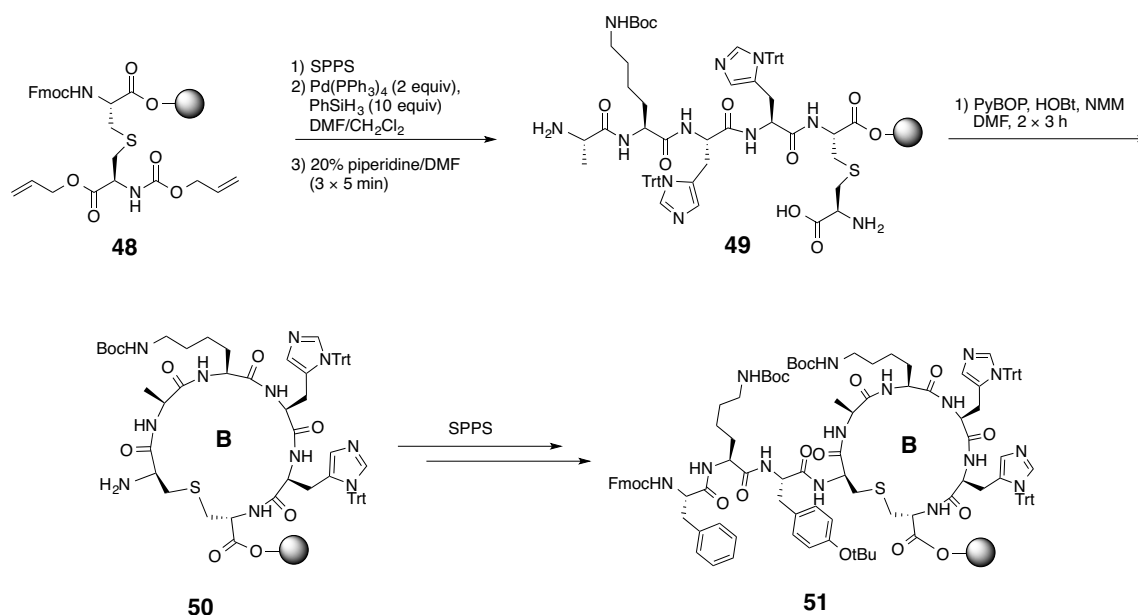
hypothesis is that A-ring lanthionine oxidation is extremely deleterious to physiological activity. By circumventing sulfoxide formation at this position, antimicrobial activity can be retained for prolonged periods of time. However, analogue **42** still lost considerable activity over the 24-hour assay, likely due to the oxidation of one or both of the remaining sulfurs in Met12 or ring B lanthionine. Substitution of DAP in the B-ring of lanthionine for both **43** and **44** qualitatively decreased activity compared to the parent analogue,⁶⁶ and would not be a good model for further analogue development. The B-ring contains three basic amino acids (positively charged at physiological pH) proposed to interact with negatively charged lipids exterior to bacterial cells. A zwitterionic sulfoxide within this ring may not be as deleterious to this electrostatic interaction. Therefore, we hypothesized that Met12 oxidation was likely the result of the diminishing activity of A-DAP and should be the next position to be targeted.

2.2.2 Synthesis of NleDAP-lactocin S (47), a doubly sulfur-substituted lactocin S analogue⁶⁸

Following the successful substitution and antimicrobial activity testing of Nle12 lactocin S⁶⁸ and A-DAP lactocin S,⁶⁶ we wanted to combine both successful modifications into one macromolecule: NleDAP lactocin S (**47**). This would hypothetically enhance oxidative stability to atmospheric oxygen, while retaining the inherent antimicrobial activity of lactocin S.

Orthogonally protected lanthionine was previously prepared by Dr. Avena Ross⁴⁵ according to literature procedure⁵⁶ and was loaded onto 2-chlorotriptyl chloride resin (**48**) at a low molar loading to promote intramolecular cyclization. Subsequent

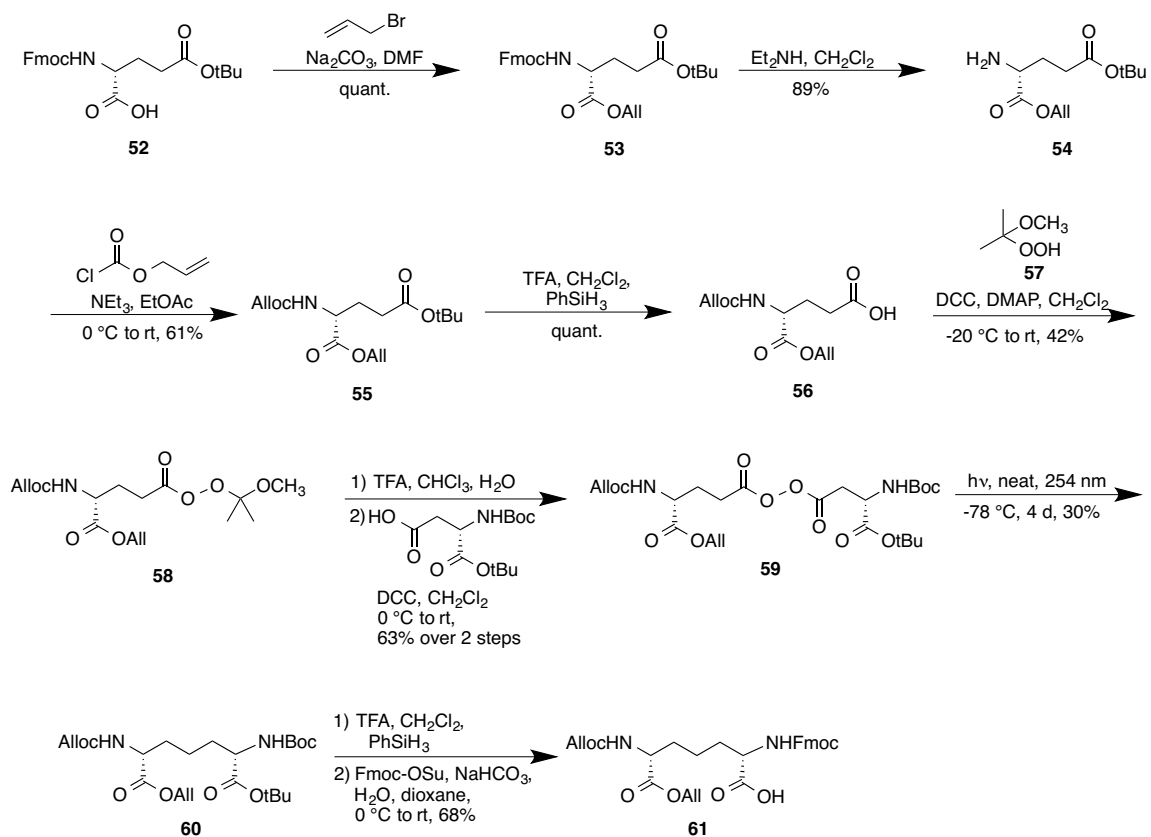
rounds of SPPS were performed to elongate the peptide chain to include all amino acids that would be contained within lanthionine ring B. Pd-catalyzed deprotection of the lanthionine allyl ester and Alloc groups, followed by Fmoc deprotection of the N-terminal alanine moiety generated **49**. The addition of coupling reagents (PyBOP, HOBT, and NMM) in the absence of additional amino acid promoted an on-resin intramolecular cyclization to form **50**. Cyclic hexapeptide **50** was N-terminally extended by an additional three amino acids to give macrocyclic nonapeptide **51** (Scheme 2.3).



Scheme 2.3 – Synthesis of lactocin S B-ring and N-terminal extension to nonapeptide 51.⁶⁸

To incorporate an orthogonally protected diaminopimelic acid derivative in lactocin S ring A, this lanthionine isostere was synthesized with the desired *meso* stereochemistry at the two α -carbons following literature protocol (Scheme 2.4).⁶⁶ Fmoc-D-Glu(tBu)-OH (**52**) was protected as allyl ester **53**, then the Fmoc group was

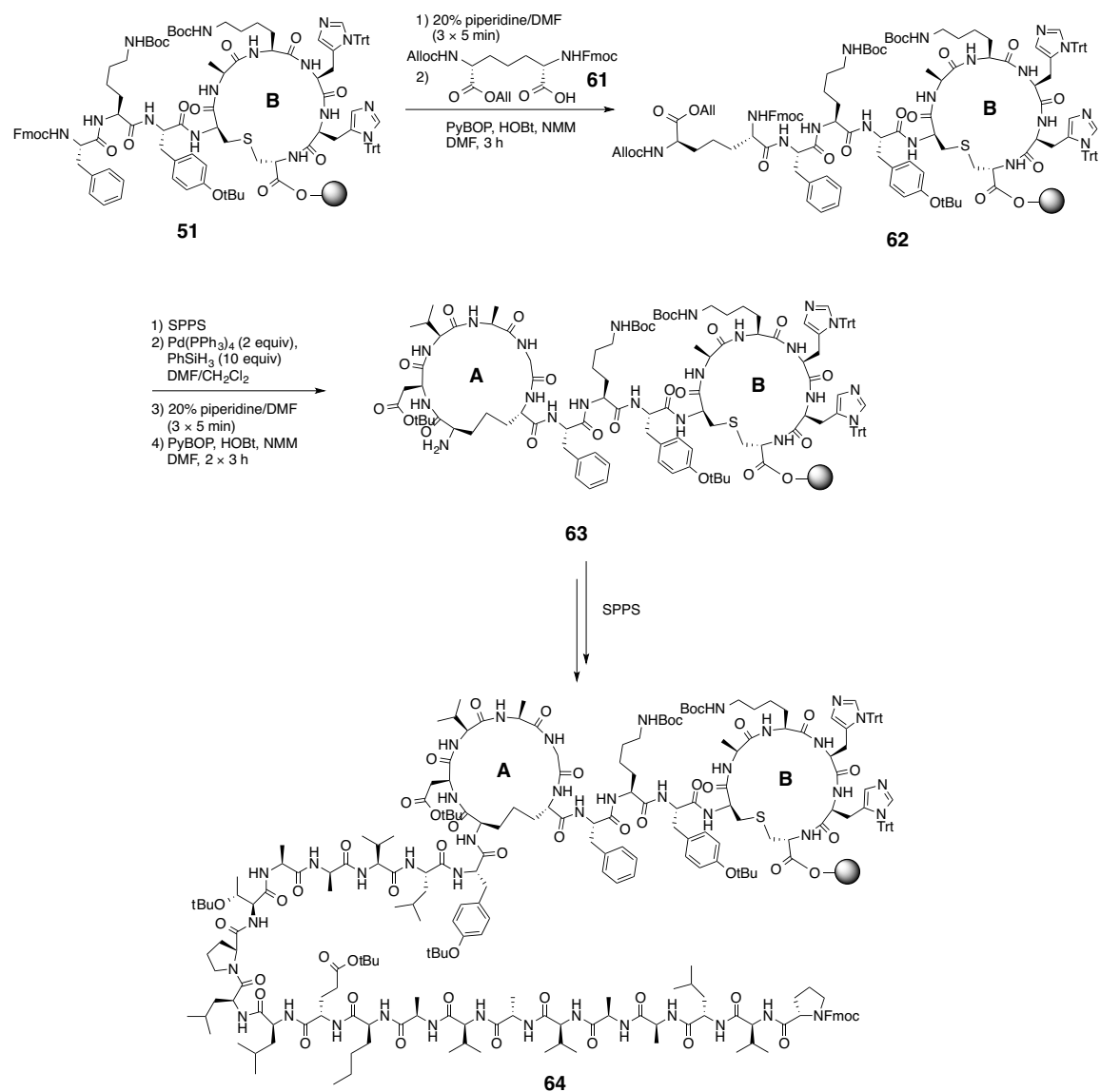
removed in the presence of diethylamine, producing **54** in 89% yield after 2 steps. Alloc protection of the amine generated compound **55**, followed by *tert*-butyl ester deprotection afforded the free acid **56**. The side chain carboxylate was coupled to 2-methoxyprop-2-yl hydroperoxide (**57**), the product of the ozonolysis of 2,3-dimethylbutene in the presence of MeOH, to give perester **58**. After purification by column chromatography, **58** was carefully hydrolyzed in the presence of aqueous TFA to the peracid, then immediately coupled to Boc-L-Asp-OtBu to form stable diacyl peroxide **59**. The UV-induced photolysis of diacyl peroxide **59** was performed at -78 °C under neat conditions for 4 days. Although this reaction was low yielding, took a considerable number of days to go to completion, and could only be performed on less than 500 mg of starting material at a time, it was advantageous in preserving the necessary stereochemistry at both α -carbons.⁶⁹ However, recent developments in the synthesis of orthogonally-protected diaminopimelic acid derivatives are considerably more efficient and amenable to scale up.⁷⁰ DAP derivative **60** had its Boc and *tert*-butyl groups concomitantly deprotected following treatment with TFA in CH₂Cl₂. Following Fmoc-protection of the amino group attached to the (*S*)- α -carbon (formerly from aspartic acid), the desired orthogonally-protected **61** diaminopimelic acid derivative was synthesized.



Scheme 2.4 – Synthesis of orthogonally protected diaminopimelic acid derivative 61.^{66,68}

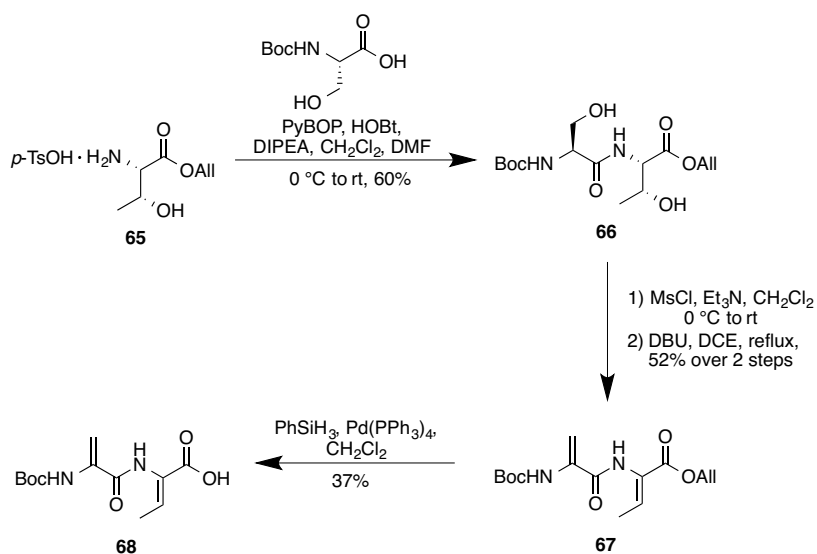
Resin-bound nonapeptide **51** was subsequently Fmoc-deprotected, then coupled to **61** to afford **62**. An analogous strategy to that done for Ring B was performed, where the N-terminus of the peptide chain was elongated by an additional four amino acids: Fmoc-Gly-OH, Fmoc-Ala-OH, Fmoc-Val-OH, and Fmoc-Asp(tBu)-OH, respectively. Macrocyclization of the A-ring of this DAP derivative was achieved by deprotecting the Alloc/All groups and N-terminal Fmoc group, then coupling with PyBOP, HOBt and NMM in the absence of additional amino acid. After bicyclic **63** was generated, additional rounds of SPPS were done to introduce the D-alanine residues at amino acid positions 7, 11 and 19, and to incorporate the advantageous norleucine replacement for

Met12. As the chain was elongated, the very hydrophobic N-terminal region became increasingly difficult to deprotect, sometimes taking up to 5 cycles to remove the N-terminal Fmoc protecting group. However, TFA-induced resin cleavage and MALDI-TOF analysis were performed after every coupling past Nle12 to ensure that the desired peptide was being formed, eventually generating the 35mer **64** (Scheme 2.5).



Scheme 2.5 – Solid-phase peptide synthesis of bicyclic 35-mer **64.**⁶⁸

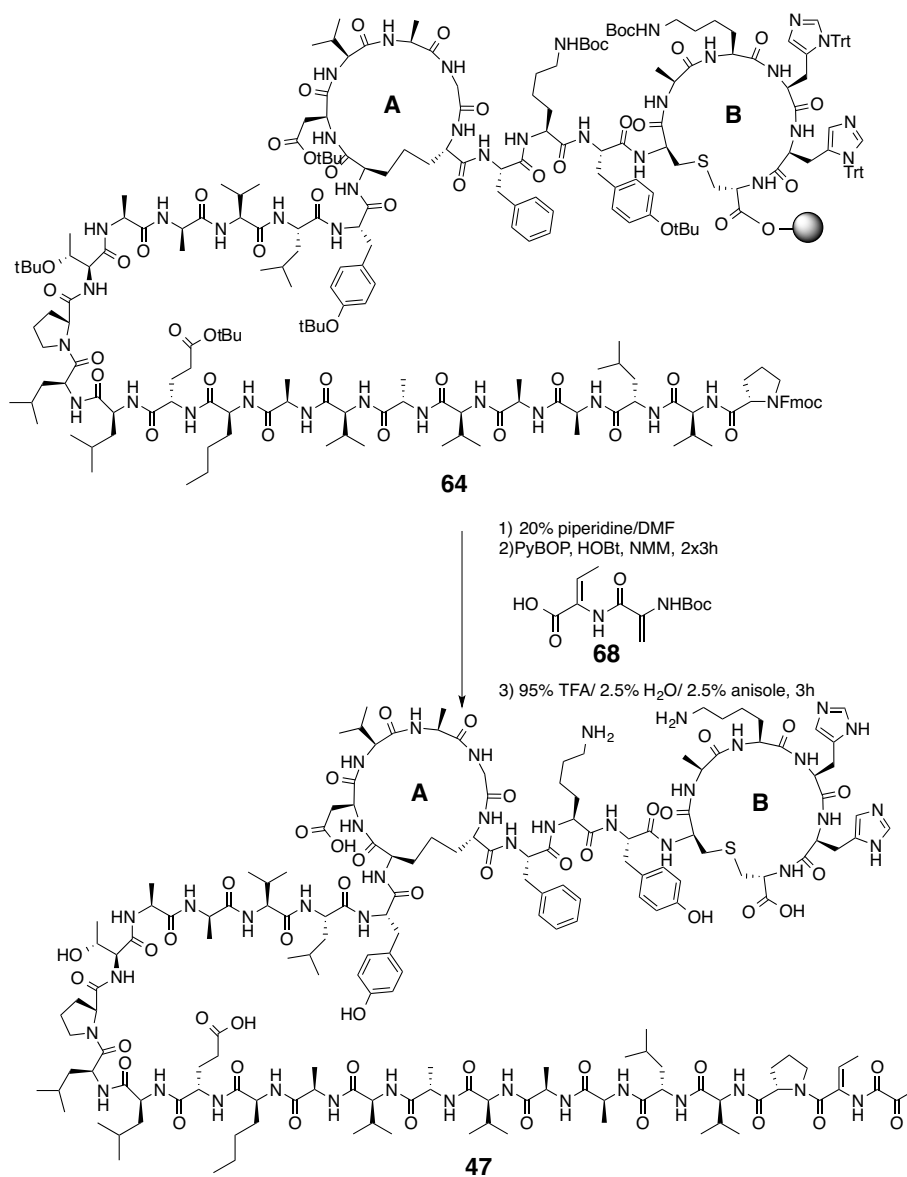
To cap the N-terminus of **64** with the required dehydrobutyryne and α -ketoamide moieties, the di-dehydrated peptide **68** was prepared in solution by a literature procedure.^{45, 66} Briefly, H-Thr-OAll *p*-toluenesulfonate salt (**65**) was coupled to Boc-Ser-OH with PyBOP, HOBT and DIPEA to generate dipeptide **66**. Both side chain hydroxyl groups were mesylated in the presence of methanesulfonyl chloride and triethylamine, and eliminated by DBU in refluxing DCE to afford di-dehydroamino acid **67**. A final deprotection of the allyl ester with Pd(PPh₃)₄ and phenylsilane gave the free acid **68** (Scheme 2.6).



Scheme 2.6 – Synthesis of N-terminal dipeptide **68.**^{45, 66, 68}

Resin bound 35-mer **64** was Fmoc deprotected in the presence of 20% piperidine in DMF, then an activated solution of **68** was added and bubbled under Ar gas for 3 hours. This procedure was repeated one additional time to ensure complete coupling of this dipeptide to the N-terminus of the peptide. Following MALDI-TOF confirmation of the formation of the 37-mer lactocin S derivative, the peptide was

cleaved from resin with a solution of 95:2.5:2.5 TFA:H₂O:anisole under an Ar atmosphere. This concomitantly cleaved the acid-labile side chain protecting groups and formed the desired α -ketoamide moiety at the N-terminus after Boc-deprotection, enamine tautomerization, and imine hydrolysis (Scheme 2.7). To preserve the reduced B-ring lanthionine of **47**, purification via C₂/C₁₈ RP-HPLC took place with the addition of TCEP (1.5 mg/L) to HPLC solvents and fractions were collected under a stream of Ar gas. Double sulfur-substituted lactocin S analogue **47** was obtained in 1.8% yield as a white solid following lyophilization.



Scheme 2.7 – Synthesis of NleDAP-analogue 47.⁶⁸

2.2.3 Activity testing of NleDAP lactocin S (47)⁶⁸

To assess the spectrum of antimicrobial activity of NleDAP lactocin S (**47**), the same panel of organisms previously examined for DAP analogues of lactocin S were assessed.⁶⁶ Analogue **47** showed a similar spectrum of antimicrobial activity to native lactocin S (**26**) via spot-on-lawn assays. Both *Pediococcus acidilactici* PAC1.0 and

Lactobacillus delbrueckii subsp. *bulgaricus* 11842, showed zones of clearing, while lactocin S-insensitive organisms (*L. helveticus* 18009, *L. acidophilus* 4356, and *P. pentosaceus* FBB63) showed no inhibition of growth. Minimum inhibitory concentrations were qualitatively estimated using serial dilution assays, and showed that **47** lost antimicrobial ability against *P. acidilactici* between 50 – 100 μ M and against *L. delbrueckii* subsp. *bulgaricus* between 100 – 200 μ M (Figure 2.12). NleDAP lactocin S (**47**) was also tested against the producing organism *Lactobacillus sakei* L45, and was shown to have no antimicrobial effects. This implies that the changes in structure of **47** were conservative enough to maintain recognition by the innate immunity protein responsible for the protection of *L. sakei* L45 against the action of its own lantibiotic.

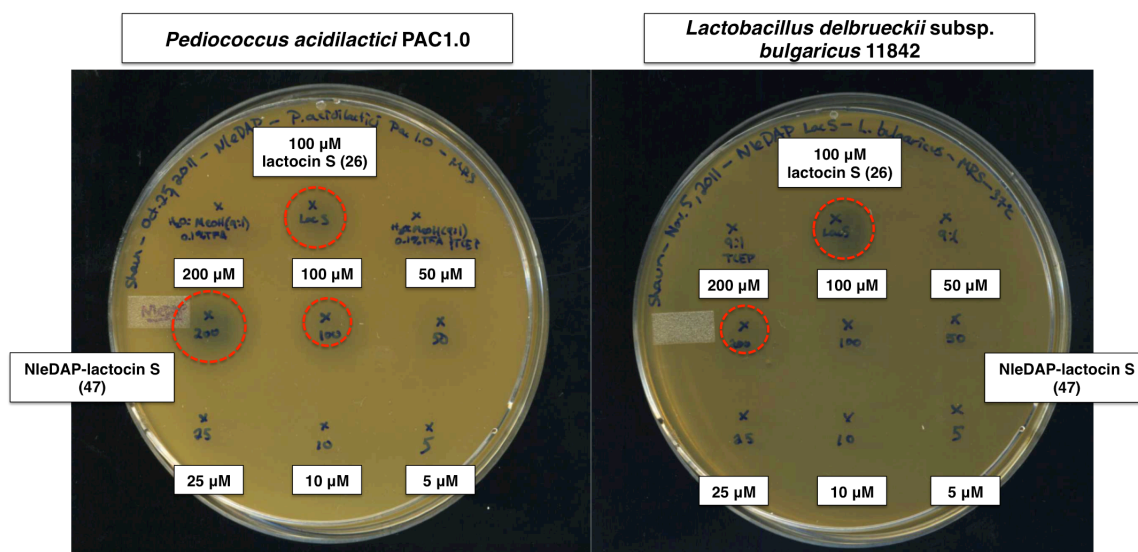


Figure 2.12 - Spot on lawn activity testing of 100 μ M lactocin S (26) and dilutions of NleDAP lactocin S analogue (47) against *Pediococcus acidilactici* PAC1.0 (left) and *Lactobacillus delbrueckii* subsp. *bulgaricus* 11842 (right).⁶⁸

In comparison to single sulfur-substituted analogues A-DAP (**42**), Leu12 (**45**), or Nle12 lactocin S (**46**), **47** showed a reduced potency of antimicrobial activity, especially

towards *L. delbrueckii* subsp. *bulgaricus*. The loss of antimicrobial activity following serial dilution assays between the organisms is highlighted in Table 2.1. However, it was encouraging to see that antimicrobial activity was retained in **47** after two sulfur-substitutions.

Table 2.1 – Loss of antimicrobial activity based on zones of clearing after serial dilutions of lactocin S (26) and sulfur-substituted analogues (42-47).^{66, 68}

Lactocin S Analogue	Sulfur substitution	Loss of antimicrobial activity (μM) (<i>P. acidilactici</i>)	Loss of antimicrobial activity (μM) (<i>L. delbrueckii</i>)
lactocin S (26)	-	10 – 50	10 – 50
A-DAP (42)	A-ring Lan	1 – 10	10 – 50
B-DAP (43)	B-ring Lan	50 – 100	50 – 100
D-DAP (44)	A and B ring Lans	50 – 100	100 – 200
Leu12 (45)	Met12	20 – 50	20 – 50
Nle12 (46)	Met12	20 – 50	20 – 50
NleDAP (47)	Met12 and A-ring Lan	50 – 100	100 – 200

2.2.4 Oxygen-stability testing of Met12-substituted lactocin S analogues⁶⁸

Analogues of lactocin S with Met12 substitutions (**45-47**) were exposed to an atmosphere of pure oxygen for 6 h and 24 h, and then assessed for antimicrobial activity against the two previously analyzed sensitive organisms (Figure 2.13). While the antimicrobial activity of lactocin S (**26**) was completely abolished after 24 h of oxygen exposure, all three methionine substituted analogues retained antimicrobial activity after this time. This validated the initial hypothesis that Met12 oxidation is the most deleterious to the inherent antimicrobial activity of lactocin S. Parent analogue **46** was considerably more potent against both bacterial strains than doubly sulfur-substituted **47**.

However, the observed zone of clearing did decrease over the 6 and 24 h oxygen exposure, indicating that A-ring DAP oxidation plays a role in the lessening of activity. While 47 showed a smaller zone of clearing, its activity was largely retained throughout oxygen exposure, accomplishing our initial goal of stabilizing the antimicrobial activity of lactocin S to the presence of oxygen gas.

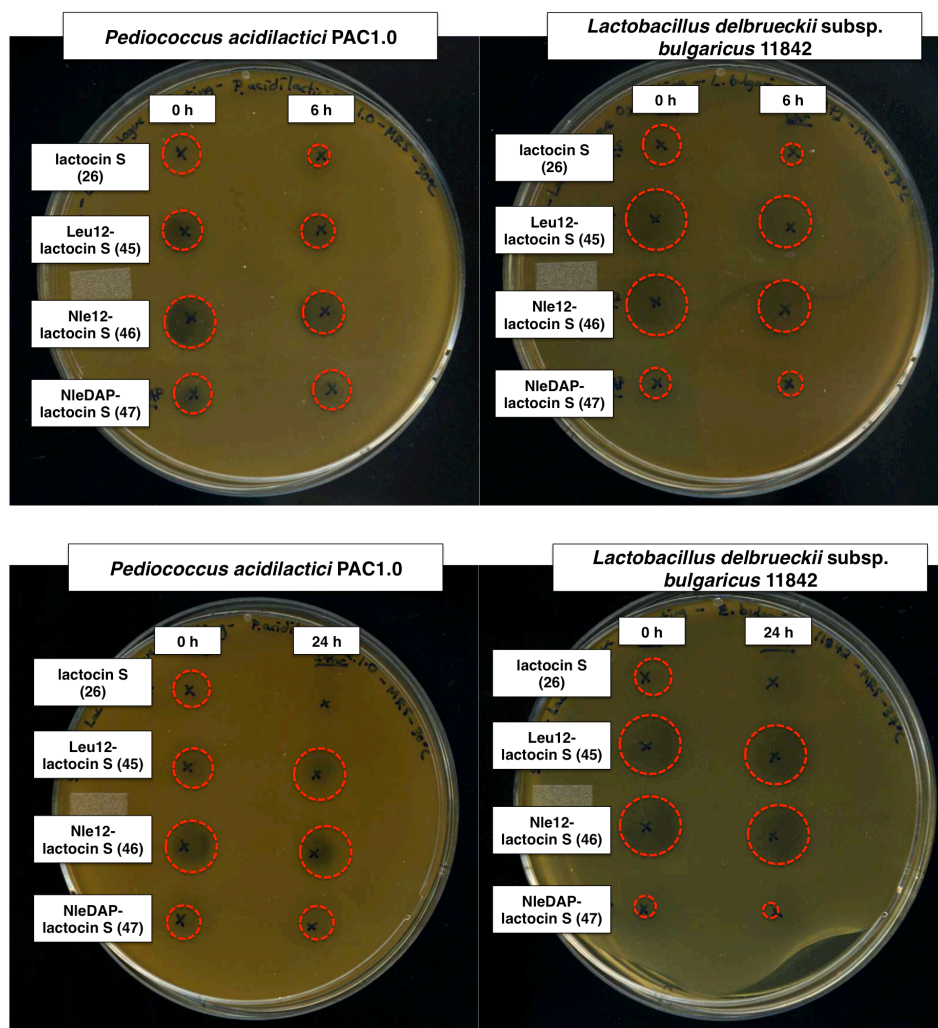


Figure 2.13 –Spot-on-lawn activity testing of 100 μ M lactocin S (26), methionine-substituted Leu12 (45), and Nle12 (46) lactocin S, and double substituted NleDAP lactocin S (47) against *Pediococcus acidilactici* PAC1.0 (left) and *Lactobacillus delbrueckii* subsp. *bulgaricus* 11842 (right) after exposure to oxygen gas for 6 h (top) or 24 h (bottom).⁶⁸

2.3 Conclusions and future directions

In this chapter, an assessment of the antimicrobial activity of five single sulfur-substituted analogues of lactocin S was performed. These experiments showed that the isosteric replacement of lanthionine or methionine amino acid residues results in a conservation of antimicrobial activity while enhancing the oxidative stability of these peptides. A double sulfur-substituted analogue, NleDAP lactocin S (**47**) was synthesized via solid-phase peptide synthesis after the preparation of orthogonally protected diaminopimelic acid **61** and di-dehydro dipeptide **68** in solution. Analogue **47** was found to retain antimicrobial activity, albeit slightly reduced, yet showed a minimal decrease in activity after 24 h of exposure to accelerated oxidation conditions.

This project serves as a good ‘proof-of-principle’ that isosteric sulfur-substitutions can be used to improve the stability of susceptible amino acids within the framework of lantibiotic peptides. Although the cellular machinery does not currently exist to incorporate DAP molecules into lantibiotic backbones through an analogous ‘lanthionine-forming’ mechanism, methionine substitution is achievable through site-directed mutagenesis. The substitution of methionine-12 with canonical amino acid leucine (**45**) generated a particularly potent analogue, which could lead to the preparation of more durable lantibiotic peptides for commercial or industrial applications.

3 Apelin

3.1 Introduction

3.1.1 Apelin structure and processing

Apelin is a recently discovered peptide hormone⁷¹ shown to have a wide variety of effects in human physiology, including roles in cardiovascular regulation, body fluid homeostasis, and the adipoinular axis.^{72,73} Beginning from a 77-amino acid precursor prepropeptide, apelin gets processed into three main isoforms: apelin-36, apelin-17, and pyr-1-apelin-13 (Figure 3.1). These peptides have different distributions in different organ systems, with pyr-1-apelin-13 being the dominant isoform in the cardiovascular system.⁷⁴ Although there is still considerable work needed to understand apelin prepropeptide processing and secretion, a recent report has identified proprotein convertase subtilisin kexin 3 (PCSK3 or furin) preferentially cleaves proapelin directly to apelin-13.⁷⁵ All three dominant isoforms share an identical C-terminus, and the C-terminal 23 amino acids of the prepropeptide are also conserved among all mammals. Comparing the remainder of the native apelin prepropeptide sequence, there is over 90% sequence identity across mammalian apelins.⁷⁶

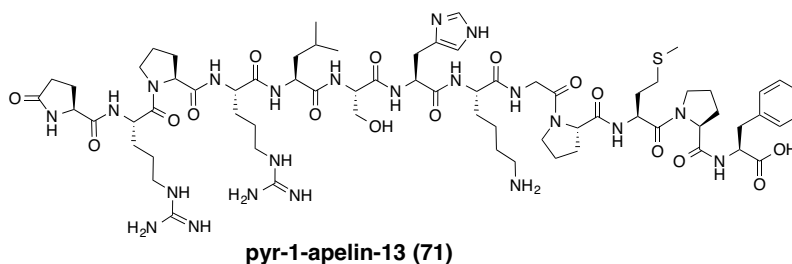
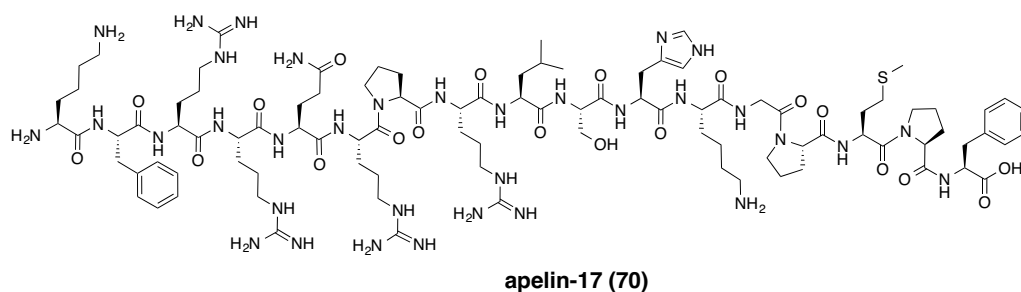
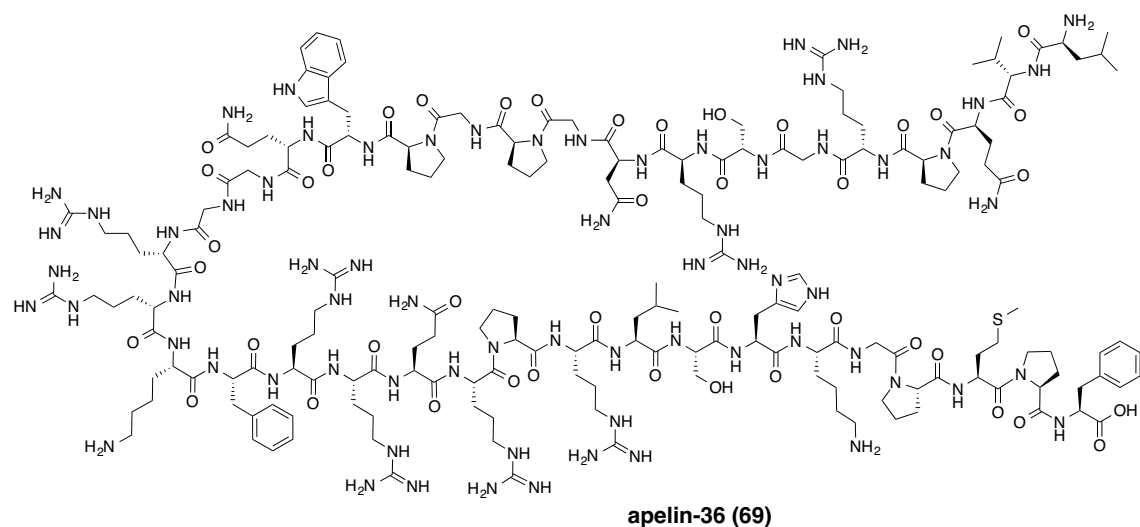


Figure 3.1 – Structures and sequences of native isoforms of apelin.

To analyze the secondary structure of apelin peptides in aqueous solutions, circular dichroism (CD) studies were performed on all isoforms at 5 °C and 35 °C.⁷⁷ Analysis at both temperatures indicated that all isoforms largely adopt a random coil

orientation in solution, with some but not all elements of polyproline-II (PP_{II}) helix structures.⁷⁷ The authors also propose some conformational restriction surrounding the C-terminal phenylalanine based on the CD spectra.

A more thorough structural investigation was also conducted via NMR spectroscopy at 5 °C and 35 °C.⁷⁷ Analogous to the CD studies, the effect of temperature on the amide backbone was negligible. The major structural analysis was performed on apelin-17, and two distinct conformations of apelin were found via *cis-trans* isomerization surrounding the C-terminal G13-F17 region. The majority of the structure showed a random coil distribution of signals, corroborating the circular dichroism findings. However, pockets of well-defined structure were observed in the 'RPRL' region (R6-L9) and between P14-F17. These two regions showed an increased abundance for polyproline-II type helix and type IV β -turn motifs, and are believed to be the most significant for inducing apelin conformations.

3.1.2 Apelin receptor interactions

The discovery of apelin as a physiologically active peptide hormone was made after the initial discovery of the apelin receptor (APJ) in 1993.⁷⁸ This G-protein coupled receptor (GPCR) was identified due to its high sequence homology to the angiotensin II receptor type 1, yet showed no physiological response in the presence of angiotensin II.⁷⁸ Five years later, the receptor was deorphanized by the discovery of an endogenous ligand, apelin-36, from bovine colostrum extracts.⁷¹ The apelin receptor is a type A rhodopsin-like GPCR composed of the characteristic seven transmembrane helices, and is subdivided into the same subfamily alongside both angiotensin II receptors type 1 and

2, and bradykinin receptors B1 and B2 based on sequence homology. It is interesting to note that both bradykinin and angiotensin II are also cardiovascular peptide hormones.

Classical GPCR activation by an extracellular ligand results in a structural reorganization of the seven transmembrane helices, leading to downstream effects inside of the cell mediated by a heterotrimeric ($\alpha\beta\gamma$) G-protein; the four different classes of α subunits differentiate the corresponding physiological effects. The apelin receptor primarily associates with the $G\alpha_{i/o}$ subfamily,⁷⁹ although signaling through the $G\alpha_{q/11}$ subunit has also been reported in different cell lines.⁸⁰ $G\alpha_{i/o}$ activation by apelin leads to the inhibition of intracellular cyclic AMP and causes phosphorylation of ERK (extracellular signal-regulated kinases) and Akt (protein kinase B) kinases (Figure 3.2 A).⁷⁹ Akt phosphorylation activates eNOS,⁸¹ which in turn generates nitric oxide and promotes vasodilation. The apelin signaling pathway is known to go through this enzyme based on inhibition experiments.⁸² $G\alpha_{q/11}$ activation leads to many similar physiological effects, beginning with the phosphorylation of PLC β . This phosphorylation leads to an influx of cytosolic calcium ions, and increase in activity of calmodulin, which can also activate eNOS-induced vasodilation (Figure 3.2 B). The apelin receptor is also known to participate in the β -arrestin pathway with subsequent endosomal internalization,^{83,84} leading to activation of ERK (Figure 3.2 C).⁸⁵ This endocytosis is via a clatherin-mediated mechanism,⁸⁶ and β -arrestin activation has been hypothesized to play a role in ‘biased agonism’ at GPCRs, influencing particular pathways over others.^{87,88} Although this represents a dramatic simplification of the complexity associated with GPCR signal transduction, a basic understanding will help to explain the diverse physiological effects of apelin and its isoforms in mammals.

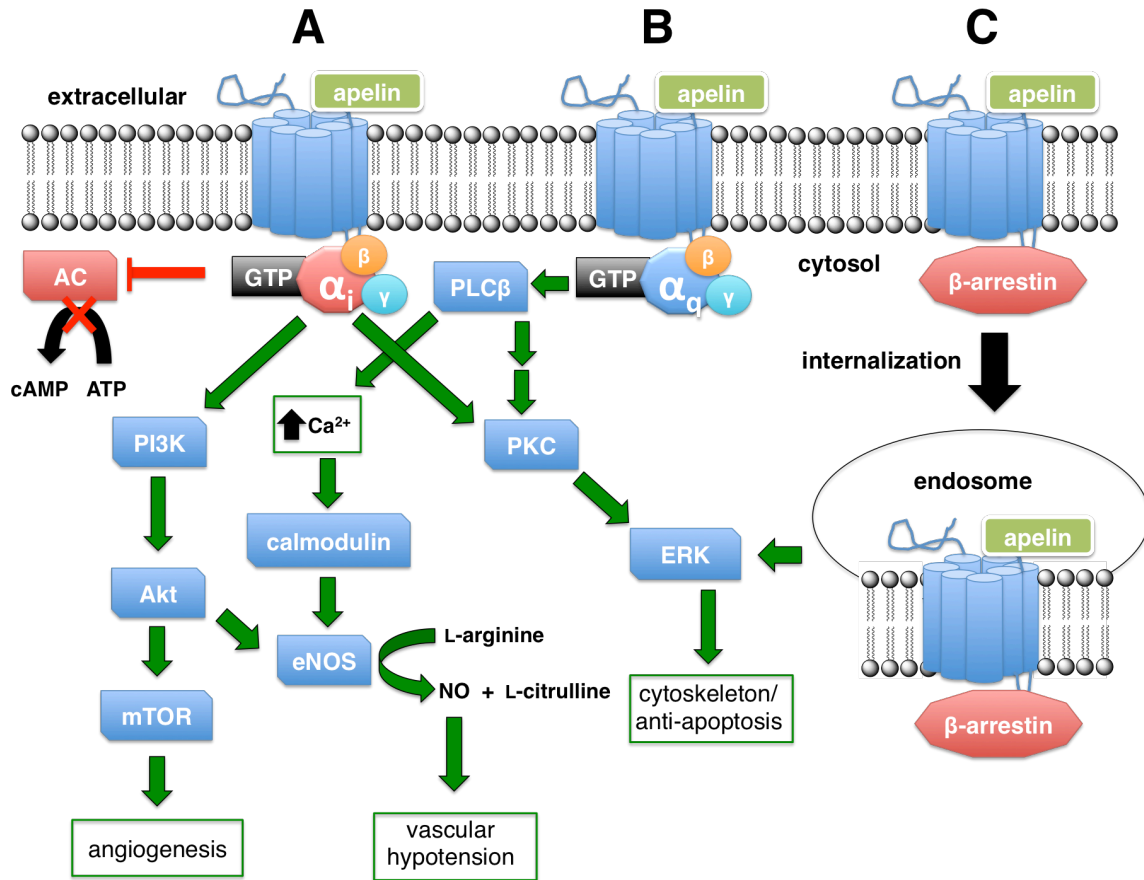


Figure 3.2 – Key signaling pathways activated by apelin-APJ interactions. A) $G_{\alpha_{i/o}}$ activation leading to downstream activation of mTOR and eNOS and the inhibition of AC; B) $G_{\alpha_{q/11}}$ activation leading to an increase in intracellular calcium concentration and subsequent activation of eNOS and ERK pathways; C) β -arrestin mediated internalization of the apelin receptor, leading to the activation of ERK pathway. AC = adenylate cyclase, cAMP = cyclic adenosine monophosphate, ATP = adenosine triphosphate, GTP = guanosine triphosphate, PI3K = phosphoinositol 3-kinase, Akt = protein kinase B, mTOR = mechanistic/mammalian target of rapamycin, eNOS = endothelial nitric oxide synthase, NO = nitric oxide, PLC β = phospholipase C- β , PKC = protein kinase C, ERK = extracellular signal-regulated kinase. Figure modified from Chapman *et al.*⁸⁹ and Kalea *et al.*⁸⁵

The human apelin receptor still remains to have its crystal structure solved, making definitive ligand-receptor interactions elusive. Three unique apelin receptor models have been constructed based on common GPCR scaffolds and have been examined for key interactions between the substrate and receptor.⁹⁰ These models

indicate that substrate interactions with the apelin receptor are strongly electrostatic, with key interactions proposed between Arg2, Arg4, and Lys8 of apelin-13 with acidic amino acids in the extracellular region of the receptor. However these negatively charged receptor amino acids vary depending on the GPCR backbone selected. To experimentally determine the significance of these acidic residues, alanine mutants of the rat apelin receptor were generated via site-directed mutagenesis. Asp92, Glu172, and Asp282 alanine mutants showed dramatically reduced apelin binding and reduced internalization upon exposure to pyr-1-apelin-13. This activity could be restored with the apelin receptor mutation to the corresponding amide isostere in Asp92Asn or Glu172Gln. However Asp282Asn showed neither binding nor *in vitro* activity in the presence of pyr-1-apelin-13, highlighting the essential nature of electrostatic attraction of the aspartic acid at this position of the receptor.⁹⁰ The significance of these electrostatic interactions are supported by the NMR-solution structure of the first transmembrane segment of the apelin receptor in DPC micelles and subsequent molecular dynamics simulations.⁹¹

Another key interaction proposed from modeling experiments involves the C-terminal phenylalanine of apelin interacting in a hydrophobic aromatic pocket of the apelin receptor.⁹² This interaction had previously been observed in the homologous angiotensin II-AT₁ receptor system.⁹³ Apelin receptor amino acids Trp154, Phe257 and Trp261 form a pocket which anchors the ligand through π - π stacking interactions. Site-directed mutagenesis experiments mutated Phe255 and Trp259 of the rat apelin receptor to non-aromatic amino acids. These mutations abolished the ability of the apelin receptor to be internalized, but showed only small deviations from native ligand binding

and forskolin-induced cAMP inhibition. Truncation^{86,92} or alanine-substitution⁹⁴ of this C-terminal phenylalanine residue in apelin showed a similar effect; analogue binding to wild-type apelin receptors and inhibition of cAMP was not disturbed but receptor internalization did not occur. Additional investigations into [Phe13Ala]-substituted ppy-1-apelin-13 analogues showed a dose-dependent inhibition of key physiological effects attributed to the apelinergic system, behaving as a functional antagonist.⁹⁴ In combination, these studies conclude that the C-terminal phenylalanine residue is critical for the full physiological effects of apelin.

Rainey and coworkers have suggested that a conformational switching occurs in which apelin peptides initially bind to the apelin receptor, then undergo a structural isomerization putatively in the C-terminal PMPF region.⁷⁷ This two-step mode of binding then activation has been observed before for other ligand-receptor interactions for class A chemokine⁹⁵ and class B GPCRs⁹⁶ and correlates well with current experimental evidence.

3.1.3 Physiological effects of the apelinergic system

Apelin mRNA has been found to be upregulated in a wide variety of vascular compartments of many organ systems in the human body,⁹⁷ including the central nervous system, heart, lung, placenta, liver, kidneys, spleen and stomach.^{98,99,100} Due to its diverse tissue distribution, apelin has a wide variety of physiological roles and has been implicated in body fluid regulation,^{101,102} energy metabolism,^{103,104} diabetes,^{105,106,107} and the inhibition of HIV infection.^{108,109} However, the remainder of this section, and our interest in this project will focus solely on the role of the apelinergic system in the cardiovascular system.^{85,89}

One of the dominant physiological effects of apelin-receptor interactions involves the decrease in mean arterial blood pressure (MABP), which has been shown in both rats^{98,110} and humans^{111,112,113} through a NO-mediated pathway.¹¹¹ A direct correlation has been established between apelin receptor internalization and the induction of hypotensive activity.⁸⁶ Clinical investigations have taken place *in vivo* in human patients suffering from heart failure, and have shown an increased cardiac output when supplied with exogenous apelin.^{111,112,113} The pyr-1-apelin-13 and apelin-36 isoforms of apelin elicited a comparable physiological response; however, the duration of activity varied between the two. Pyr-1-apelin-13 showed a dose-dependent response that was reproducible after a ‘washout’ period, implying a more transient apelin-receptor interaction.¹¹¹ The introduction of apelin-36 generated a durable response that was not recapitulated following this washout, implying a different pharmacodynamic interaction between APJ and the two apelin isoforms.¹¹¹

Apelin also shows anti-apoptotic effects in glucose-starved cardiomyocytes.¹¹⁴ This effect has been attributed to the prevention of injury associated with a period of ischemia post-myocardial infarction.¹¹⁵ The prevention of oxygen-deprived heart cells from triggering apoptosis following a traumatic event such as a heart attack (myocardial infarction), would contribute greatly to cardiac viability, and patient survival. Apelin is also an extremely potent inotropic agent, improving cardiac contractility in both isolated cardiac tissue from rats⁸⁰ and humans⁷⁴ in the picomolar range.

Through the activation of the mTOR pathway, apelin-APJ interactions have also been shown to induce angiogenesis.¹¹⁶ In terms of cardiovascular health, the proliferation of new blood vessels is beneficial for applications in the treatment of heart

disease, particularly after traumatic heart events. However, increased angiogenesis is often negatively associated with the proliferation of cancer. Apelin and its receptor are upregulated in select colon cancers, and have been shown to inhibit apoptosis in these carcinomas.¹¹⁷ Interestingly, the application of functional apelin receptor antagonist [Phe13Ala]-pyr-1-apelin-13 analogue was shown to minimize tumor growth.¹¹⁷

3.1.4 Structure-activity relationship of apelin

With the recent discovery of apelin as an important physiological agent, it has become a target for optimization by a variety of research groups as it represents a promising subject for therapeutic development. Structure-activity relationship studies have been done in an effort to better understand the critical residues for apelin's broad biological activity.⁷³

Two unique alanine-scans have been performed on pyr-1-apelin-13 to determine critical amino acids for apelin receptor binding and biological activity.^{98,109} Although some slight discrepancies exist, they both arrive at the same conclusions that the RPRL motif of pyr-1-apelin-13 is essential for binding and physiological activity (Figure 3.3). It was interesting to note that [His7Ala]-pyr-1-apelin-13 generated an analogue with improved binding and greater physiological activity in both experiments. As well, both studies found that alanine substitution of either of the two arginine amino acids (Arg2, Arg4) dramatically decreased binding to the apelin receptor, but had a range of effects on the downstream signaling abilities, including an increase in intracellular Ca^{2+} .^{98,109}

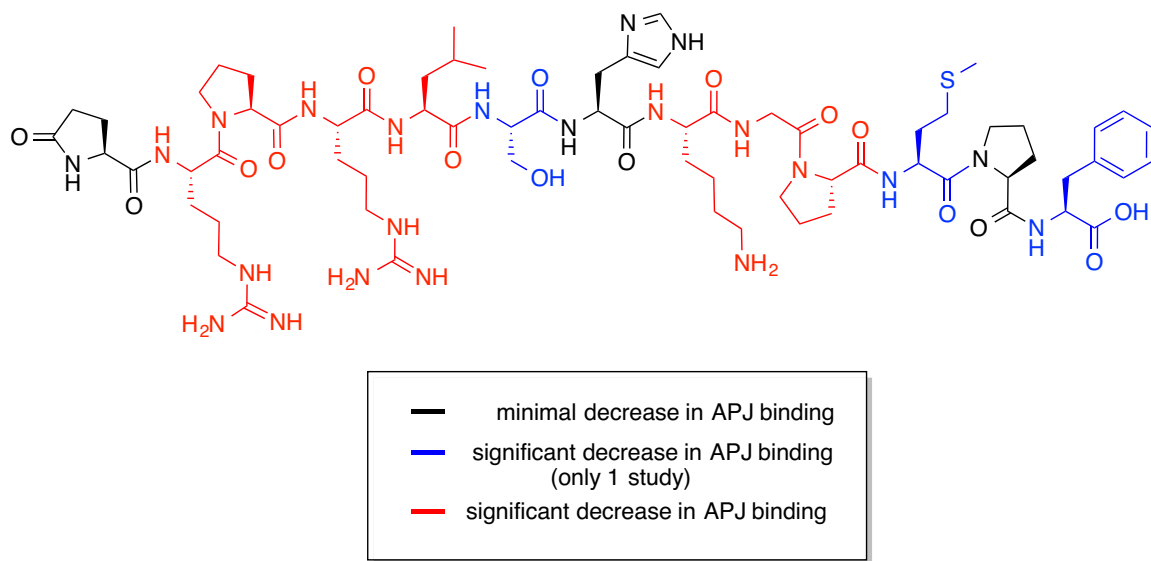


Figure 3.3 – Alanine-scan data for pyr-1-apelin-13 (71) based on decreased binding to the apelin receptor (APJ).^{98,109}

The replacement of each amino acid with its enantiomeric D-amino acid helps to identify regions of critical structure for the binding or activity of a peptide. None of the D-amino acid substitutions improved ligand binding to the receptor based on IC_{50} inhibition of radiolabelled apelin binding.¹¹⁸ The most detrimental epimerizations were observed in the N-terminal ‘RPRLS’ region of pyr-1-apelin-13 and at Pro10 (Figure 3.4).¹¹⁸ This result supports the hypothesis that these two regions of the peptide possess a more defined structure that is critical for receptor interactions.⁷⁷

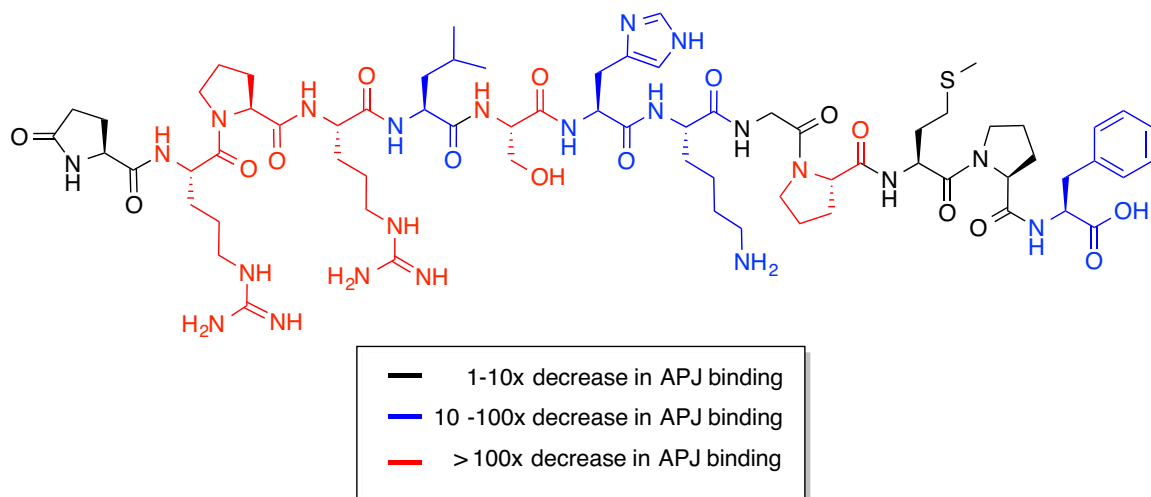


Figure 3.4 – D-amino acid scan data for pyr-1-apelin-13 (71) based on decreased binding to the apelin receptor (APJ).¹¹⁸

Truncation analyses have also been done on pyr-1-apelin-13 and apelin-17 isoforms to determine critical residues binding and physiological activity.^{86,98} Medhurst *et al.* eliminated N-terminal regions of the peptide, generating acetylated 5-13 and acetylated 8-13 fragments. Both truncated peptides showed a substantially reduced affinity for APJ and minimal biological activity.⁹⁸ El Messari *et al.* took a more systematic approach by sequentially deleting individual amino acids from the N-terminus of pyr-1-apelin-13 and the C-terminus of apelin-17.⁸⁶ The authors monitored receptor binding, receptor internalization, and cAMP production in stable cell lines in addition to blood pressure changes in anesthetized rats. The removal of pyroglutamic acid generated an equipotent apelin analogue to pyr-1-apelin-13, but additional elimination of Arg2 abolished receptor binding and physiological activity.⁸⁶ Sequential C-terminal truncation of apelin-17, removing Phe17 (K16P), Pro16Phe17 (K15M), and Met15Pro16Phe17 (K14P), showed comparable binding and inhibition of cAMP production to native apelin-17.⁸⁶ This implies that these 3 C-terminal amino acids are not critical for $G\alpha_{i/o}$

phenyl moiety of Phe13 with benzophenone (**74**) showed an improvement in the inhibition of cAMP 30-fold. Replacement of Phe13 with Tyr(OBn) (**75**) improved binding 60-fold and exhibited stronger hypotensive effects in anesthetized rats than the native peptide (Figure 3.6). This pharmacodynamic ‘fine-tuning’ of apelin-receptor interactions represents an interesting approach to creating ‘biased analogues’ for the selective activation of particular GPCR pathways.

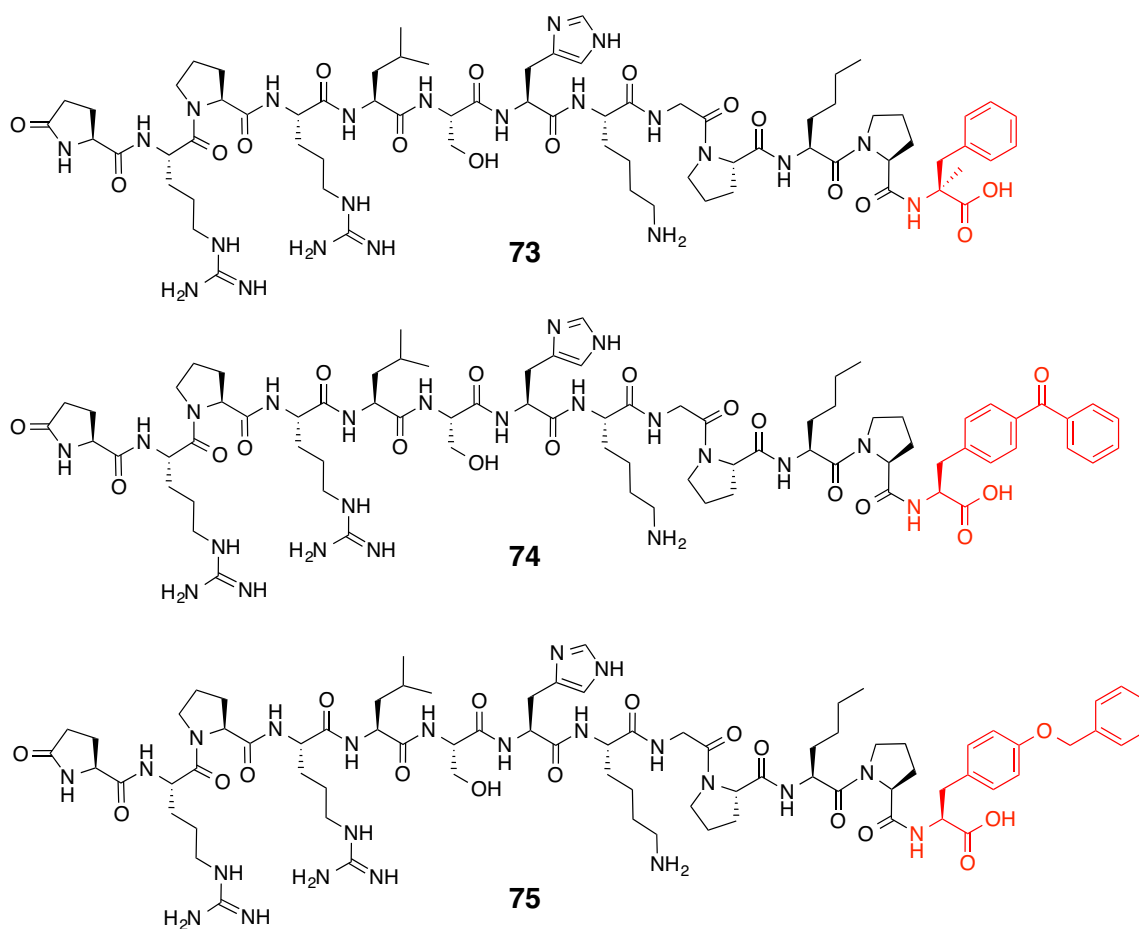


Figure 3.6 – Phe13-substituted pyr-1-apelin-13 analogues 73 -75.¹²³

3.2 Role of angiotensin converting enzyme 2

3.2.1 Introduction to angiotensin converting enzyme 2

One of the major limitations of peptides as therapeutics is their susceptibility to proteolytic degradation. To date, only one protease has been implicated in the degradation of apelin in the cardiovascular system: angiotensin converting enzyme 2 (ACE2).¹²⁴ ACE2 is an important regulatory enzyme in terms of cardiovascular function,¹²⁵ with its primary *in vivo* activity involving the degradation of angiotensin II (78) to angiotensin 1-7 (79). However, this enzyme has many other peptide substrates, including opioid peptides, the vasoactive des-Arg9-bradykinin, and all isoforms of apelin.¹²⁴

ACE2, a zinc-dependent monocarboxypeptidase, has a high specificity for the hydrolysis of phenylalanine from the conserved C-terminal proline-phenylalanine end of these peptides. However this enzyme specificity is not universal, as ACE2 can remove the C-terminal residues from neurotensin 1-8 (pELYENKPR), dynorphin A (YGGFLRRIRPKLK) and β -casomorphin (YPFVEPI) *in vitro* with high catalytic efficiency.¹²⁴ After proteolysis, ACE2 does not degrade these peptide fragments further, suggesting a highly regulated specificity of cleavage.

The physiological relevance of ACE2 hydrolysis in the angiotensin system has been heavily studied since the discovery of this enzyme. While decapeptide angiotensin I (77) is cleaved *in vitro* by ACE2 to angiotensin 1-9,¹²⁴ the catalysis of octapeptide angiotensin II to angiotensin 1-7 is catalytically 1000 times faster.¹²⁶ Angiotensin I (77) has also been shown to inhibit the activity of ACE2 *in vitro* with a modest K_I of 2.2 μ M.¹²⁷ The proteolysis of angiotensin II (78) has been shown *in vivo* to be relevant,

truncating the potent vasoconstrictor to peptide **79**, which has been shown to have vasodilation effects.¹²⁸ The inhibition of ACE2 in the angiotensin system has been shown to have detrimental effects, mostly due to the accumulation of angiotensin II.¹²⁵ However, a thorough investigation into the role of ACE2 on the apelinergic system had yet to be performed, and was recently investigated by our collaborators Dr. Gavin Oudit and Mr. Wang Wang (University of Alberta, Department of Medicine, Division of Cardiology).

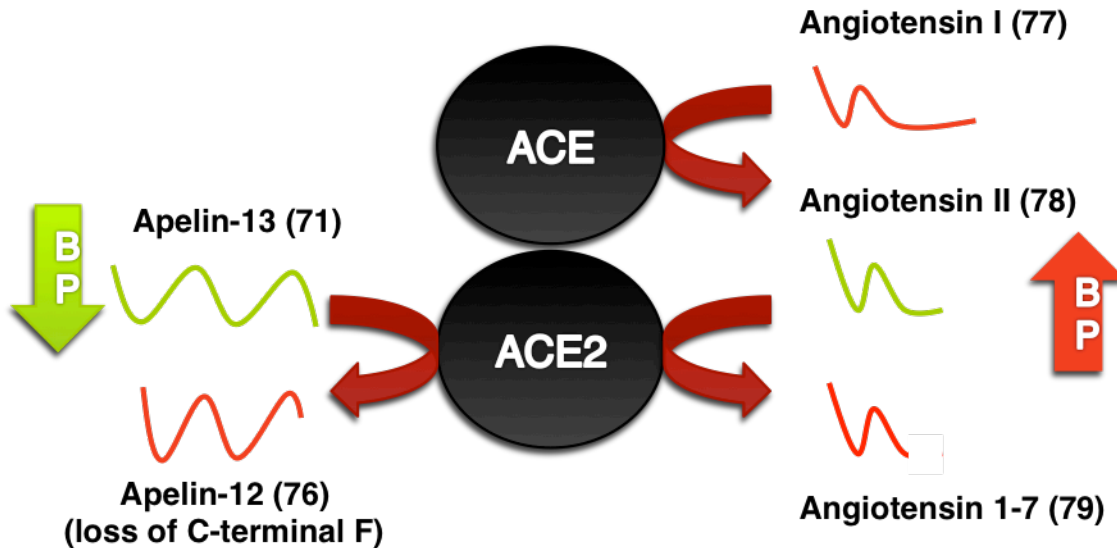


Figure 3.7 – Hydrolysis of angiotensin II and apelin-13 by ACE2 and the relative effect on blood pressure in the cardiovascular system.

The relevance of ACE2 in the apelinergic system has been suggested due to the reduction of physiological activity of C-terminally truncated or substituted phenylalanine analogues. Analogues lacking this critical phenylalanine residue show no diminished ability to bind to the receptor⁹⁸ or activate ‘surface-level’ GPCR pathways.¹²⁹ However, truncation or substitution of phenylalanine prevents receptor internalization via the β -

arrestin pathway and a host of downstream effects essential for the full activation of the apelinergic system.^{92,94}

Recently performed experiments have been completed by the Oudit lab designed to support the physiological relevance of ACE2 as an important apelin regulatory enzyme and in the cardiovascular system.¹³⁰ Physiological experiments have been performed on pyr-1-apelin-13 (**71**), apelin-17 (**70**), and their truncated des-phenylalanine variants pyr-1-apelin-12 (**76**) and apelin-16 (**80**). Results obtained show that the products of ACE2 proteolysis (**76**, **80**) have a diminished capacity to induce NO-mediated vasodilation (Figure 3.8 A) and have no ability to alleviate myocardial ischemic reperfusion injury post-infarction (Figure 3.8 B/C).¹³⁰ Apelin-16 (**80**) had previously been shown to have a diminished ability to induce both NO-mediated hypotension in mice and receptor internalization in cell cultures.⁸⁶ To further emphasize the physiological significance of ACE2, this enzyme was genetically knocked-out (ACE2-KO) in select mice. A heightened and prolonged hypotensive response was observed after the injection of pyr-1-apelin-13 and apelin-17 for ACE2-KO mice (Figure 3.8 D/E).¹³⁰

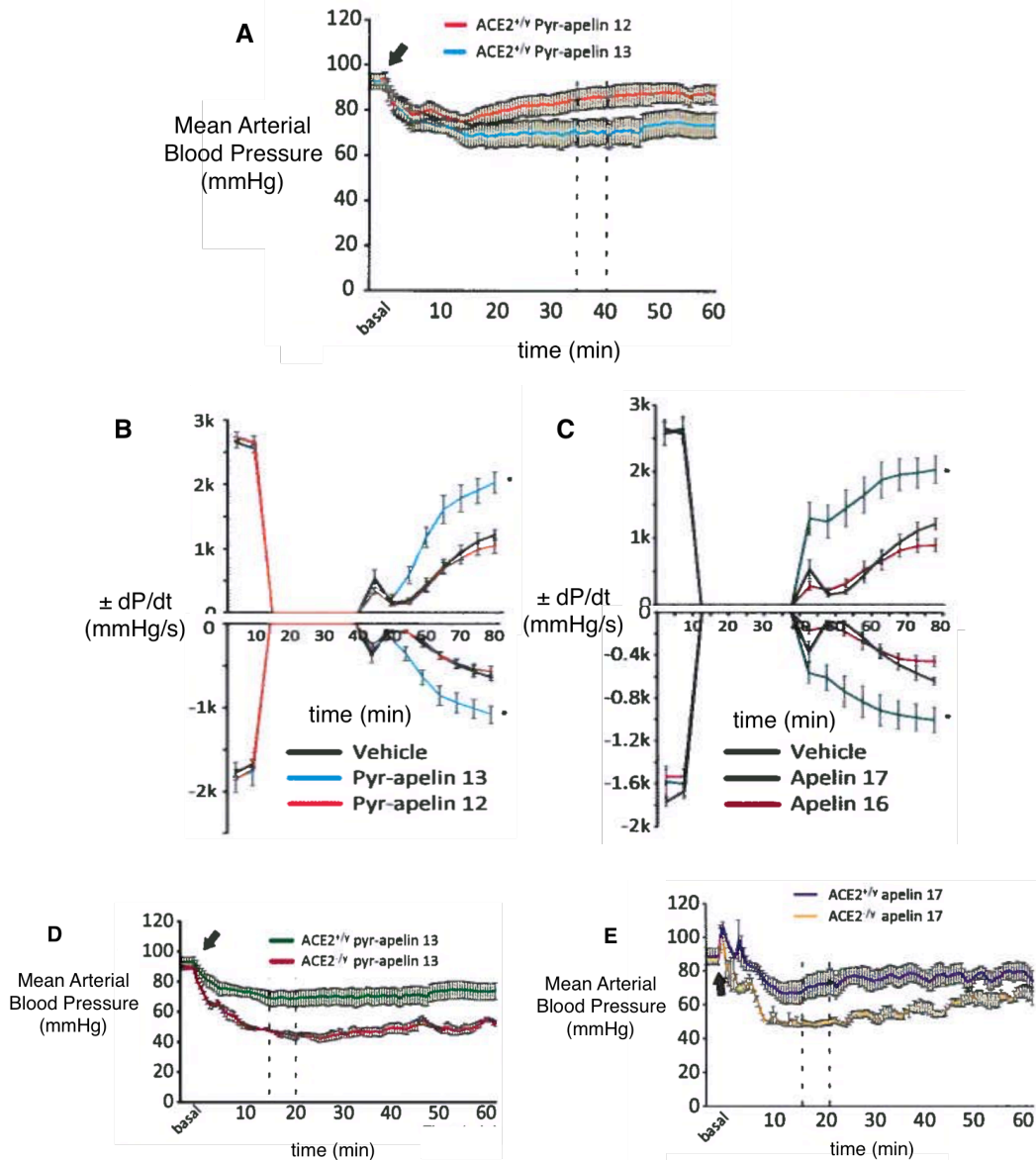


Figure 3.8 – Physiological experiments highlighting the significance of ACE2.¹³⁰ A) Hypotension assay showing the decrease of mean arterial blood pressure over time in mice after the injection of 20 μ M of pyr-1-apelin-13 (blue) or pyr-1-apelin-12 (red), n = 5; B) Langendorff assay showing the maximum and minimum rate of change in left ventricular pressure (\pm dP/dt) during a period of ischemia (0 – 30 min) and post ischemia (30 + min) with reperfusion of 1 μ M of pyr-1-apelin-13 (blue), pyr-1-apelin-12 (red), or saline (black), n = 8; C) Langendorff assay with reperfusion of 1 μ M of apelin-17 (grey), apelin-16 (magenta), or saline (black), n = 8; D) Hypotension assay in wild-type (green) and ACE2 knockout (pink) mice after the addition of 20 μ M of pyr-1-apelin-13, n = 5; E) Hypotension assay in wild-type (purple) and ACE2 knockout (yellow) mice after the addition of 20 μ M of apelin-17, n = 5.

3.2.2 Results - *In vitro* ACE2 experiments with pyr-1-apelin-13 and apelin-17¹³⁰

An initial time-course was examined for the *in vitro* ACE2-mediated degradation of pyr-1-apelin-13 and apelin-17 to confirm the ability and rate of proteolysis. Under optimized literature buffer conditions,¹²⁴ apelin substrates were incubated with recombinant human ACE2 at 37 °C, quenching the enzyme with EDTA to chelate the essential zinc ion. Following C₁₈ RP-HPLC analysis, peptide fragments eluting at different retention times were collected and assessed by MALDI-TOF to confirm that the desired peptide products were being produced. Quantitation was performed by comparing the area under the peak of the product to that of the starting material, and converting this ratio to a percentage of hydrolysis according to the following formula:

$$\% \text{ hydrolyzed product} = (\text{product area}) / ((\text{product area}) + (\text{starting material area})) \times 100$$

A rapid and quantitative conversion of pyr-1-apelin-13 and apelin-17 to their shorter fragments, pyr-1-apelin-12 and apelin-16, respectively, was observed after only a few minutes' incubation with ACE2 (Table 3.1).¹³⁰

Table 3.1 – *In vitro* ACE2 hydrolysis of pyr-1-apelin-13 and apelin-17 peptides to pyr-1-apelin-12 and apelin-16, respectively.¹³⁰ (n = 3 except pyr-1-apelin-13 incubation at 240 and 480 s (n = 1))

Time	% pyr-1-apelin-12	% apelin-16
30 s	30 ± 3	12 ± 1
60 s	68 ± 3	22 ± 4
120 s	100	49 ± 2
240 s	100	93 ± 2
480 s	100	100

ACE2 kinetic experiments had been performed on the apelin-13 substrate lacking the pyroglutamyl functionality at the N-terminus in literature,¹²⁴ but had not been completed for apelin-17 or the pyr-1-apelin-13 isoform. By varying the concentration of apelin substrates between 5 and 100 μM at a constant enzyme concentration, the kinetics of ACE2 hydrolysis were determined for these two apelin isoforms (Table 3.2).¹³⁰ The amount of product was quantified by comparing the ratio of product to starting material and converting the percentage of hydrolysis into micromoles of substrate formed. The initial velocities of product formation over time were calculated and graphed against substrate concentration, using GraphPad PRISM version 4.0 software to determine kinetic parameters. A calculated ACE2 molecular mass of 85,314 Da was used to determine the turnover numbers (k_{cat}) analogous to that previously reported.¹²⁴

Table 3.2 – ACE2 kinetic parameters for apelin-13,¹²⁴ pyr-1-apelin-13 and apelin-17.¹³⁰ (n = 2)

	apelin-13¹²⁴	pyr-1-apelin-13	apelin-17
K_m (μM)	6.8 ± 0.3	12 ± 1	19 ± 4
k_{cat} (s^{-1})	13.0 ± 0.1	19.1 ± 0.6	7.7 ± 0.4
k_{cat}/K_m ($\text{s}^{-1}\text{M}^{-1}$)	2.0×10^6	$(1.6 \pm 0.1) \times 10^6$	$(0.40 \pm 0.09) \times 10^6$
V_{max} ($\mu\text{M}/\text{min}$)	-	22.9 ± 0.7	9.2 ± 0.5

While pyr-1-apelin-13 and the literature apelin-13 degradations showed comparable kinetic parameters, particularly the ratio of k_{cat}/K_m , there was a four-fold decrease for the k_{cat}/K_m of ACE2 relative to apelin-17. ACE2 had a lower affinity for the longer apelin substrate based on the higher K_m , a slower catalytic rate based on the rate of catalysis, and a correspondingly lower V_{max} . In all parameters assessed, ACE2 showed a diminished affinity towards apelin-17 in comparison to the shorter isoforms.

3.2.3 Quantification of pyr-1-apelin-13 and apelin-17 in wildtype and ACE2-knockout plasma¹³⁰

To follow up the *in vitro* recombinant ACE2 quantification and kinetics, the next step involved the addition of exogenous peptide to mouse plasma in an effort to quantify the amount of apelin remaining over time. To support the relevance of ACE2 in the degradation of apelin, the lifetime of this peptide in ACE2 knockout (ACE2-KO) and littermate wild-type organism (WT) mouse plasma (obtained from collaborator Dr. Gavin Oudit) would be compared.

Aliquots of apelin were incubated with WT or ACE2-KO mouse plasma *in vitro* at 37 °C for 10 or 30 minutes. Experiments were quenched by the addition of 10% TFA to prevent any further protease-mediated degradation of apelin peptides. A non-hydrolyzable internal standard (Fmoc-Asp-OH) was added prior to the work up of individual experiments to account for any losses during purification. Peptide and protein components were isolated from the plasma through the use of a C₁₈ Harvard Apparatus centrifugation column, and the eluted compounds were resolved with C₁₈ RP-HPLC. The ratio of apelin peptide to internal standard at 0 minutes was compared to the same ratios over the 10 and 30 minute time points, and used to quantitate the amount of remaining pyr-1-apelin-13 and apelin-17 (Table 3.3). To account for the inherent variability in plasma from different organisms, triplicate experiments were performed at each time point and for each apelin isoform.

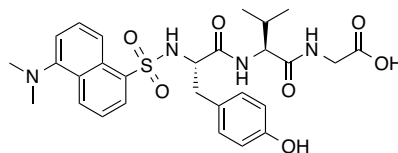
Table 3.3 – Quantification of pyr-1-apelin-13 and apelin-17 after incubation with wild-type (WT) and ACE2-knockout (KO) plasma.¹³⁰ (n = 3)

Plasma incubation time (min)	% pyr-1-apelin-13 remaining		% apelin-17 remaining	
	WT	KO	WT	KO
0	100	100	100	100
10	47 ± 9	77 ± 9	62 ± 1	63 ± 2
30	15 ± 3	40 ± 5	6 ± 3	27 ± 1

These experiments highlighted a large increase in the amount of remaining pyr-1-apelin-13 after *in vitro* incubation in ACE2-KO mouse plasma in comparison to wild-type at both time points examined. This data suggests that ACE2 plays a very significant role in the degradation of pyr-1-apelin-13. However, a negligible difference was observed after 10 minutes' incubation with apelin-17 in ACE2-deficient plasma. While a larger quantity of apelin-17 persisted after longer incubation times in ACE2-KO plasma, these results seem to indicate that ACE2 is potentially less significant for the initial degradation of apelin-17. In comparing the two apelin isoforms, the major difference in structures involve the N-terminal four amino acid extension in apelin-17, as well as the cyclic lactam formation of the N-terminal glutamine residue in pyr-1-apelin-13. Pyroglutamylation is known to minimize the impact of aminopeptidase degradation, a likely source of degradation in the extended apelin-17. These knockout experiments support our claim that ACE2 is a critical regulatory enzyme for pyr-1-apelin-13; however other proteases, particularly aminopeptidases, may play a more significant role in the initial degradation of apelin-17 in mouse plasma.

3.2.4 Quantification of pyr-1-apelin-13 and apelin-17 in human plasma¹³⁰

The methodology used to measure the time-dependent degradation of pyr-1-apelin-13 and apelin-17 in mouse plasma was also used to study their degradation in human plasma. However, considerably more plasma protein was eluted from the Harvard Apparatus C₁₈ spin columns with human plasma in comparison to that found after incubation in mouse plasma. This excess of plasma protein unfortunately co-eluted with the Fmoc-Asp-OH reference compound used to standardize samples to each other in the mouse experiments. After a preliminary screen, synthetic tripeptide dansyl-Tyr-Val-Gly-OH (dansyl-YVG, Sigma-Aldrich, **81**), was selected due to its advantageous retention time, which did not interfere with human plasma proteins, and its strong UV absorbance properties.



81

Figure 3.9 – Structure of internal standard dansyl-YVG (81**) used for the standardization of apelin in human plasma samples.**

Through the use of internal standard **81**, human plasma samples were incubated with pyr-1-apelin-13 and apelin-17 for 30 and 60 minute time intervals in triplicate and analyzed by C₁₈ HPLC as described previously (Table 3.4). Similar results were observed in that pyr-1-apelin-13 was degraded rapidly in comparison to that of apelin-17. However, some N-terminal fragments of apelin-17 had an identical retention time as the full 17-mer after HPLC runs and MALDI-TOF analysis, which complicated the analysis.

Table 3.4 – Incubation of pyr-1-apelin-13 and apelin-17 in human plasma.¹³⁰

Plasma incubation time (min)	% pyr-1-apelin-13 remaining	% apelin-17 remaining
0	100	100
30	45 ± 8	51 ± 17
60	12 ± 2	40 ± 7

3.2.5 Attempted synthesis of ACE2 inhibitor MLN-4760 and ACE2 inhibition in human plasma

To support the relevance of ACE2 as a significant regulatory factor in the degradation of apelin in human plasma, an analogous experiment to that performed with the ACE2-KO mouse plasma was required. Without the ability to genetically remove ACE2 from human plasma, an alternative approach involving the selective inhibition of ACE2 was envisioned. Two highly potent ACE2 inhibitors were selected from literature: the amino dicarboxylate small molecule MLN-4760,¹²⁷ and peptide-based DX-600¹³¹ (Figure 3.10).

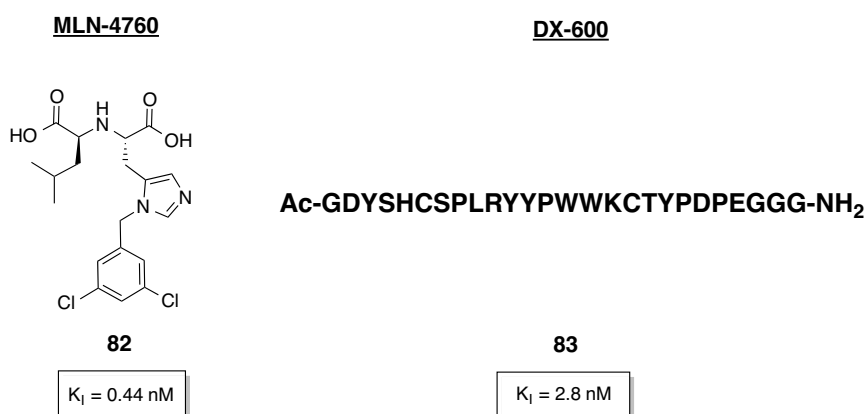


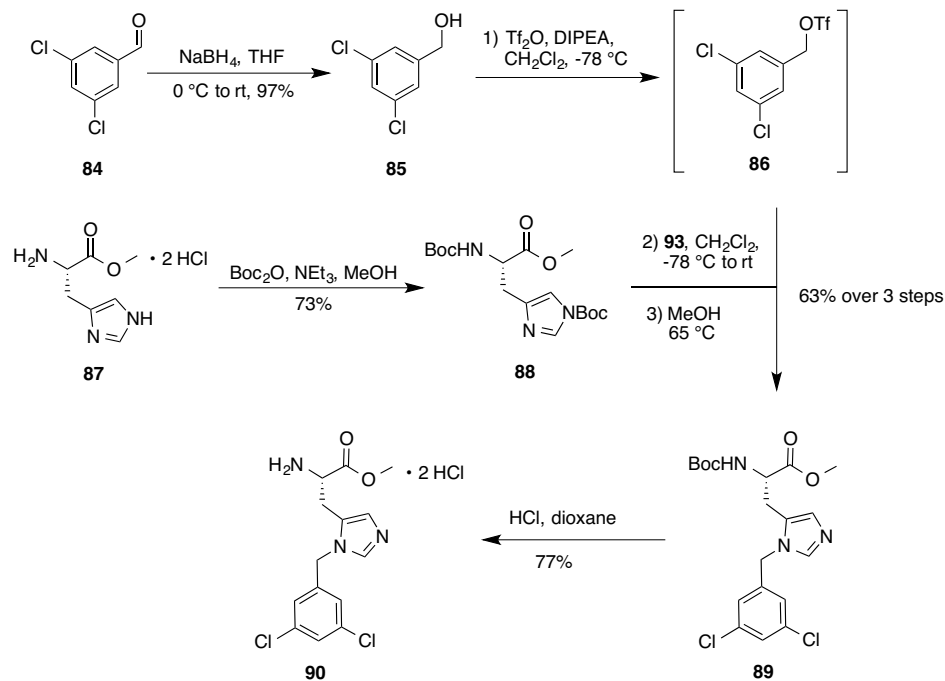
Figure 3.10 – Selected ACE2 inhibitors MLN-4760 (82)¹²⁷ and DX-600 (83).¹³¹

Both inhibitors had been previously shown to inhibit the degradation of angiotensin II to angiotensin 1-7 by ACE2.^{132,133} While MLN-4760 successfully inhibits both human and murine ACE2-mediated cleavage of angiotensin II at low micromolar concentrations, linear peptide DX-600 only is active at inhibiting human ACE2 in purified solutions, with limited inhibition in plasma.¹³² Alternatively, MLN-4760 was capable of inhibiting the formation of angiotensin 1-7 in ACE2-WT mice when the concentration of angiotensin II was <100 nM, although higher concentrations of substrate showed no noticeable inhibition, which would not be ideal for our assay conditions.

Regardless of literature complications, we opted to use these ACE2 inhibitors in an effort to pharmacologically negate the impact of ACE2 on *in vitro* apelin proteolysis in human plasma. While DX-600 was commercially available, literature reports indicated that small-molecule inhibitor MLN-4760 was no longer purchasable.¹³³ Fortunately, the initial communication outlining the syntheses of these amino dicarboxylate inhibitors was available,¹²⁷ and we decided to synthesize the inhibitor instead.

To synthesize the precursor to the MLN-4760 inhibitor, the two halves of the molecule were prepared separately. 3,5-Dichlorobenzaldehyde (**84**) was reduced with sodium borohydride to corresponding alcohol **85** in excellent yield,¹³⁴ and di-Boc protected L-histidine methyl ester **88** was obtained after Boc protection of L-histidine methyl ester dihydrochloride (**87**). To combine the two fragments, 3,5-dichlorobenzylalcohol (**85**) was reacted with triflic anhydride at -78 °C, generating triflate **86** which was immediately reacted with **88** to achieve histidine N-alkylation with

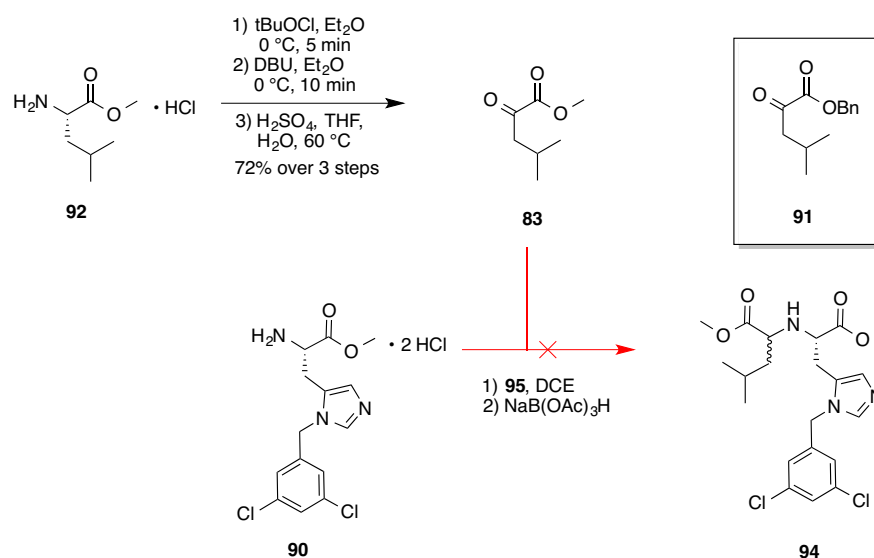
the desired regiochemistry. Thermal decomposition of the N-Boc imidazole protecting group and column chromatography yielded **89** in 63% yield over three steps. The remaining N-Boc group was deprotected under acidic conditions, forming dihydrochloride salt **90** in 77% yield after trituration (Scheme 3.1).¹²⁷



Scheme 3.1 – Synthesis of N π -arylated histidine derivative **90.**¹²⁷

The literature synthesis of MLN-4760 involved the reductive amination of **90** with benzyl-protected α -ketoester **91**, separating the resulting diastereomers by HPLC.¹²⁷ Because of immediate resource availability, methyl ester derivative **93** was prepared instead by literature protocols.¹³⁵ Beginning with H-Leu-OMe \cdot HCl (**92**), the amine was chlorinated in the presence of *tert*-butyl hypochlorite, followed by the elimination of the *N*-chloride through DBU-deprotonation of the leucine α -hydrogen. The resultant imine was hydrolyzed to α -ketoester **93** under aqueous acidic conditions and used without

further purification. Amine **90** was mixed with the α -ketoester prior to the addition of sodium triacetoxyborohydride, but unfortunately no desired product was observed (Scheme 3.2). Because of the poor stability of the α -ketoester intermediate as well as poor literature characterization and diastereomer purification procedures of **94**, we decided to approach the synthesis of this inhibitor with a novel, stereoselective approach.



Scheme 3.2 – Attempted reductive amination approach to di-methylester protected **94**.

Although all stereoisomers of MLN-4760 (**82**) were shown to inhibit ACE2 *in vitro*, there was a huge difference in IC_{50} values between the 4 diastereomers, exemplifying the need for a stereoselective synthesis (Figure 3.11).¹²⁷ We wanted to selectively generate the (*S,S*) diastereomer for its extremely potent ACE2 inhibition while minimizing the (*S,R*) diastereomer because of its significantly diminished capacity to inhibit ACE2.

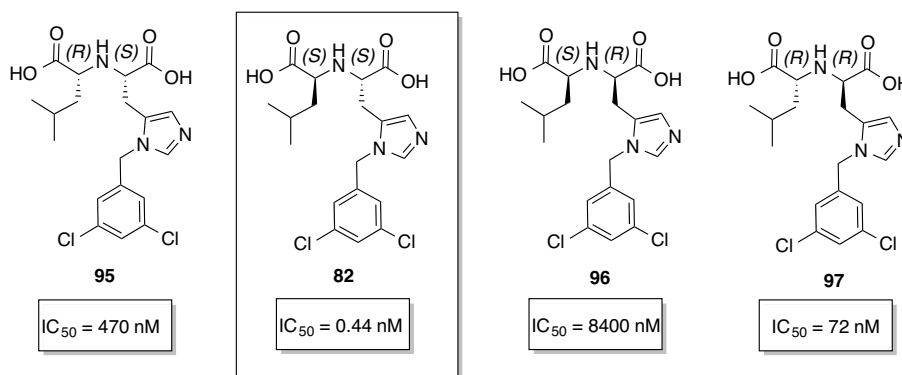
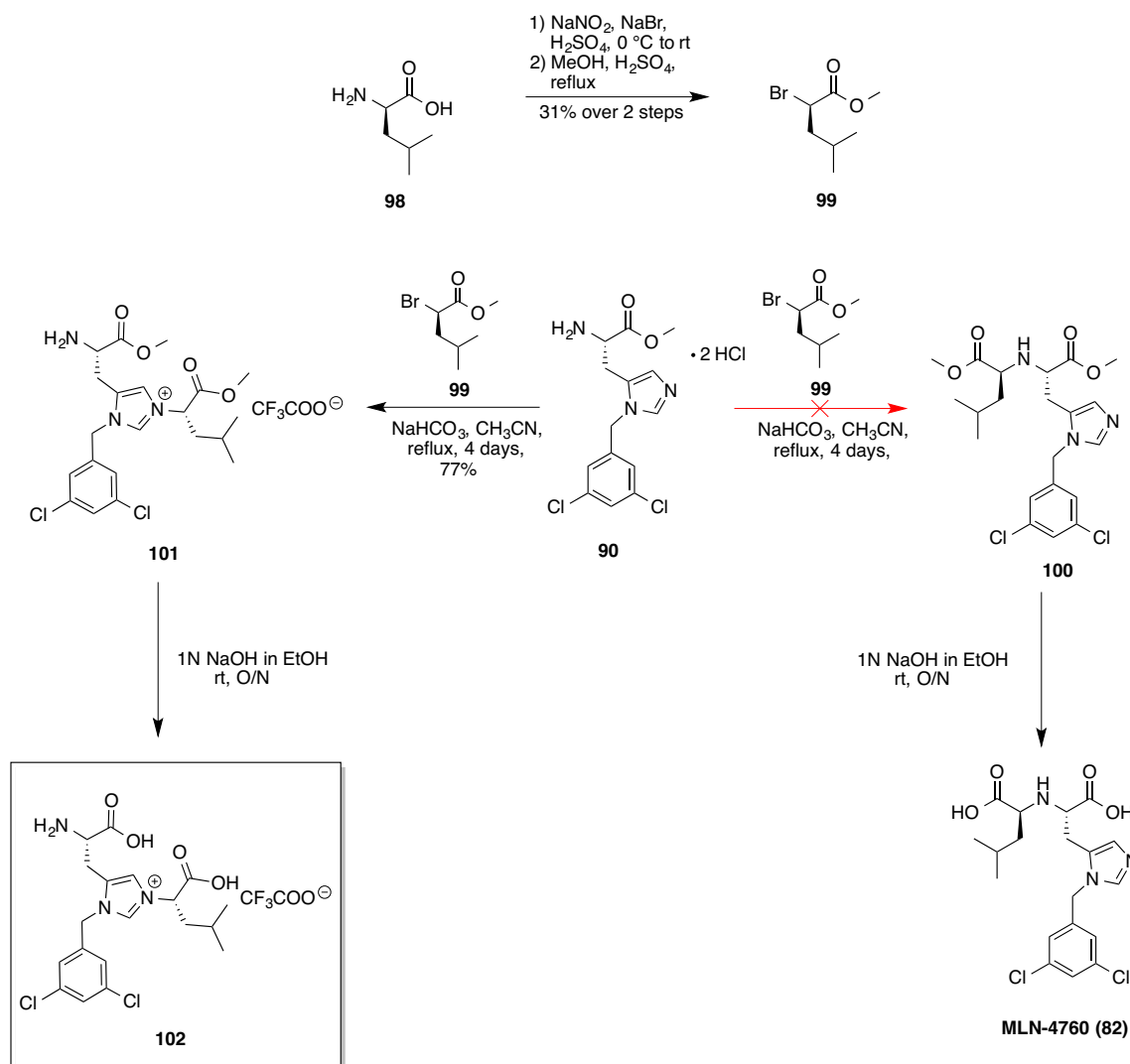


Figure 3.11 – Differences in ACE2 inhibition for MLN-4760 (82) diastereomers 95-97.¹²⁷

We envisioned that a stereospecific S_N2 displacement of α -brominated leucine derivative **99** with the $N\alpha$ amine of **90** could be used to generate the desired (*S*, *S*) stereochemistry at the amino dicarboxylate core. The α -bromo-acid was initially prepared by reacting the amine of D-leucine (**98**) with sodium nitrite in the presence of excess sodium bromide and sulfuric acid to form the diazonium salt. This unstable diazonium species would quickly be displaced by the anchimeric assistance of the neighboring carboxylic acid, forming a highly strained α -lactone. The α -lactone could be stereoselectively opened by the bromide nucleophile to retain the original stereochemistry at the α -position.¹³⁶ Compound **99** was formed by the methyl ester protection of the resulting α -bromoacid in poor yield, but with excellent retention of chirality. The nucleophilic substitution reaction between **90** and **99** was monitored by LC-MS and only began to show conversion to a product of the desired mass after refluxing in acetonitrile in the presence of sodium bicarbonate¹³⁷ after 2 days. The reaction was stopped after 4 days and the HPLC purification of **101** via a C_{18} RP-HPLC column yielded a compound with the correct mass. Compound **101** was hydrolyzed with

sodium hydroxide in ethanol, giving diacid **102** after HPLC purification. Compound **102** had the correct mass and similar, but not identical $^1\text{H-NMR}$ spectra to literature inhibitor **82** (Scheme 3.3). After *in vitro* incubation of ACE2 with a solution of **102** showed no inhibition in the cleavage of pyr-1-apelin-13, a more thorough investigation into the structure of **102** was performed.



Scheme 3.3 – Synthesis of α -bromo leucine derivative **99 and attempted stereoselective synthesis of MLN-4760 (**82**).**

Fortunately, a small quantity of commercial sample MLN-4760 was obtained (EMD Millipore) and the key differences in the NMR spectra were observed to be centered around the added 'leucine' moiety (Figure 3.12). A large chemical shift difference for the Leu-CH α was seen for **102** (~ 5.3 ppm) while the commercial MLN-4760 showed the corresponding hydrogen at a significantly upfield shift (~ 4.2 ppm). The Leu-CH $_2\beta$ protons were also deshielded by approximately 0.3 ppm in **102** in comparison to the commercial sample, appearing at a higher chemical shift than the Leu-CH γ . ROESY experiments showed a through-space NOE interaction between the His and Leu α -hydrogens for commercial MLN-4760; this interaction was not observed in **102**. However, strong NOE interactions were seen between the Leu-CH α and both imidazole hydrogen atoms, supporting a structural reassignment of **102** to the imidazolium salt instead of the desired amino dicarboxylate structure.

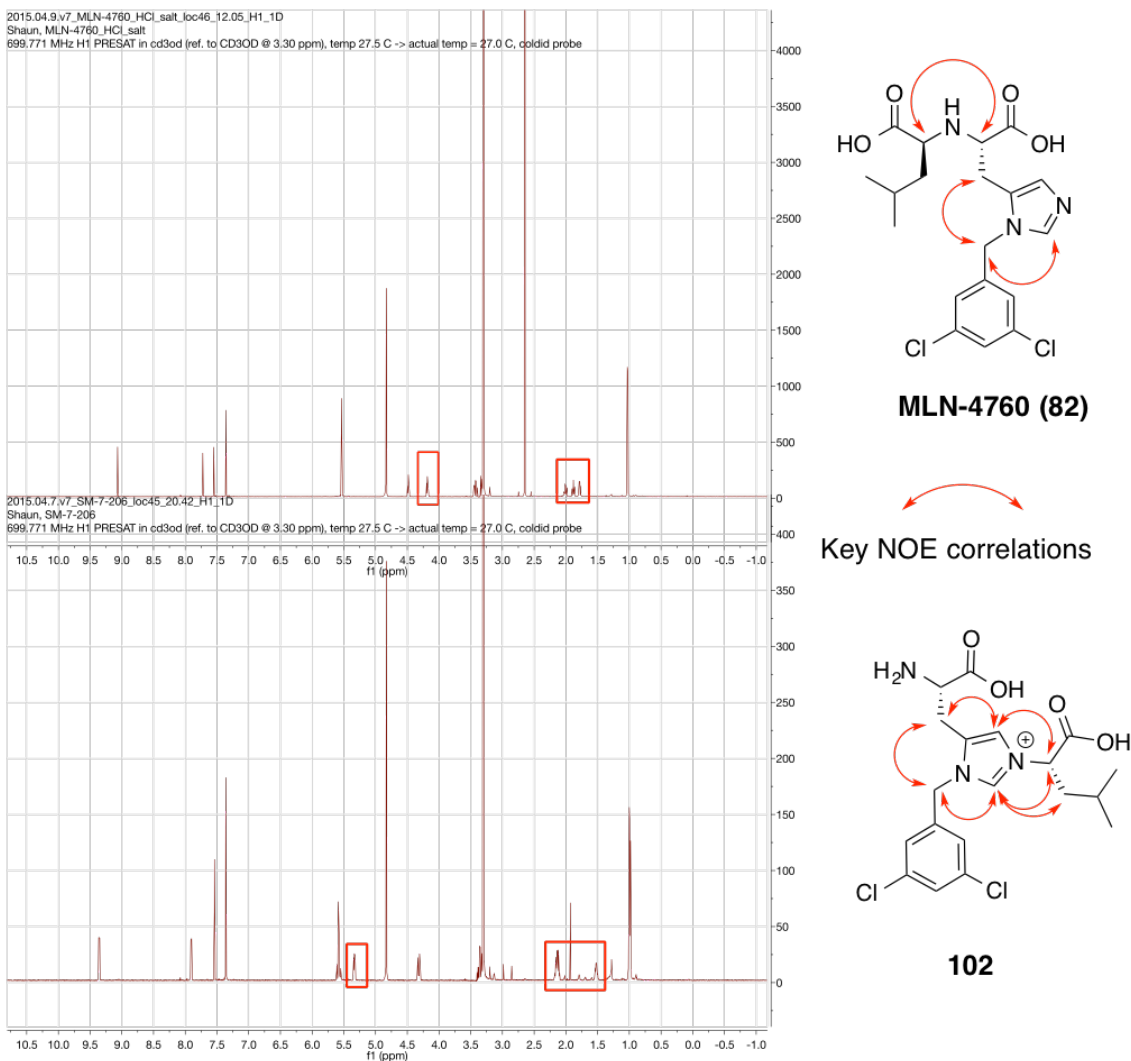


Figure 3.12 – ¹H-NMR comparison of commercial MLN-4760 (82) with 102. ‘Leucine’ CH α , CH $_2\beta$ and CH γ chemical shifts are highlighted in red boxes, and key NOE correlations supporting the imidazolium salt structure of 102 are shown.

Unsurprisingly, the lack of the amino dicarboxylate moiety rendered the imidazolium regioisomer **94** unable to inhibit ACE2 in degrading pyr-1-apelin-13 *in vitro*. Although commercial MLN-4760 showed potent *in vitro* ACE2 inhibition as expected, this did not adequately translate to the inhibition of ACE2 in human plasma samples. Plasma was pre-incubated with inhibitor (MLN-4760 (**82**), DX-600 (**83**), or

102) for 5 minutes at 37 °C prior to the addition of apelin analogues for 30 minutes. Virtually no difference was observed between any attempts at ACE2 inhibition in plasma. An alternative approach for supporting the relevance of ACE2 in the proteolysis of pyr-1-apelin-13 in human plasma could be done by observing any differences in the degradation patterns of ACE2-resistant analogues.

3.3 Synthesis of ACE2 resistant apelin analogues

3.3.1 Previous SAR work surrounding ACE2 cleavage site

To minimize the impact of ACE2 on the degradation of apelin analogues, we proposed to synthesize protease-resistant analogues of pyr-1-apelin-13 through chemical modification at the Pro12 and Phe13 positions. Two strategies were envisioned: the susceptible C-terminal amide bond could be masked by modifying the surrounding amino acid side chains; or through isosteric replacement of the amide bond with a non-hydrolyzable moiety. It was also essential that any synthetic modification to the apelin C-terminus not inhibit the inherent activity of ACE2, as it is an important regulatory enzyme in the angiotensin system, and its removal exacerbates a host of cardiovascular diseases.¹²⁵

Significant SAR studies had been performed on Pro12 and Phe13 in the pyr-1-apelin-13 backbone through single amino acid substitutions. Marsault and coworkers have performed an extensive analysis of the structure-activity relationship surrounding the ACE2 cut site and effects of these substitutions on: binding to the apelin receptor; functional assays associated with GPCR activation; and plasma stability.¹¹⁸ Pro12 and Phe13 substituted analogues with improved receptor-binding capabilities compared to native pyr-1-apelin-13 are highlighted in Table 3.5.¹¹⁸ However, no assessment of ACE2 stability and physiological activity were performed on any of these analogues. We proposed to combine two successful amino acid substitutions at the Pro12 and Phe13 positions of pyr-1-apelin-13 and examine the physiological activities and *in vitro* stabilities of these analogues to ACE2.

Table 3.5 – Literature pyr-1-apelin-13 analogues incorporating C-terminal substitutions and corresponding apelin receptor binding and % peptide remaining after 3 h.¹¹⁸ Substitutions are highlighted in red. Legend: Nle – norleucine, Nal – naphthylalanine, Cha – cyclohexylalanine, Aib – aminoisobutyric acid, Acpc – aminocyclopropane carboxylic acid, Inp – isonipecotic acid.

Literature analogue number ¹¹⁸	C-terminal tripeptide structure	Met11 sub.	Pro12 sub.	Phe13 sub.	Binding IC ₅₀ [nM]	% remaining (3h)
-		-	-	-	5.7 ± 0.3	0
1		Nle	-	-	2.6 ± 0.3	0
17		Nle	-	2Nal	1.2 ± 0.1	6
18		Nle	-	Cha	2.3 ± 0.6	30
20		Nle	-	<i>p</i> -BrPhe	1.2 ± 0.1	2
21		Nle	-	2,4,5 trifluoro Phe	0.83 ± 0.2	5
24		-	Aib	-	0.76 ± 0.1	12
26		Nle	Acpc	-	2.4 ± 0.4	0
29		Nle	Aib	-	1.8 ± 0.2	6
30		Nle	Inp	-	5.0 ± 0.9	31
32		Nle	Aib	2Nal	3.6 ± 1.0	7

3.3.2 Synthesis of substituted Pro12-Phe13 pyr-1-apelin-13 analogues¹¹⁵

Two select analogues were envisioned, both of which replaced the native Met11 and Phe13 for norleucine and *para*-bromo-L-phenylalanine, respectively. The norleucine substitution was selected due to its enhanced oxidative stability and negligible effect on apelin receptor binding (literature analogue 1, Table 3.5), while the *para*-bromo-L-phenylalanine modification improved binding compared to native apelin (literature analogue 20, Table 3.5).¹¹⁸ Although not part of the initial design strategy, the presence of the bromine atom in the *para*-bromo-L-phenylalanine gave these analogues a unique isotope distribution pattern. This feature proved advantageous when analyzing the degradation of these apelin analogues in plasma (Section 3.4). However, the two analogues differed by the amino acid selected at proline-12. Isonipecotic acid was chosen due to its improved analogue stability after 3 h incubation in rat plasma (literature analogue 30, Table 3.5). Aminoisobutyric acid was selected for its significant improvement to apelin receptor binding (entries 24 and 29, Table 3.5). The syntheses of Nle11Inp12BrPhe13 pyr-1-apelin-13, (pyr-1-apelin-13 A1, **103**) and Nle11Aib12BrPhe13 pyr-1-apelin-13, (pyr-1-apelin-13 A2, **104**) were targeted.

To initiate the syntheses of these analogues, Fmoc-*p*-bromo-L-phenylalanine was loaded onto Wang resin by first preparing the symmetrical anhydride in the presence of diisopropyl carbodiimide (DIC). The two analogues were divergently synthesized by manual (**103**) or automated SPPS (**104**), cleaved from resin with concomitant amino acid side chain removal using a solution of 95:2.5:2.5 TFA:H₂O:TIPS, purified by C₁₈ RP-HPLC and lyophilized. Pyr-1-apelin-13 A1 and A2 analogues were isolated in 26% and 36% yields respectively (Figure 3.13).¹¹⁵

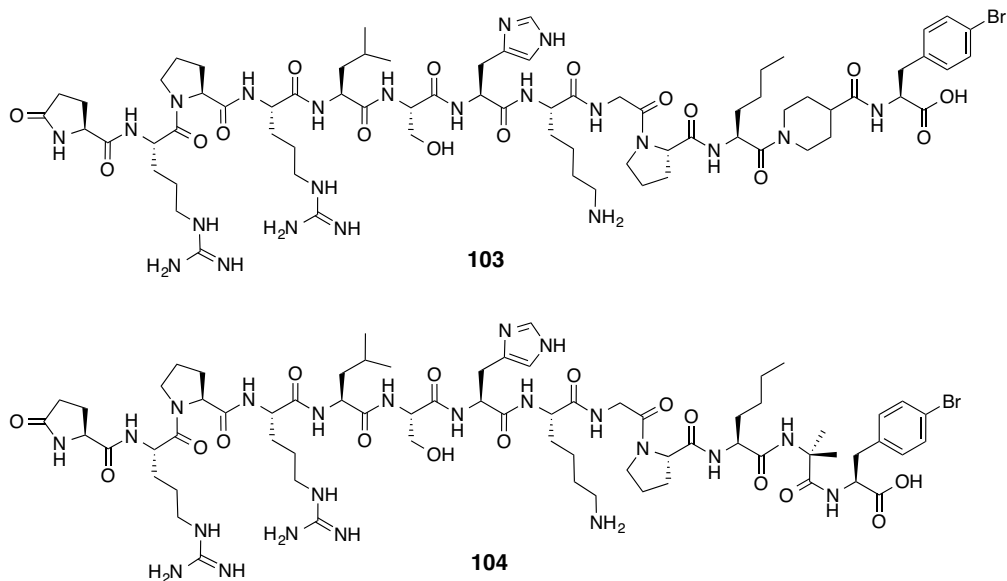


Figure 3.13 – Structures of Nle11Inp12BrPhe13 pyr-1-apelin-13 (pyr-1-apelin-13 A1, 103) and Nle11Aib12BrPhe13 pyr-1-apelin-13 (pyr-1-apelin-13 A2, 104) analogues.¹¹⁵

3.3.3 Assessment of ACE2 stability of Pro12-Phe13 pyr-1-apelin-13 analogues¹¹⁵

C-terminally substituted pyr-1-apelin-13 analogues **103** and **104** were then assessed for *in vitro* ACE2 stability. Exposure of apelin analogues **103** and **104** to optimal ACE2 proteolysis conditions yielded no observed degradation after the prolonged incubation of 48 h at 37 °C (Figure 3.14).¹¹⁵ In contrast, native pyr-1-apelin-13 was completely degraded to pyr-1-apelin-12 under the same conditions after 2 minutes, as observed in section 3.2.2.

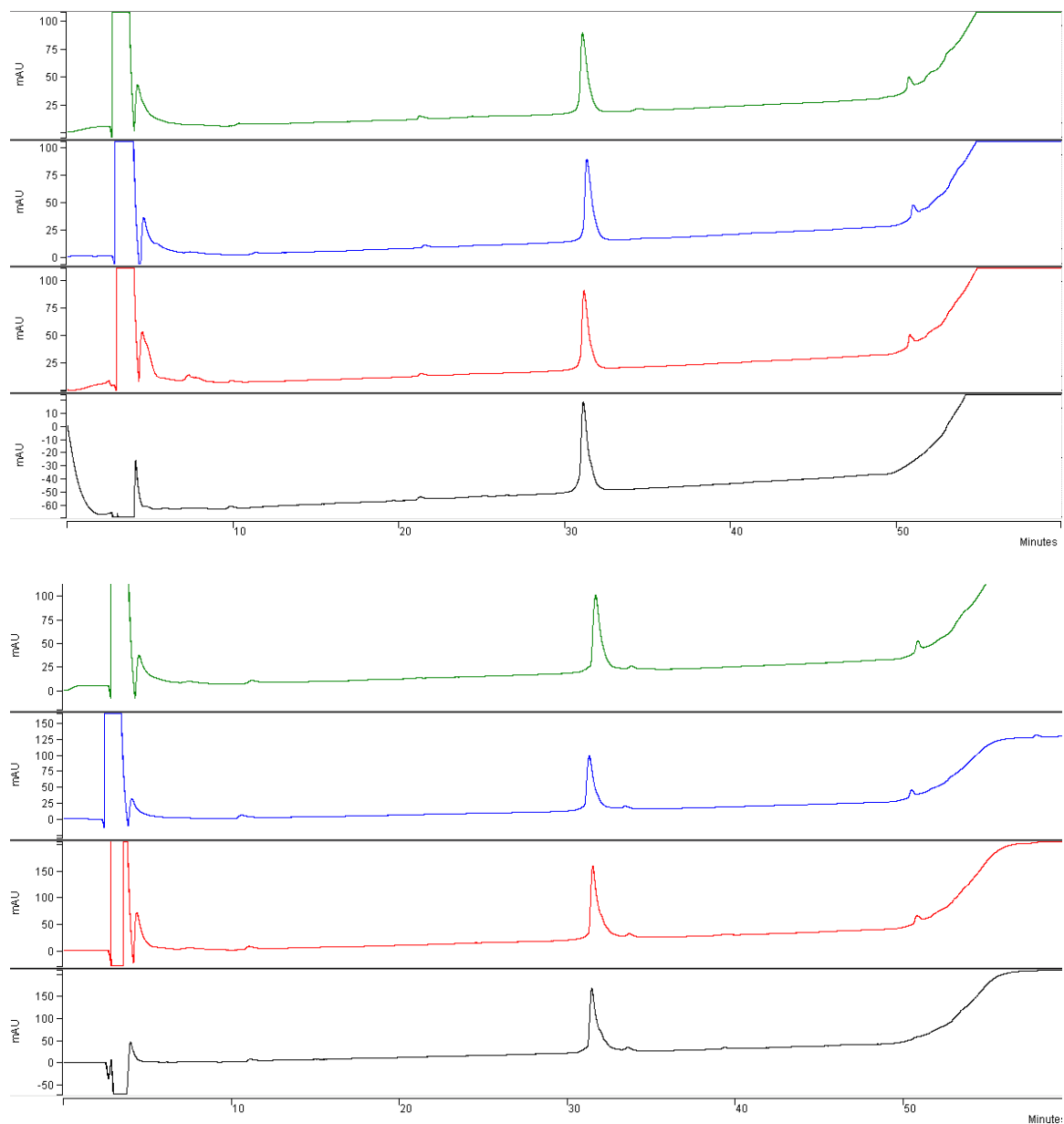


Figure 3.14 – Analytical C₁₈ RP-HPLC traces of *in vitro* ACE2 incubation of pyr-1-apelin-13 A1 (103, top) and pyr-1-apelin-13 A2 (104, bottom). Incubation times: black – 0 min; red – 1 h; blue – 24 h; green – 48 h at 37 °C.¹¹⁵

With significant resistance to ACE2 proteolysis achieved, the ability of analogues **103** or **104** to inhibit ACE2 activity was examined. The ability of **103** or **104**

to inhibit ACE2 through a time-dependent method was done by pre-incubating the enzyme with the analogues for 1 h. Addition of the native pyr-1-apelin-13 substrate and HPLC analysis indicated that pre-incubation of either analogue with ACE2 had a negligible effect on the ability of the enzyme to cleave pyr-1-apelin-13 (Figure 3.15). Analogous experiments were performed with ten times the concentration of **103** and **104** to determine the extent of time-independent inhibition of ACE2; again a negligible effect was observed.

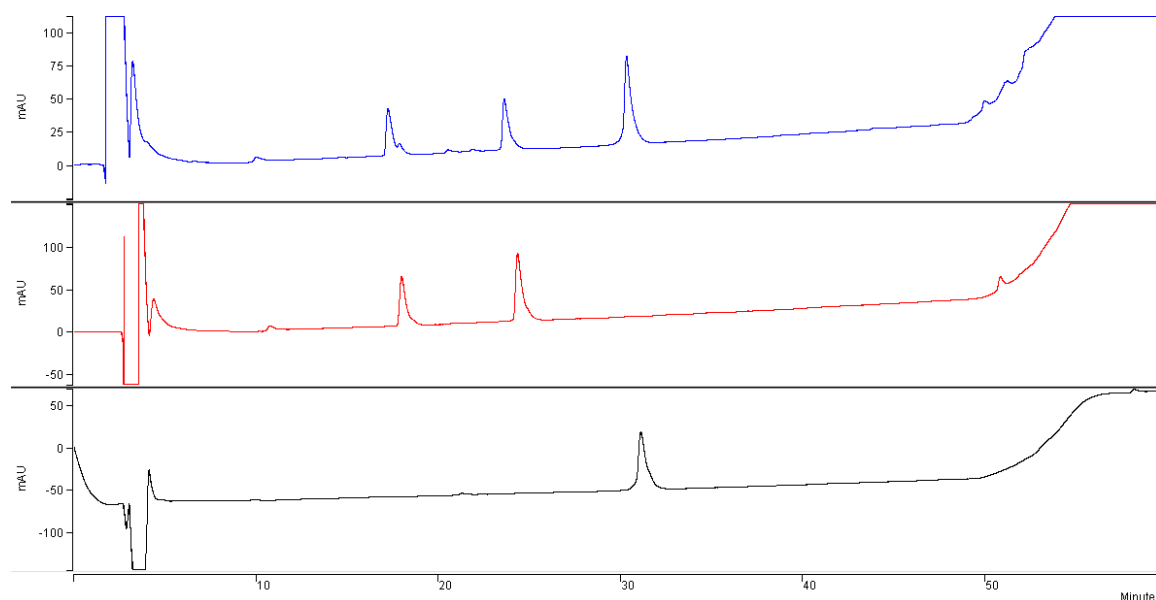


Figure 3.15 – Analytical C₁₈ RP-HPLC traces of *in vitro* ACE2 inhibition assay. black - pyr-1-apelin-13 A1 (**103**); red – pyr-1-apelin-13 1 minute ACE2 incubation; blue – pyr-1-apelin-13 1 minute ACE2 incubation with pre-incubated analogue **103**.

Because both amino acid sidechains flanking the susceptible amide bond were modified in analogues **103** and **104**, the exact substitution necessary to impart resistance to ACE2 degradation was unknown. With the assistance of Mr. Kelvin Tran (Alberta Innovates Health Solutions summer student, 2013), the individually substituted pyr-1-

apelin-13 analogues **105** – **107** (literature analogues 20, 29 and 30 respectively¹¹⁸) were synthesized by automated SPPS and tested for stability to ACE2 *in vitro* (Figure 3.16). The substitution of Pro12 with either Aib12 (**106**) or Inp12 (**107**) conferred resistance to ACE2. However, the substitution of Phe13 with BrPhe13 (**105**) was cleaved at a comparable rate to pyr-1-apelin-13. These results indicate that Pro12 substitution can contribute to ACE2 resistance.

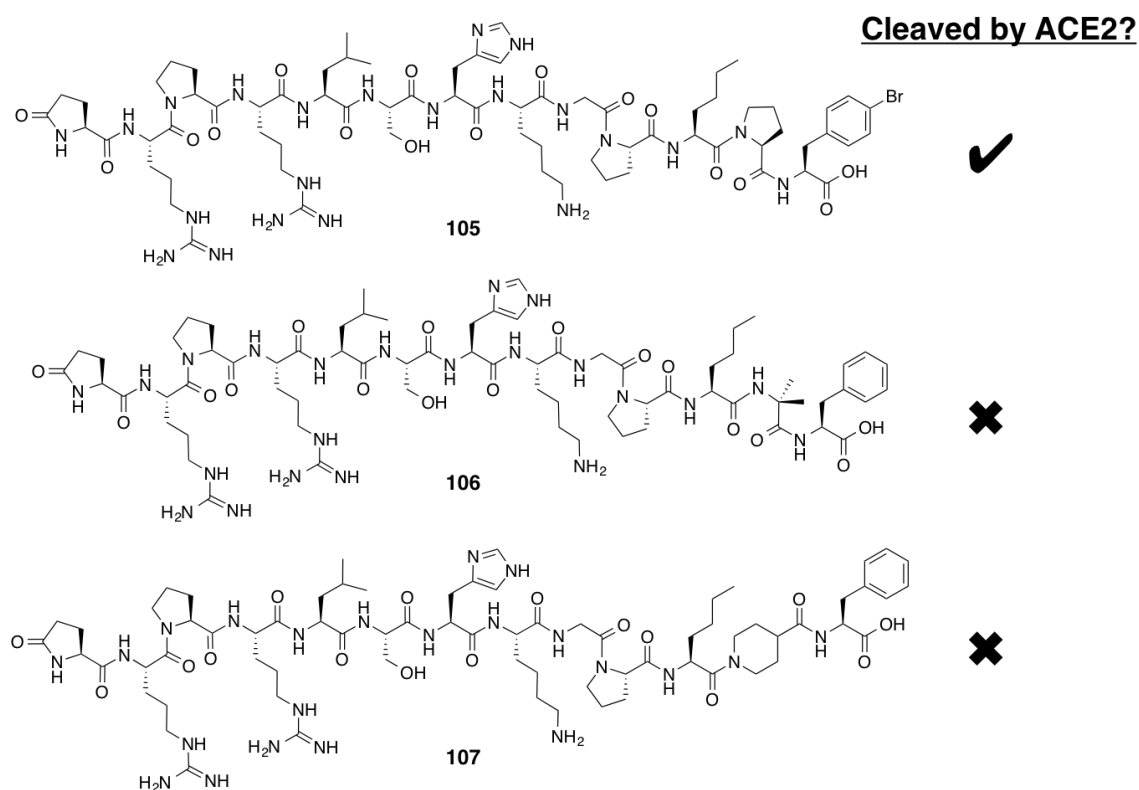


Figure 3.16 – Pyr-1-apelin-13 analogues 105 – 107 and their *in vitro* ACE2 stability.

3.3.4 Physiological testing of Pro12-Phe13 substituted pyr-1-apelin-13 analogues¹¹⁵

Pyr-1-apelin-13 analogues **103** and **104** were investigated for their physiological properties by collaborators Mr. Wang Wang and Dr. Gavin Oudit. Although many physiological tests were performed on these analogues, the results that will be focused on in this thesis are their effects on: NO-mediated vasodilation; the prevention of myocardial ischemic reperfusion injury; and the induction of angiogenesis. Direct apelin receptor binding studies were not performed on disubstituted **103** or **104**, but their literature monosubstituted parent analogues showed similar IC₅₀ values to native pyr-1-apelin-13 itself.¹¹⁸ It was proposed that the differences in **103** and **104** binding to the apelin receptor would be negligible. However these two pyr-1-apelin-13 analogues exhibited a large difference in physiological effects (Figure 3.17).

Both **103** and **104** exhibited an ability to induce NO-mediated vasodilation when introduced to mice at a 20 μ M concentration, although the magnitude and duration of the hypotensive effect was limited for **103** in comparison to either **104** or native pyr-1-apelin-13 (Figure 3.17 A). These two analogues differed greatly when analyzed by Langendorff and angiogenesis assays. The reperfusion of Inp12-substituted **103** post-infarction showed no difference from the wildtype phenotype when supplemented to the *ex vivo* mouse heart after a period of ischemia. However, the introduction of **104** showed a statistically significant ($p < 0.05$) increase in the ability of the heart to recover from this traumatic event (Figure 3.17 B).¹¹⁵ Likewise, **104** showed a strong ability to induce an increase in length and number of new blood vessels in murine aortic ring cultures ($p < 0.05$), while **103** had no effect (Figure 3.17 C).¹¹⁵

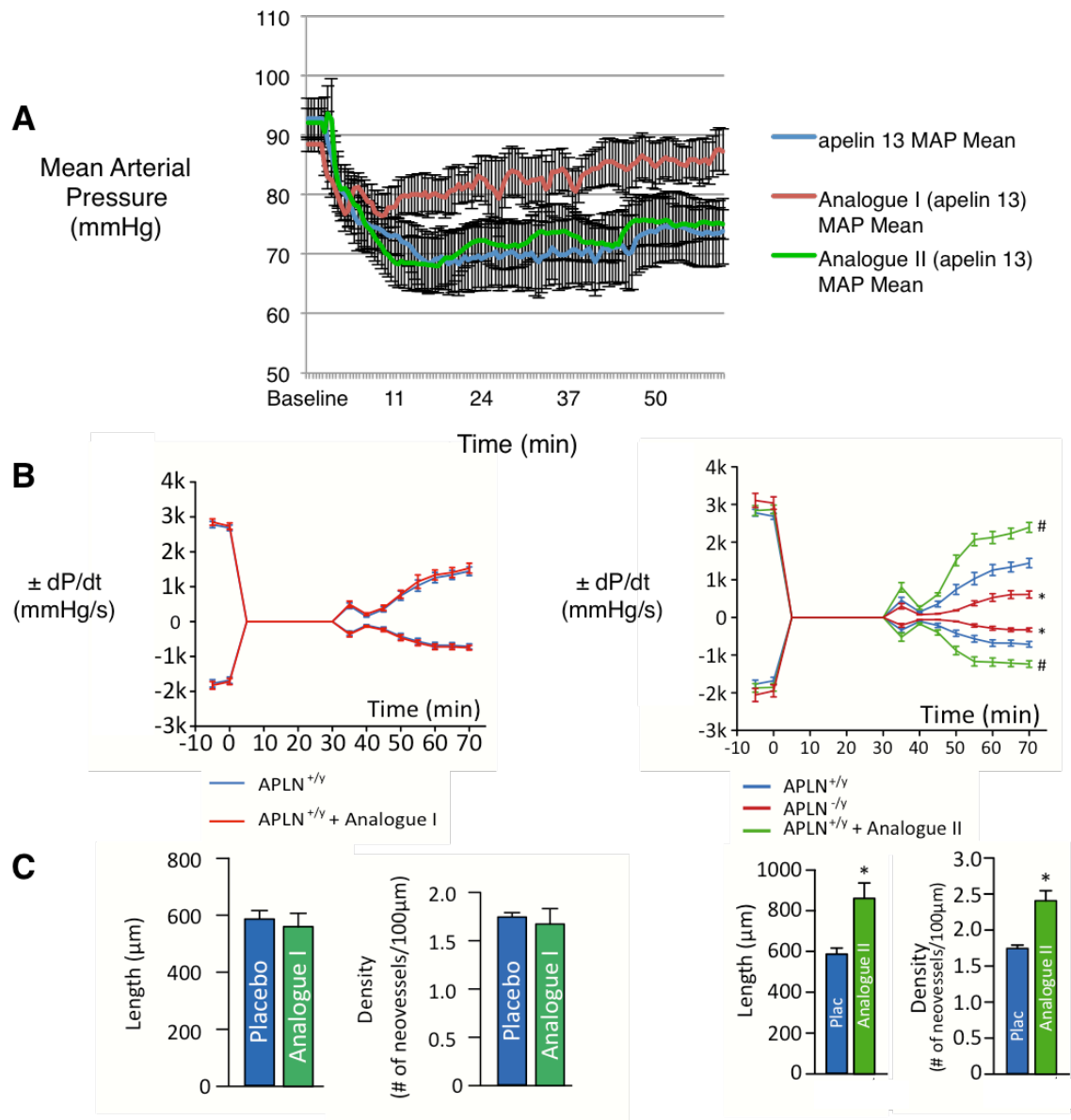


Figure 3.17 – Physiological testing performed on pyr-1-apelin-13 analogue 1 (103) and analogue 2 (104). A) Hypotension assay showing the decrease of mean arterial blood pressure over time in mice after the addition of 20 μ M of apelin analogue, n = 5; B) Langendorff assay showing the maximum and minimum rate of change in left ventricular pressure (\pm dP/dt) during a period of ischemia (0 – 30 min) and post-ischemia (30+ min) with or without reperfusion of 1 μ M of apelin analogues n = 8; C) Angiogenesis assay showing the ability of apelin analogues to induce the growth and number of new blood vessels in ACE2 wild type murine aortic ring cultures, n = 5.¹¹⁵

These results mirrored those observed in the physiological comparison of pyr-1-apelin-13 with pyr-1-apelin-12 as previously described in section 3.2.1. The introduction of Inp12 as a Pro12 substitute likely positions the critical C-terminal phenylalanine in a disadvantageous orientation for apelin receptor activation and internalization. This suggests that **103** serves as a ‘biased’ agonist, limiting its utility to solely induce NO-mediated vasodilation. This result is consistent with the trends observed previously with the physiological results of des-phenylalanine containing apelin peptides pyr-1-apelin-12/apelin-16, and the F17A-analogue of apelin-17.⁹²

3.3.5 Synthesis and physiological testing of elongated and internally substituted apelin A2 analogues

With the ACE2-resistant and physiologically potent **104** analogue in hand, this successful C-terminal modification (NleAibBrPhe, subsequently referred to as ‘A2’) was applied to the apelin-17 isoform, synthesizing analogue **108** by manual SPPS. A subsequent report also highlighted the potentially beneficial role of select internally substituted analogues of apelin-13.¹³⁸ Analogues were prepared containing substitutions at the histidine-7 and lysine-8 positions in the pyr-1-apelin-13 backbone. Alanine-7 and arginine-8 substituted analogues showed a dramatically improved IC₅₀ (0.12 nM for Ala7Arg8-pyr-1-apelin-13, 0.10 nM for the N-terminally elongated Arg-Arg-Ala7Arg8(*p*ClPhe)13-apelin-13) when displacing a bound radiolabelled pyr-1-apelin-13 substrate (1.4 nM) at the APJ receptor.¹³⁸ These advantageous apelin receptor-binding substitutions were combined with the ACE2-resistant A2 C-terminus to generate apelin analogues **109** and **110** after preparation by manual SPPS (Figure 3.18).

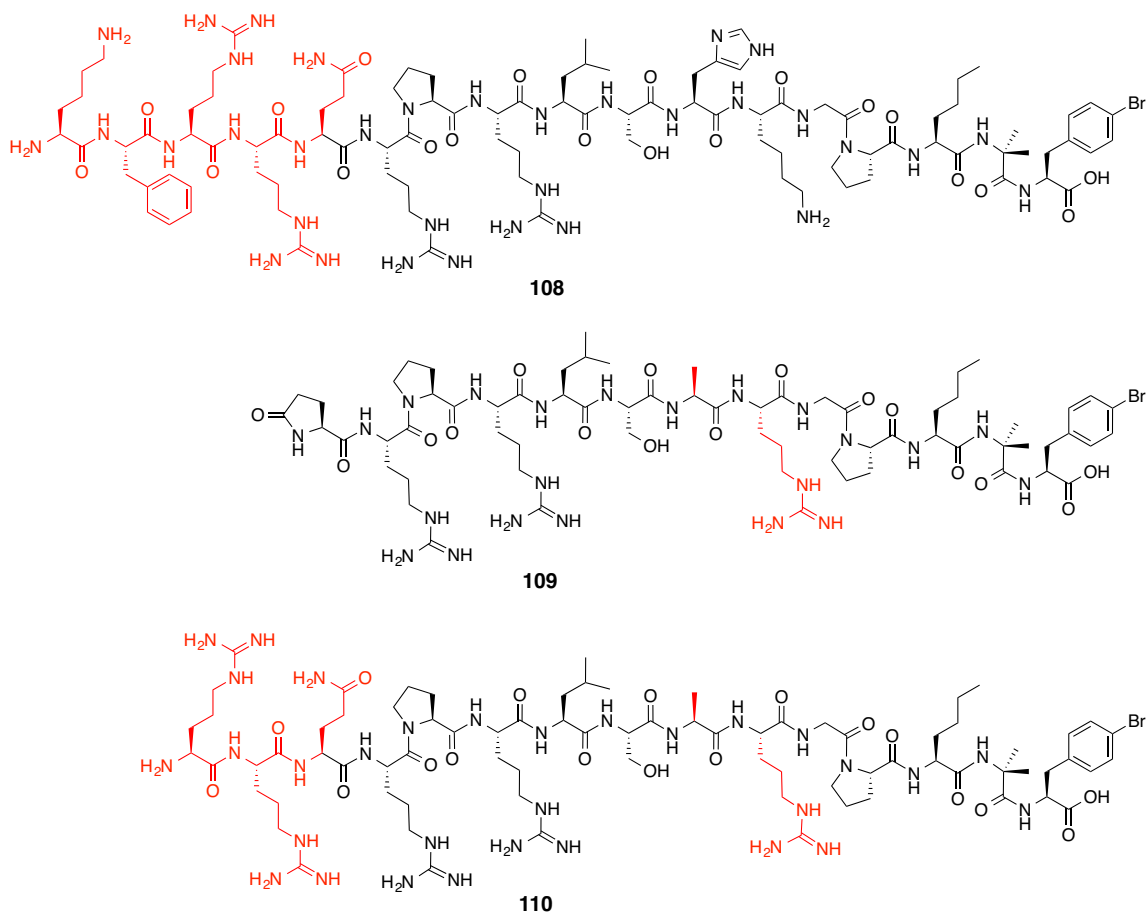


Figure 3.18 – Structures of apelin-17 A2 (108) and internally substituted analogues 109 and 110. Structural differences from **104** are highlighted in red.

Analogues **108 – 110** were assessed for physiological activity by collaborators Mr. Wang Wang and Dr. Gavin Oudit, solely investigating their ability to activate NO-mediated hypotension and to prevent myocardial ischemic reperfusion injury (Figure 3.19). In comparison to the parent **104** analogue, apelin-17 A2 (**108**) had a pronounced effect in the hypotension assay, dramatically lowering the blood pressure of test mice (Figure 3.19 A). Although no direct comparison is shown in Figure 3.19 B, **108** again showed an exaggerated effect in the Langendorff experiments, dramatically increasing

the ability of *ex vivo* mouse hearts to survive prolonged periods of ischemia. Analogues **109** and **110** showed a similar effect to that observed with **104** in both assays examined. While the internal His7Ala and Lys8Arg substitutions seemed to retain physiological activity in the Langendorff experiment, no significant beneficial pharmacodynamic effect was observed, so no further analogues incorporated these internal His7 and Lys8 amino acid substitutions.

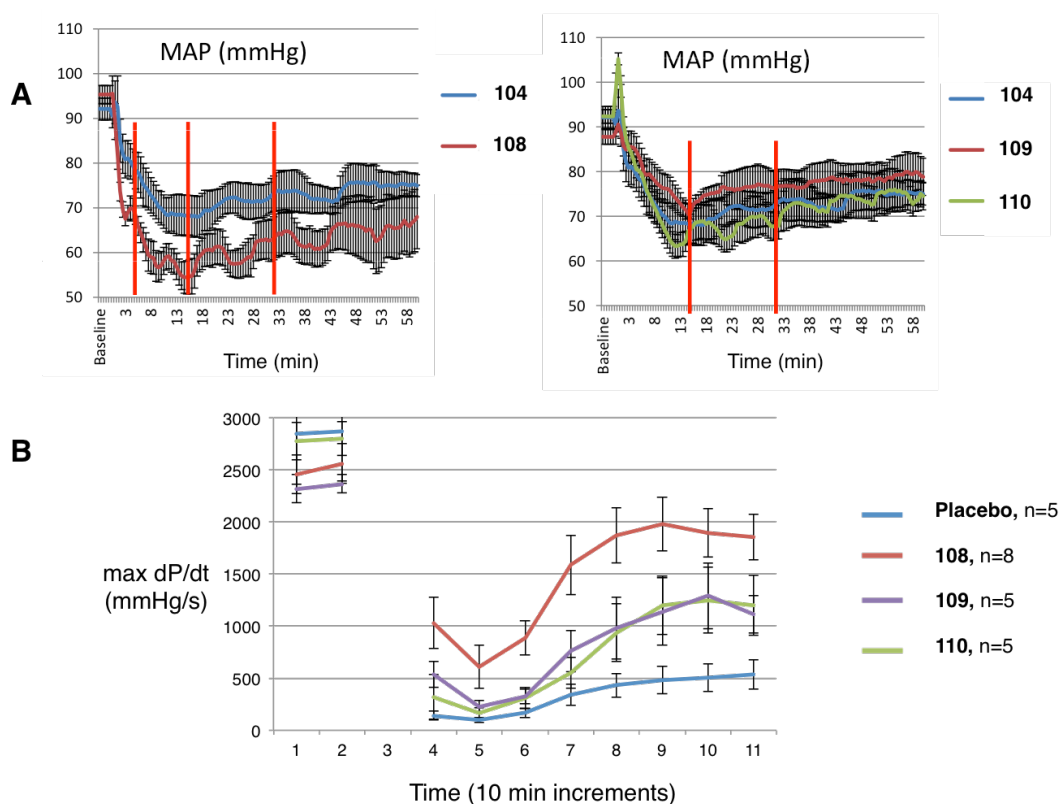


Figure 3.19 – Physiological testing performed on extended apelin A2 analogue 108, and internally substituted analogues 109 and 110. A) Hypotension assay showing the decrease of mean arterial blood pressure over time in mice after the addition of 20 μ M of apelin analogue, n = 5; B) Langendorff assay showing the maximum rate of change in left ventricular pressure (max dP/dt) during a period of ischemia (0 – 30 min) and post-ischemia (30+ min) with reperfusion of 1 μ M of apelin analogues for 20 minutes, n = 5 for placebo, **109**, **110**; n = 8 for **108**.

3.3.6 *In vitro* human plasma stability of ACE2 resistant analogues

With a variety of ACE2 resistant analogues now available, an alternative approach was used to investigate the role of ACE2 as a major factor in the degradation of pyr-1-apelin-13 and apelin-17 in human plasma. An increased plasma lifespan for an ACE2 resistant analogue compared to the native peptide would suggest that ACE2 plays a role in the degradation of this peptide hormone. With the assistance of Mr. Tyler McDonald (Alberta Innovates Health Solutions summer student, 2015), synthetic apelin analogues were incubated in human plasma and quantified as previously described (Table 3.6).¹³⁰

Table 3.6 – Remaining percentage of ACE2 resistant apelin analogues in human plasma comparison to native apelin.¹³⁰ (n = 3)

Apelin modification	compound number	% remaining 30 min	% remaining 60 min
pyr-1-apelin-13 analogues			
pyr-1-apelin-13	71	45 ± 8	12 ± 2
NleInpBrPhe (A1)	103	95 ± 4	97 ± 8
NleAibBrPhe (A2)	104	77 ± 19	65 ± 14
Ala7Arg8 A2	109	92 ± 8	87 ± 1
apelin-15 analogue			
Ala9Arg10-apelin-15 A2	110	78 ± 5	32 ± 9
apelin-17 analogues			
apelin-17	70	51 ± 17	39 ± 7
NleAibBrPhe (A2)	108	43 ± 1	35 ± 5

ACE2 resistant pyr-1-apelin-13 analogues **103**, **104** and **109** all showed an appreciable increase in plasma stability compared to the native peptide. It is important to note that although **103** showed virtually no decrease in this *in vitro* plasma stability assay, its inability to activate certain cardio-protective pathways associated with apelin makes it an unattractive candidate for further development. The internally substituted

15mer **110** showed an enhanced stability to plasma proteolysis in comparison to native pyr-1-apelin-13, but showed an accelerated hydrolysis in comparison to the other A2 substituted analogues. This is likely due to the presence of a free amino terminus and lack of N-terminal pyroglutamylation on this 15 amino acid analogue. However, the most physiologically potent analogue **108** showed a negligible difference from the native degradation of apelin-17 in human plasma. All combined, these results shadow those highlighted in the mouse ACE2 knockout experiments (Table 3.3) in that ACE2 has a significant role in the degradation of pyr-1-apelin-13 but a lesser effect on apelin-17 breakdown.

3.3.7 Synthetic efforts towards Pro12-Phe13 pyr-1-apelin-13 isosteres

The substitution of Pro12 and Phe13 amino acid side chains in **103** and **104** gratifyingly generated ACE2 resistant apelin analogues via the incorporation of commercially available amino acids. However, a parallel strategy involving the isosteric replacement of the C-terminal Pro12-Phe13 amide bond with non-hydrolyzable amide derivatives was also proposed in order to maximize the biological stability of apelin. Due to the physiological significance of ACE2 in the cardiovascular system, isosteric moieties were selected to minimize potential enzyme inhibition.^{125,128,139} We initially targeted three unique isosteric moieties: ketone (**111**); triazole (**112**); and aza-analogues (**113**) that could serve as core isosteres for further modification and analogue generation (Figure 3.20). Synthetic efforts were initiated on all three of these molecules, but due to the retention of physiological activity, simplicity, and potency of amino acid-substituted ACE2 resistant analogue **104**, isosteric replacements of the terminal amide bond were not completed for any of these analogues.

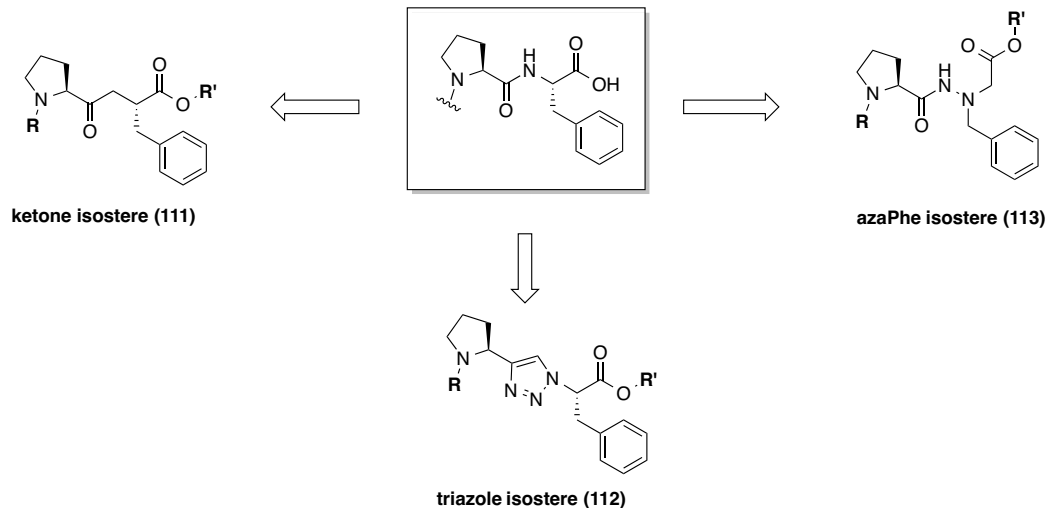
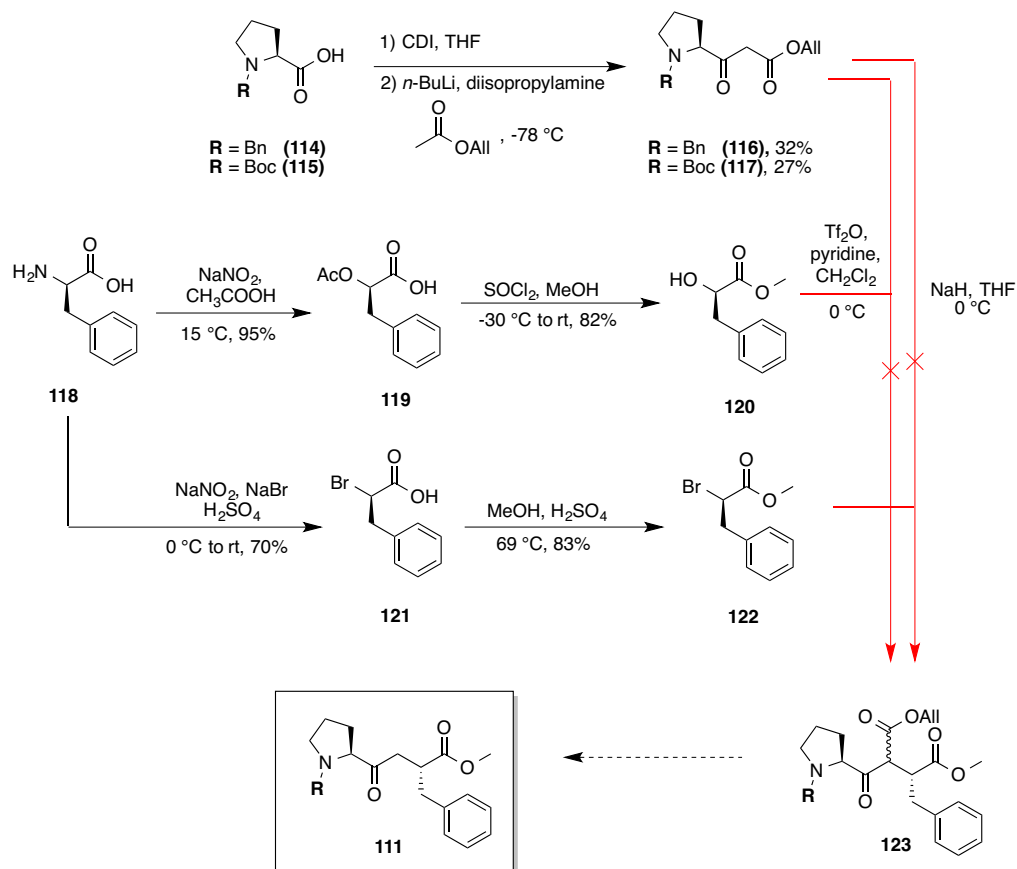


Figure 3.20 – Initial amide bond isostere targets for Pro12-Phe13.

To initiate the synthesis of ketone isostere **111**, the carboxylic acid of benzyl or Boc-protected L-proline (**114**, **115**) was activated with 1,1'-carbonyldiimidazole (CDI), then reacted with the enolate of allyl acetate to generate an allyl β -keto ester in poor yields (**116** and **117** respectively).¹⁴⁰ Substitution at the α -position of phenylalanine was achieved through the acid-catalyzed reaction of D-phenylalanine (**118**) with sodium nitrite. The intermediate diazonium salt quickly collapses to an α -lactone with extrusion of nitrogen gas due to the neighboring carboxylic acid. The presence of glacial acetic acid or excess sodium bromide and sulfuric acid stereoselectively opens the intermediate α -lactone to form **119**¹⁴¹ or **121**,¹³⁶ respectively, with excellent retention of configuration. Subsequent methyl ester protection generated **120**¹⁴¹ and **122**¹³⁶ (Scheme 3.4). However, deprotonation of the allyl β -keto ester compounds with non-nucleophilic base at 0 °C followed by the addition of **122** or the triflate of **120**¹⁴² failed to alkylate between the two carbonyl moieties.¹⁴⁰ Further investigations into the formation of **123**

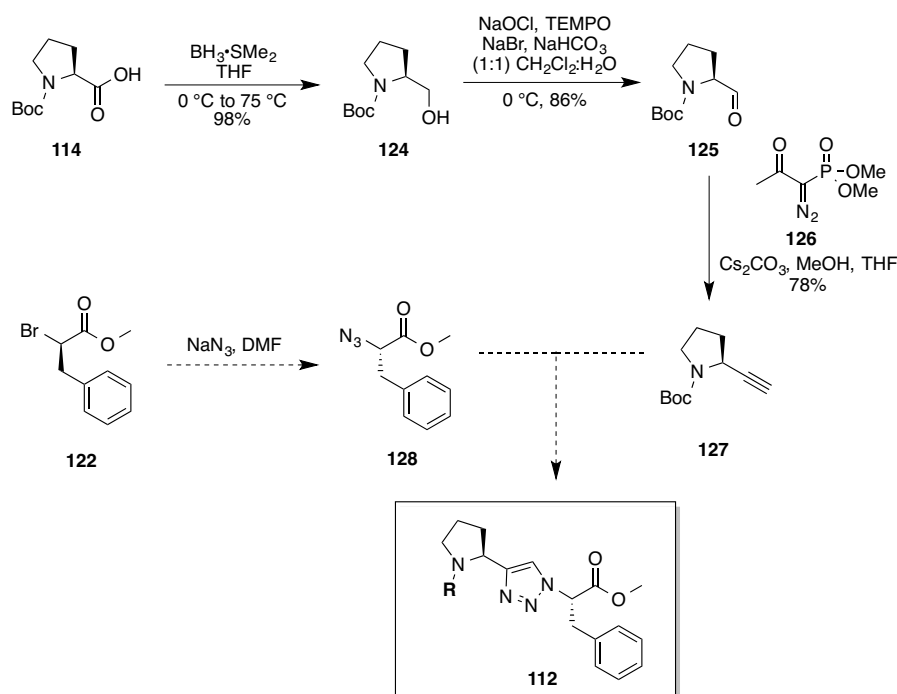
were not performed, though if successful, the desired ketone isostere (**111**) could be prepared through allyl ester deprotection and β -keto acid decarboxylation.¹⁴⁰



Scheme 3.4 – Efforts towards the synthesis of Pro-Phe ketone isostere 111.

The synthesis of the Pro-Phe triazole isostere (**112**) was initiated by the reduction of Boc-L-Pro-OH (**114**) to alcohol **124** by borane dimethylsulfide,¹⁴³ followed by Anelli oxidation to Boc-L-prolinal (**125**).¹⁴⁴ A Bestmann-Ohira reaction with reagent **126** in the presence of cesium carbonate and methanol was performed on aldehyde **125** to generate terminal alkyne **127** in 78% yield.¹⁴⁵ The corresponding azide partner **128**

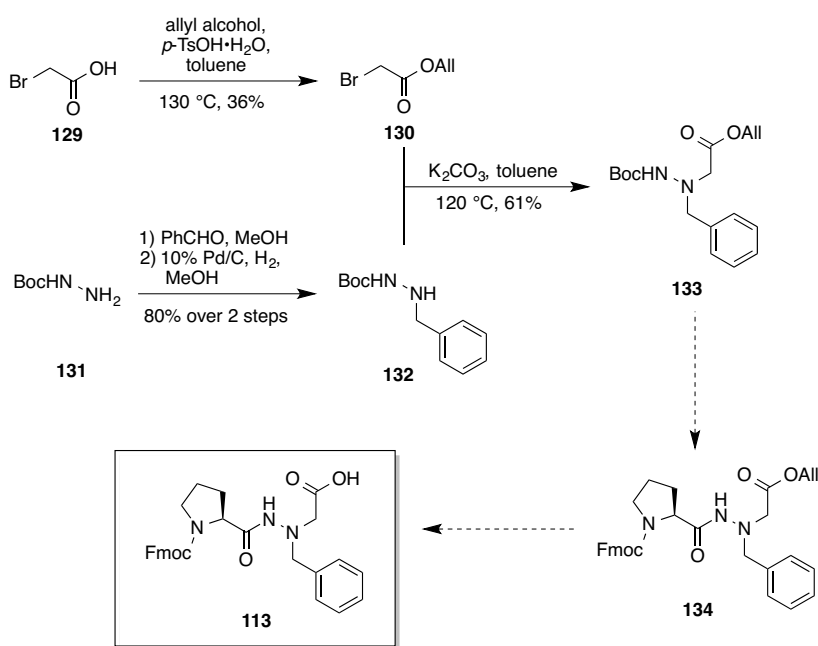
could be prepared from the S_N2 displacement of the α-bromide in **122** with sodium azide (Scheme 3.5).



Scheme 3.5 – Efforts towards the synthesis of Pro-Phe triazole isostere 112.

Aza-analogue **113** was also targeted in an effort to stabilize the susceptible amide bond. A further discussion of aza-analogues will take place later in this chapter (section 3.5.5), but in retrospect, the α-carbon substitution should have occurred at the proline position to create an analogue with improved protease stability. Aza-analogue **113** was also extended by a methylene, generating an aza-β-amino acid because of the instability of N-carbamic acids. Ester **130** was prepared by allyl protecting bromoacetic acid (**129**) under Dean Stark conditions, while its hydrazine counterpart (**132**) was prepared by reacting Boc-hydrazine (**131**) with benzaldehyde followed by palladium-

catalyzed hydrogenation of the intermediate hydrazone.¹⁴⁶ These two fragments were coupled together in the presence of potassium carbonate and refluxing toluene to afford the Boc-protected β -aza phenylalanine moiety **133** in 61% yield.¹⁴⁷ Subsequent Boc deprotection, coupling with Fmoc-Pro-OH and allyl ester deprotection could afford the final methylene-extended aza analogue **113** (Scheme 3.6).

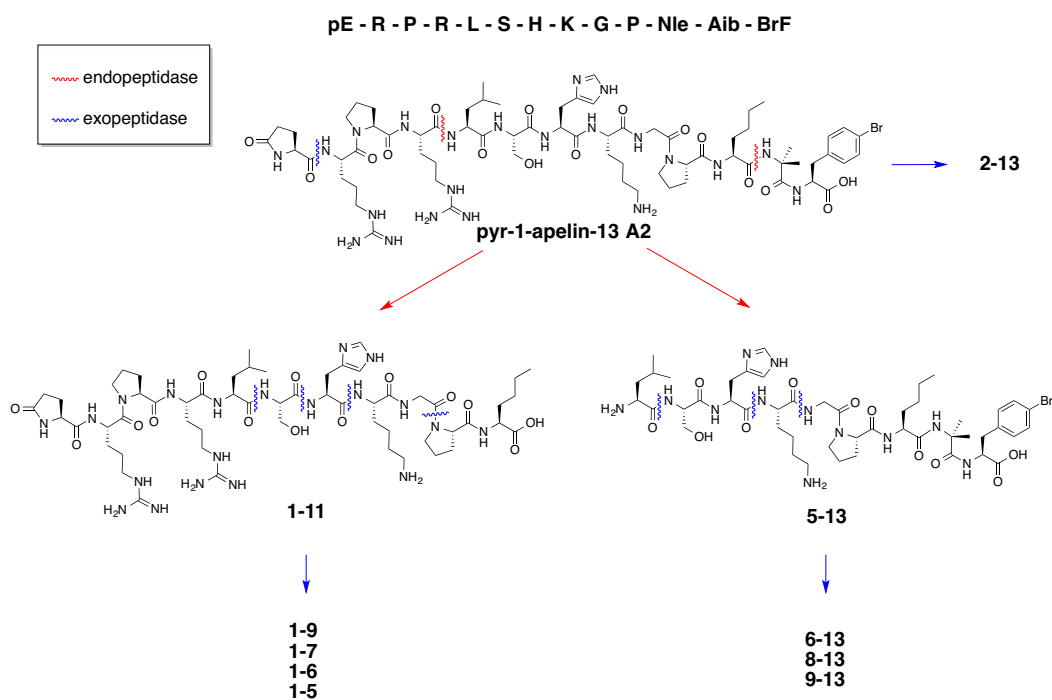


Scheme 3.6 – Efforts towards the synthesis of Pro-Phe azadipeptide 113.

3.4 Further protease degradation of ACE2 resistant apelin analogues

3.4.1 Identification of additional sites of protease cleavage in ACE2 resistant analogue 104

Although ACE2 resistant analogue **104** exhibited an improved lifespan in comparison to native pyr-1-apelin-13, our next objective involved the locating other sites of proteolytic degradation in plasma. With the assistance of Mr. Kelvin Tran, **104** was incubated in both human and mouse plasma for decreasing time periods and the resulting peptide fragments were isolated using a C₁₈ RP-silica based purification method. These analogue fragments were analyzed by LC-MS/MS and identified by Mascot database searching to give the projected sites of protease cleavage (Scheme 3.7).



Scheme 3.7 – Observed LC-MS/MS fragments and proposed protease degradation pathways of pyr-1-apelin-13 analogue 104 after incubation in mouse plasma.

Theoretical endopeptidase cuts are shown in red and exopeptidase cuts are shown in blue. Fragments (1-11, etc.) are numbered according to the amino acid sequence of pyr-1-apelin-13.

The results obtained from LC-MS/MS suggested a pattern of degradation of peptide fragments resulting from internal endopeptidase cleavage, then non-specific exopeptidase degradation. The plasma incubation time of **104** was decreased in an effort to find the initial endopeptidase fragments, and we proposed that two distinct regions of proteolytic degradation existed in mouse plasma. By analyzing the remaining fragments, we extrapolated these results back to propose a fragmentation site between Arg4-Leu5, and Nle11-Aib12 in mouse plasma. These experiments were repeated in human plasma, and an analogous N-terminal cleavage was found between Arg4-Leu5. However, no evidence of the C-terminal Nle11-Aib12 hydrolysis was observed in human plasma at this time (Figure 3.21). We decided to initially investigate the Arg4-Leu5 site of proteolysis, as previous truncation studies had shown that removal of any of the ‘RPRL’ amino acids completely abolished receptor binding and physiological activity.^{86,98} This protease responsible for this N-terminal degradation is physiologically relevant for the regulation of the activity of apelin and its potential application as a therapeutic for the treatment of cardiovascular disease.

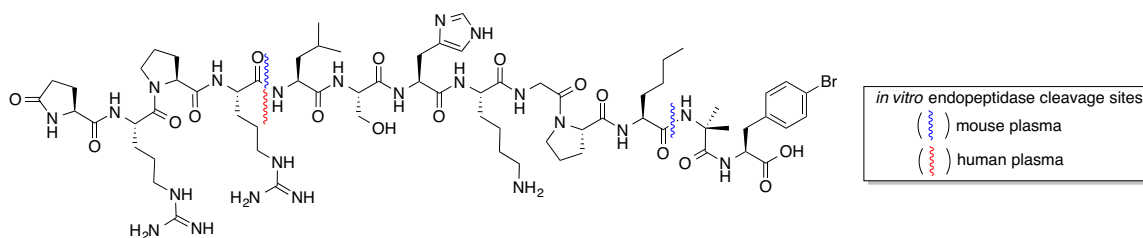


Figure 3.21 – Proposed sites of proteolytic degradation of pyr-1-apelin-13 analogue 104 in mouse and human plasma after LC-MS/MS analyses.

3.4.2 Additional literature sites of degradation

At a similar time to our experiments, other research groups performed their own analyses on the breakdown of pyr-1-apelin-13 and analogues.^{148,149} Overall, similar patterns were observed, including the observation of two unique sites of degradation. However, differences were observed in the precise location of endoprotease degradation and the relevance of these proteases *in vivo* or *in vitro*.

Marsault and coworkers performed *in vitro* pyr-1-apelin-13 degradation experiments in mouse, rat and human plasma and analyzed the resultant peptide fragments by LC-MS.¹⁴⁸ The authors found a few key differences from our results, most notably placing the location of the N-terminal cut site between Leu5-Ser6 due to an accumulation of octapeptide 6-13 (Figure 3.22).

The *in vivo* degradation of apelin peptides was also examined after injection in rats. In addition to the removal of C-terminal phenylalanine, likely by ACE2, the major proposed degradation was located between Pro10-Nle11, followed by N-terminal degradation between Ser6-His7 (Figure 3.22).

In addition to native pyr-1-apelin-13, two additional analogues were tested in these assays. An α -Me-L-Phe13-substituted pyr-1-apelin-13 analogue (**73**) showed an identical fragmentation pattern to the native peptide in both the *in vivo* and *in vitro* experiments. The authors also the *in vitro* degradation patterns of D-Leu5 pyr-1-apelin-13 and proposed that this analogue moved the initial site of endoprotease degradation to the His7-Lys8 position.

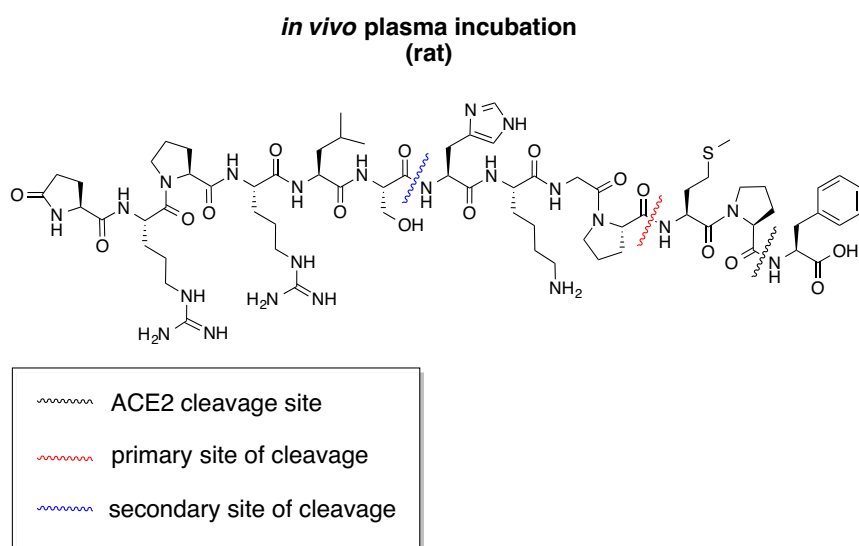
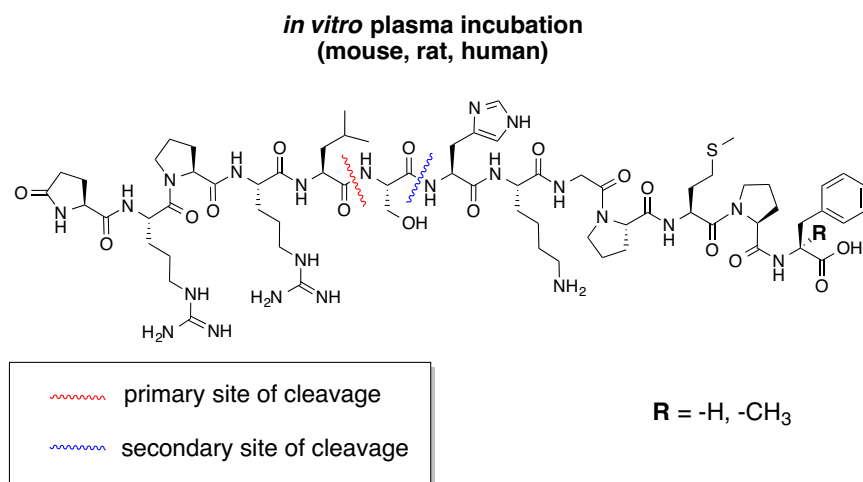
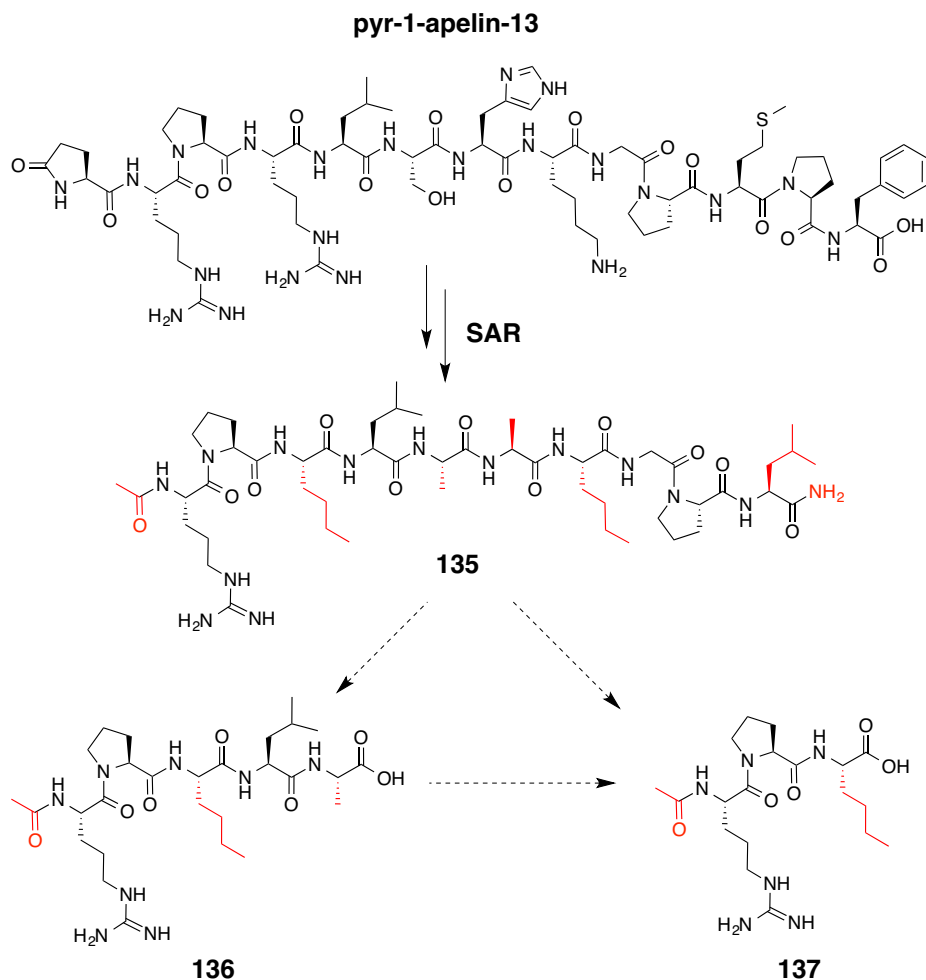


Figure 3.22 – Proposed pyr-1-apelin-13 pattern of fragmentation based on HPLC-MS analyses.¹⁴⁸

In contrast, Runyon and coworkers had performed structure-activity relationship studies on the apelin-13 scaffold, using an apelin-receptor induced calcium mobilization assay to guide analogue development.¹⁴⁹ Having arrived at optimized compound **135**, which removed the site of ACE2 hydrolysis altogether, the authors found that **135** was rapidly degraded *in vitro*, lasting less than 15 minutes when incubated in rat plasma. LC-MS and subsequent LC-MS/MS analyses confirmed the product peptides as **136** and **137**,

the acetylated penta- and tripeptides respectively (Scheme 3.8). This final conversion of **135** or **136** to final tripeptide product **137** aligned with our proposed Arg4-Leu5 site of protease degradation in the original apelin sequence. However, the replacement of the P1' Arg4 with Nle4 in compound **135** deviates largely from the native apelin structure.



Scheme 3.8 - Fragmentation of apelin analogue 135 *in vitro* in rat plasma.¹⁴⁹

A critical examination of these conflicting results was necessary before moving forward. Marsault and coworkers' results disagreed with our proposed Arg4-Leu5 cleavage site, but had been performed on samples after a considerable period of time (30

to 180 minutes)¹⁴⁸ and the fact that only LC-MS analyses had been performed gave no precise sequence analysis of the resultant peptide fragments. As well, the quantities of the resultant apelin and analogues fragments were not reported, analogous to our own LC-MS/MS experiments. Although Runyon and coworkers' ultimate location of proteolysis supported our proposed location of degradation, the substitution of Arg4 with Nle4 at the N-terminal location to the cleavage site raised concerns about the relevancy of an unnatural cleavage site.¹⁴⁹ Taking both experiments into account, we hypothesized that because our analyses on **104** were performed for shorter time periods than the Marsault study, our experiments minimized the role of non-specific exopeptidases. This prolonged exposure of pyr-1-apelin-13 and related analogues to mammalian plasma could result in the degradation of the initial 5-13 peptide fragment to the 6-13 octapeptide. However, a more thorough quantitative experiment would be required to definitively support this theory.

3.4.3 The synthesis of a fluorescent probe to aid in the activity-guided fractionation of human plasma

Due to the high complexity of mammalian plasma, we required a tool to aid in the activity-guided fractionation of the human plasma to isolate the desired protease. To identify the reported protease responsible for the N-terminal degradation of pyr-1-apelin-13 and **104** in human plasma, we envisioned applying a Förster resonance energy transfer (FRET) based assay to assist in the activity-guided fractionation of human plasma. By having a fluorophore and quenching moiety on opposing sides of a susceptible amide bond, the intensity of any fluorescent signal would be intramolecularly suppressed; upon protease-mediated cleavage of an internal amide bond, the inherent

fluorescence of the fluorophore would be increased (Figure 3.23). This synthetic fluorescent probe could be applied to human plasma and subsequent fractions to identify the presence of a protease with a defined sequence specificity. We decided to use the aminobenzoate (Abz) and 3-nitrotyrosine (NO₂Y) fluorophore/quencher pair due to their previous successes in the literature.^{150,151}

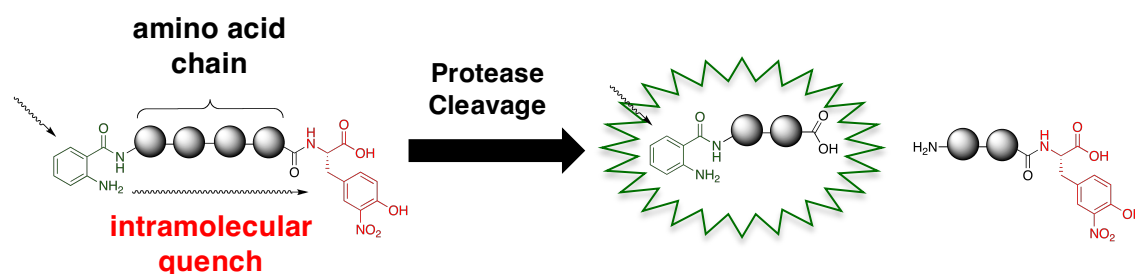
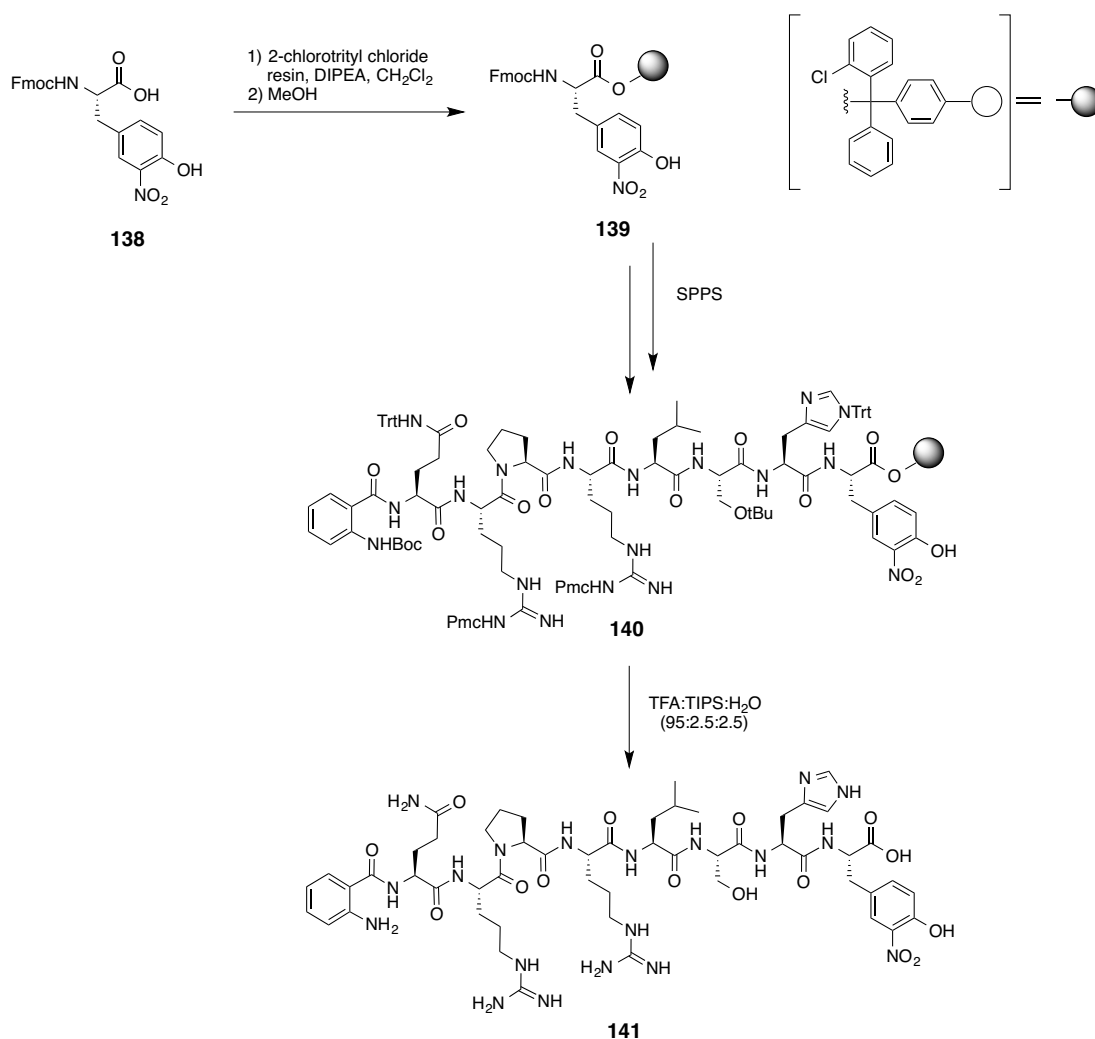


Figure 3.23 – General approach of FRET assay with fluorescent Abz moiety and intermolecular quencher 3-nitrotyrosine.

Fmoc-3-nitrotyrosine (**138**) was loaded onto 2-chlorotrityl chloride resin (**139**) and elongated by solid phase peptide synthesis through HATU/HOAt/DIPEA coupling conditions. A final coupling of 2-(Boc-amino)benzoic acid capped the N-terminus of the fluorescent probe (**140**). The 9-mer peptide **141** was liberated from resin with concomitant side chain deprotection in the presence of 95:2.5:2.5 TFA:H₂O:TIPS and was purified by C₁₈ RP-HPLC (Scheme 3.9).



Scheme 3.9 – Solid phase peptide synthesis of FRET probe 141.

To assess the ability of **141** to serve as an adequate fluorescent probe for the activity-guided purification of the unknown N-terminal apelin protease, we assessed its ability to be degraded in the presence of human plasma. The optimization of the excitation ($\lambda_{\text{ex}} = 325 \text{ nm}$) and emission ($\lambda_{\text{em}} = 420 \text{ nm}$) wavelengths for the Abz fluorophore within the **141** scaffold remained consistent with previous reports.¹⁵⁰ Incubation of this fluorescent probe in the presence of human plasma for 1 h at room temperature caused a significant increase in fluorescence compared to incubation in

sodium phosphate buffer (Figure 3.24). To serve as a positive control, **141** was incubated with trypsin for 1 h to cleave after either arginine moiety, showing the anticipated increase in fluorescence at 420 nm. A time-dependent increase in fluorescence was also observed upon the incubation of **141** in human plasma.

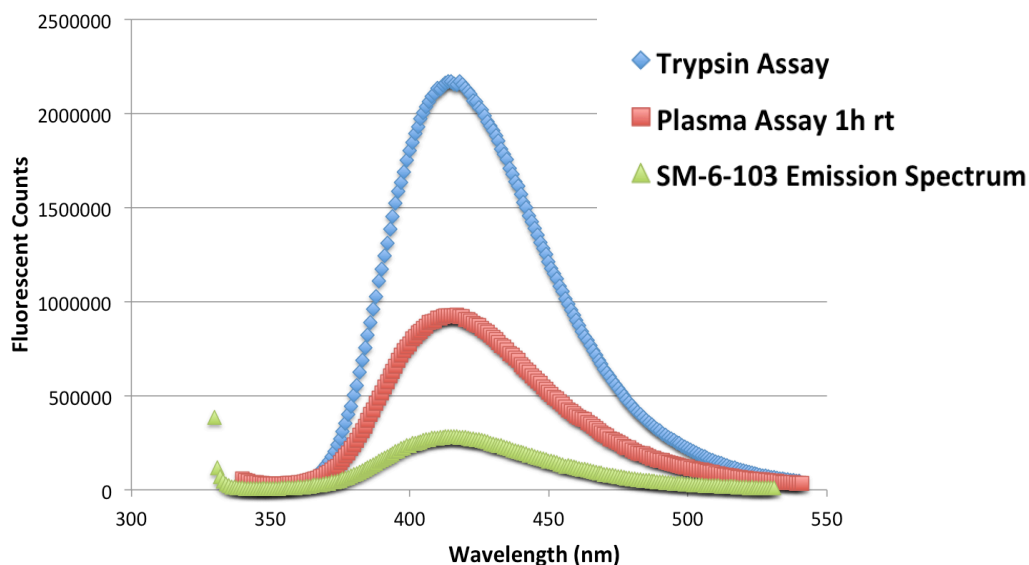


Figure 3.24 – Initial FRET assays with fluorescent probe 141. Probe **141** was incubated with plasma (red), trypsin (blue, positive control), and sodium phosphate buffer (green, negative control) for 1 h at room temperature.

With the initial success of human plasma cleaving **141**, we wanted to synthesize a more selective fluorescent probe with a smaller amino acid linker between the fluorophore and quenching units. Ms. Andrea Werny (Heritage Youth Researcher Summer Program Student, July – Aug 2014) aided in the synthesis of two additional shorter fluorescent probes by manual SPPS, containing 6 (**142**) and 5 (**143**) amino acids between these moieties. These shorter fluorescent probes would be more selective for

the predicted Arg4-Leu5 protease, provided the decreasing length between the unnatural amino acids does not perturb the recognition of the native cut site (Figure 3.25).

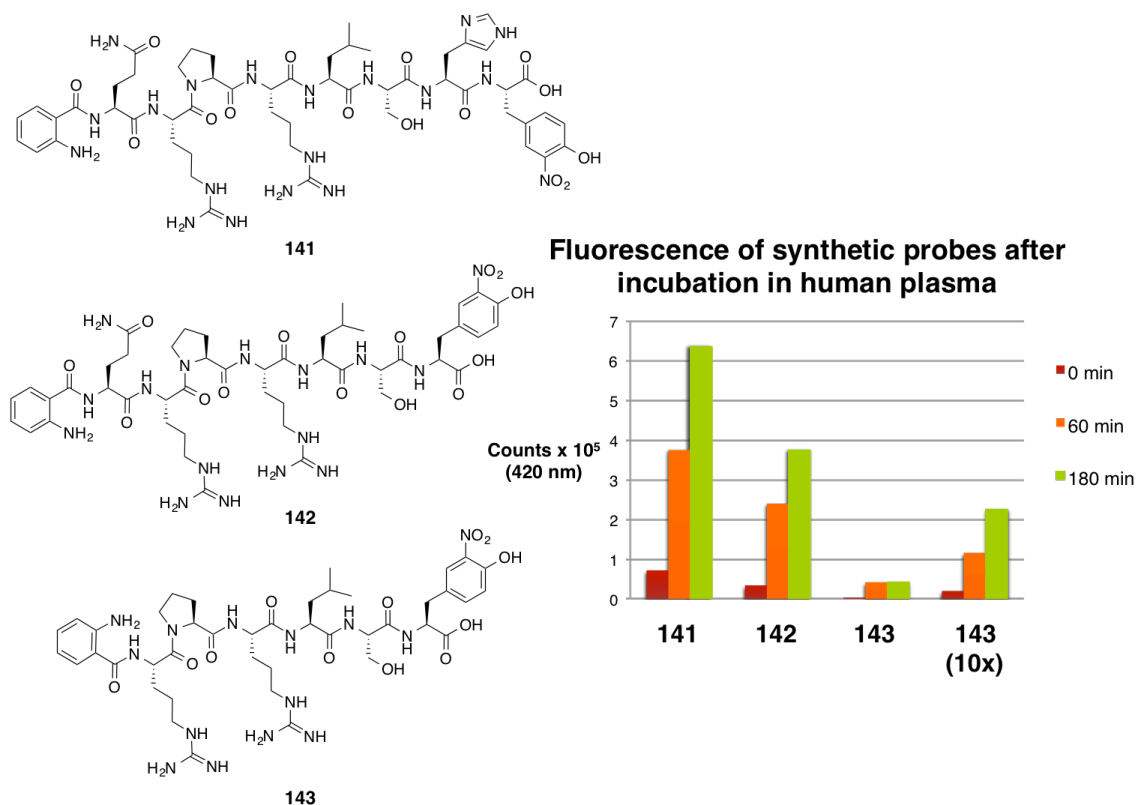
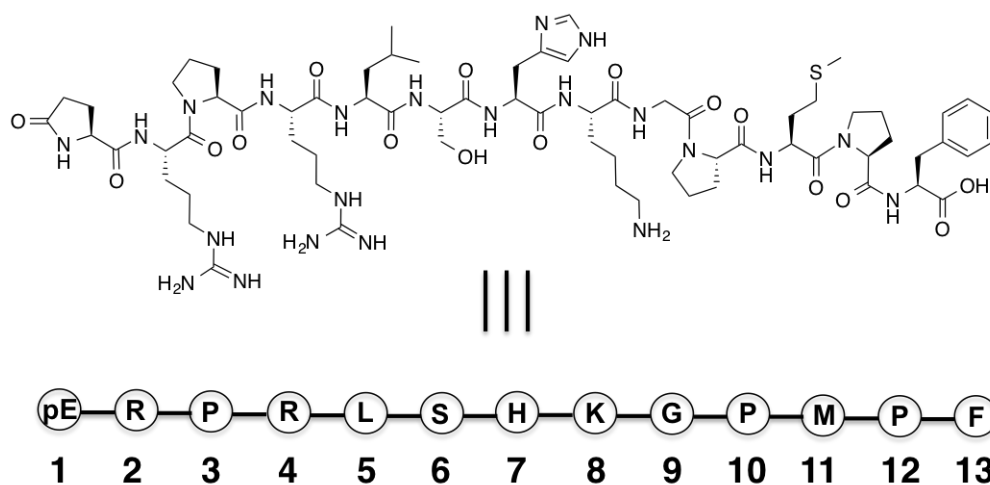


Figure 3.25 – Chemical structures of synthetic fluorescent probes 141, 142 and 143 (left), and their increased fluorescence after incubation in human plasma (right).

All three synthetic fluorescent probes showed a time-dependent increase in fluorescence after exposure to human plasma, albeit at 10x the concentration for the shortest analogue **143**. The largest increase in fluorescence over the assayed time was observed from the original **141** analogue and this was used for the activity-guided fractionation.

3.4.4 Activity-guided fractionation of human plasma

Prior to any fractionation, the amino acid sequence of native pyr-1-apelin-13 was inputted into the ExPASy Peptide Cutter tool (http://web.expasy.org/peptide_cutter/) to predict *in silico* any potential sites of protease degradation (Figure 3.26). A closer examination of literature enzymes with similar specificities for the N-terminal region of apelin yielded many enzymes with no known homologues in humans (thermolysin, clostripain, proteinase K).



Proteases that cut between Arg4-Leu5	Putative degradation site	Proteases that cut at other positions	Putative degradation site
Arg-C proteinase	2, 4	Chymotrypsin (low specificity)	5, 7, 13
Clostripain	2, 4	Lys C	8
Thermolysin	4, 12	Lys N	7
Trypsin	4, 8	Pepsin	5
		Proline-endopeptidase	3
		Proteinase K	5

Figure 3.26 – ExPASy predicted degradation sites of pyr-1-apelin-13. Putative degradation positions are located C-terminal to amino acid residue number.

During the activity-guided fractionation process, fluorescent probe **141** was incubated with the plasma fractions and compared to **141** incubated in sodium phosphate buffer (negative control) over the same period of time. The comparison of the fluorescence of plasma fractions to the negative control would help to determine the presence of any proteases capable of hydrolyzing the suspect amide bond.

To initiate the activity-guided fractionation of human plasma, 20% and 40% ammonium sulfate precipitations were performed, generating three fractions, the 20% and 40% cuts and the remaining 40% ammonium sulfate supernatant. All fractions were desalted prior to incubation with **141**, and a dramatic increase in Abz fluorescence was observed in the 40% ammonium sulfate pellet (40% ASP) compared to the other fractions (Figure 3.27). Subsequent repetitions of this experiment validated this observation, and it was also observed that by-passing the 20% ammonium sulfate step led to a quicker inactivation of this increase in fluorescence. This 40% ASP was further separated using G100 size exclusion chromatography, and the strongest increase in fluorescence after incubation with **141** was observed on the right side of the major chromatogram peak. SDS-PAGE analyses were performed on the most active size exclusion fractions to assess their relative purity, but substantial protein co-elution was observed. Despite this, trypsin digestion was done on the most active size exclusion fractions and LC-MS/MS analyses were performed with the assistance of Ms. Jing Zheng (University of Alberta Mass Spectrometry Lab). Mascot database searching on the resulting fragments gave a large number (~50) of protein hits, but the presence of a sequence matching 'kininogen-1 isoform 2' was a particularly interesting discovery. This protein is involved in the processing of bradykinin via tissue

kallikrein/kininogenin/endoproteinase Arg-C/KLK1. As this enzyme had been previously identified as a potential protease candidate *in silico*, this coincidence was not to be overlooked.

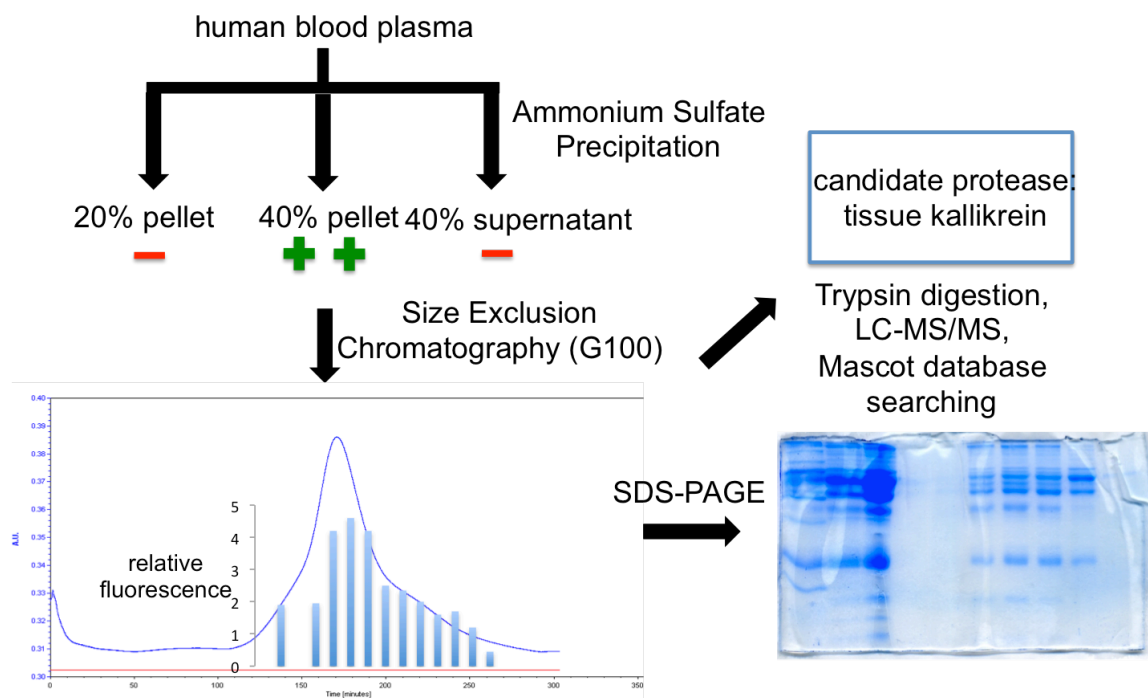


Figure 3.27 – Activity-guided fractionation of human plasma using FRET-based assay with fluorescent probe 141.

Additional experiments to elucidate the identity of the human plasma protease were also performed on the 40% ASP. Ion-exchange chromatography was a good option to further resolve contaminating proteins from the desired protease based on the isoelectric point (pI) of the protein. Although the pI would be unknown for this protease, it could be experimentally determined through an incubation assay with ion-exchange resins at varying pHs (Figure 3.28). Aliquots of strong anion exchanger Q-sepharose and strong cation exchanger SP-sepharose were equilibrated in Tris buffer at pHs between

5.0 to 9.0 varying by 0.5 pH increments. The 40% ASP was applied to these ion exchange resins and incubated for 30 minutes, finally pelleting the resin and any bound proteins by centrifugation. Unbound proteins would remain in the supernatant and could be assayed for the ability to cleave the fluorescent substrate **141** in the FRET assay, thereby giving an approximate pI for the unknown protease. To account for the effect of pH on the change in fluorescence of the Abz moiety and on the unknown plasma protease, the activities of the ion exchange resin-incubated supernatants were compared to samples of **141** incubated in buffer only (negative control), or **141** incubated in buffer with an equivalent volume of 40% ASP (positive control).

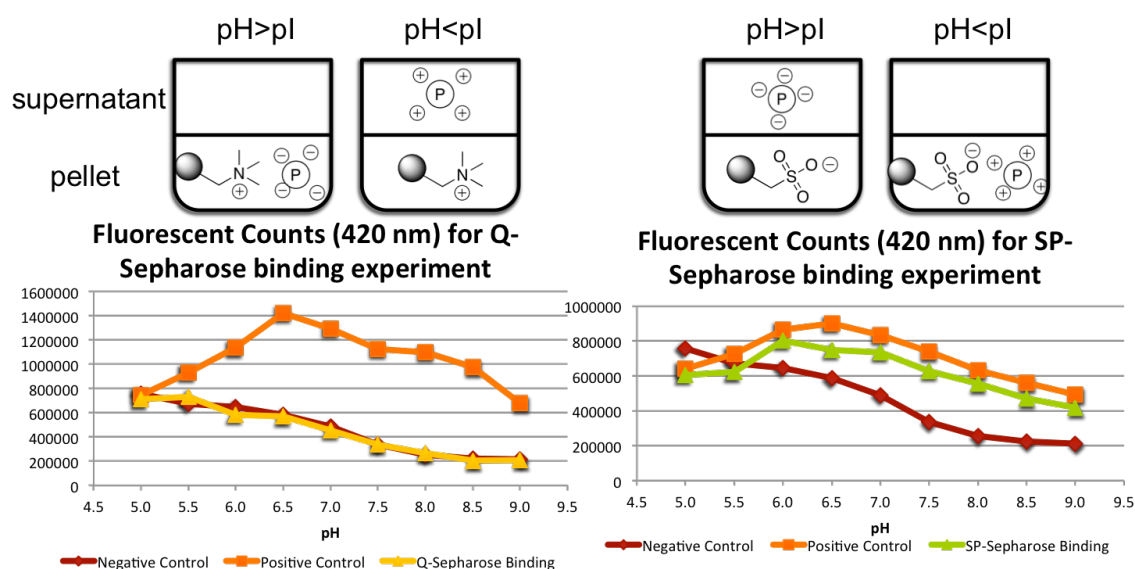


Figure 3.28 – Isoelectric point approximation of unknown plasma protease in 40% ASP fraction. Incubation of 40% ASP with Q-sepharose anion exchange resin (yellow) and SP-sepharose strong cation exchange resin (green) were compared to the incubation of 141 at varying pH (red) and with 40% ASP at varying pH (orange).

Strong anion exchange chromatography experiments with Q-sepharose were initially performed, showing a minimal difference between the Q-sepharose supernatant

(yellow line, Figure 3.28) and the native fluorescence of **141** (red line, Figure 3.28) at pHs above 5.5. However, because the plasma protease showed no ability to cleave the fluorescent substrate at pH 5.0, further analysis of the pI using Q-sepharose resin would not be helpful. By switching to the strong cation exchange resin SP-sepharose and repeating the same experiment, the ability of the plasma protease to cleave fluorescent probe **141** in the supernatant of the SP-incubated 40% ASP (green line, Figure 3.27) was restored between pH 5.5 and 6.0. This indicates that at a more basic pH, the plasma protease is repelled from the SP-sepharose and remains unbound in the supernatant. From these results, we predicted a rough pI of the plasma protease being between pH 5.5 and 6.0. Despite these interesting results, efforts towards applying ion exchange chromatography to the activity-guided fractionation of human plasma were unsuccessful. Scaling up the amount of 40% ASP applied to the resin prevented the protease from binding and eluting at compatible pHs to retain physiological activity. When comparing this to the *in silico* predicted pI of 4.7 for monomeric KLK1 (based solely on amino acid sequence without any additional posttranslational modifications), our experimental result was within an order of magnitude of our protease candidate.

The 40% ASP was also used for preliminary inhibition experiments to crudely assign a protease family to our unknown protease could belong to. Five compounds were selected for their various selective inhibitory properties: sulfonyl fluorides AEBSF (**144**) and PMSF (**145**) for serine proteases; EDTA (**146**) for metalloproteases; IA (**147**) for cysteine proteases; and finally TCEP (**148**) to determine the importance of structure-inducing disulfide bonds. Fluorescent probe **141** was incubated with 1 mM inhibitor in

buffer (negative control) or with 40% ASP fraction and 1 mM inhibitor (n = 2) and the relative increase in fluorescence was assessed (Figure 3.29).

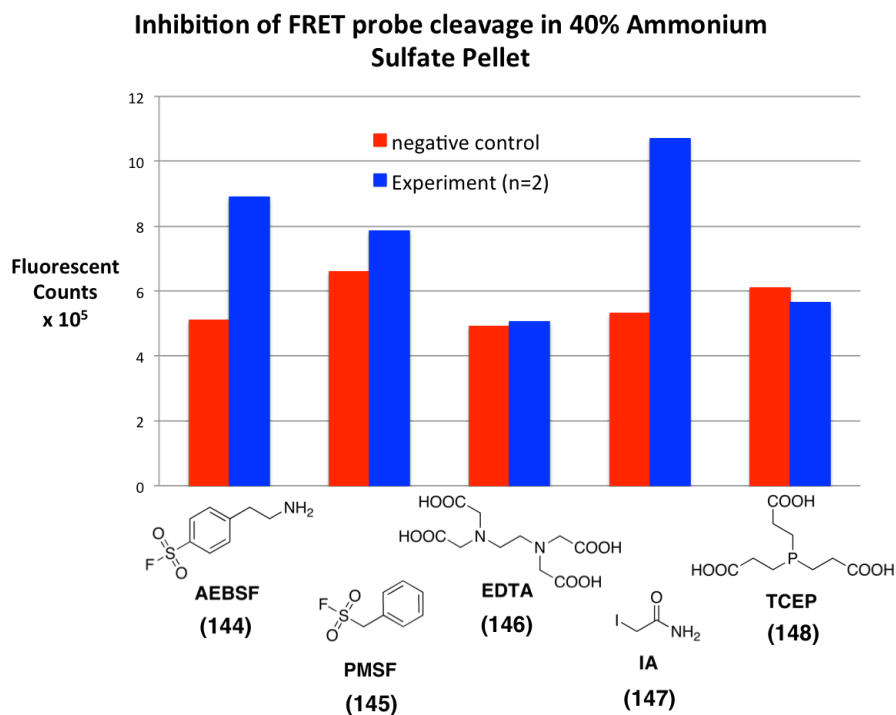


Figure 3.29 – Inhibition experiments performed on 40% ASP fraction. Inhibitors used included: 1 mM of AEBSF and PMSF (serine protease inhibitors); EDTA (metalloprotease inhibitor); IA (cysteine protease inhibitor); and TCEP (disulfide reducing agent).

The presence of both EDTA and TCEP were highly detrimental for the ability of the plasma protease to cleave **141**, while showing no increase in Abz fluorescence over the negative control. AEBSF and IA seemed to have no inhibitory effect on the 40% ASP fraction, while PMSF showed a reduced difference between the experiment and negative control. These results suggested that the unknown plasma protease responsible for apelin N-terminal degradation could be a metalloprotease with significant disulfide bonds, or potentially another type of protease with bound metal ions required

for activity. Marsault and coworkers also noted the disappearance of any N-terminally truncated apelin fragments after *in vitro* rat plasma treatment with either EDTA or 1,10-*o*-phenanthroline.¹⁴⁸ Our proposed protease candidate, KLK1, a serine protease, was inhibited by PMSF,^{152,153} but despite having five disulfide bridges, had remarkable stability and activity in the presence of reducing agent DTT at extremely high concentrations (20 mM).¹⁵⁴ The effect of iodoacetamide or EDTA on KLK1 had not been assessed in the literature, but select activity stimulation of KLK1 in the presence of Ca²⁺ ions had been reported.¹⁵⁵ We hypothesize that the chelation of essential calcium ions by EDTA could potentially have an impact on the activity of KLK1, partially explaining this inhibition.

3.4.5 Kallikrein experiments identifying degradation

While not all experimental parameters perfectly matched that of tissue kallikrein, enough circumstantial evidence had accumulated to support KLK1 as a protease candidate in the N-terminal degradation of apelin. Physiologically, kallikrein enzymes are a family of serine proteases distributed throughout the human body and separated into 15 unique tissue kallikreins (KLK1-15) and one plasma kallikrein (KLKB1).¹⁵⁶ KLK1 is most notably involved in the liberation of (lys)bradykinin, a vasoactive peptide hormone, from high-molecular weight kininogen (HMWK). There is considerable cross talk between the regulation of the kinin, angiotensin and apelin pathways by ACE2,¹²⁴ and both angiotensin and bradykinin are substrates for angiotensin-converting enzyme (ACE). Additional interplay between these cardiovascular pathways is seen between the heterodimerization of the apelin receptor with both the angiotensin II¹⁵⁷ and bradykinin¹⁵⁸ receptors in cell cultures. This receptor

oligomerization has an inhibitory impact on the action of angiotensin II,¹⁵⁹ but seems to enhance the physiological effects associated with bradykinin GPCR activation.¹⁵⁸ Considering these factors, plus the identification of kininogen-1-isoform 2 from the LC-MS/MS activity-guided purification of human plasma, it seemed reasonable to investigate the ability of KLK1 to serve as a regulatory protease for effects of apelin.

Initially, the mouse homologue of tissue kallikrein, mouse-submaxillary Arg-C endoproteinase (Boehringer Mannheim), was obtained and a preliminary assay with pyr-1-apelin-13 and other analogues were set up. To our surprise, pyr-1-apelin-13, apelin-17 and pyr-1-apelin-13 analogues **104** and **106** were nearly completely converted to the 5-13 fragment after 90 minutes incubation at 37 °C after MALDI-TOF analysis. By prolonging the incubation time to 24 h, no traces of the parent 1-13 peptide were seen and the 5-13 fragment had additionally been degraded by one amino acid to the 6-13 piece. C₁₈-RP-HPLC was used to separate these peptide fragments (Figure 3.30), and their sequences were confirmed by LC-MS/MS. These experiments support our proposed Arg4-Leu5 cut site, but also agreed with the results observed by Marsault *et al.*,¹⁴⁸ in which prolonged plasma incubation times produced an accumulation of the 6-13 apelin fragment.

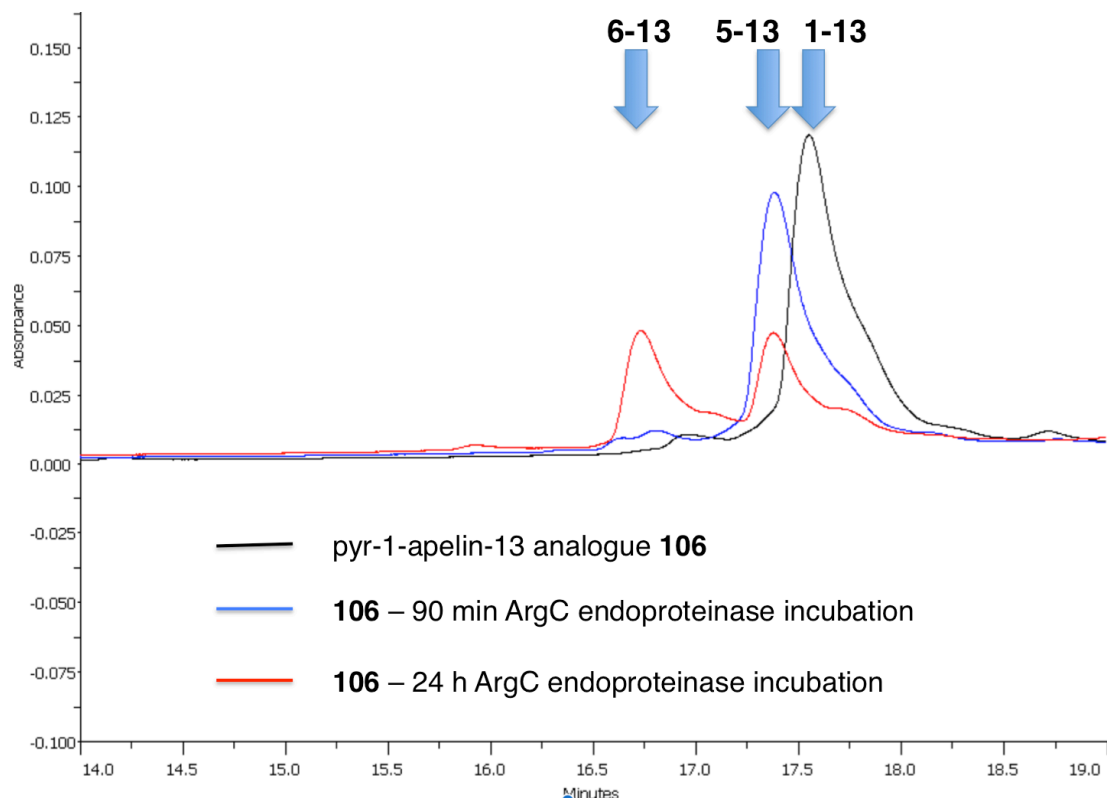


Figure 3.30 – Analytical C₁₈ RP-HPLC traces of pyr-1-apelin-13 analogue 106 with mouse Arg-C endoproteinase at 37 °C. Arg-C endoproteinase incubation times: black - 0 minutes, blue - 90 minutes, red - 24 h.

With the success of the mouse kallikrein experiments, recombinant human tissue kallikrein (KLK1) and plasma kallikrein (KLKB1) were obtained from a commercial supplier (R&D systems). Because both kallikrein enzymes have high inherent proteolytic activity and are capable of cleaving themselves in solution, they were supplied in an inactive prokallikrein zymogen form. The presence of an additional enzyme, bacterial thermolysin, cleaves the N-terminus of the zymogen, converting the kallikrein into its active form. To avoid additional kallikrein degradation, thermolysin is quenched by the addition of EDTA or 1,10 *o*-phenanthroline for KLKB1 and KLK1 respectively, chelating the required zinc ion away from the metalloprotease. The extent

of kallikrein activation was assessed with kallikrein-specific substrate PFR-AMC (Bachem, **149**). Proteolysis of **149** by activated kallikrein hydrolyzes the C-terminal amide bond, liberating tripeptide **150** from fluorophore 7-amino-4-methylcoumarin (**151**). The fluorescence of **151** can then be used to assess the proteolytic activity of the enzyme (Figure 3.31 A). Treatment of both KLKB1 and KLK1 with thermolysin successfully activated both enzymes (Figure 3.31 B-C).

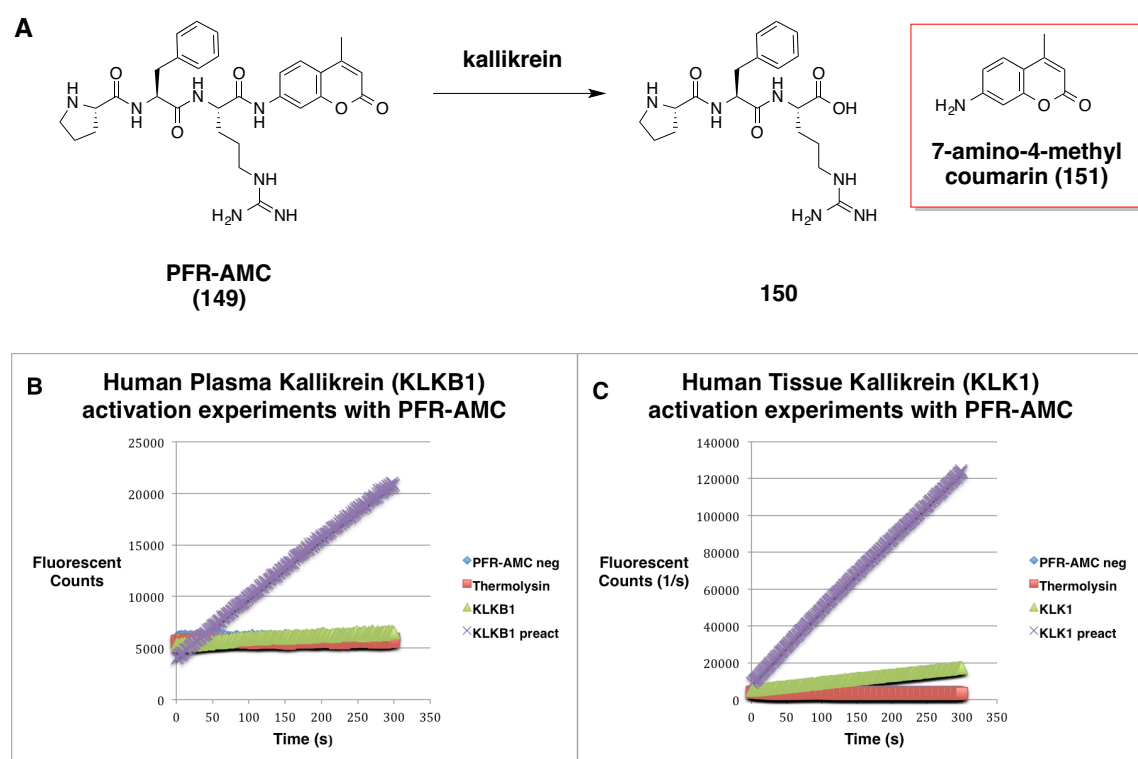


Figure 3.31 – Kallikrein activation assay. A) Scheme for PFR-AMC (**149**) cleavage by kallikrein, liberating fluorophore 7-amino-4-methylcoumarin (**151**). Fluorescent counts over time for thermolysin activation experiments with B) recombinant human plasma kallikrein (KLKB1) and C) tissue kallikrein (KLK1). In both activation experiments, PFR-AMC is incubated with: buffer (negative control) – blue; thermolysin – red; zymogen kallikrein – green; and thermolysin-treated kallikrein (preactivated kallikrein) – purple.

With active KLKB1 and KLK1 in hand, the ability of these enzymes to cleave pyr-1-apelin-13 and apelin-17 was examined. *In vitro* kallikrein assays and corresponding control experiments were incubated in buffer (50 mM Tris pH 7.5, 250 mM NaCl) at 37 °C overnight (18 h for KLKB1, 24 h for KLK1), using MALDI-TOF to analyze peptide fragments (Table 3.7).

The KLKB1 experiments showed no activity towards the shorter pyr-1-apelin-13 substrate under any conditions examined. In contrast, KLKB1 cleaved apelin-17 between Arg3-Arg4 in the N-terminal extension that differentiates the two isoforms. This activity was observed regardless of enzyme activation by thermolysin, as apelin-17 incubation with zymogen KLKB1 showed a MALDI-TOF peak for the 4-17 fragment as well. However as this was not our desired site of proteolysis, this result was not further investigated at this time.

From the right-hand side of Table 3.7, the degradation of pyr-1-apelin-13 and apelin-17 was observed in the activated form of KLK1 at the predicted Arg-Leu location, and subsequent N-terminal degradation was observed to form the C-terminal nonapeptide and octapeptides (5-13 and 6-13 using pyr-1-apelin nomenclature) respectively. However, a similar peptide fragmentation was observed when incubating exclusively thermolysin with either apelin isoform. This was not entirely surprising as thermolysin was identified earlier by the ExPASy *in silico* analysis of putative proteolytic sites in the pyr-1-apelin-13 scaffold. The addition of metalloprotease-specific inhibitors EDTA or 1,10-phenanthroline in the activations of KLKB1 and KLK1 respectively, prevented thermolysin-mediated apelin degradation *in vitro* in the absence of any kallikrein.

Table 3.7 – *In vitro* KLKB1 (left) and KLK1 (right) experiments with apelin substrates. Legend: 13 = pyr-1-apelin-13, 17 = apelin-17, K = kallikrein, T = thermolysin, activated K = kallikrein pre-incubated with thermolysin prior to thermolysin inhibitor addition.

Experiment	KLKB1 assay conditions	Cleaved?	MALDI Products	KLK1 assay conditions	Cleaved?	MALDI Products
13 (-)	13	No	-	13	No	-
13 K	13 zymogen K	No	-	13 zymogen K	No	-
13 T	13 T	Yes	1-13 5-13 6-13	13 T	Yes	1-13 5-13 6-13
13 T-inhib	13 T EDTA	No	-	13 T 1,10- phenanth.	No	-
13-KT	13 activated K	No	-	13 activated K	Yes	1-13 5-13 6-13
17 (-)	17	No	-	17	No	-
17 K	17 zymogen K	Yes	4-17 1-17	17 zymogen K	No	-
17 T	17 T	Yes	9-17 10-17 1-8 1-9	17 T	Yes	9-17 10-17 1-8 1-9 1-17
17 T-inhib	17 T EDTA	No	-	17 T 1,10- phenanth.	No	-
17-KT	17 activated K	Yes	4-17 1-17	17 activated K	Yes	9-17 10-17 1-8 1-9 1-17

To ensure that only the activated kallikrein was degrading the apelin substrate, similar *in vitro* assays were performed in which apelin substrates were exposed to

thermolysin at varying concentrations of inhibitor. EDTA inhibited thermolysin cleavage at all dilutions tested, validating KLKB1 as a relevant protease for the degradation of apelin-17. However, as the concentration of 1,10-phenanthroline was diluted, thermolysin-mediated cleavage of apelin re-appeared in the absence of KLK1, indicating that 1,10-phenanthroline is not completely inhibiting the proteolytic activity of the bacterial metalloprotease. It should be noted that all dilutions of 1,10-phenanthroline used involved the presence of superstoichiometric quantities of the inhibitor. Substituting 1,10-phenanthroline with EDTA in the activation of KLK1 has successfully cleaved apelin at the desired Arg4-Leu5 position. However, the activity of KLK1 in the presence of EDTA is dramatically reduced after 24 h incubation time at 4 °C based on the proteolysis of fluorescent substrate **149**. Dr. Conrad Fischer and Mr. Fabricio Mosquera are currently optimizing the activation protocol of KLK1 to fully inhibit thermolysin, yet retain active kallikrein over an extended time period.

One additional discrepancy in results obtained from the human and murine enzyme assays is that the rate of KLK1 proteolysis is very slow in comparison to the mouse ArgC endoproteinase enzyme. This may be due to sub-optimal enzyme conditions or a difference in glycosylation states of the recombinant KLK1 protein. Because of the age of the mouse protease sample used in these experiments, no information was available to determine if this enzyme was activated with a secondary enzyme such as thermolysin, and tryptic digestion of the ArgC enzyme and LC-MS/MS identification of peptide fragments was unfortunately inconclusive. Despite this ambiguity, I believe that KLK1 is still an appropriate protease candidate for the N-terminal degradation of apelin. Additionally, analogous to KLK1 activation by

thermolysin, one of the numerous biological enzymes that regulate the activity of KLK1 may be an additional plasma protease responsible for this degradation.

3.4.6 Quantification of *in vitro* human plasma degradation products of ACE2-resistant apelin analogues

One question that remained was the identification of the precise location of this N-terminal plasma protease and quantitative assessment of peptide fragments remaining after *in vitro* incubation of apelin in human plasma. In collaboration with Mr. Bela Reiz and Dr. Angelina Morales-Izquierdo (University of Alberta Mass Spectrometry Laboratory), we used an LC-MS assay to quantify the relative changes of fragments of pyr-1-apelin-13 A2 (**104**) and apelin-17 A2 (**108**) analogues at shorter time points than those previously examined.¹⁴⁸ A2-substituted apelin analogues were used to negate the inherent action of ACE2 in the degradation of apelin. The addition of non-canonical amino acids, particularly the bromine atom in the *p*-bromophenylalanine, made the identification of C-terminal A2 fragments unique from background peptide fragments due to the isotope distribution pattern of the bromine atom. These experiments would support the location and relative significance of endoproteinase cleavage, and potentially identify additional sites of protease-mediated cleavage *in vitro* in plasma.

Plasma samples were pre-incubated at 37 °C to simulate physiological conditions prior to the addition of ACE2-resistant analogues **104** or **108**. Aliquots (25 µL) were removed immediately following apelin analogue addition, and then again every 10 minutes. After the addition of internal standard dansyl-YVG (**81**), acidic work up, and purification by Harvard Apparatus C₁₈ spin columns, samples were analyzed by LC-

MS. A database was prepared with all potential single protease cleavage permutations of **104** and **108** for rapid analysis of peptide fragments.

We had initially planned on using strictly an LC-MS methodology to quantify the peptide fragments over time, but significant co-elution of peptide fragments was observed, particularly with analogue **108**. Instead, the extracted ion chromatograms (EIC) were isolated for each apelin fragment based on their predicted masses and molecular formulae by MassHunter software. Although typically not a quantitative measurement, the EIC counts were used to directly compare the relative amounts of individual apelin peptide fragments over the course of time, while negating the differences in ionization ability of different peptide fragments.

Unfortunately, the incubation of pyr-1-apelin-13 A2 analogue **104** with human plasma *in vitro* did not help to resolve the ambiguity surrounding the N-terminal protease location. Although observed in small quantities, our proposed 1-4 and 5-13 fragments, shown in red and pink respectively (Figure 3.31), did not seem to increase over time or be particularly relevant. By comparison, the 1-5 and 6-13 fragments, shown in dark and light green respectively, had significantly higher EIC quantities over all time points analyzed; however these peptide fragments did not seem to increase over the course of the experiment. The action of non-specific exopeptidases could explain the lack of increase in the 1-5 and 6-13 peptide fragments over time, but the products of this degradation (1-4, 7-13) did not increase either. These results did not add any additional evidence to our claim that Arg4-Leu5 is a significant site of proteolysis at short time points, although these *in vitro* experiments may not necessarily represent the entire physiological perspective.

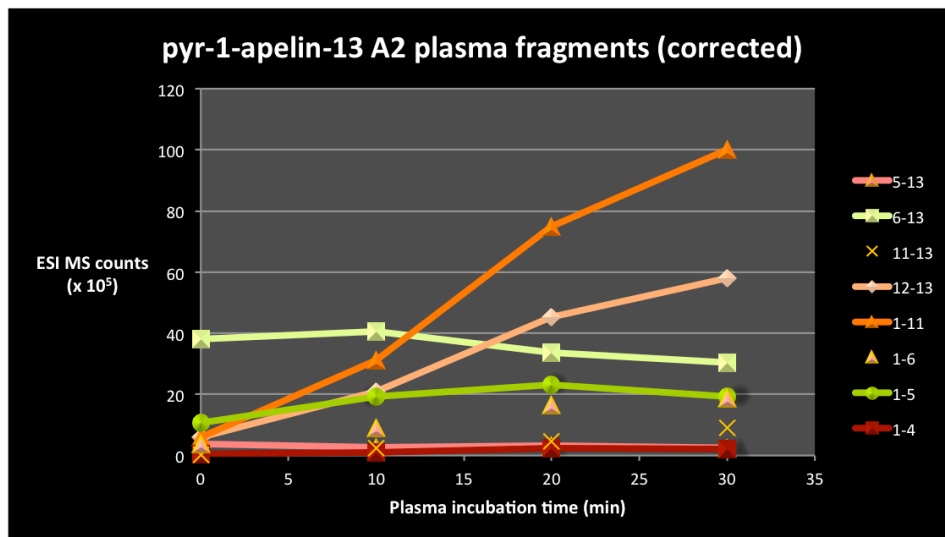
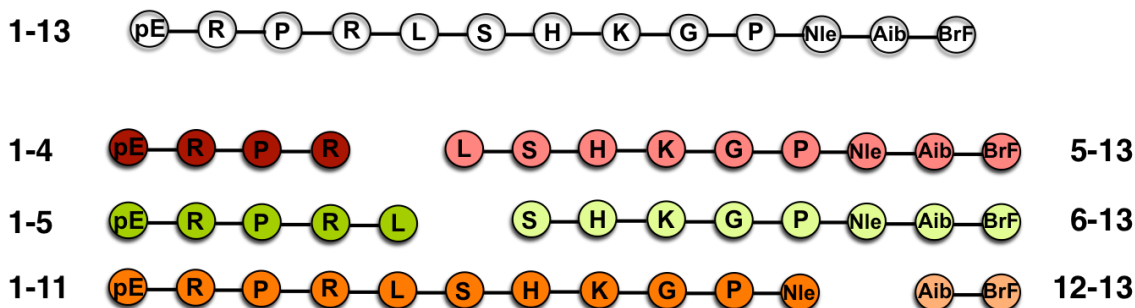


Figure 3.32 – Quantification of major peptide fragments of pyr-1-apelin-13 A2 (104) by LC-MS and EIC following the incubation in human plasma for 0 – 30 minutes.

One interesting result was the observation of an additional C-terminal site of degradation between Nle11-Aib12, which had previously been observed with murine *in vitro* plasma incubation (Section 3.4.1). Peptide fragments 1-11 and 12-13 (dark and light orange respectively, Figure 3.31) significantly increased over time, implying a specific endoprotease recognition and degradation. Due to the fact that this site of proteolysis is flanked by two unnatural amino acids, it may not be relevant in the physiological processing of pyr-1-apelin-13. However, it may be relevant for limiting the physiological activity of our ACE2 resistant analogue and represents an area for

future investigation. These experiments were performed in triplicate to minimize erroneous results; while data from a single run is shown in Figure 3.32, the trends for this data remained consistent throughout.

Identical experiments performed for apelin-17 A2 analogue **108** highlighted a different degradation pattern to that observed with pyr-1-apelin-13 A2 analogue **104** (Figure 3.33). The corresponding N and C-terminal Arg-Leu-Ser cleavages were not seen in appreciable quantities in these time-course plasma experiments, indicating that these protease locations are less significant for the degradation of **108**. Similar to the pattern observed with **104**, C-terminal dipeptide 16-17 (light orange) increased over the time course examined. The remaining N-terminal 1-15 fragment was not seen at any time point, suggesting that this C-terminal dipeptide removal is secondary to an additional degradative pathway. Analysis of the other major fragments highlighted the relevance of nonspecific aminopeptidases in the breakdown of **108**. Aminopeptidases were hypothesized to play a more dominant role in the amount of remaining apelin-17. This was based on the ACE2 knock out studies in mouse plasma (Section 3.2), and minimal difference in apelin-17 A2 stability compared to native apelin-17 in human plasma (Section 3.3). Significant N-terminal truncation was observed, with sequential amino acid removal occurring from 2-17 (light green) down to the 6-17 fragment (yellow). Subsequent truncations past 6-17 (7-17, 8-17, . . .) were observed in minor quantities, but did not show an increase in ion count over the monitored time. However, the largest increase was seen for **108** fragment 4-17 (dark red), especially between the 0 and 10-minute time points. Fortunately, tripeptide 1-3 (pink) was just hydrophobic enough to be retained on the C₁₈ LC column, and EIC quantitation showed a

corresponding linear increase in the amount of peptide. Based on these results, we propose an endoproteinase cleavage site between Arg3-Arg4 in **108**. This had previously been shown to be the precise location of plasma kallikrein (KLKB1) degradation of apelin-17 *in vitro*, and we believe that this highlights a role of KLKB1 in the breakdown of apelin-17. The full physiological role of KLKB1 in apelin degradation still remains to be studied.

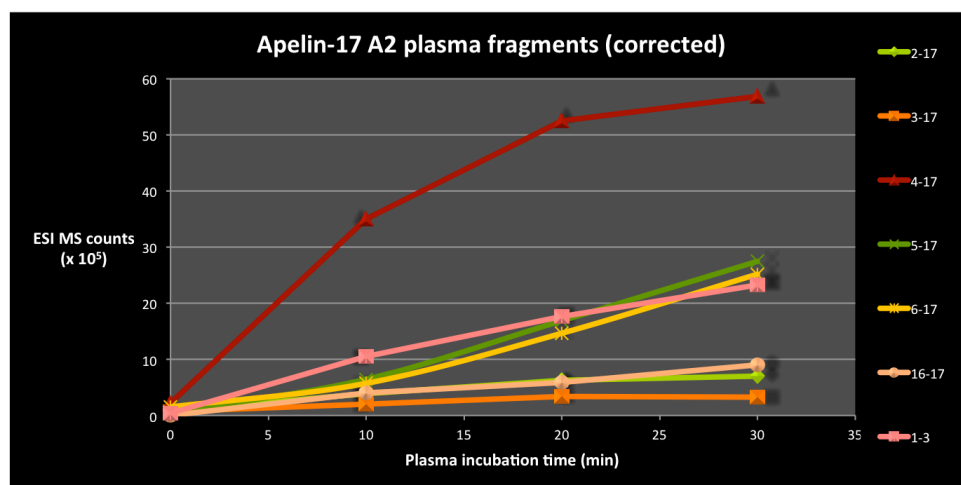
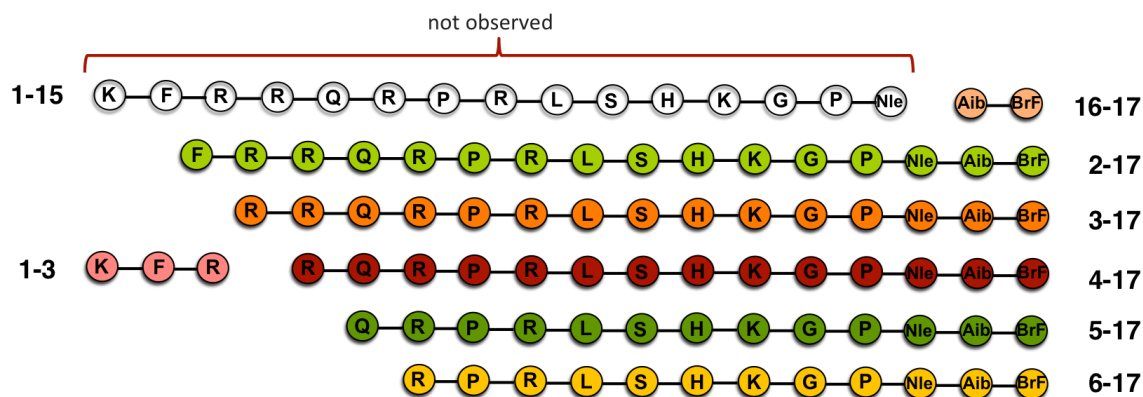


Figure 3.33 – Quantification of major peptide fragments of apelin-17 A2 (108) by LC-MS and EIC following the incubation in human plasma for 0 – 30 minutes.

After the identification of a cleavage site between Arg3-Arg4 (red) and Nle15-Aib16 (blue) in apelin-17 A2 analogue **108**, we wanted to determine the relative order of

degradation (Figure 3.34), also taking into account the inherent activity of non-specific aminopeptidases (black). The MassHunter Qualitative analysis software was adapted to search for the products of multiple protease degradations, showing an increase in **108** fragment 6-15 over time. No 4-15 or 5-15 pieces were observed from these searches, implying that Arg3-Arg4 proteolysis (red arrow) happens first, followed by sequential aminopeptidase degradation (black arrows). Finally, C-terminal dipeptide excision (blue arrow) would be done, as all peptide fragments along this degradation pathway have been identified.

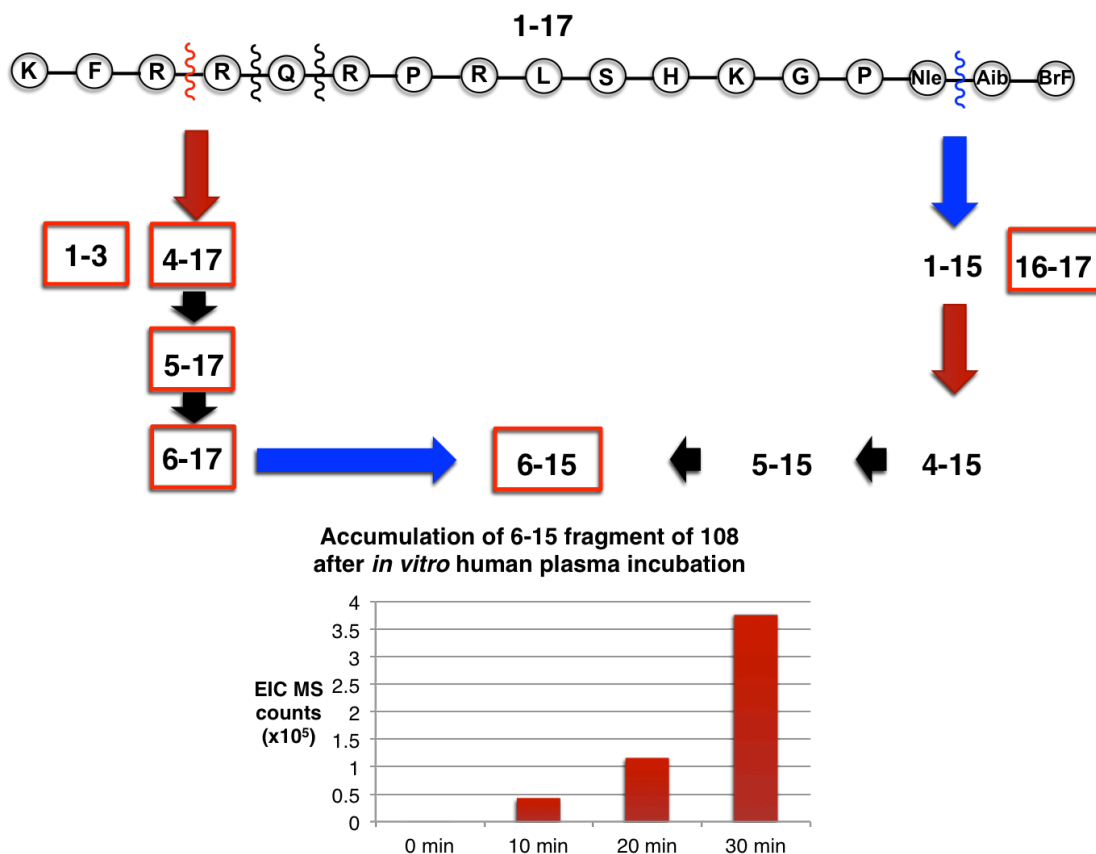


Figure 3.34 – Proposed degradation pathway of apelin-17 A2 analogue 108 for *in vitro* human plasma. Two alternative pathways to the accumulation of fragment 6-15 are shown, beginning with either Arg3-Arg4 proteolysis (red arrow, left) or Nle15-Aib16 proteolysis (blue arrow, right) with sequential aminopeptidase degradation shown with black arrows. Peptide fragments identified by MassHunter analysis are highlighted with red boxes.

Although these short time course plasma experiments did not support our hypothesis that a significant endoprotease cut site exists between Arg-Leu in the apelin backbone, it opens up additional areas to explore for the future stabilization of apelin peptides. It also highlighted the putative importance of plasma kallikrein, or a protease with related specificity, as a candidate for the breakdown of apelin-17 in human plasma. The proteolysis of peptides *in vitro* may also not be a complete representation of the *in vivo* physiological process, as has been observed before in the discrepancies observed between rat *in vitro* and *in vivo* apelin processing.¹⁴⁸ However, it represents a good platform for further development and investigation. In summary, these experiments have led to the proposal of three distinct novel locations of endopeptidase activity, of which two putative protease candidates are hypothesized (Figure 3.35). The identity of the C-terminal dipeptidase, which was shown not to be angiotensin converting enzyme, is currently under investigation by Mr. Fabricio Mosquera.

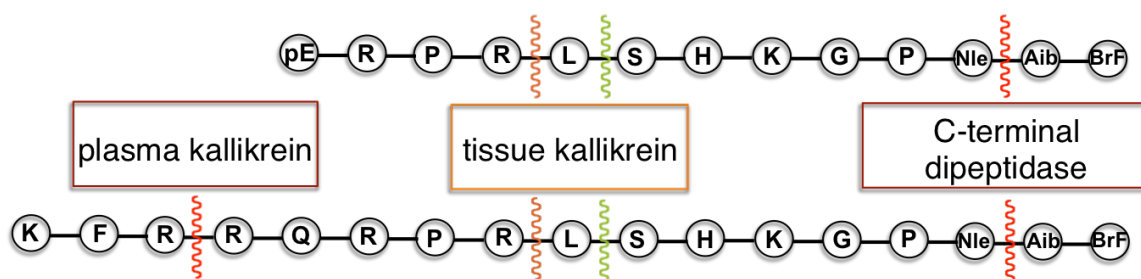


Figure 3.35 – Proposed sites of endopeptidase degradation of pyr-1-apelin-13 A2 analogue 104 and apelin-17 A2 analogue 108.

3.5 Synthesis of Arg-Leu analogues

3.5.1 Introduction and synthetic targets

In order to improve the stability of apelin analogues against the action of the N-terminal protease, a variety of structural modifications surrounding our predicted Arg-Leu amide bond were envisioned. Because of the recent discovery and ambiguity in literature as to the precise location of the exact site of proteolysis,^{148,149} extensive SAR studies had yet to be performed at this N-terminal position of pyr-1-apelin-13. We proposed to use a variety of accessible synthetic modifications at amino acid residues surrounding our proposed Arg-Leu degradation site, including the incorporation of: D-amino acids; N-methylations; α -methylations; and aza-analogues (Figure 3.36).

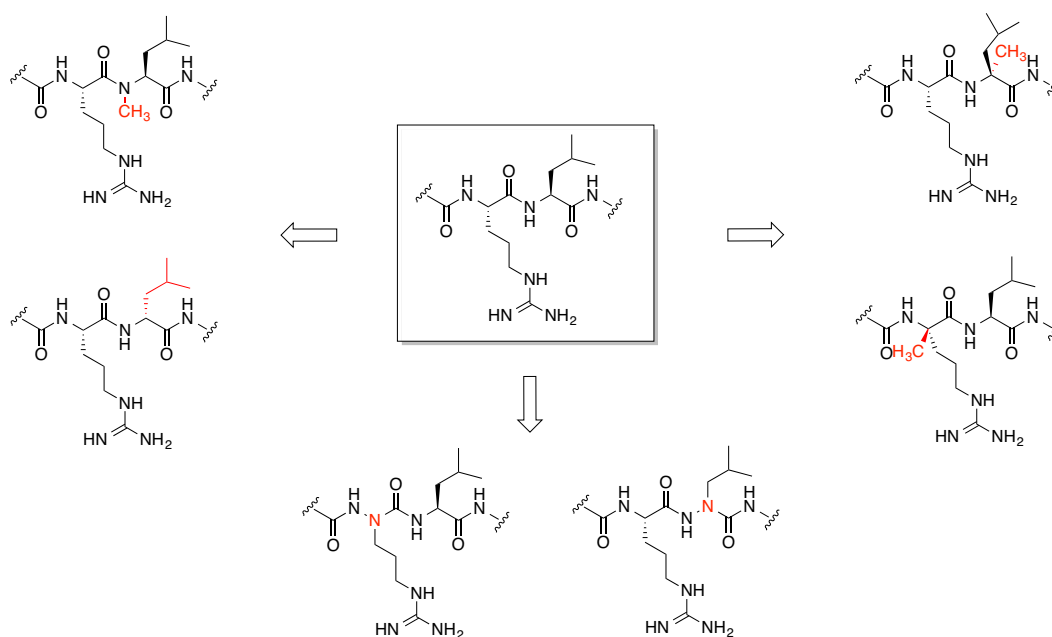
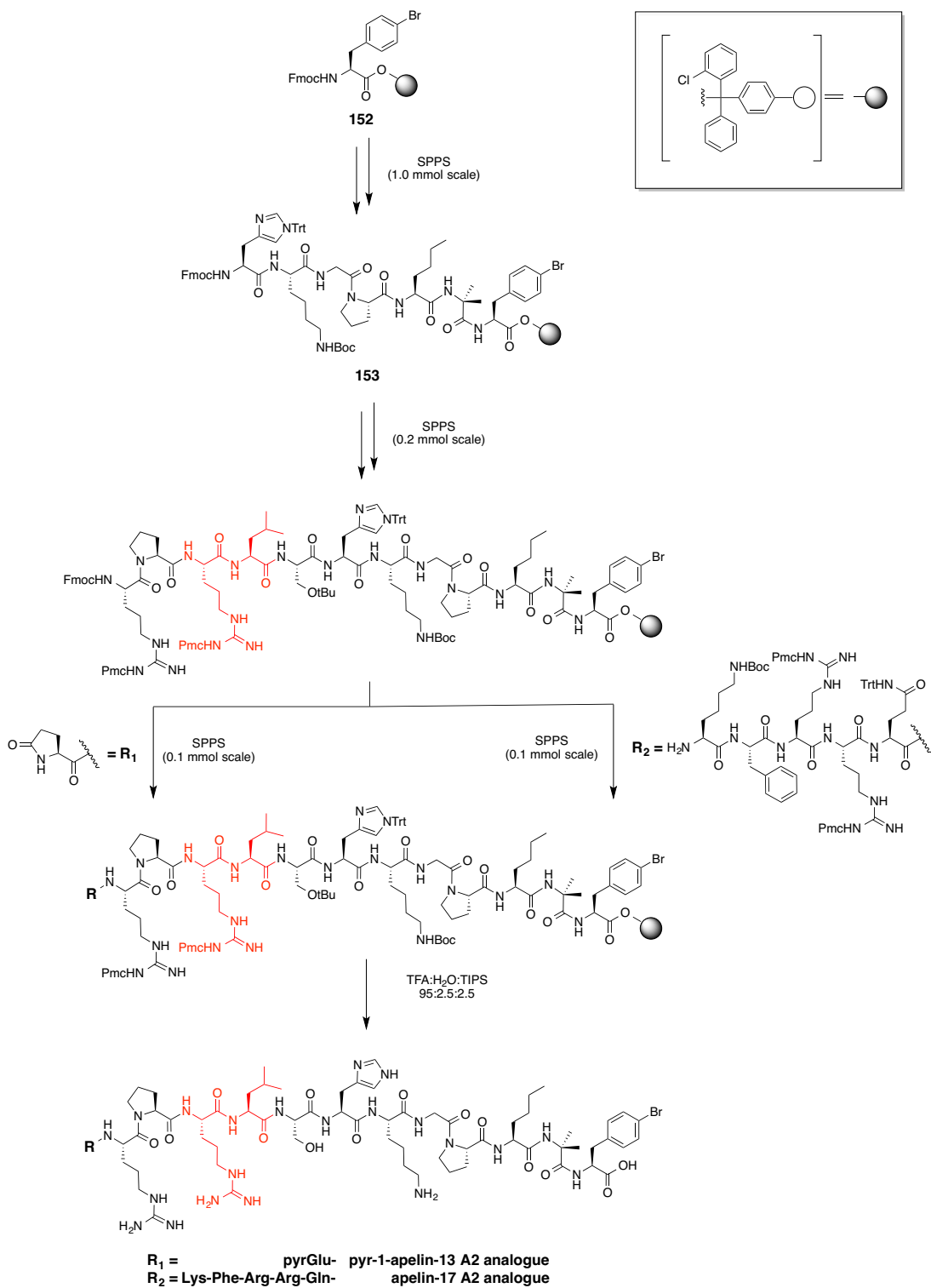


Figure 3.36 – Synthetic modifications surrounding the proposed Arg-Leu cut site.

In addition to the enhanced proteolytic resistance of these apelin analogues to the predicted N-terminal protease, the synthesis of analogues surrounding this Arg-Leu position could have an effect on the secondary structure of the 'RPRL' region. Although both apelin isoforms are largely disordered in aqueous solutions, it is believed that some secondary structure elements do exist in the apelin-17 isoform, particularly when interacting with the apelin receptor.⁷⁷ A combination of structural analysis, proteolytic stability, as well as physiological activity of these Arg-Leu apelin analogues could give an interesting insight into this significant region.

To negate the impact of ACE2 cleavage on these novel apelin analogues, the resistant A2 C-terminus (NleAibBrPhe) would be incorporated in all Arg-Leu analogues. To prepare for efficient syntheses of multiple different apelin analogues, large quantities (1.0 mmol batches) of resin-bound peptide **153** were prepared by manual SPPS and portioned into 0.1 mmol equivalents (Scheme 3.10). Novel analogues were initiated from common heptapeptide **153** on 0.2 mmol scale, incorporating the desired modifications at the appropriate position as orthogonally protected individual amino acids, dipeptides, or tripeptides. After the successful incorporation of Arg-Leu modifications, analogues would be extended N-terminally to the dodecapeptide stage and divided in half to 0.1 mmol portions. This approach allows for the divergent syntheses of pyr-1-apelin-13 A2 analogues by coupling half the material with L-pyroglutamic acid, while the other 0.1 mmol could be extended by the sequential addition of the 5 N-terminal amino acids (Fmoc-Gln(Trt)-OH, Fmoc-Arg(Pmc)-OH, Fmoc-Arg(Pmc)-OH, Fmoc-Phe-OH, and Fmoc-Lys(Boc)-OH) and a final Fmoc-deprotection to synthesize

apelin-17 A2 analogues. Apelin analogues were cleaved from the 2-chlorotrityl resin with a cleavage cocktail of 95:2.5:2.5 TFA:H₂O:TIPS, concomitantly removing any sidechain protecting groups. All peptide analogues were purified by C₁₈ RP-HPLC and lyophilized.



Scheme 3.10 – General SPPS approach to the synthesis of Arg4-Leu5 apelin analogues beginning from common heptapeptide 153. Locations of synthetic modifications to native apelin are shown in red.

3.5.2 D-Leu analogues

The simplest analogues to access synthetically involve the incorporation of a D-amino acid around the susceptible amide bond. Fmoc-protected D-amino acids are commercially accessible and do not require any additional solution-phase syntheses in the preparation of unique analogues. Based on literature precedent, the only moderately conservative D-amino acid substitution within the desired region of pyr-1-apelin-13 was Leu5, which had a 10-fold decrease in affinity for the apelin receptor.¹¹⁸ Conversely, substitution of D-Arg4 or D-Ser6 in pyr-1-apelin-13 was incredibly detrimental to apelin receptor binding (Table 3.8). Although literature apelin receptor binding values have not always correlated to physiologically active compounds, exemplified with the discrepancy between **103** and **104**,¹¹⁵ it is advisable to avoid a significant decrease in apelin receptor binding when selecting desirable modifications for apelin analogues.

Table 3.8 – Apelin receptor binding affinity of D-Scan analogues.¹¹⁸

Apelin analogue sequence	Apelin receptor binding IC ₅₀ (nM)	Relative decrease in apelin receptor affinity
native pyr-1-apelin-13	5.7 ± 0.3	1.0
D-Arg4 pyr-1-apelin-13	1279 ± 271	220
D-Leu5 pyr-1-apelin-13	61 ± 10	11
D-Ser6 pyr-1-apelin-13	642 ± 118	110

Beginning from the chlorotriptyl-resin-bound intermediate **153**, peptide analogues **154** and **155** were individually synthesized by manual SPPS on 0.1 mmol scale each, incorporating the unnatural Fmoc-D-Leu-OH at amino acid positions 5 and 9 respectively (Figure 3.37).

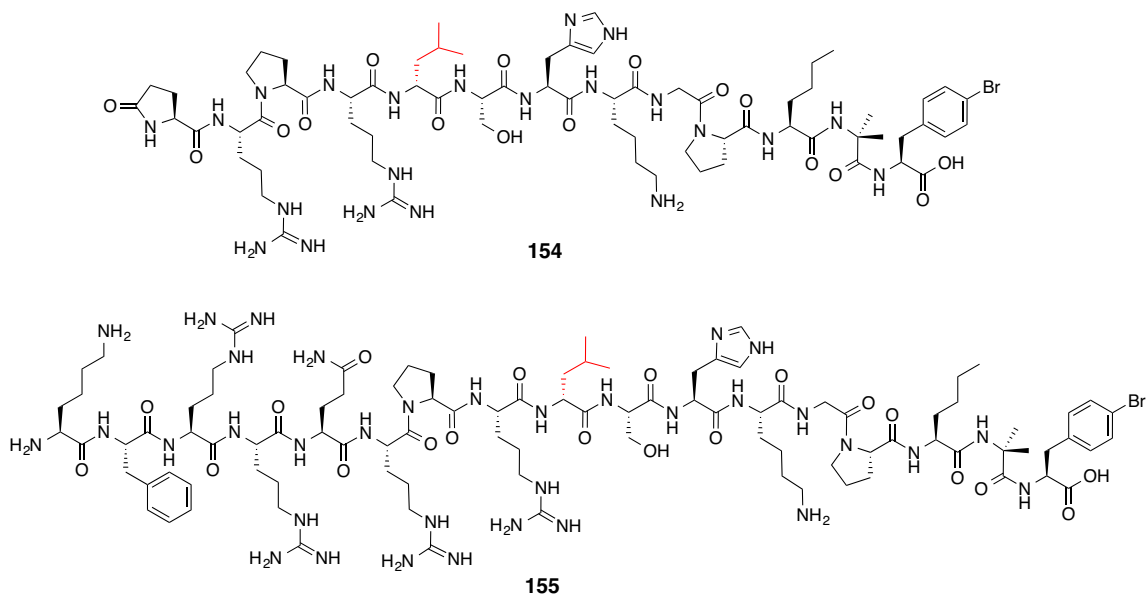


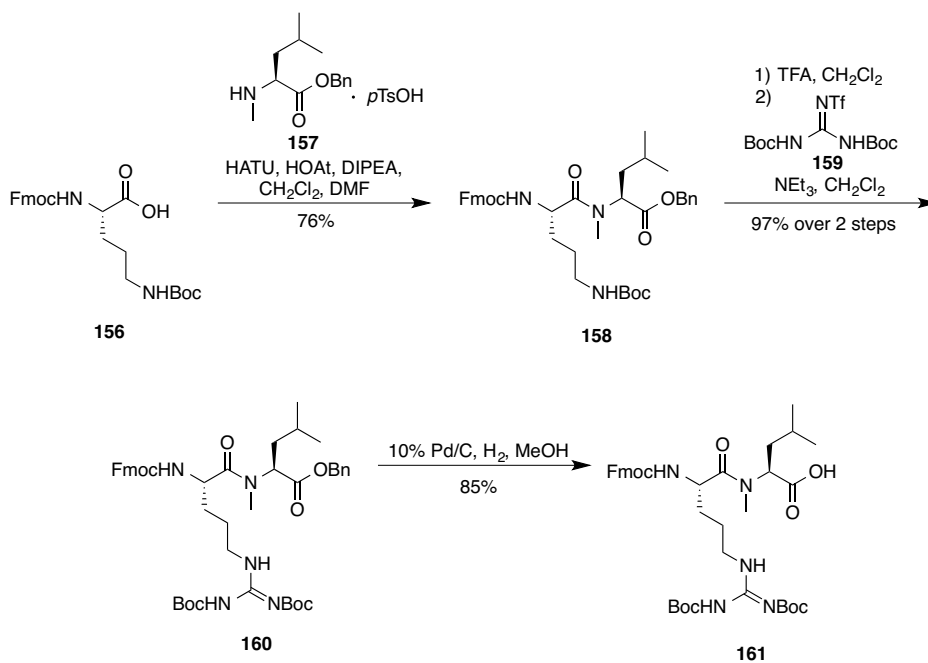
Figure 3.37 – Structures of D-Leu⁵ pyr-1-apelin-13 A2 (154) and D-Leu⁹ apelin-17 A2 (155) analogues.

3.5.3 N-MeLeu analogues

Additional simple analogues that could be prepared using commercially available amino acids involve the incorporation of N-methylated amino acids surrounding the susceptible amide bond. We targeted this Arg-Leu proposed proteolytic site for methylation, incorporating an N-methyl-L-leucine at the 5 and 9 position for pyr-1-apelin-13 and apelin 17 respectively. The N-methylated dipeptide was synthesized in solution and coupled as a protected dipeptide onto the apelin scaffold through manual SPPS to avoid complications via enhanced steric constraints surrounding the methylated amide bond.

Commercially available N-methyl-L-leucine benzyl ester *p*-toluenesulfonate salt (**157**) was coupled with Fmoc-L-Orn(Boc)-OH (**156**) using standard HATU/HOAt/DIPEA coupling conditions. The ornithine side chain amine was

deprotected under acidic conditions, then guanidinylated with 1,3-di-Boc-2-(trifluoromethylsulfonyl)guanidine (**159**). The C-terminal benzyl ester was removed under hydrogenolysis, generating the desired dipeptide **161** (Scheme 3.11).



Scheme 3.11 – Synthesis of Fmoc-Arg(diBoc)-NMeLeu dipeptide 161.

Direct coupling of the N-methyl-L-leucine benzyl ester *p*-toluenesulfonate salt with a protected Fmoc-Arg-OH derivative was not attempted for two reasons: the propensity of arginine to react intramolecularly to form lactams when activated in solution,^{160,161} particularly when being coupled to a sterically hindered amino acid; and the incompatibility of Pbf or Pmc protecting groups with benzyl ester hydrogenolysis.

Resin-bound intermediate **153** was N-terminally extended by the coupling of Fmoc-Ser(*t*Bu)-OH, followed by the coupling of dipeptide **161**. A small sample of the peptide was cleaved from the resin using 95:2.5:2.5 TFA:H₂O:TIPS, and analyzed using

MALDI-TOF. After confirmation of the desired mass for the decapeptide, subsequent elongation rounds of SPPS were employed to generate both the N-MeLeu pyr-1-apelin-13 and apelin-17 analogues **162** and **163** (Figure 3.38).

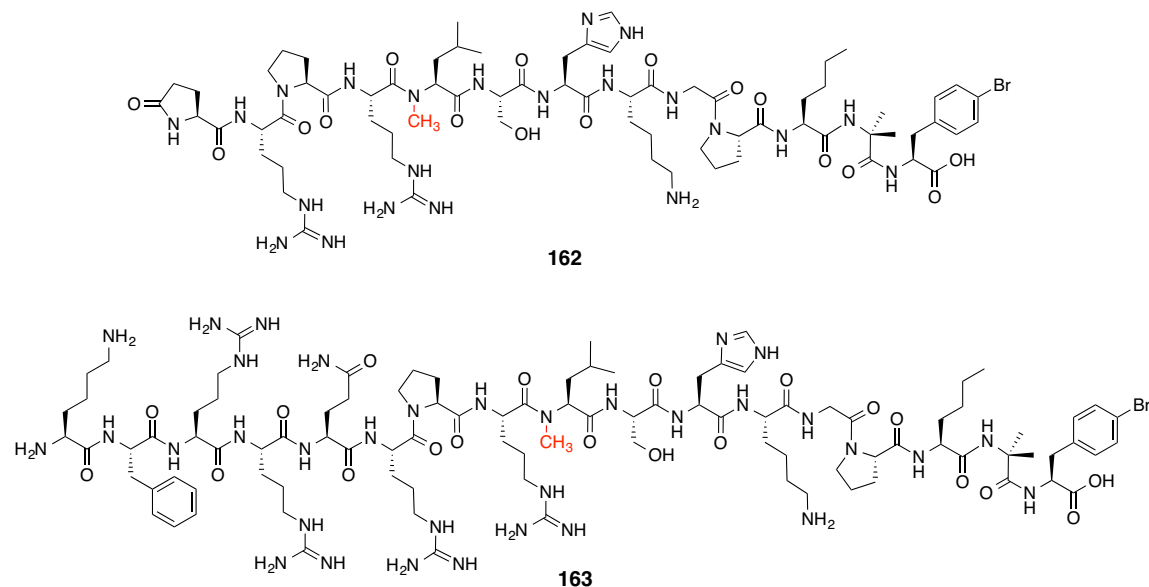


Figure 3.38 – Structures of NMeLeu₅ pyr-1-apelin-13 A₂ (162) and NMeLeu₉ apelin-17 A₂ (163) analogues.

3.5.4 α -Methyl analogues

Another approach to sterically occluding the susceptible amide bond involves C-methylation at the α -position of the amino acid on either side of the amide. This approach was previously successful in conferring resistance to ACE2 proteolysis through the substitution of the penultimate proline with aminoisobutyric acid,¹¹⁵ and it was hopeful that an analogous modification could have a similar effect at this new site of proteolysis.

Although many Fmoc-protected α -methylated amino acids are commercially available, at the time this project was initiated, no sources for Fmoc- α -Me-L-Arg were found. Fortunately, a large amount of methodologies exist to synthesize unnatural amino acids through the alkylation of chiral glycine amino acid scaffolds. We opted to use Ni-Schiff base complex **166** due to its relative ease of synthesis, the ability to recover and reuse the chiral ligand, and reported ease of purification and crystallization of individual diastereomers (Figure 3.39).

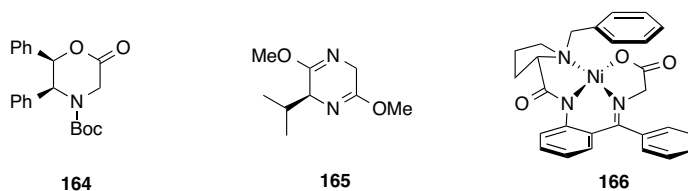
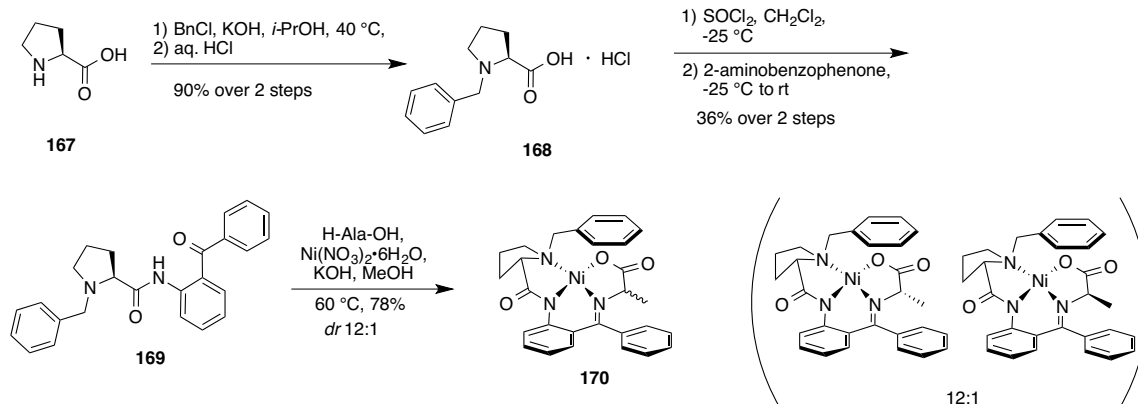


Figure 3.39 – Williams (164),¹⁶² Schollkopf (165)¹⁶³ and Ni-Schiff base (166)¹⁶⁴ chiral glycine auxiliaries for the stereoselective syntheses of amino acids.

Synthesis of the Ni-Schiff base complex was accomplished following literature procedure (Scheme 3.12).¹⁶⁴ The amine of L-proline (**167**) was benzylated in the presence of benzyl chloride and potassium hydroxide, then acidified to precipitate the resultant N-benzylproline hydrochloride salt (**168**). The free carboxylic acid was converted into an acid chloride through reaction with thionyl chloride, and amidated with 2-aminobenzophenone. L-Benzylproline-2-aminobenzophenone (*S*-BPB) ligand (**169**) was heated under basic conditions in the presence of nickel (II) nitrate hexahydrate and excess L-alanine, to afford Ala-Ni-(*S*)-BPB (**170**) as a bright red solid. Significant scale up of these compounds was done by Mr. Kevin Kalin (Alberta Innovates Health Solutions summer student, 2014).



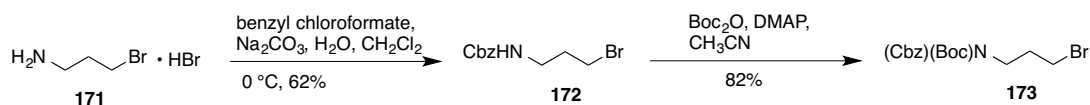
Scheme 3.12 – Synthesis of Ala-Ni(*S*)-BPB complex **170.¹⁶⁴**

Despite utilizing enantiomerically pure L-alanine for this reaction, two distinct diastereomers, differing at the stereochemistry at the alanine α -carbon, were obtained in a 12:1 ratio based on $^1\text{H-NMR}$ characterization. This could be explained through the increased acidity of the α -hydrogen upon imine formation between the benzophenone carbonyl and alanine amine moieties. However, both **170** diastereomers could be separated via silica flash chromatography by using slow gradients of MeOH in EtOAc; a feature that would be very advantageous in resolving di-alkylated Ni-Schiff base complexes. After characterization of the major diastereomer, both configurations of Ala-Ni(*S*)-BPB were synthetically useful so were pooled and carried forward for further alkylation reactions.

3.5.4.1 α -Methyl arginine analogues

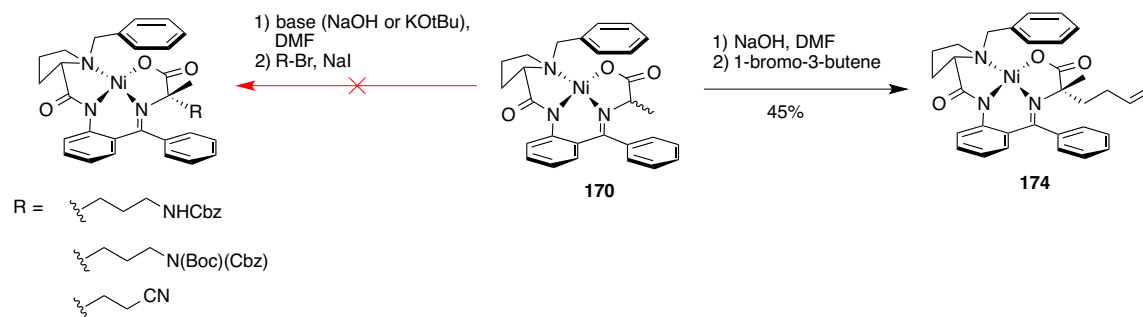
With Ni-Schiff base complex **170** in hand, test alkylations were attempted in an effort at installing the desired protected propylamine sidechain. Initially, benzyl (3-

bromopropyl)carbamate **172** was prepared by reacting 3-bromopropyl amine hydrobromide salt (**171**) with benzyl chloroformate under biphasic conditions. A second potential electrophile, di-carbamate protected **173** was obtained after protection of **172** under neutral conditions with Boc anhydride and catalytic DMAP (Scheme 3.13).¹⁶⁵ Commercial 3-bromopropionitrile was selected as a third electrophile.



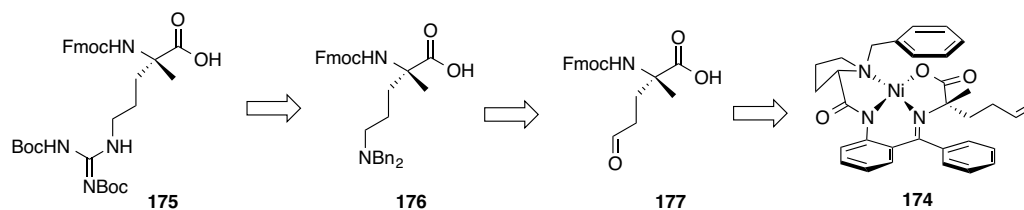
Scheme 3.13 – Syntheses of protected propylamine bromide electrophiles.

The literature protocol for alkylation of Ala-Ni-(S)-BPB **170** involved mixing the complex with either 10 equivalents of sodium hydroxide, or 1.1 equivalents of potassium *tert*-butoxide, turning the resultant anionic species a black color.¹⁶⁶ After a few minutes of exposure to these basic conditions, three equivalents of the alkyl bromides in the presence of 10 mol% sodium iodide were added. This returned the reaction immediately back to a bright red color, suggesting the anion was being quickly quenched by the addition of the electrophile. However, after leaving the reaction for the recommended reaction time of 180 minutes,¹⁶⁶ no conversion of starting material to the di-alkylated species was observed (Scheme 3.14). It was hypothesized that the regeneration of **170** resulted from the deprotonation of acidic hydrogen atoms on the carbamate of electrophile **172**, or on the carbon adjacent to the primary bromide for **173** and 3-bromopropionitrile, favoring bromide elimination.



Scheme 3.14 – Efforts towards dialkylation of Ala-Ni-(S)-BPB (170).

The dialkylated compound **174** was successfully synthesized according to literature procedures with 1-bromo-3-butene as the electrophile (Scheme 3.11).¹⁶⁶ Although the resulting amino acid derivative did not have the desired δ -amino functionality, a synthetic route was envisioned to access the α -methylated arginine. After decomplexation and Fmoc protection of the amine, the terminal alkene could be converted to aldehyde **177** by ozonolysis, and further transformed to amine **176** through reductive amination with a protected secondary amine. Benzyl deprotection and guanidinylation could afford amino acid **175** (Scheme 3.15). The absence of δ -amino functionality in **174** added many additional steps however, so this scheme was reserved as a back up plan.

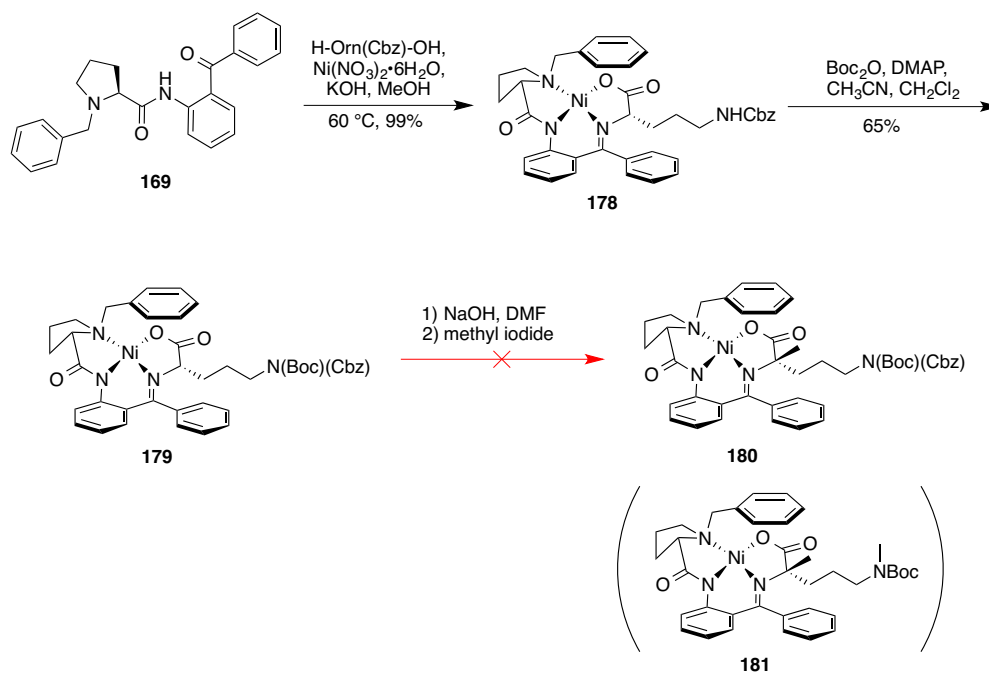


Scheme 3.15 – Retrosynthetic approach to access 175 from Ni-complex 174.

With limited success at installing a propylamine group onto Ala-Ni-(*S*)-BPB, a less-universal approach to the synthesis of **175** was created, where a protected ornithine derivative was initially complexed to **169**, and the α -methyl group would be installed afterwards. Although the incoming electrophile would conventionally be added from the bottom face to avoid steric clashing of the N-benzyl group with the amino acid side chain, the steric effect of the methyl iodide electrophile would be negligible in comparison to that of the attached aminopropyl group, likely affording some of the desired diastereomer **180**.

Orn(Cbz)-Ni-(*S*)-BPB **178** was synthesized in an analogous fashion to the alanine-complex (Scheme 3.16). The ornithine side chain carbamate N-H was masked by protection with Boc anhydride and catalytic DMAP,¹⁶⁵ while adapting the literature solvent system through the addition of CH₂Cl₂ to improve the solubility of the Ni-complex in acetonitrile. The dicarbamate-protected complex **179** was mixed with 10 equivalents of sodium hydroxide in dry DMF to form the black enolate. Three equivalents of methyl iodide were added to the enolate with stirring for 90 minutes, followed by an additional 3 equivalents of methyl iodide and an additional 90-minute reaction time. After an aqueous workup and purification of the main components of the reaction mixture, it was determined that while all of the starting material had been consumed, all isolated products lacked the Cbz protecting group. The main product from this reaction (~20% yield) was characterized by HRMS as being methylated twice, with ¹H-NMR analysis supporting methylation at the ornithine NH and at the α -carbon (Scheme 3.5.4.5). No stereochemical information could be obtained from bis-methylated product **181**, and it was predicted to be a mixture of diastereomers. Although ornithine

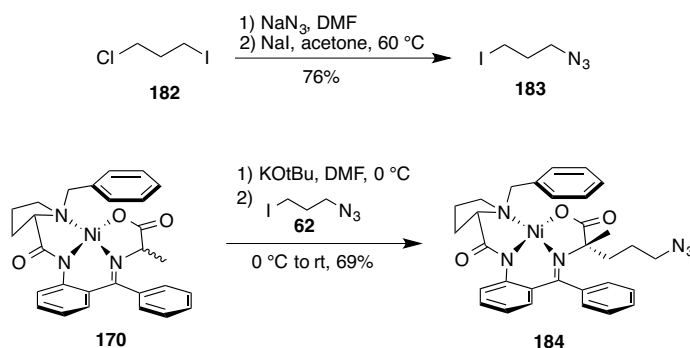
N-methylation was detrimental for further elaboration of this synthetic route, it was gratifying to see that α -carbon methylation was possible from this strategy.



Scheme 3.16 – Attempted α -methylation of Orn(Boc)(Cbz)-Ni-(S)-BPB complex **179**.

A more thorough literature investigation uncovered a patent that used the electrophile 1-iodo-3-azidopropane (**183**) to synthesize the desired α,α -disubstituted Ni-complex.¹⁶⁷ **183** was prepared by nucleophilic substitution of the iodide from 1-chloro-3-iodopropane (**182**) with sodium azide, followed by a Finkelstein reaction with sodium iodide in refluxing acetone to regenerate the primary alkyl iodide. Under modified reaction conditions, Ala-Ni-(S)-BPB complex **170** was initially cooled to 0°C with dry potassium *tert*-butoxide, then dissolved in dry DMF. As a solution of **183** in DMF was added, the solution maintained a dark black color for a prolonged period of time;

qualitatively indicating that immediate re-protonation of the Ni-complex was not occurring. The (*S,S*) α,α -dialkylated diastereomer **184** was purified by silica flash chromatography in 69% yield (Scheme 3.17).



Scheme 3.17 – Preparation of dialkylated α Me-L-azidoOrn-Ni(*S*)-BPB **184.**

Initially, the relative stereochemistry of complex **184** was confirmed by NOE correlations of the α -methyl group with the *N*-benzyl aromatic hydrogens using a ROESY experiment. To confirm the absolute stereochemistry of this complex, crystals were grown using a slow evaporation method out of minimal CH_2Cl_2 and hexanes. The absolute stereochemistry was assigned as (*S*) at the α carbon of the amino acid (Figure 3.40) with the assistance of Dr. Bob McDonald (University of Alberta X-ray Crystallography Laboratory).

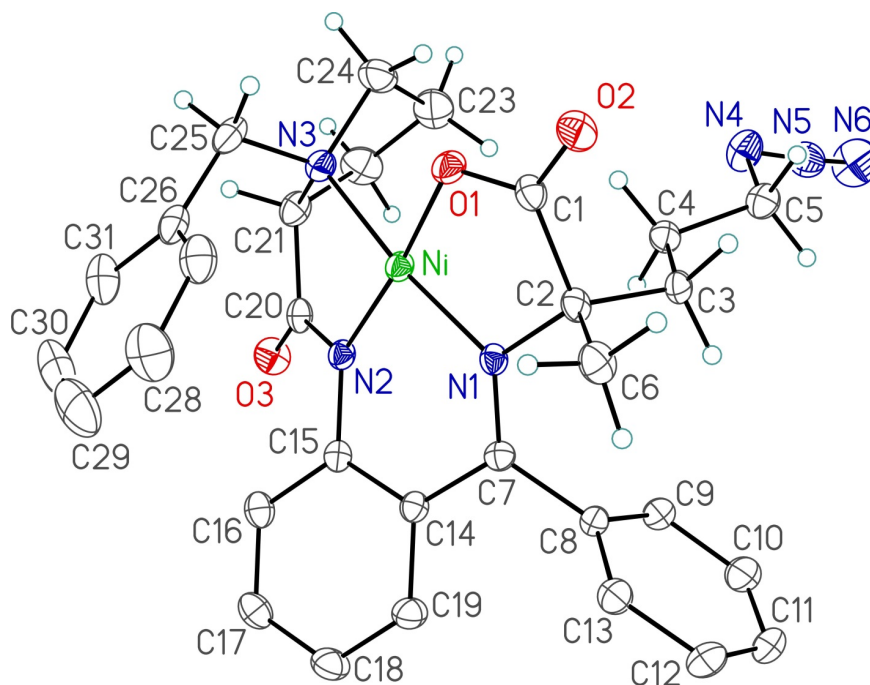
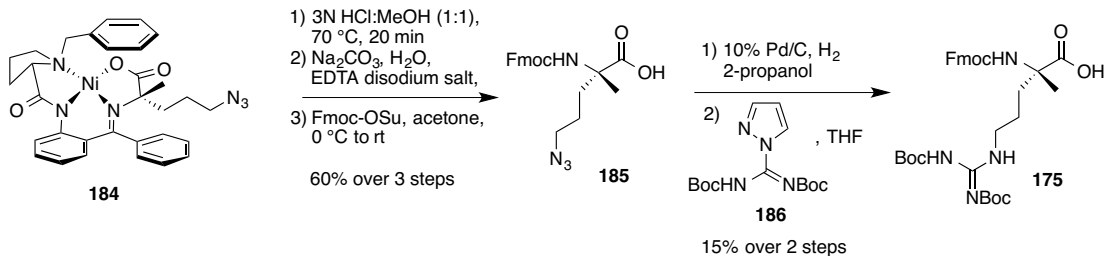


Figure 3.40 – Crystal structure of 184 confirming the (*S*) absolute stereochemistry at amino acid α -carbon C2.

Ni-complex **184** was then hydrolyzed under acidic conditions, producing the recoverable BPB ligand, aqueous Ni salt, and the free amino acid.¹⁶⁷ Initial attempts at Fmoc-protection of the amino acid according to literature yielded disappointing results (<10 %), so a modified procedure was adapted by chelating the aqueous Ni²⁺ in solution with EDTA prior to Fmoc protection. Subsequent hydrogenolysis of the azido group of **185** generated a free δ -amine that was guanidylated using pyrazole-based reagent *N,N'*-di-Boc-1*H*-pyrazole-1-carboxamide (**186**). The desired Fmoc- α -Me-L-Arg(di-Boc)-OH (**175**) was obtained in a disappointing yield over the final two steps (Scheme 3.18). It was postulated that the overnight exposure to hydrogen gas in the azide hydrogenolysis step might have begun to deprotect the Fmoc-group. Residual guanidinylation at both the N α and N δ positions would limit the amount of desired amino acid **175**.



Scheme 3.18 – Synthesis of Fmoc- α Me-L-Arg(di-Boc)-OH (175).

Despite the poor yield of **175**, enough material was present to attempt a small-scale on-resin coupling. Resin-bound peptide **153** was N-terminally extended by sequential addition of Fmoc-Ser(tBu)-OH, then Fmoc-Leu-OH. After Fmoc-deprotection of the nonapeptide using a 20% piperidine in DMF solution, a preactivated solution of **175** was added to the resin and bubbled under Ar gas for 2 h. A small portion of the resin was cleaved by 95:2.5:2.5 TFA:H₂O:TIPS and the resulting crude peptide was analyzed by MALDI-TOF. Unfortunately, the dominant mass observed was that of the deprotected nonapeptide, with only a small trace of the desired Fmoc-protected decapeptide. Two problems were postulated: in addition to the increased prevalence of carbamate-protected α,α -disubstituted amino acids at intramolecular cyclization to form an oxazolone (**188**), it was hypothesized that the free δ -amino group of the arginine guanidine sidechain could react intramolecularly with the activated amino acid **187** to form a δ -Freidinger lactam (**189**, Figure 3.41).¹⁶⁰ Initially forming the unnatural dipeptide in solution with **185**, then coupling this to the resin could help to circumvent this problem.

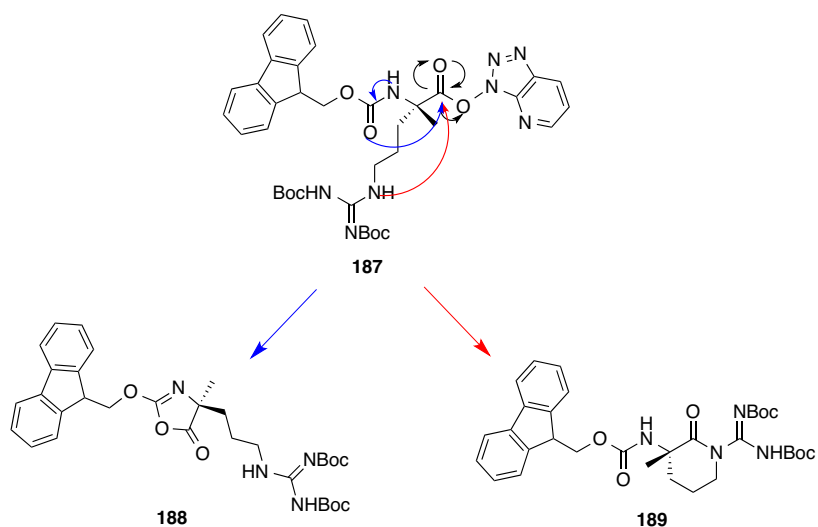
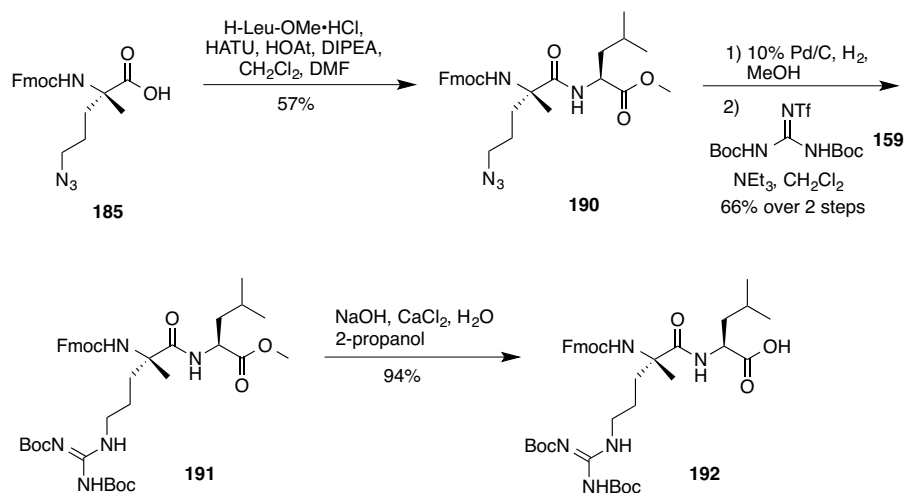


Figure 3.41 – Proposed side product formation from activated 175 (187).

To test this hypothesis, **185** was briefly preactivated with HATU/HOAt/DIPEA in DMF for 2 minutes and then added to a solution of H-Leu-OMe hydrochloride in CH_2Cl_2 , affording the desired dipeptide **190** in a moderate yield of 57% (Scheme 3.19). The azide of **190** was converted to a primary amine under palladium-catalyzed hydrogenolysis, then capped by guanidinylation reagent 1,3-di-Boc-2-(trifluoromethylsulfonyl)guanidine in the presence of triethylamine. Finally, the methyl ester of **191** was hydrolyzed through exposure to 2 equivalents of sodium hydroxide in a 0.8 M CaCl_2 solution,¹⁶⁸ giving the desired Fmoc- α Me-L-Arg(diBoc)-Leu-OH dipeptide **192**.



Scheme 3.19 – Synthesis of Fmoc- α Me-L-Arg(diBoc)-Leu-OH dipeptide 192.

To complete the syntheses of the α MeArg-containing analogues, peptide analogue **153** was elongated by manual SPPS cycles to introduce Fmoc-Ser(tBu)-OH, then the **192** dipeptide. A small sample of resin was cleaved by 95:2.5:2.5 TFA:H₂O:TIPS at this decapeptide stage and analyzed by MALDI-TOF. After positive confirmation of the desired decapeptide mass, the next amino acid (Fmoc-Pro-OH) was added after Fmoc-deprotection of the resin-bound decapeptide. A small sample of resin was again cleaved under aqueous TFA conditions and analyzed by MALDI-TOF to ensure complete coupling of amino acid residues surrounding the unnatural modification. After the desired undecapeptide mass was observed, SPPS was continued, extending the N-terminus by 2 or 6 amino acids to synthesize pyr-1-apelin-13 analogue **193** and apelin-17 analogue **194** respectively (Figure 3.42). One notable deviation to the conventional SPPS procedure involved eliminating the addition of end-capping solutions of 20% acetic anhydride in DMF between couplings after the addition of unnatural **192** to avoid any potential N δ -acetylation of the di-Boc protected arginine moiety.

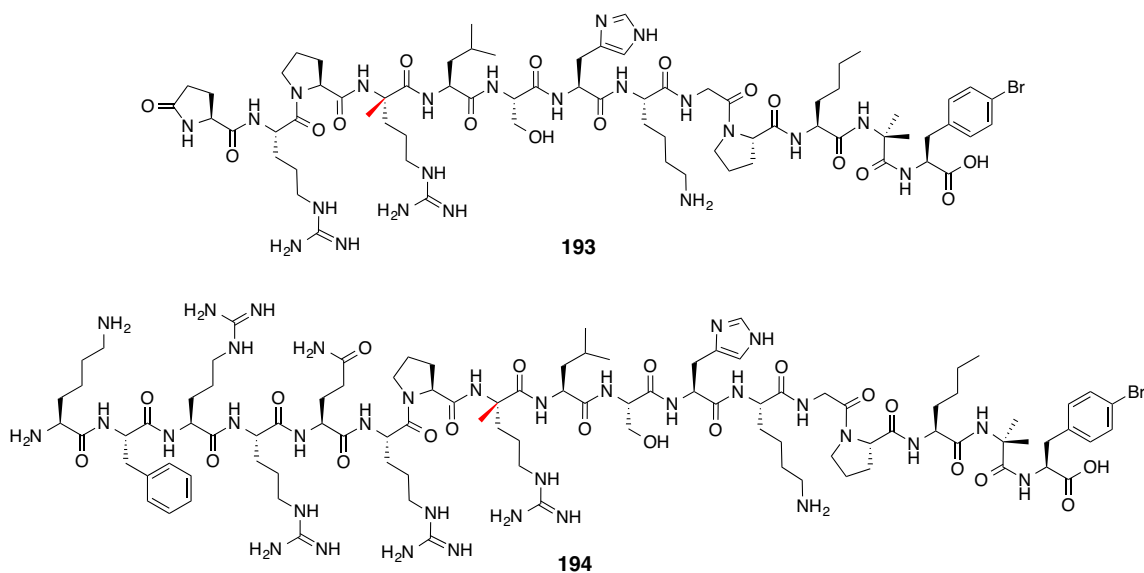


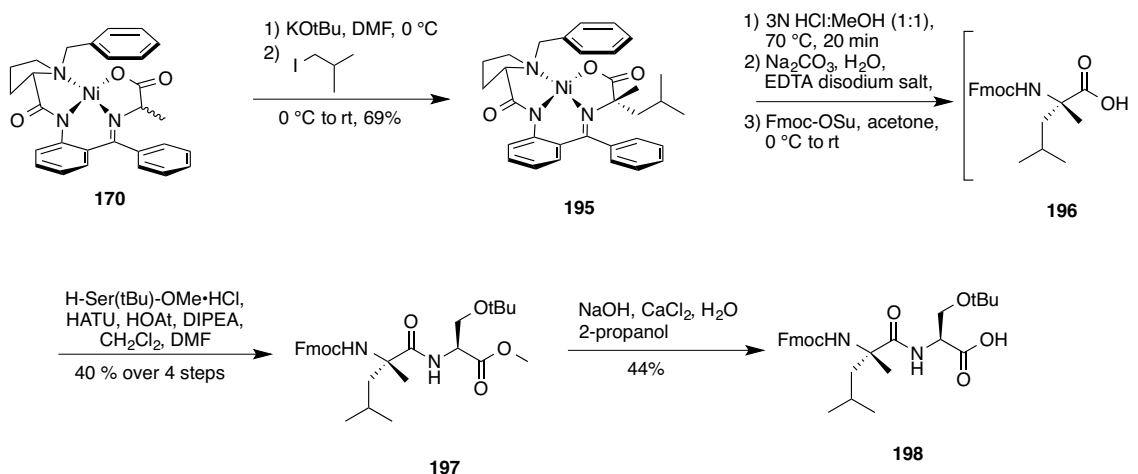
Figure 3.42 – Structures of α MeArg4 pyr-1-apelin-13 A2 (193) and α MeArg8 apelin-17 A2 (194) analogues.

3.5.4.2 α -Methyl leucine analogues

The α -methylation methodology established in the syntheses of the α -MeArg analogues could additionally be extended to the Leu5 position of the pyr-1-apelin-13 scaffold. The introduction of steric bulk C-terminal to our proposed cut site could have an effect at stabilizing the peptide to proteolysis. While Fmoc- α -Me-L-Leu-OH is commercially available at a high cost (\$365 USD/g, Chem-Impex International), all necessary intermediates for the synthesis of this amino acid were already prepared or accessible in our lab.

Preliminary work on the synthesis of these analogues was done with the assistance of Mr. Kevin Kalin. Ala-Ni-(S)-BPB complex **170** was alkylated using 2-methyl-1-iodopropane in an analogous method to the α -methyl arginine synthesis. The

desired (*S*)-diastereomer of **195** was purified by silica flash column chromatography in a 69% yield. Preliminary NMR ROESY experiments of **195** showed a *syn*-relationship between the α -methyl and N-benzyl moiety of proline, supporting the relative stereochemistry. The absolute stereochemistry was later confirmed by crystallographic analysis (Figure 3.43) with the assistance of Dr. Bob McDonald (University of Alberta X-ray Crystallography Laboratory). Dialkylated complex **195** was hydrolyzed under acidic conditions to liberate BPB and the free amino acid. EDTA was used to chelate residual Ni²⁺ salts followed by Fmoc-protection of the amine. Instead of attempting an on-resin coupling with amino acid **196**, dipeptide **197** was formed in solution with HATU/HOAt/DIPEA coupling conditions and H-Ser(*t*Bu)-OMe hydrochloride. The NMR signals surrounding the amide bond were again broadened in this molecule, as previously observed in α -MeArg dipeptide **190**. Methyl ester hydrolysis in the presence of excess CaCl₂ to protect the Fmoc under basic conditions¹⁶⁸ afforded the final dipeptide **198** after column chromatography (Scheme 3.20).



Scheme 3.20 – Synthesis of Fmoc- α Me-L-Leu-Ser(tBu)-OH dipeptide 198.

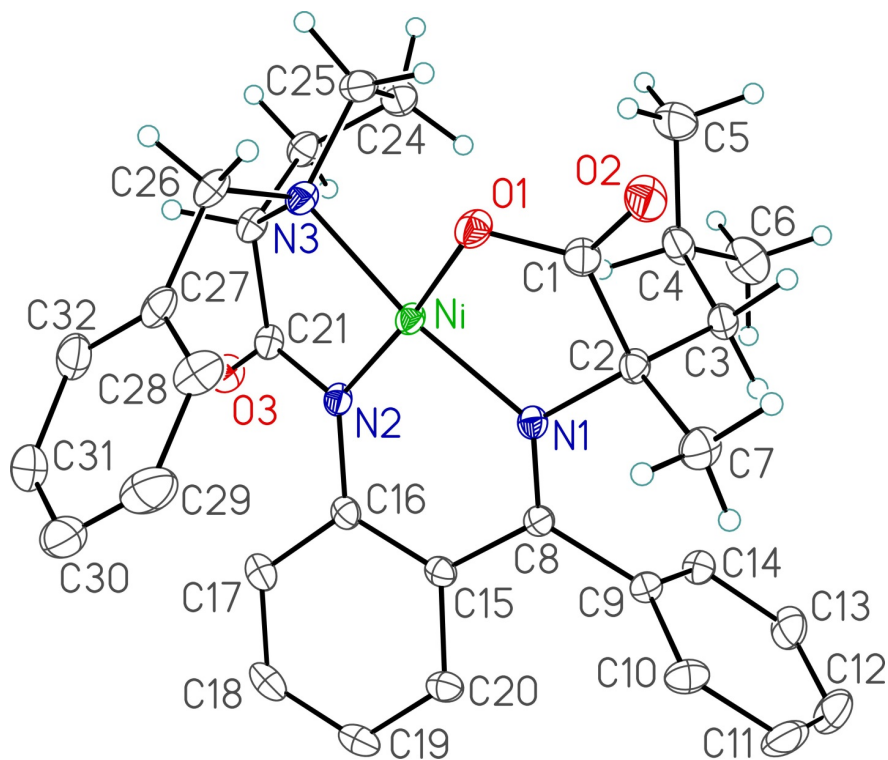


Figure 3.43 – Crystal structure of 195 confirming the (*S*) absolute stereochemistry at amino acid α -carbon C2.

To complete the synthesis of the α -Me-L-Leu containing analogues, 0.2 mmol of **153** were Fmoc-deprotected with 20% piperidine in DMF, and a preactivated solution

of **198** was coupled to the resin. A small sample of the resin was cleaved and analyzed by MALDI-TOF, showing the correct mass for the desired nonapeptide. Fmoc-Arg(Pmc)-OH, the next amino acid in the sequence, was coupled following standard SPPS conditions and a small sample of resin was cleaved and analyzed by MALDI-TOF. After confirmation of the correct mass for the decapeptide, two additional rounds of SPPS were performed, sequentially adding Fmoc-Pro-OH, then Fmoc-Arg(Pmc)-OH. The resin was split into half, divergently synthesizing the pyr-1-apelin-13 analogue **199** and the apelin-17 analogue **200** in 0.1 mmol scale each (Figure 3.44).

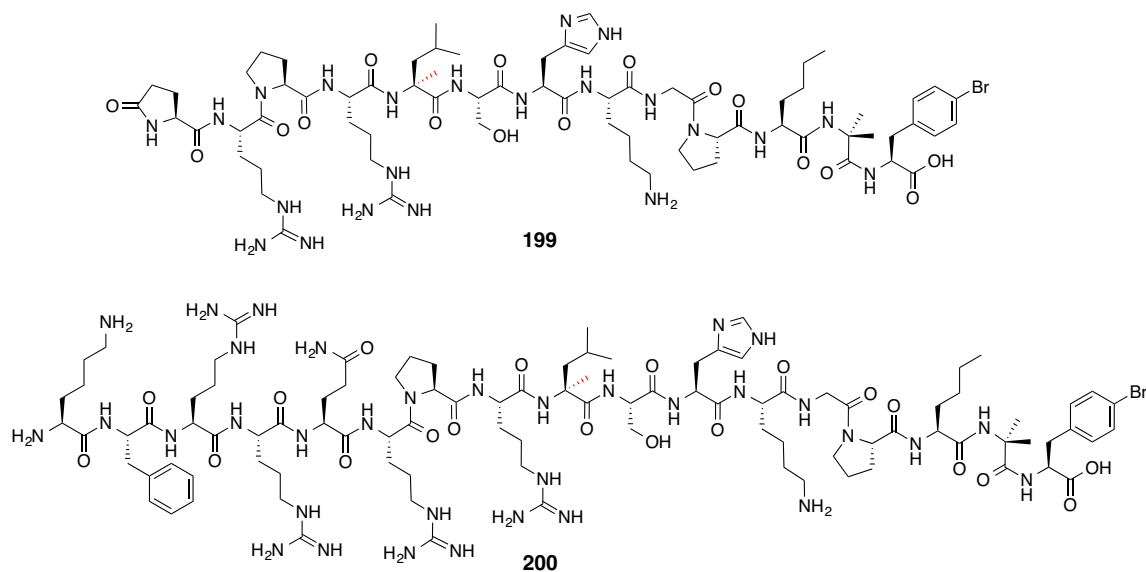


Figure 3.44 – Structures of α MeLeu⁵ pyr-1-apelin-13 A2 (199**) and α MeLeu⁹ apelin-17 A2 (**200**) analogues.**

3.5.5 aza-Analogues

3.5.5.1 Introduction and Background

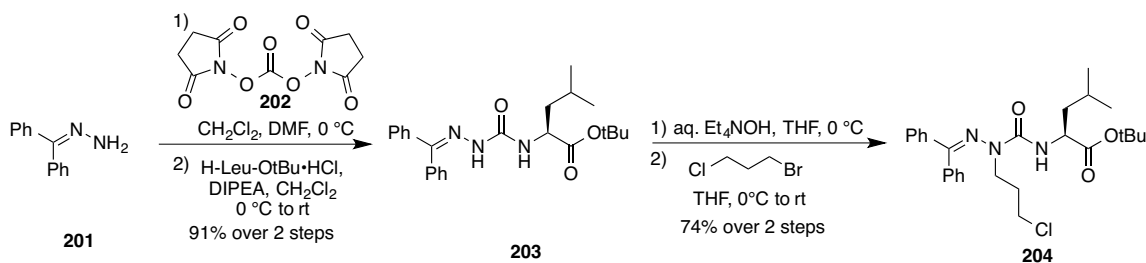
aza-Analogues involve the substitution of an amino acid α -carbon with nitrogen, generating an aminoacylated semicarbazide moiety upon incorporation into the amino acid scaffold.¹⁶⁹ The semicarbazide carbonyl of aza-peptides will be significantly more stable to proteolysis than the corresponding amide carbonyl due to the presence of the two flanking nitrogen atoms. The first successful application of azapeptides in a biological system was the synthesis of [azaVal³]-angiotensin II (bovine), which was shown to have a smaller hypertensive response but a prolonged duration compared to the native peptide.¹⁷⁰ Subsequent aza-analogue derivatives of natural peptides have had a comparable increase in half-life while retaining or enhancing biological activity.^{169,171}

In terms of peptide backbone structure, α -nitrogen substitution can have a profound effect as the amino acid moiety has a more ‘configurationally labile’ α -center due to the more sp^2 -like α -nitrogen center. Chirality at this position may be influenced by the preference of surrounding amino acids to the semicarbazide moiety, or additional interactions with the biological receptor. Additionally, the adjacency of the two nitrogen atoms to each other in the diacylhydrazine moiety prefers a perpendicular orientation of the nitrogen lone pairs based on computational work.^{172,173} This can influence a variety of β -turn and polyproline helix structures in the peptide backbone.^{169,172} It is hard to predict the effect of an aza-peptide substitution on the structure and activity of potential analogues, however these analogues seemed like viable synthetic targets to study the structure and *in vitro* stability of this Arg-Leu region of apelin.

3.5.5.2 aza-Arg analogues

These analogues were initiated after a recent publication from Lubell and coworkers in which they synthesized nitrogen-containing aza-amino acids by alkylating semicarbazone backbones with α -bromo- ω -chloroalkanes.¹⁷⁴ Subsequent displacement of the primary chloride with nitrogen nucleophiles generates the desired aza-diaminobutyrate, ornithine, or lysine moieties. This work was an expansion of their previous efforts using propargyl-substituted semicarbazones to perform Mannich-like A³ reactions, forming acetylenic aza-lysine moieties.¹⁷⁵

The construction of the semicarbazone backbone of the aza-arginine analogue was accomplished by reacting benzophenone hydrazone (**201**) with disuccinimidyl carbonate (**202**), then adding a solution of H-Leu-OtBu hydrochloride and DIPEA in CH₂Cl₂ via cannulation. The alkylation of semicarbazone **203** required some optimization to achieve a moderate yield while retaining the desired stereochemistry at the leucine (Scheme 3.21). The literature alkylation methodology of benzhydrylidene-protected semicarbazones utilizing 1.2 equivalents of tetraethylammonium hydroxide and 1.5 equivalents of 3-chloro-1-bromopropane unfortunately yielded no desired product after 3 h reaction time at 0 °C.¹⁷⁴ By increasing the equivalents of base and electrophile to 5.0 and 7.5 respectively, chloroalkylated semicarbazone **204** was obtained in 35% yield after 3 h at 0 °C. Extending the reaction time to 72 h and slowly allowing the reaction to warm to room temperature increased the yield of **204** to 74% (Table 3.9).



Scheme 3.21 – Synthesis of chloropropyl-alkylated semicarbazide precursor 204.

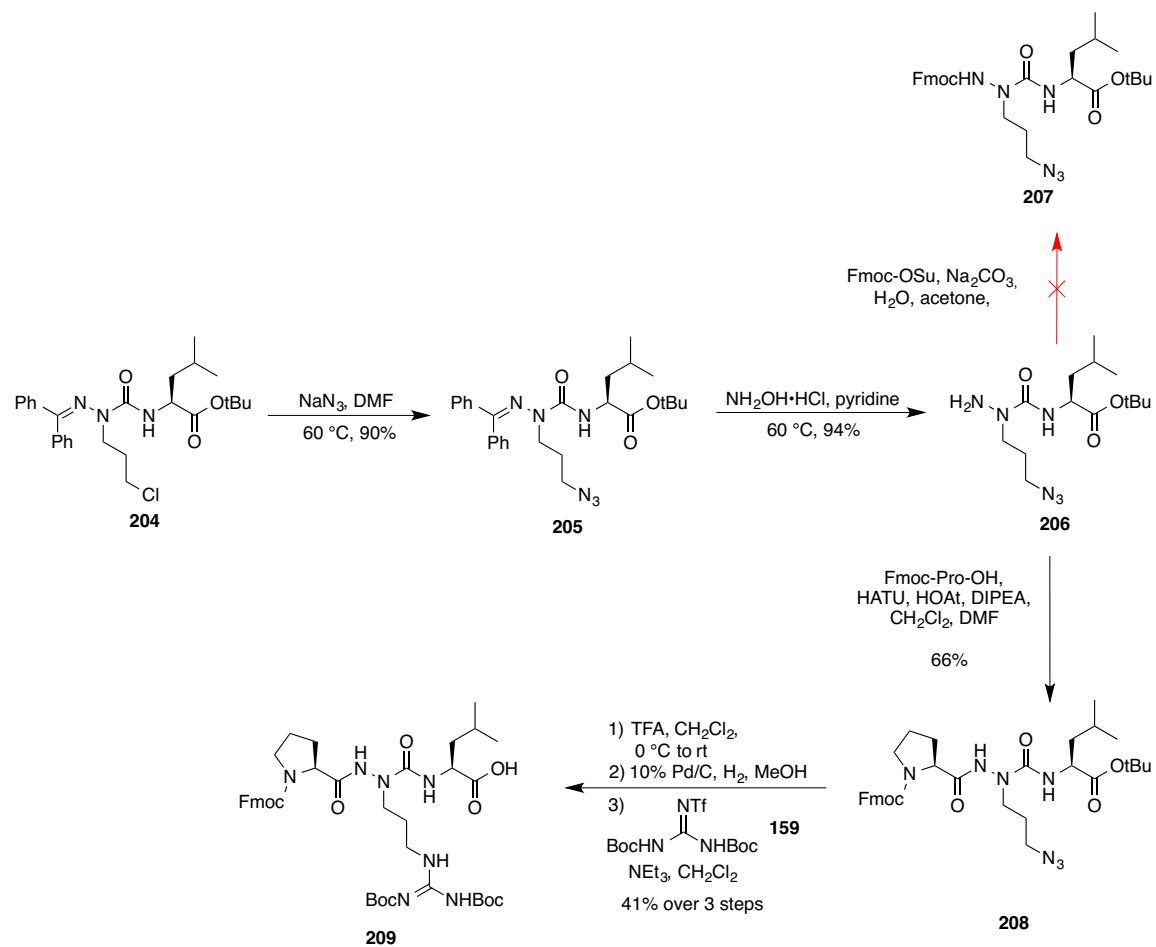
The initial methodology paper indicated the propensity of C-terminal *tert*-butyl ester-protected semicarbazones to partially racemize (up to 15%) at temperatures above 0 °C during the 3 h reaction time; this racemization could be prevented by maintaining the reaction at 0 °C or using a C-terminal amide instead.¹⁷⁴ To assess the extent of loss of optical purity, compounds **203** and **204** were recovered from the reaction conditions exclusively held at 0 °C for 3 h and from the reaction conditions allowed to warm to room temperature over 72 h and analyzed by optical rotation (Table 3.9). Comparison of the $[\alpha]_D^{26}$ values of the starting material and **204** product showed that minimal racemization took place after elevated reaction temperatures and prolonged times.

Table 3.9 – Reaction conditions for the optimization of 204.

Reaction Conditions	Et ₄ NOH equiv.	Alkyl-Br equiv.	temp. (°C)	time (h)	Yield (%)	$[\alpha]_D$ 203	$[\alpha]_D$ 204
1	1.2	1.5	0	3	0	-	-
2	5.0	7.5	0	3	35	-	64
3	5.0	7.5	0 – 20	72	74	31	61
			starting material 203			36	

With **204** in hand, azidopropyl semicarbazone **205** was prepared in 90% yield by the displacement of the primary alkyl chloride with sodium azide at 60 °C. The N-benzophenone protecting group was liberated in the presence of hydroxylamine

hydrochloride, forming semicarbazide **206** in excellent yield. An Fmoc protection was attempted on semicarbazide **206**, but no desired product (**207**) was formed, recovering 95% of the starting material. An alternative approach was envisioned in which the next N-terminal amino acid, Fmoc-Pro-OH, would be coupled to the semicarbazide, effectively protecting the N-terminus with the desired Fmoc-group and reducing the number of solid-phase couplings required by one. Under HATU coupling conditions with 10 mol% HOAt, aza-tripeptide **208** was synthesized and purified by column chromatography. The desired guanidylated analogue **209** was prepared by removing the C-terminal *tert*-butyl ester under acidic conditions, palladium-catalyzed hydrogenolysis of the primary azide, and guanidinylation using 1,3-di-Boc-2-(trifluoromethylsulfonyl)guanidine in the presence of triethylamine (Scheme 3.22).



Scheme 3.22 – Synthesis of Fmoc-Pro-aza-Arg(diBoc)-Leu-OH aza-tripeptide 209.

With the desired modification in hand, 0.2 mmol of **153** were extended by one round of SPPS by the addition of Fmoc-Ser(tBu)-OH and subsequently deprotected with a solution of 20% piperidine in DMF. 1.25 equivalents of **209** were briefly preactivated for 2 minutes, then added to the resin and bubbled under Ar gas for 3 h. This procedure was immediately repeated a second time with 1.1 equivalents of **209** to maximize coupling of the synthetic tripeptide. After resin cleavage and MALDI-TOF confirmation of the desired undecapeptide mass, the peptide chain was elongated by Fmoc-Arg(Pmc)-OH, a small portion cleaved and the mass again confirmed by MALDI-TOF analysis.

The resin was then split into half, divergently synthesizing the pyr-1-apelin-13 analogue **210** and the apelin-17 analogue **211** in 0.1 mmol scale each (Figure 3.45).

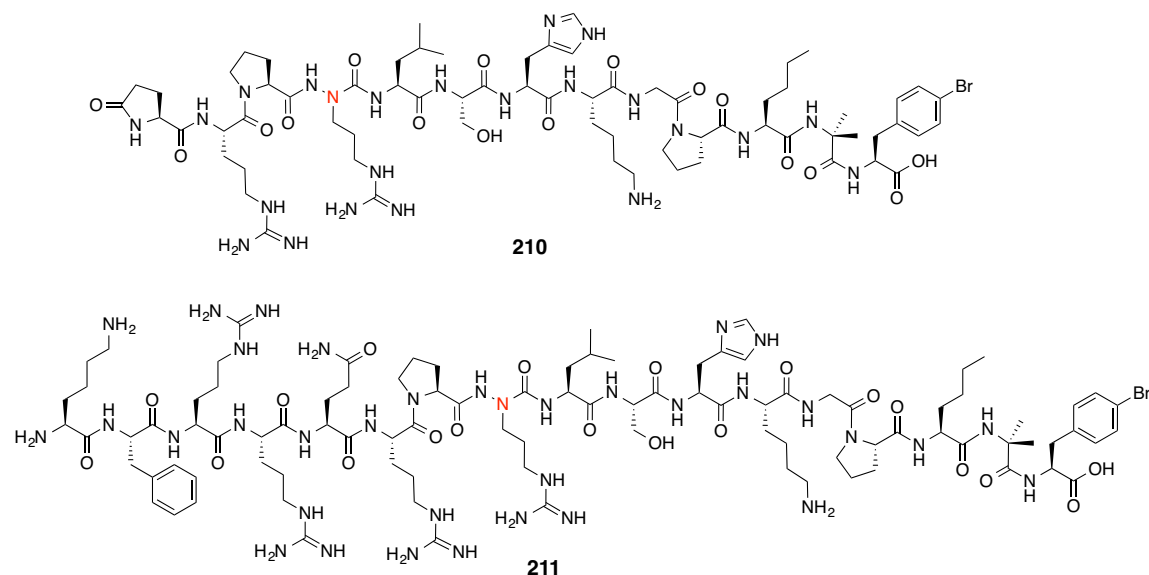
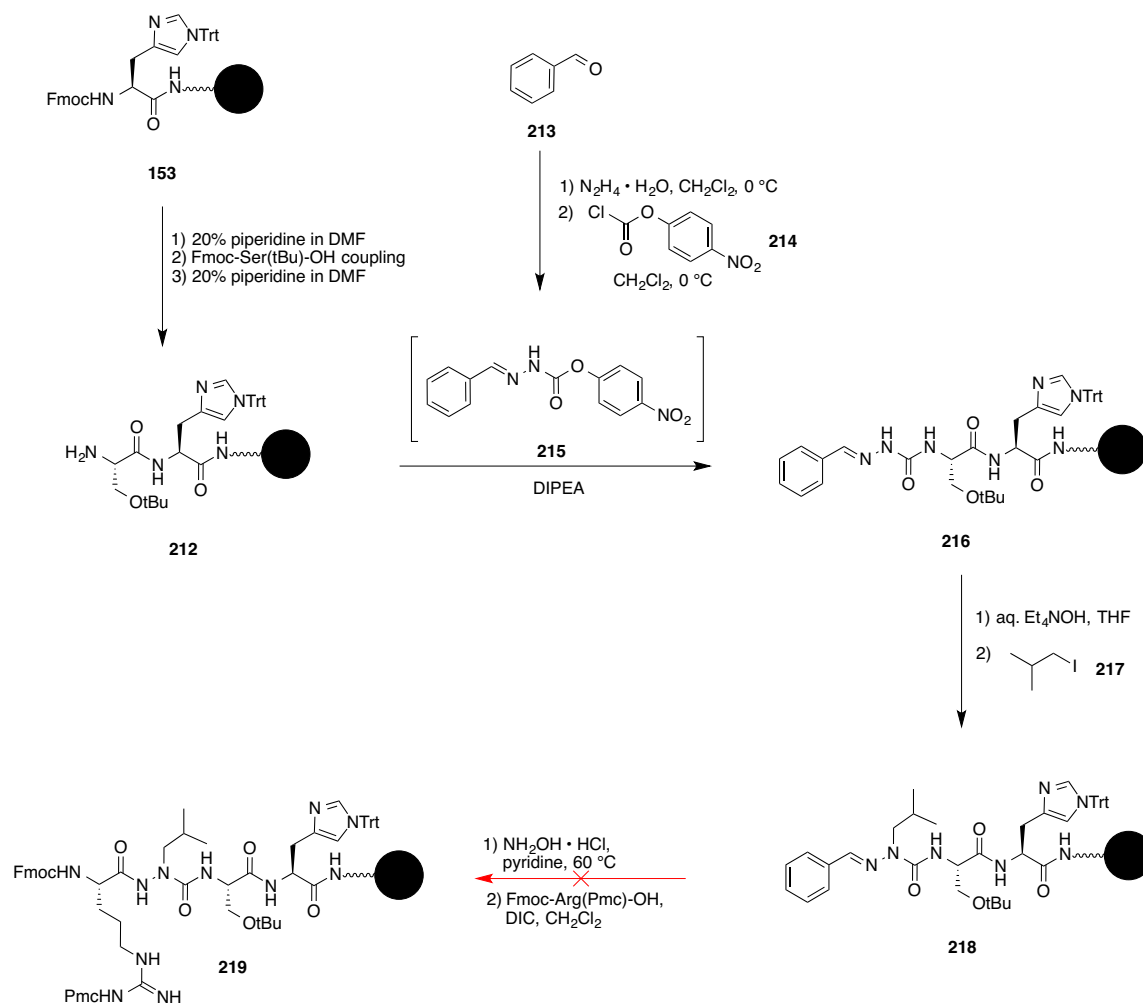


Figure 3.45 – Structures of aza-Arg4 pyr-1-apelin-13 A2 (210) and aza-Arg8 apelin-17 A2 (211) analogues.

3.5.5.3 aza-Leu analogues

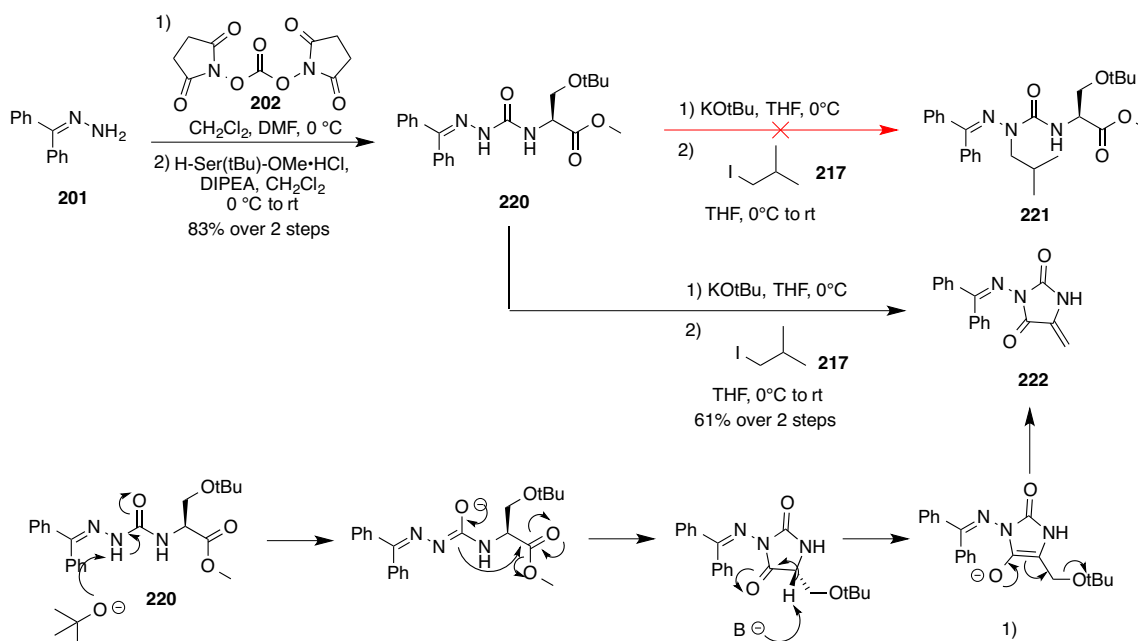
Initially we opted to use an on-resin approach to the synthesis of these analogues to minimize purification steps.^{176,177} Resin-bound **153** was extended by one round of SPPS and deprotected with 20% piperidine in DMF, yielding the resin-bound octapeptide **212**. In a separate flask, benzaldehyde (**213**) was mixed with hydrazine monohydrate at 0 °C to form a hydrazone, then activated with *p*-nitrophenyl chloroformate (**214**) to yield **215**. This compound was immediately reacted with **212** for 24 h under Ar without any purification or further characterization. A small sample of resin was cleaved at this point using 95:2.5:2.5 TFA:H₂O:TIPS, analyzed by MALDI-

TOF, and the desired mass for **216** was observed. Initial attempts to alkylate **216** with 2-methyl-1-iodopropane (**217**) with aqueous tetraethylammonium hydroxide over 3 h were unsuccessful, but by increasing the reaction time to 48 h, the mass of alkylated product **218** was observed by MALDI-TOF analysis. Unfortunately, subsequent efforts to deprotect the N-terminal semicarbazone and aminoacylate it with Fmoc-Arg(Pmc)-OH yielded no desired product (**219**) or easily discernable by-product masses by MALDI-TOF analyses (Scheme 3.23). An in-solution approach to the synthesis of the aza-leucine analogues would be investigated instead.



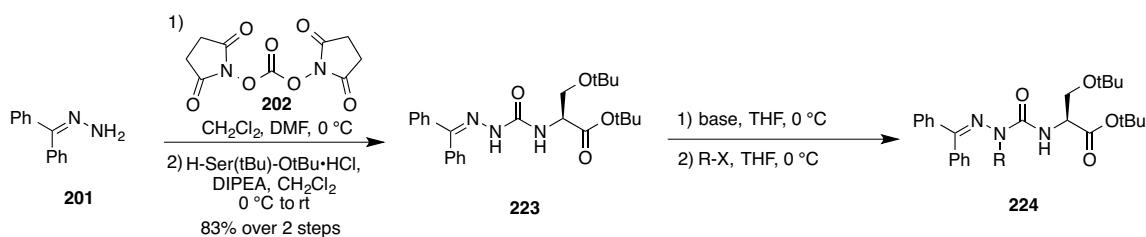
Scheme 3.23 – Attempted on-resin aza-leucine formation.

Initially, methyl-ester protected semicarbazone **220** was prepared by reacting benzophenone hydrazone (**201**) with disuccinimidyl carbonate (**202**), then the addition of a solution of H-Leu-OMe hydrochloride and DIPEA in CH₂Cl₂ via cannulation. Attempts to alkylate the semicarbazone nitrogen with tetraethylammonium hydroxide as a base led to a decomposition of the product via methyl ester hydrolysis. When the base was exchanged for potassium *tert*-butoxide (1.1 equivalents at 0 °C), dehydrated hydantoin **222** product was formed in appreciable yield, instead of **221**. Previous alkylation experiments had reported some hydantoin byproduct formation with methyl-ester protected semicarbazones as a result from the 5-*exo*-trig cyclization, suggesting that would be the initial mechanistic step.¹⁷⁸ Subsequent deprotonation of the serine α -hydrogen, followed by the elimination of the *tert*-butyl group could lead to the formation of **222** (Scheme 3.24).



Scheme 3.24 – Formation and proposed mechanism for the synthesis of dehydrated hydantoin **222**.

Fortunately, subsequent studies by Lubell and coworkers showed that the utilization of C-terminal *tert*-butyl esters in semicarbazone alkylations minimized the amount of hydantoin byproducts.¹⁷⁸ Semicarbazone **223** was constructed in an identical fashion to the methyl ester derivative **220** and a small sample was exposed to tetraethylammonium hydroxide for 4 h at 0 °C. After no decomposition was observed by TLC, test alkylation conditions were examined to install the desired isobutyl side chain onto the aza-glycine backbone (Scheme 3.25).

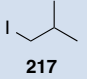
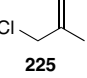
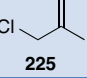
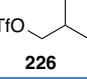
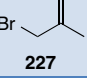
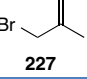
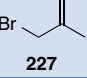


Scheme 3.25 – Synthesis of *tert*-butyl ester protected semicarbazone **223 and test alkylation scheme overview.**

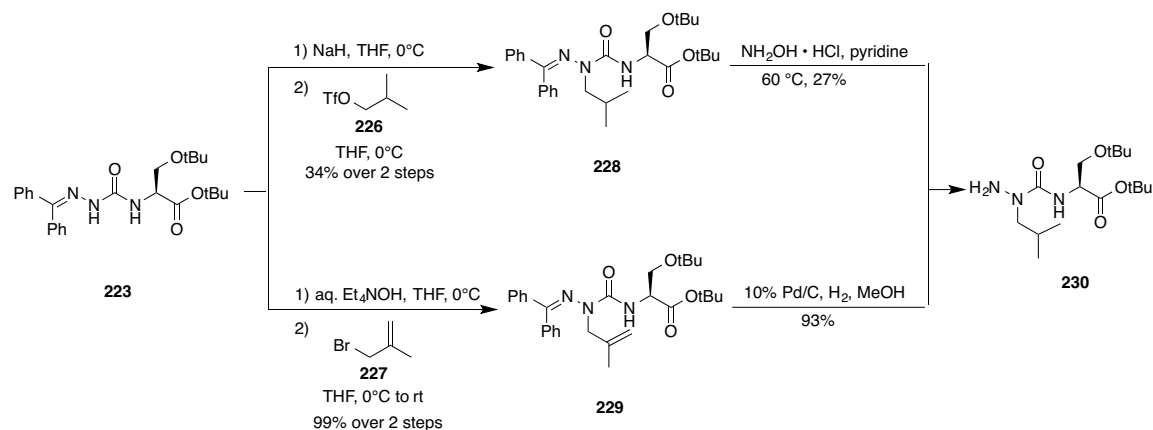
A variety of bases and electrophiles were used in an effort to alkylate semicarbazone **223** (Table 3.10). Any combinations of tetraethylammonium hydroxide and either 1-iodo-2-methylpropane (**217**) or 3-chloro-2-methylpropene (**225**) were unsuccessful at transforming any starting material to its alkylated derivative even after prolonged reaction times and elevated temperatures (entries 1-3). The decision to change to the non-nucleophilic sodium hydride resulted in modest product formation when paired with either isobutyl triflate (**226**, entry 4), or 3-bromo-2-methylpropene (**227**, entry 5). Repeating the deprotonation and alkylation of **223** with sodium hydride and increased quantity of 3-bromo-2-methylpropene on a larger scale led to a disappointing

decrease in yield (entry 6). However, after adapting identical alkylation conditions used in the aza-arginine synthesis, the desired product was obtained in a nearly quantitative yield (entry 7).

Table 3.10 – Test alkylation conditions for semicarbazone 223. * larger scale

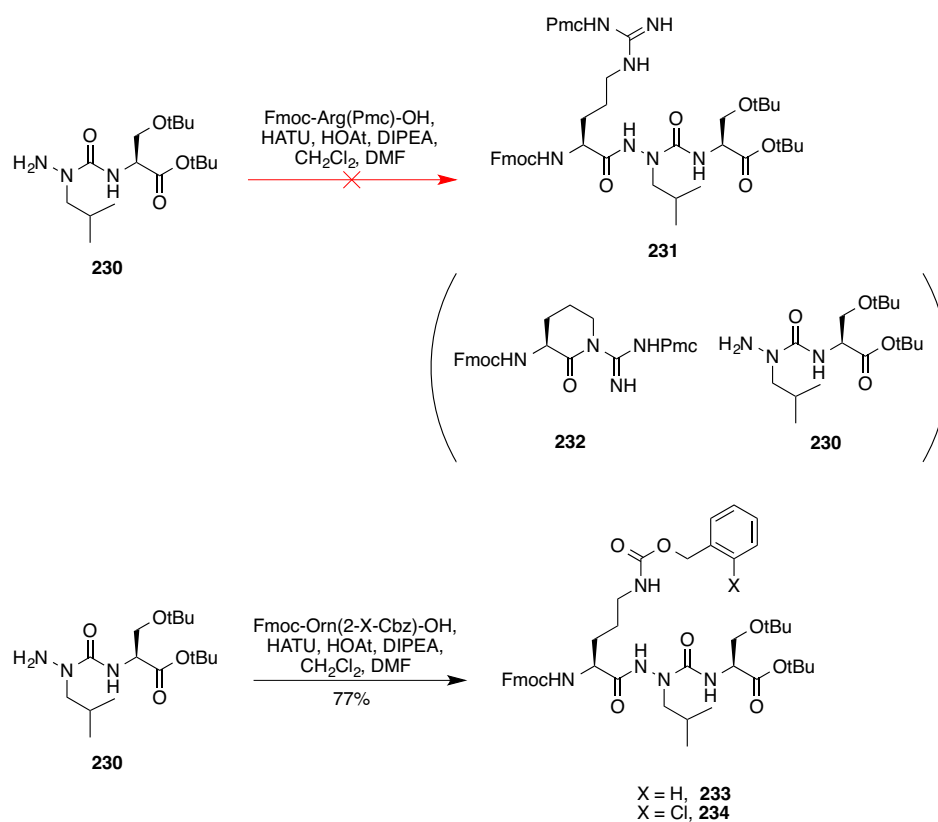
Reaction Conditions	Base used	Base equiv.	R-X	R-X equiv.	temp (°C)	time (h)	Yield (%)
1	Et ₄ NOH	1.2	 217	1.5	0	5	0
2	Et ₄ NOH	1.5	 225	2.0	0 – 20	18	0
3	Et ₄ NOH	5.0	 225	10.0	0 – 20	18	0
4	NaH	1.2	 226	1.5	0	6	34
5	NaH	1.2	 227	1.5	0	5.5	39
6	NaH	1.3	 227	2 x 3.0	0	5.5	28*
7	Et ₄ NOH	5.0	 227	7.5	0 – 20	60	99*

After successfully alkylating semicarbazone **223** to form **229**, the product was exposed to an atmosphere of hydrogen gas in the presence of 10% palladium on carbon to hydrogenate the alkene and concomitantly remove the N-terminal benzophenone moiety. Semicarbazide **230** was also accessed by the deprotection of alkylated semicarbazone **228** with hydroxylamine hydrochloride in pyridine. Due to the dramatically improved yields employing the allylation/hydrogenation strategy, this methodology was used for future scale-ups (Scheme 3.26).



Scheme 3.26 – Alternate approaches to synthesis of semicarbazide 230.

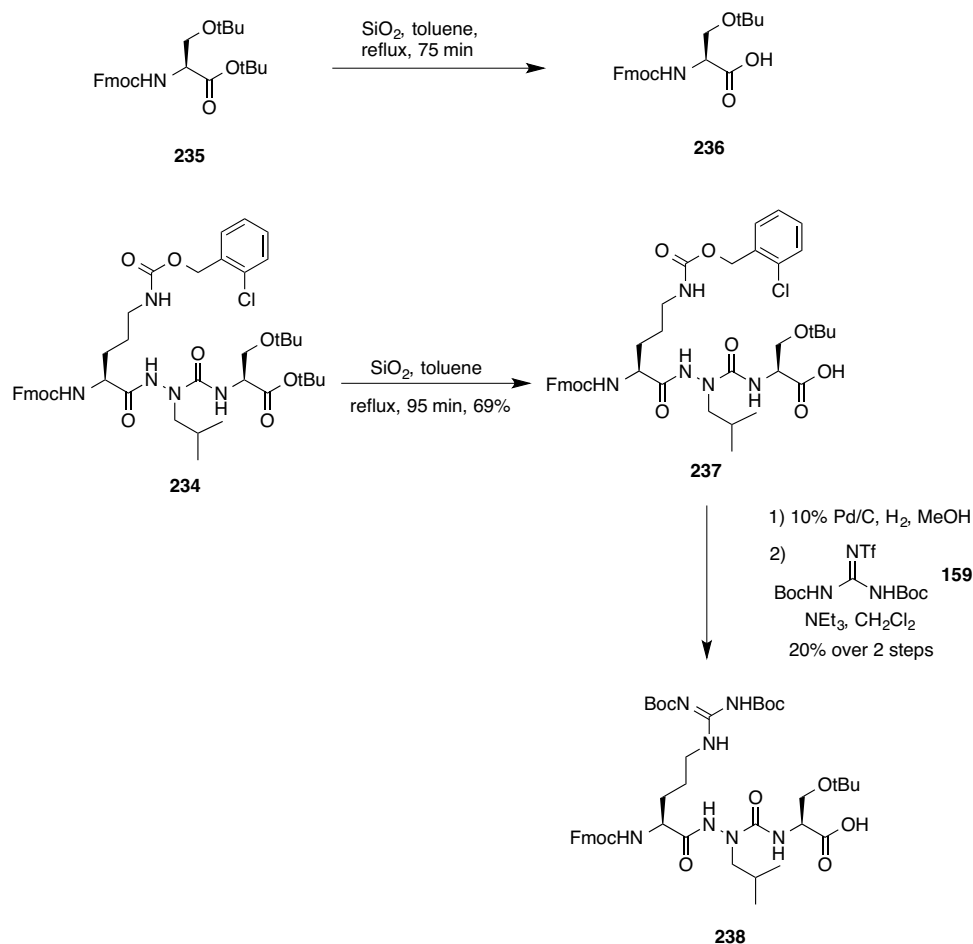
Because of the difficulty in Fmoc protecting semicarbazide **206** in the aza-Arg synthesis, a similar reaction was not attempted for the aza-Leu synthesis, targeting the aza-tripeptide instead. Semicarbazide **230** was added to a briefly preactivated solution of Fmoc-Arg(Pmc)-OH, HATU, 10 mol% HOAt and DIPEA in DMF and CH₂Cl₂, but the tripeptide **233** was not formed. Starting material **223** was largely recovered from this attempted coupling along with Fmoc-Arg(Pmc) lactam (**232**) after flash chromatography. This δ -lactam sideproduct was assigned based on ¹H-NMR and MS analysis. By repeating the same coupling reaction with a δ -carbamate protected ornithine, the desired aza-tripeptides **233** and **234** were obtained (Scheme 3.27). The success of this approach was proposed to be due to the diminished ability of the carbamate δ -nitrogen to react with the activated amino acid.



Scheme 3.27 – Attempted coupling of semicarbazide **230** with Fmoc-Arg(Pmc)-OH and syntheses of aza-Leu-containing tripeptides **233** and **234**.

Deprotection conditions to remove the *tert*-butyl ester while retaining the serine *tert*-butyl ether were next explored. This chemoselective deprotection was reported by refluxing model di-protected substrates in toluene in the presence of silica.¹⁷⁹ Model substrate **235** was synthesized by Fmoc protecting H-Ser(*t*Bu)-OtBu hydrochloride, and this compound was refluxed at 110 °C in toluene with 25% w/v flash-grade silica added for 75 minutes. TLC and ¹H-NMR analyses indicated that the product had been completely consumed with the dominant species remaining being the *tert*-butyl ester deprotected compound **236**. These reaction conditions were then adapted to aza-tripeptide **234**, monitoring the conversion by TLC and LC-MS every 30 minutes. After 95 minutes, the first trace of di-*tert*-butyl deprotection was observed by LC-MS, so the

reaction was quenched, purifying free acid **237** by silica flash chromatography in a 69% yield (Scheme 3.28). The loss of the *tert*-butyl ester hydrogens at ~1.4 ppm were observed as the only major difference in the ¹H-NMR spectra of **234** and **237** (Figure 3.46). Subsequent Cbz deprotection and guanidinylation of the ornithine δ-amine yielded aza-tripeptide **238**.



Scheme 3.28 – Test *tert*-butyl ester deprotection conditions on Fmoc-Ser(*t*Bu)-OtBu (**235**) and aza-tripeptide **234** and completion of aza-tripeptide **238**.

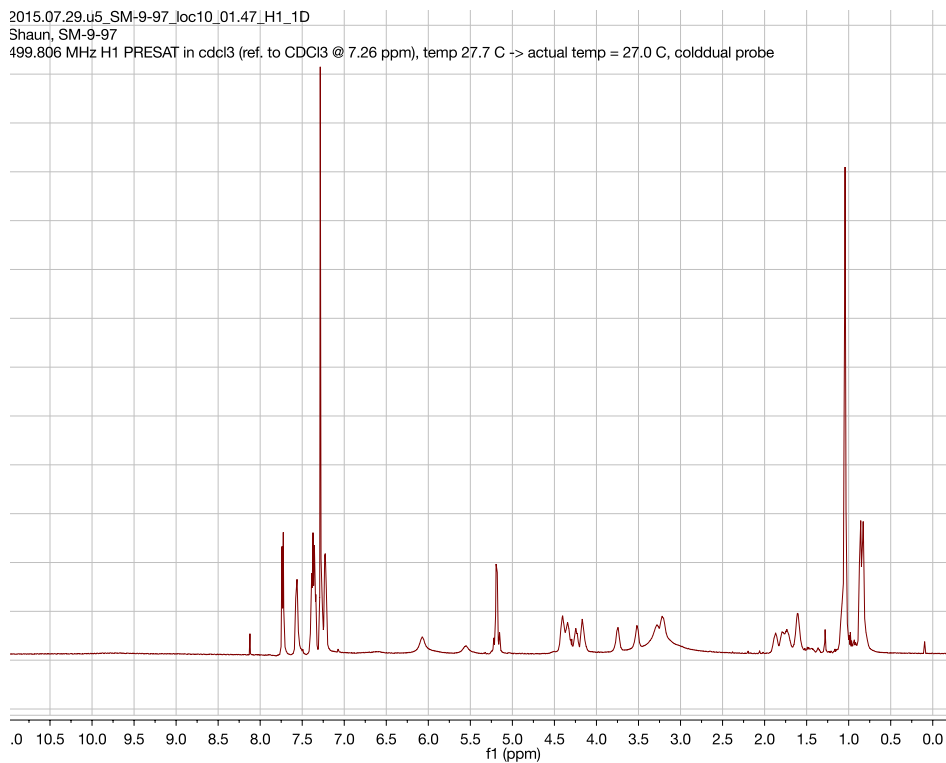
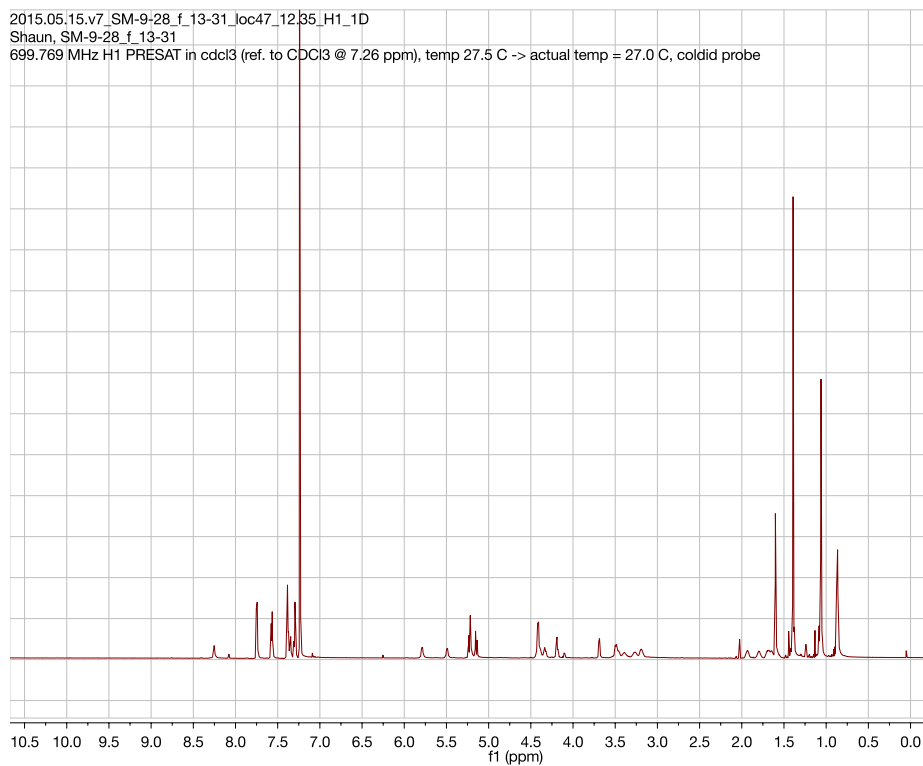


Figure 3.46 – ^1H -NMR spectra of aza-tripeptide **234** (top) and **237** (bottom). The absence of the *tert*-butyl ester ^1H signals at 1.4 ppm are evident for compound **237**.

To complete the syntheses of these aza-Leu analogues, two equivalents (0.2 mmol) of **153** were Fmoc-protected with a solution of 20% piperidine in DMF, then 0.95 equivalents of a briefly preactivated solution of aza-tripeptide **238** were added to the resin and bubbled under Ar gas for 3 h. An additional 1.3 equivalents of **238** were added without any additional SPPS steps and coupled for an additional 2 h. A small sample of the resin was cleaved and the resultant mass analyzed by MALDI-TOF; after confirmation of the desired decapeptide, the amino acid chain was elongated by the addition of Fmoc-Pro-OH, again analyzing the mass through resin cleavage and MALDI-TOF. SPPS was continued, generating pyr-1-apelin-13 analogue **239** and apelin-17 analogue **240** (Figure 3.47).

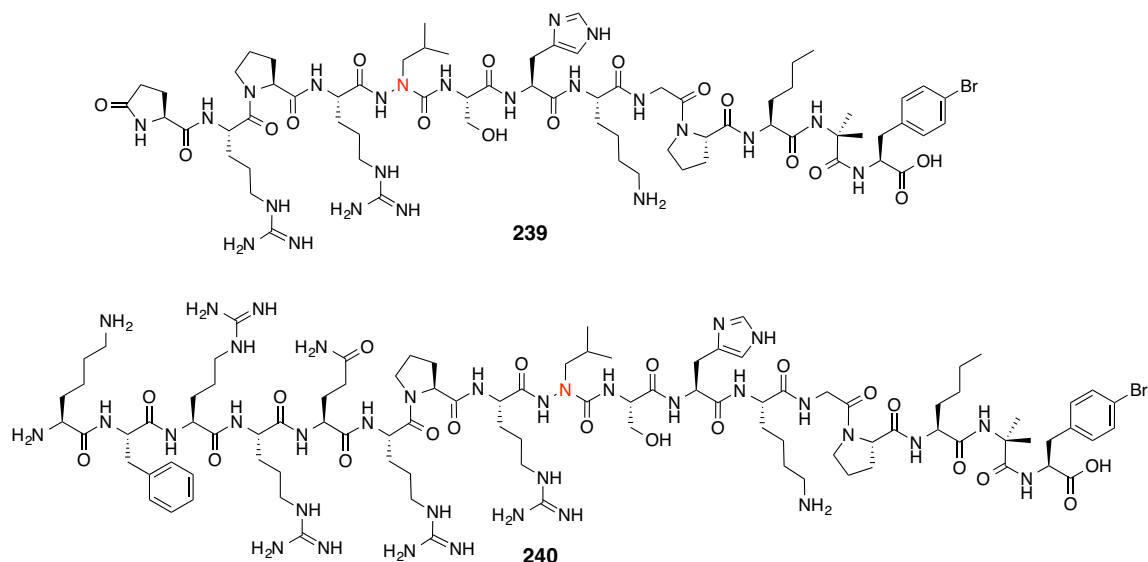
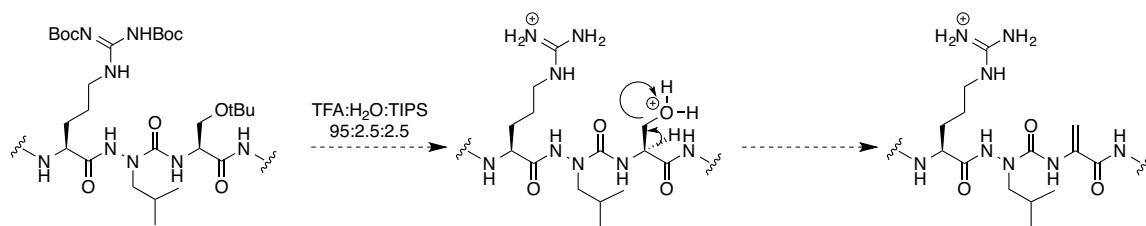


Figure 3.47 – Structures of aza-Leu5 pyr-1-apelin-13 A2 (239) and aza-Leu9 apelin-17 A2 (240) analogues.

Unlike the majority of the other analogues synthesized by manual SPPS, the dominant mass observed after resin cleavage was actually the $(M-H_2O)^+$ peak for both

pyr-1-apelin-13 analogue **239** and apelin-17 analogue **240**. The dehydrated product was carefully isolated from the desired analogue using C₁₈-RP-HPLC by Mr. Tyler McDonald and will undergo LC-MS analysis to determine the location of the unexpected dehydration. Initial proposals suggest that the prolonged exposure of resin-bound aza-Leu analogues to the strongly acidic cleavage conditions may have led to the elimination of the serine hydroxyl group (Scheme 3.29). This is likely due to the enhanced acidity of α -hydrogens adjacent to the semicarbazide functionality in the aza-Leu, observed by their propensity to racemize at the dipeptide stage.¹⁷⁸



Scheme 3.29 – Proposed dehydration of aza-Leu-containing apelin analogues.

3.5.6 Pharmacokinetics of Arg4-Leu5 apelin analogues in human plasma

To help assess the pharmacokinetics of Arg4-Leu5 modified apelin analogues in human plasma, replicate experiments were incubated at 37 °C for varying lengths of time. After removing lipid components and larger plasma proteins with a Harvard apparatus spin concentration column, remaining apelin analogues were quantified using C₁₈ RP-HPLC, comparing replicate samples against a known quantity of internal standard dansyl-YVG (**81**). Triplicate runs at 30 and 60 minute incubation times of all peptide analogues were performed by Mr. Tyler McDonald (Table 3.11).

Table 3.11 – Remaining percentage of Arg4-Leu5 apelin analogues after incubation in human plasma and C₁₈ RP-HPLC analysis. (n = 3)

	pyr-1-apelin-13 A2 analogues			apelin-17 A2 analogues		
Arg-Leu Modification	analogue number	% apelin 30 min	% apelin 60 min	analogue number	% apelin 30 min	% apelin 60 min
None	104	77 ± 19	65 ± 14	108	43 ± 1	35 ± 5
D-Leu	154	32 ± 2	22 ± 1	155	80 ± 3	80 ± 4
NMeLeu	162	77 ± 3	59 ± 6	163	49 ± 10	47 ± 7
αMeArg	193	88 ± 4	62 ± 6	194	61 ± 10	55 ± 4
αMeLeu	199	45 ± 6	38 ± 3	200	77 ± 4	48 ± 7
azaArg	210	83 ± 3	57 ± 1	211	96 ± 6	94 ± 3
azaLeu	239	19 ± 5	2 ± 1	240	82 ± 1	68 ± 4
native apelin	71	45 ± 8	12 ± 2	70	51 ± 17	39 ± 7

A clear trend can be observed from the pharmacokinetic data performed on the pyr-1-apelin-13 A2 analogues. Analogues substituted at the Arg4 α-position (**193, 210**) and the amide of Leu5 (**162**) seem to retain a similar quantity of apelin analogue compared to **104** following 30 and 60 minutes of exposure to plasma. Conversely, alteration of the Leu5 α-position (**154, 199, 239**) seems to accelerate hydrolysis of the pyr-1-apelin-13 analogue. On a strict steric crowding basis, modification at Leu5 should have a universal effect at prolonging the half-life of the pyr-1-apelin-13 analogue in plasma if a Leu5-Ser6 site of degradation is the correct location as previously reported.¹⁴⁸ Since the beneficial stabilizing effects are crowded around the Arg4-Leu5 amide bond, these results seem to support our proposal of a site of protease degradation existing between Arg4-Leu5.

In terms of the electronic stability of the amide bond, the large discrepancy between the half-lives of aza-analogues **210** and **239** also supports our proposed site of proteolysis. Flanking the susceptible amide bond with nitrogen atoms on either side of the carbonyl carbon would significantly improve its stability to proteolysis, as observed

in **210**. If the aza-analogue is included C-terminal to the susceptible amide bond, proteolysis could actually be enhanced due to the extrusion of a stable C-terminal semicarbazide (Figure 3.48).

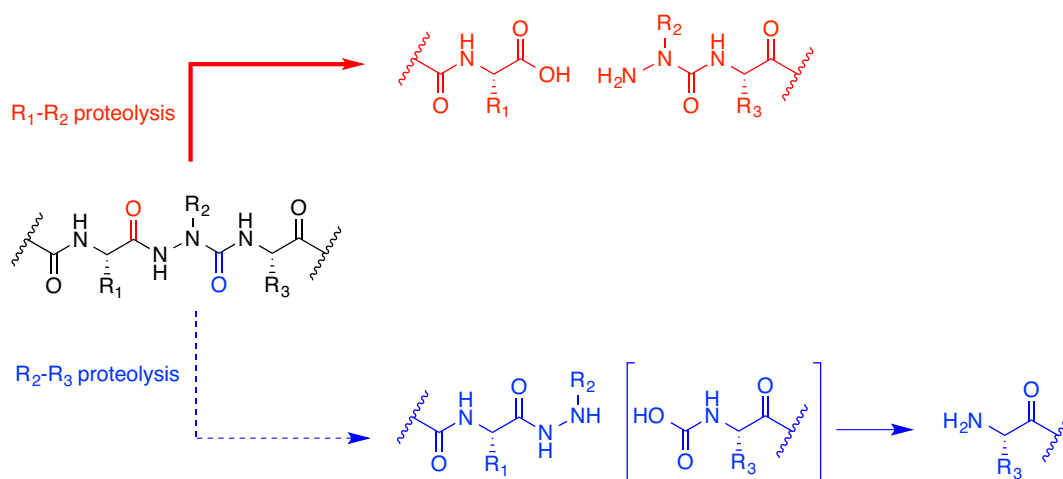


Figure 3.48 – Stability of aza analogues to hydrolysis. Protease-mediated hydrolysis between R₁ and R₂ (red carbonyl) would be accelerated due to the stability of the resultant amino acid and semicarbazide moieties; hydrolysis between R₂ and R₃ (blue carbonyl) would be diminished due to the instability of the N-carbamic acid intermediate.

A clear trend cannot be as easily drawn with the apelin-17 A2 analogues, with virtually all of the analogues showing an improved percentage of remaining peptide after 30 and 60 minutes of incubation time. Of particular interest was the enhanced stability of aza-Arg8-apelin-17 A2 (**211**), which showed virtually no decomposition over the 60-minute assays. These results suggest that any modification surrounding the Arg-Leu-Ser site of apelin-17 results in an enhanced stability, putatively highlighting the role of this N-terminal protease in the degradation of apelin-17. However, after the *in vitro* plasma quantitation experiments had been performed, it was observed that a few of the N-

terminal truncated apelin-17 fragments co-elute with the parent apelin-17, so these results are likely artificially high.

However with all peptide analogues, *in vitro* plasma stability is only a portion of what is necessary to generate a successful analogue; physiological activity must be assessed alongside the pharmacokinetics to determine the significance of a particular modification on apelin itself. As observed with **103**, which had exceptional *in vitro* plasma stability but minimal physiological activity, synthetic manipulation of the apelin scaffold may certainly generate inactive compounds.

3.5.7 Physiological testing of Arg4-Leu5 apelin analogues

At the time of completion of this thesis, only D-Leu5-pyr-1-apelin-13 A2 (**154**) had been examined for any physiological activity (Figure 3.49). The hypotensive activity of this analogue yielded a very interesting result as the inversion of one stereocenter at the Leu5 position in **154** completely negated any physiological activity of the previously potent **104** analogue. This further highlights the physiological significance of the 'RPRL' motif in apelin, and shows an importance of not only the sequence in this region but also the structure. Past receptor-binding studies had highlighted that D-Leu5-pyr-1-apelin-13 had only a minimal contribution in decreasing APJ binding,¹¹⁸ further emphasizing the disparity between receptor binding and physiological activity. In combination with the current pharmacokinetic stability experiments, further physiological results on the remaining Arg-Leu analogues will help to determine the significance of this region of the peptide for both activity as well as protease stability.

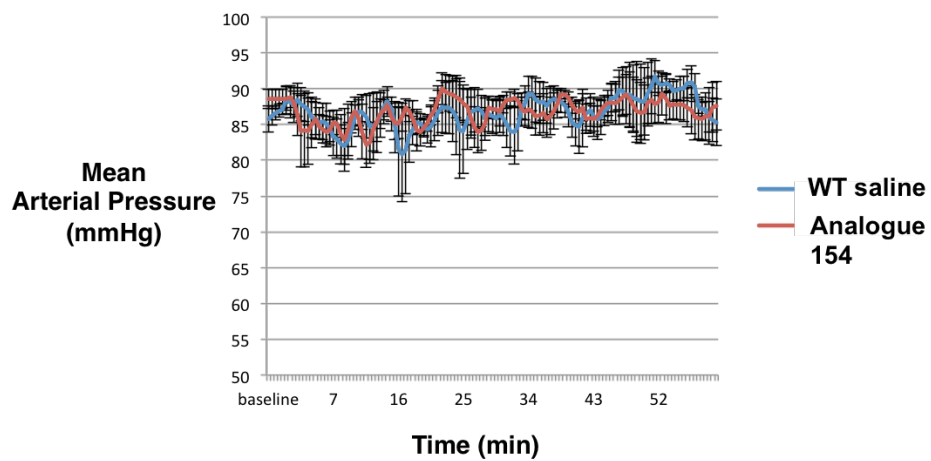


Figure 3.49 – Hypotension assay testing for D-Leu⁵-pyr-1-apelin-13 analogue 154. No statistically significant difference was observed between saline injection and injection of 20 μ M **154** in rats, n = 5.

3.6 Conclusions and future directions

In this chapter, biochemical evidence was presented to suggest that ACE2 is a significant regulatory enzyme in the proteolysis of pyr-1-apelin-13 in mouse plasma. This was observed through the increased quantity of apelin isoforms after *in vitro* incubation and HPLC analyses in ACE2 knockout plasma versus wild type plasma. Kinetic studies with recombinant human ACE2 highlighted a difference in affinity of ACE2 for pyr-1-apelin-13 over the longer apelin-17 isoform under optimized *in vitro* conditions. Two unique pyr-1-apelin-13 analogues (**103**, **104**) were synthesized with C-terminal substitutions that showed complete stability to ACE2, and were subsequently used to highlight the relevance of this protease as a regulatory enzyme in the *in vitro* degradation of pyr-1-apelin-13 human plasma. In contrast, ACE2 is suspected to not dominate in the proteolysis of apelin-17.

It was determined that Pro12 substitution in the pyr-1-apelin-13 scaffold is the modification responsible for conferring ACE2 resistance; however, this enhanced stability does not necessarily translate into physiologically active peptide hormones. Pyr-1-apelin-13 A2 analogue (**104**) showed comparable activity to the native peptide in all physiological assays examined, with the added benefit of enhanced *in vitro* plasma stability. This advantageous ‘A2’ C-terminus was applied to synthesize 3 additional analogues with improved physiological parameters, including the most potent apelin-17 A2 (**108**) analogue.

Initial investigations into the *in vitro* plasma degradation of **104** highlighted a putative proteolytic site between Arg4-Leu5 in the pyr-1-apelin-13 backbone. Through the use of a fluorescent substrate **141** and a FRET-based assay, the activity-guided

fractionation of human plasma yielded tissue kallikrein (KLK1) as a candidate protease for this degradation. There are still questions surrounding whether KLK1 or its activating metalloprotease thermolysin is responsible for proteolysis, and this is currently being investigated in our lab. However, plasma kallikrein, KLKB1 was discovered to selectively cleave apelin-17 and analogues between Arg3-Arg4 *in vitro*. Subsequent efforts to quantitatively analyze the fragments of ACE2 resistant **108** highlighted this location as a site of rapid proteolysis after *in vitro* human plasma incubation. The increase in the unnatural Aib-*p*-BrPhe C-terminal dipeptide from these quantitative experiments highlights yet another position for proteolytic degradation common to both **104** and **108**.

Lastly, six unique synthetic modifications have been incorporated at the Arg-Leu position, generating a total of twelve 'A2'-substituted apelin analogues. *In vitro* human plasma pharmacokinetic experiments have been performed on these analogues, and have highlighted Arg4-substituted analogues as having improved plasma stability in the pyr-1-apelin-13 backbone. In contrast, most analogues showed improved stability with the apelin-17 scaffold. Future physiological testing and structural characterization of these Arg-Leu analogues will give some insight into the proteolysis of this region, as well as the structure-activity relationship of this critical region of the peptide.

4 Experimental Procedures

4.1 General information

4.1.1 Reagents, solvents and purification

Commercially available chemical and biological reagents were purchased from Sigma-Aldrich Canada, Chem-Impex International Inc., Fisher Scientific Ltd., Alfa Aesar Ltd., R&D Systems, Tocris Bioscience, Harvard Apparatus, Caledon or VWR International, and used without further purification unless otherwise stated. All solvents were of American Chemical Society (ACS) grade and were used without further purification. All anhydrous reactions were conducted under positive pressure of argon using flame-dried glassware. Solvents for anhydrous reactions were distilled prior to use: dichloromethane and dichloroethane were distilled over calcium hydride, tetrahydrofuran and diethyl ether were distilled over sodium with benzophenone as an indicator, and methanol was distilled over magnesium. HPLC grade acetonitrile, dimethylformamide, 2-propanol, hexanes and methanol were used without further purification. Commercially available ACS grade solvents (>99.0% purity) were used for column chromatography without further purification. Deionized water was obtained from a Milli-Q reagent water filtration system (Millipore Co., Milford, MA). All reactions and fractions from column chromatography were monitored by thin layer chromatography (TLC) using glass plates with a UV fluorescent indicator (normal SiO₂, Merck 60 F₂₅₄). Visualization was performed following: UV absorption by fluorescence quenching, staining with phosphomolybdic acid in ethanol (10 g/100 mL), ninhydrin (ninhydrin : acetic acid : *n*-butanol, 0.6 g : 6 mL : 200 mL) or potassium permanganate

(KMnO₄ : K₂CO₃ : NaOH : H₂O, 1.5 g : 10 g : 0.12 g : 200 mL). Flash chromatography was performed using Merck type 60, 230 – 400 mesh silica gel. The removal of solvents *in vacuo* was performed via evaporation under reduced pressure using a Büchi rotary evaporator. Analytical scale high performance liquid chromatography (HPLC) was performed on one or more of the following systems: Varian ProStar chromatograph equipped with model 210 pump heads, a model 325 dual wavelength UV detector, and a Rheodyne 7725i injector fitted with a 100 µL sample loop; a Gilson chromatograph equipped with model 322 pump heads, a model 171 diode array detector, a FC 203B fraction collector and a Rheodyne 7725i injector fitted with a 1000 µL sample loop. Preparative and semi-preparative scale HPLC was performed on a Gilson chromatograph equipped with model 322 pump heads, a model UV/VIS-156 detector and a GX-271 liquid handler. Columns used for purification were: Phenomenex Luna 5u, C18(2) 100 Å, 5 µm, 10.00 x 250 mm, analytical column - Vydac Protein-Peptide Column 300 Å, 5 µm, 4.6 mm x 250 mm; Alltech Prosphere 300 Å, 5 µm, 4.6 mm x 250 mm; GE Healthcare stainless steel walled µRPC C2/C18 (3 µm, 4.6 × 100 mm). HPLC solvents were filtered through a Millipore filtration system under vacuum prior to use.

4.1.2 Characterization

Optical rotations were measured on a Perkin Elmer 241 polarimeter with a microcell (10 cm, 1 mL) at ambient temperature and are reported in units of 10⁻¹ deg cm² g⁻¹. All reported optical rotations were referenced against air and measured at the sodium D line ($\lambda = 589.3$ nm).

Infrared spectra (IR) were recorded on a Nicolet Magna 750 or a 20SX FT-IR spectrometer. Cast refers to the evaporation of a solution on a NaCl plate.

Nuclear magnetic resonance (NMR) spectra were recorded on an Agilent/Varian Inova 600, Inova 400, Inova 300, DD2 MR 400, VNMRS 700 or Unity 500 spectrometer at 27 °C. For ^1H (300, 400, 500, 600. or 700 MHz) spectra, δ values were referenced to CDCl_3 (7.26 ppm), D_2O (4.79 ppm) or CD_3OD (3.30 ppm), and for ^{13}C (100, 125, 150 or 175 MHz) spectra, δ values were referenced to CDCl_3 (77.0 ppm) or CD_3OD (49.0 ppm), as the solvents. Reported splitting patterns are abbreviated as s = singlet, d = doublet, t = triplet, q = quartet, sept = septet, m = multiplet.

Mass spectra (MS) were recorded on a Kratos AEIMS-50, Bruker 9.4T Apex-Qe FTICR (high resolution, HRMS) or on a Perspective Biosystems VoyagerTM Elite MALDI-TOF MS using either 4-hydroxy- α -cyanocinnamic acid (HCCA) or 3,5-dimethoxy-4-hydroxycinnamic acid (sinapinic acid) as matrices. MS/MS was performed on a Bruker Ultraflex extreme MALDI/TOF/TOF. LCMS was performed on an Agilent Technologies 6130 LCMS.

Fluorescence experiments were performed on a Photon Technology International (PTI) MP1 Fluorescence System.

4.2 Lactocin S synthesis

4.2.1 General procedure for elongation using Fmoc SPPS⁶⁸

NMM (6 equiv) was added to a solution of Fmoc protected amino acid (5.0 equiv to resin loading), HOBt (5.0 equiv) and PyBOP (4.9 equiv) in DMF (10 mL). The solution was allowed to pre-activate for 5 min. The solution was transferred to the reaction vessel containing pre-swelled resin and was bubbled with argon for 3 h. A small sample of the peptide was cleaved from the resin (by treatment with 95% TFA/2.5%

TIPS or anisole/2.5% H₂O for 2 h) and the completion of the reaction was determined by MALDI-TOF analysis [TIPS was used as a scavenger for peptide cleavage up until residue 13. Afterwards, anisole was used instead as it produced cleaner MALDI spectra]. Resin was washed with DMF (3 × 10 mL), then 20% Ac₂O in DMF (10 mL) was added to the resin for 10 min to effect end capping. Resin was again washed with DMF (3 × 10 mL). Then 20% piperidine in DMF (3 × 10 mL) was added to remove the N-terminal Fmoc protecting group, this reaction was monitored by UV-Vis spectroscopy, observing the dibenzofulvene-piperidine adduct at $\lambda = 301$ nm.

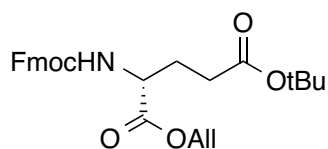
4.2.2 General procedure for cleavage and purification of lactocin S analogues⁶⁸

To simultaneously cleave the peptide from 2-chlorotrityl resin, remove side chain protecting groups, and generate the α -ketoamide functionality at the N-terminus of the peptides, a solution of 95:2.5:2.5 TFA:anisole:H₂O was added to the resin-bound peptide for 2 hours. The resin beads were removed via filtration through glass wool and the filtrate was concentrated *in vacuo*. The crude peptide was obtained by precipitation with cold Et₂O. All cleavage and precipitation steps were done under an atmosphere of argon gas to reduce the oxidation of remaining sulfur atoms in methionine or lanthionine residues. The crude peptide was dissolved in a 1:1 water:methanol (0.1% TFA) and injected onto a C₂/C₁₈ RP-HPLC column (GE Healthcare, 4.6 x 100 mm, 3 μ m) using water (0.1% TFA) and methanol (0.1% TFA) as eluents. TCEP (1.5 mg/L) was added to the HPLC solvents and the product was collected under a stream of argon gas to minimize oxidation of the sulfur atoms in methionine and lanthionine residues. The HPLC method followed was: gradient beginning at 5% methanol for 1 min, climb to 60% over 4 min, then climb to 100% over 8 min, remain at 100% for 2 min, return to 5%

over 2 min and remain at 5% for 8 min (flow rate 1 mL/min, UV detection at 220 nm). The peptide was collected as a broad peak at ~13.5 min and solvent was removed *in vacuo*. The residue was then dissolved in approximately 100 μ L methanol and 900 μ L water (both with 0.1% TFA) and lyophilized to give the final product.

4.2.3 Orthogonally-protected DAP synthesis⁶⁶

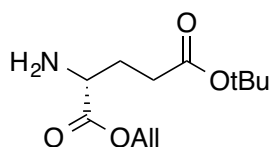
(*E*)-5-(*tert*-butyl) 1-(allyl) (((9*H*-fluoren-9-yl)methoxy)carbonyl)-D-glutamate (53**)**



A solution of Fmoc-D-Glu(*t*Bu)-OH (25.0 g, 58.8 mmol) and Na₂CO₃ (7.47 g, 70.5 mmol) in DMF (400 mL) was stirred vigorously under Ar gas. Allyl bromide (6.05 mL, 70.5 mmol) was added and the mixture was stirred for 15 h. The reaction mixture was then concentrated *in vacuo*, resuspended in EtOAc (250 mL), washed with water (2 x 150 mL) and brine (100 mL), dried over Na₂SO₄, filtered and concentrated *in vacuo*. Compound **53** was obtained as a white solid (27.7 g, quantitative) and used without any further purification. (*R_f* 0.8 on SiO₂, 1:1 hexanes:EtOAc); [α]_D²⁶ 5.6 (*c* 1.04 EtOAc); IR (EtOAc cast) 3337, 3067, 2979, 2933, 1728, 1529, 1451, 1368, 1252 cm⁻¹; ¹H (CDCl₃, 500 MHz): δ 7.76 (dd, *J* = 7.6, 1.1 Hz, 2H, Ar-H), 7.63 – 7.57 (m, 2H, Ar-H), 7.43 – 7.36 (m, 2H, Ar-H), 7.35 – 7.28 (m, 2H, Ar-H), 5.91 (ddt, *J* = 16.5, 11.0, 5.8 Hz, 1H, -OCH₂CH=CH), 5.51 (d, *J* = 8.3 Hz, 1H, N-H), 5.34 (dq, *J* = 17.2, 1.5 Hz, 1H, -OCH₂CH=CH), 5.26 (dq, *J* = 10.5, 1.3 Hz, 1H, -OCH₂CH=CH), 4.66 (d, *J* = 5.8 Hz, 2H, -OCH₂CH=CH), 4.46 – 4.33 (m, 3H, Fmoc-CH₂, Glu-CH α), 4.22 (t, *J* = 7.0 Hz, 1H,

Fmoc-CH), 2.35 (tq, $J = 16.8, 9.5, 7.9$ Hz, 2H, Glu-CH $\underline{2}\gamma$), 2.26 – 2.14 (m, 1H, Glu-CH $\underline{2}\beta$), 2.07 – 1.93 (m, 1H, Glu-CH $\underline{2}\beta$), 1.45 (s, 9H, -C(CH $\underline{3}$) $\underline{3}$); ^{13}C (CDCl $\underline{3}$, 125 MHz): δ 172.1, 171.8, 156.0, 143.9, 143.7, 141.3, 141.3, 131.5, 127.7, 127.1, 125.1, 125.1, 120.0, 119.0, 80.9, 67.1, 66.1, 53.6, 47.2, 31.5, 28.1, 27.6; HRMS (ES) Calculated for C $\underline{27}$ H $\underline{31}$ NNaO $\underline{6}$ 488.2044, found 488.2047 (M+Na) $\underline{+}$.

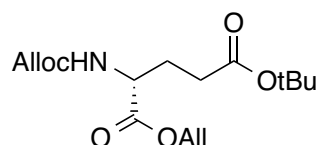
(*E*)-5-(*tert*-butyl) 1-(allyl) D-glutamate (54**)**



Orthogonally protected **53** (27.7 g, 59.5 mmol) was dissolved in a solution of CH $\underline{2}$ Cl $\underline{2}$ (150 mL) and diethylamine (150 mL) and was stirred under Ar gas for 2 h. The reaction was concentrated *in vacuo* and resuspended in EtOAc (300 mL). The free amine was extracted by washing with 10% aqueous citric acid (100 mL), water (100 mL) and brine (100 mL). The pooled aqueous fractions were adjusted to pH 9 by the addition of solid K $\underline{2}$ CO $\underline{3}$, and then washed with EtOAc (3 x 100 mL) to re-extract the desired compound. The organic layers were dried over Na $\underline{2}$ SO $\underline{4}$, filtered, and concentrated *in vacuo*. Amino acid **54** was purified via flash chromatography (silica gel, 50% EtOAc in hexanes), yielding a yellow oil (12.9 g, 89%). (R_f 0.2 on SiO $\underline{2}$, 1:1 hexanes:EtOAc); $[\alpha]_D^{26}$ -3.1 (*c* 1.45 EtOAc); IR (EtOAc cast) 3388, 3320, 2979, 2935, 1730, 1452, 1368, 1255, 1157 cm $\underline{-1}$; ^1H (CDCl $\underline{3}$, 500 MHz): δ 5.90 (ddt, $J = 17.2, 10.4, 5.8$ Hz, 1H, -OCH $\underline{2}$ CH=CH $\underline{2}$), 5.31 (dq, $J = 17.2, 1.5$ Hz, 1H, -OCH $\underline{2}$ CH=CH $\underline{2}$), 5.23 (dq, $J = 10.5, 1.3$ Hz, 1H, -OCH $\underline{2}$ CH=CH $\underline{2}$), 4.60 (dt, $J = 5.8, 1.4$ Hz, 2H, -OCH $\underline{2}$ CH=CH $\underline{2}$), 3.47 (dd, $J = 8.3, 5.2$ Hz, 1H, Glu-CH $\underline{\alpha}$), 2.35 (t, $J = 7.5$ Hz, 2H, Glu-CH $\underline{\gamma}$), 2.09 – 1.97 (m, 1H, Glu-

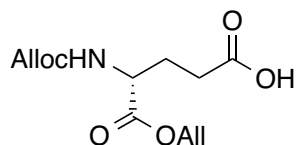
$\text{CH}_2\beta$), 1.84 – 1.73 (m, 1H, Glu- $\text{CH}_2\beta$), 1.42 (s, 9H, $-\text{C}(\text{CH}_3)_3$); ^{13}C (CDCl_3 , 125 MHz): δ 175.4, 172.4, 131.9, 118.6, 80.4, 65.6, 53.8, 31.8, 29.9, 28.1; HRMS (ES) Calculated for $\text{C}_{12}\text{H}_{22}\text{NO}_4$ 244.1543, found 244.1544 ($\text{M}+\text{H}$) $^+$.

(E)-5-(tert-butyl) 1-(allyl) ((allyloxy)carbonyl)-D-glutamate (55)



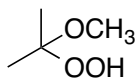
A solution of **54** (12.9 g, 52.9 mmol) and triethylamine (8.10 mL, 58.1 mmol) in EtOAc (150 mL) was cooled to 0 °C before the addition of a solution of allyl chloroformate (6.77 mL, 63.42 mmol) in EtOAc (150 mL) dropwise over 30 minutes. The reaction was slowly warmed to room temperature for 21 h. The crude reaction was washed with 10% citric acid (100 mL), water (100 mL) and brine (100 mL), and concentrated *in vacuo*. The crude product was purified by flash chromatography (silica gel, 20% EtOAc in hexanes) and isolated as a yellow oil (10.6 g, 61%). (R_f 0.7 on SiO_2 , 1:1 hexanes:EtOAc); $[\alpha]_D^{26}$ 8.9 (c 1.4 EtOAc); IR (EtOAc cast) 3349, 3082, 2979, 2934, 1728, 1527, 1368, 1257, 1153 cm^{-1} ; ^1H (CDCl_3 , 400 MHz): δ 5.94 – 5.82 (m, 2H, 2 x - $\text{OCH}_2\text{CH}=\text{CH}_2$), 5.43 (d, $J = 8.4$ Hz, 1H, N-H), 5.35 – 5.14 (m, 4H, 2 x - $\text{OCH}_2\text{CH}=\text{CH}_2$), 4.62 (dt, $J = 5.8, 1.5$ Hz, 2H, - $\text{OCH}_2\text{CH}=\text{CH}_2$), 4.54 (dt, $J = 5.7, 1.5$ Hz, 2H, $\text{OCH}_2\text{CH}=\text{CH}_2$), 4.37 (td, $J = 8.3, 4.8$ Hz, 1H, Glu- $\text{CH}\alpha$), 2.39 – 2.22 (m, 2H, Glu- $\text{CH}\gamma$), 2.19 – 2.09 (m, 1H, Glu- $\text{CH}_2\beta$), 1.97 – 1.89 (m, 1H, Glu- $\text{CH}_2\beta$), 1.42 (s, 9H, $-\text{C}(\text{CH}_3)_3$); ^{13}C (CDCl_3 , 125 MHz): δ 172.0, 171.7, 155.8, 118.9, 117.8, 80.8, 66.0, 65.8, 53.5, 31.5, 28.1, 27.6; HRMS (ES) Calculated for $\text{C}_{16}\text{H}_{26}\text{NNaO}_6$ 350.1574, found 350.1575 ($\text{M}+\text{Na}$) $^+$.

(*R,E*)-4-(((allyloxy)carbonyl)amino)-5-oxo-5-(prop-1-en-1-yloxy)pentanoic acid (56**)**



A solution of **55** (10.6 g, 32.3 mmol) and phenylsilane (3.98 mL, 32.3 mmol) in CH₂Cl₂ (100 mL) had TFA (100 mL) slowly added over 2 minutes. The reaction mixture was stirred for 3 h and concentrated *in vacuo*. The crude residue was purified using flash chromatography (silica gel, 60-100% EtOAc in hexanes gradient), yielding the free acid **56** as a yellow oil (10.8 g, quantitative). (*R_f* 0.3 on SiO₂, 1:1 hexanes:EtOAc); [α]_D²⁶ 11.6 (*c* 1.3 EtOAc); IR (EtOAc cast) 3330, 3088, 2950, 1720, 1533, 1413, 1270, 1208 cm⁻¹; ¹H (CDCl₃, 400 MHz): δ 5.97 – 5.81 (m, 2H, 2 x -OCH₂CH=CH₂), 5.66 (d, *J* = 8.4 Hz, 1H, N-H), 5.39 – 5.19 (m, 4H, 2 x -OCH₂CH=CH₂), 4.68 – 4.54 (m, 4H, 2 x -OCH₂CH=CH₂), 4.45 (m, 1H, Glu-CH α), 2.59 – 2.40 (m, 2H, Glu-CH γ), 2.24 (dtd, *J* = 12.7, 7.5, 5.2 Hz, 1H, Glu-CH₂ β), 2.01 (dt, *J* = 14.5, 7.6 Hz, 1H, Glu-CH₂ β); ¹³C (CDCl₃, 125 MHz): δ 178.2, 171.7, 156.4, 132.1, 131.1, 119.4, 118.3, 66.5, 66.4, 53.3, 29.8, 27.3, 27.1; HRMS (ES) Calculated for C₁₂H₁₇NNaO₆ 294.0948, found 294.0950 (M+Na)⁺.

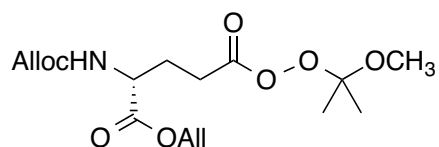
2-methoxyprop-2-yl hydroperoxide (57**)**



2,3-Dimethylbutene (2.50 mL, 21.0 mmol) and NaHCO₃ (0.009 g, 0.01 mmol) were dissolved in a 15% MeOH in CH₂Cl₂ solution (60 mL) and cooled to -78 °C. Ozone gas was bubbled into the reaction mixture for 50 minutes until a bright blue color indicative of excess ozone was observed. The vessel was purged with oxygen gas for 1

h, BHT (4.6 mg, 0.02 mmol) was added, and the reaction was warmed to room temperature. The crude reaction was concentrated *in vacuo* and used immediately without additional purification to prevent degradation. ^1H (CDCl_3 , 400 MHz): δ 7.74 (s, 1H, $-\text{OOH}$), 3.31 (s, 3H, $-\text{OCH}_3$), 1.41 (s, 6H, $-\text{(CH}_3)_2$).

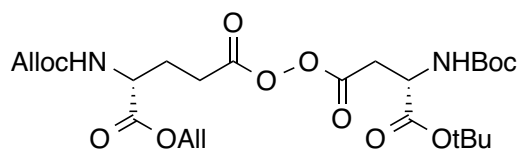
(*E*)-prop-1-en-1-yl (*R*)-2-(((allyloxy)carbonyl)amino)-5-((2-methoxypropan-2-yl)peroxy)-5-oxopentanoate (58**)**



A solution of freshly prepared **57** (21.0 mmol) in dry CH_2Cl_2 (60 mL) was cooled to $-20\text{ }^\circ\text{C}$ and had a solution of **56** (3.80 g, 14.0 mmol) in dry CH_2Cl_2 (30 mL) added, followed sequentially by DCC (4.62 g, 22.4 mmol) and DMAP (catalytic, ~ 10 mg). The reaction was stirred at $-20\text{ }^\circ\text{C}$ for 75 minutes then warmed to room temperature for 1 h. The crude reaction was filtered through a pad of Celite and concentrated *in vacuo*. Perester **58** was purified by flash chromatography (silica gel, 30% EtOAc in hexanes), yielding the desired product as a light yellow oil (2.11 g, 42%). (R_f 0.6 on SiO_2 , 2:1 hexanes:EtOAc); $[\alpha]_D^{26}$ 8.2 (c 1.25 EtOAc); IR (EtOAc cast) 3348, 3085, 2995, 2947, 1777, 1728, 1529, 1451, 1383, 1373, 1265, 1216, 1065 cm^{-1} ; ^1H (CDCl_3 , 400 MHz): δ 5.97 – 5.82 (m, 2H, 2 x $-\text{OCH}_2\text{CH}=\text{CH}_2$), 5.39 (d, $J = 8.2$ Hz, 1H, N-H), 5.37 – 5.13 (m, 4H, 2 x $-\text{OCH}_2\text{CH}=\text{CH}_2$), 4.65 – 4.61 (m, 2H, $-\text{OCH}_2\text{CH}=\text{CH}_2$), 4.59 – 4.52 (m, 2H, $\text{OCH}_2\text{CH}=\text{CH}_2$), 4.45 – 4.37 (m, 1H, Glu- CH_α), 3.31 (s, 3H, $-\text{OCH}_3$), 2.53 – 2.33 (m, 2H, Glu- CH_γ), 2.31 – 2.17 (m, 1H, Glu- $\text{CH}_2\beta$) 2.10 – 1.87 (m, 1H, Glu- $\text{CH}_2\beta$), 1.44 (s, 6H, $-\text{C}(\text{CH}_3)_2$); ^{13}C (CDCl_3 , 125 MHz): δ 171.3, 169.7, 155.8, 132.5, 131.3, 119.2,

118.0, 107.1, 66.2, 66.0, 53.3, 49.9, 27.7, 27.2, 22.5; HRMS (ES) Calculated for $C_{16}H_{25}NNaO_8$ 382.1472, found 382.1474 ($M+Na$)⁺.

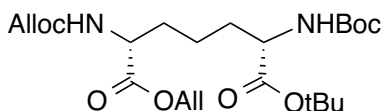
(*R,E*)-4-(((allyloxy)carbonyl)amino)-5-oxo-5-(prop-1-en-1-yloxy)pentanoic (*S*)-4-(*tert*-butoxy)-3-((*tert*-butoxycarbonyl)amino)-4-oxobutanoic peroxyanhydride (59**)**



Under vigorous stirring to a solution of perester **58** (2.11 g, 5.87 mmol) in $CHCl_3$ (100 mL), a 50% aqueous TFA solution (30 mL) was added over 20 minutes. The solution was cooled to 0 °C with vigorous stirring for 5 minutes, then saturated $NaHCO_3$ (300 mL) was added until pH 8 was achieved. The organic and aqueous phases were separated, and the aqueous phase was washed with diethyl ether (3 x 100 mL). Pooled organic layers were washed with water (100 mL) and brine (100 mL), dried over Na_2SO_4 , filtered and concentrated *in vacuo*. The peracid product was dissolved in dry CH_2Cl_2 (100 mL) and cooled to 0 °C. Boc-L-Asp-OtBu (1.61 g, 5.58 mmol) and DCC (1.33 g, 6.46 mmol) were added and stirred for 1 h, then warmed to room temperature and stirred for an additional 1.5 h. The reaction was filtered through Celite and concentrated *in vacuo*. Diacyl peroxide **59** was purified by flash chromatography (silica gel, 30% EtOAc in hexanes) as a light yellow oil (2.05 g, 63%). (R_f 0.5 on SiO_2 , 2:1 hexanes:EtOAc); $[\alpha]_D^{26}$ 9.9 (*c* 0.99 EtOAc); IR (EtOAc cast) 3347, 3085, 2980, 2937, 1813, 1784, 1722, 1515, 1369, 1253, 1155 cm^{-1} ; 1H ($CDCl_3$, 400 MHz): δ 5.98 – 5.83 (m, 2H, 2 x -OCH₂CH=CH₂), 5.45 (d, J = 7.8 Hz, 1H, N-H), 5.41 – 5.17 (m, 5H, 2 x -OCH₂CH=CH₂, N-H), 4.64 (ddd, J = 5.7, 3.4, 2.0 Hz, 2H, -OCH₂CH=CH₂), 4.57 (ddt, J = 5.9, 3.1, 1.3 Hz, 2H, -OCH₂CH=CH₂), 4.54 – 4.48 (m, 1H, Asp-CH α) 4.48 – 4.37 (m,

1H, Glu-CH α), 3.05 (dd, $J = 16.7, 4.6$ Hz, 1H, Asp-CH $_2\beta$), 2.96 (dd, $J = 16.5, 5.1$ Hz, 1H, Asp-CH $_2\beta$), 2.64 – 2.43 (m, 2H, Glu-CH γ), 2.43 – 2.17 (m, 1H, Glu-CH $_2\beta$), 2.14 – 1.93 (m, 1H, Glu-CH $_2\beta$), 1.46 (s, 9H, -C(CH $_3$) $_3$), 1.42 (s, 9H, -C(CH $_3$) $_3$); ^{13}C (CDCl $_3$, 125 MHz): δ 171.1, 168.9, 168.0, 166.8, 155.8, 155.3, 132.4, 131.2, 119.4, 117.9, 83.2, 80.3, 66.4, 66.2, 53.2, 50.4, 33.1, 30.0, 28.3, 27.8, 26.2; HRMS (ES) Calculated for C $_{25}$ H $_{38}$ N $_2$ NaO $_{12}$ 581.2317, found 581.2312 (M+Na) $^+$.

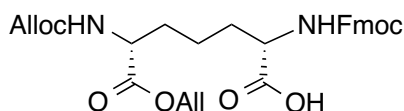
7-(*tert*-butyl) 1-((*E*)-prop-1-en-1-yl) (2*R*,6*S*)-2-(((allyloxy)carbonyl)amino)-6-((*tert*-butoxycarbonyl)amino)heptanedioate (60)



Orthogonally protected diacyl peroxide **59** (0.40 g, 0.72 mmol) was dissolved in minimal CH $_2$ Cl $_2$ (~5 mL) and transferred to the reaction vessel (a 15 cm diameter recrystallization dish with a quartz lid and two adaptors to allow a flow of argon into the vessel). The solvent was evaporated using a stream of Ar gas, leaving the crude reactant deposited onto the bottom surface of the vessel. A 2-propanol bath was cooled down to -80 °C and maintained at a constant temperature through the use of a Thermo Neslab Cryotrol/CC-100 cryo-cooler system. The reaction vessel was put under an Ar atmosphere, sealed, and cooled to -80 °C. A 0.9 Amp UV lamp (254 nm) was placed above the reaction vessel and irradiated the diacyl peroxide residue for 2 days in the absence of additional light. After the reaction vessel was warmed back up to room temperature, the crude residue was redissolved in CH $_2$ Cl $_2$ (~5 mL) to evenly distribute the reaction on the surface of the reaction vessel. The solvent was again evaporated with a stream of Ar gas, the reaction cooled down to -80 °C and irradiated as previously

described for 2 days. The crude product was collected by rinsing the reaction vessel with CH₂Cl₂, and was concentrated *in vacuo* and purified using flash chromatography (silica gel, 25% EtOAc in hexanes). The desired product **60** was obtained as a clear, colorless oil (0.104 g, 31%). (*R_f* 0.55 on SiO₂, 2:1 hexanes:EtOAc); [α]_D²⁶ 2.2 (*c* 0.65 EtOAc); IR (EtOAc cast) 3347, 3085, 2978, 2935, 2870, 1718, 1521, 1367, 1250, 1155 cm⁻¹; ¹H (CDCl₃, 400 MHz): δ 5.96 – 5.81 (m, 2H, 2 x -OCH₂CH=CH₂), 5.40 – 5.15 (m, 5H, N-H, 2 x -OCH₂CH=CH₂), 5.08 – 5.01 (m, 1H, N-H), 4.61 (dt, *J* = 5.8, 1.4 Hz, 2H, -OCH₂CH=CH₂), 4.55 (dt, *J* = 5.7, 1.4 Hz, 2H, -OCH₂CH=CH₂), 4.39 – 4.31 (m, 1H, CH α), 4.13 (dd, *J* = 7.4, 6.8 Hz, 1H, CH α), 1.88 (ddt, *J* = 16.1, 10.5, 5.2 Hz, 1H, Glu-CH₂ β), 1.82 – 1.72 (m, 1H, Asp-CH₂ β), 1.72 – 1.63 (m, 1H, Glu-CH₂ β), 1.63 – 1.51 (m, 1H, Asp-CH₂ β), 1.44 (s, 9H, -C(CH₃)₃), 1.43 – 1.40 (m, 10H, -C(CH₃)₃, CH γ), 1.38 – 1.29 (m, 1H, CH γ); ¹³C (CDCl₃, 125 MHz): δ 172.0, 171.7, 155.8, 155.3, 132.4, 131.2, 119.3, 117.9, 82.2, 80.0, 66.4, 66.2, 53.2, 53.0, 33.1, 30.0, 28.3, 27.8, 26.2; HRMS (ES) Calculated for C₂₃H₃₈N₂NaO₈ 493.2520, found 493.2516 (M+Na)⁺.

(2*S*,6*R*)-2-(((9*H*-fluoren-9-yl)methoxy)carbonyl)amino)-7-(allyloxy)-6-(((allyloxy)carbonyl)amino)-7-oxoheptanoic acid (61**)**



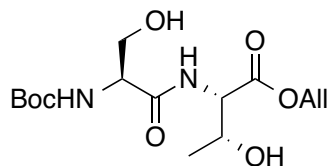
A solution **60** (0.327 g, 0.70 mmol) in CH₂Cl₂ (20 mL) had phenylsilane (0.17 mL, 1.39 mmol) added, followed by TFA (20 mL). The reaction was stirred for 3 h under an Ar atmosphere and then concentrated *in vacuo*. The crude TFA salt was dissolved in 50% aqueous dioxane (20 mL) and cooled to 0 °C with vigorous stirring. NaHCO₃ (0.250 g, 2.98 mmol) was added to the reaction mixture until pH 8, followed by

Fmoc-OSu (0.258 g, 0.77 mmol). The reaction was warmed to room temperature and stirred for an additional 2 h before concentration *in vacuo*. The crude reaction was dissolved in EtOAc (50 mL) and washed with water (2 x 50 mL) and 10% citric acid (50 mL). Pooled aqueous layers were washed with EtOAc (3 x 50 mL), and all EtOAc fractions were combined, dried over Na₂SO₄, filtered and concentrated *in vacuo*. DAP Compound **61** was purified by flash chromatography (silica gel, 70% EtOAc in hexanes) producing a white solid (0.253 g, 68%). (*R_f* 0.25 on SiO₂, 1:1 hexanes:EtOAc 1% AcOH); [α]_D²⁶ 6.8 (*c* 0.25 EtOAc); IR (EtOAc cast) 3328, 3068, 2928, 2856, 1721, 1528, 1450, 1247, 1060 cm⁻¹; ¹H (CD₃OD, 400 MHz): δ 7.80 (d, *J* = 7.5 Hz, 2H, Ar-H), 7.72 – 7.60 (m, 2H, Ar-H), 7.43 – 7.36 (m, 2H, Ar-H), 7.31 (td, *J* = 7.4, 1.2 Hz, 2H), 6.00 – 5.84 (m, 2H, 2 x -OCH₂CH=CH₂), 5.36 – 5.25 (m, 2H, 2 x -OCH₂CH=CH₂), 5.24 – 5.13 (m, 2H, -OCH₂CH=CH₂), 4.60 (dd, *J* = 5.7, 1.2 Hz, 2H, -OCH₂CH=CH₂), 4.53 (d, *J* = 4.8 Hz, 2H -OCH₂CH=CH₂), 4.40 – 4.33 (m, 2H, Fmoc-CH₂), 4.27 – 4.07 (m, 3H, Fmoc-CH, 2 x CH α), 1.92 – 1.81 (m, 2H, CH₂ β), 1.75 – 1.63 (m, 2H, CH₂ β), 1.56 – 1.41 (m, 2H, CH γ); ¹³C (CDCl₃, 125 MHz): δ 175.1, 166.0, 159.0, 158.4, 147.3, 145.7, 142.6, 134.2, 133.4, 128.7, 128.1, 126.1, 121.0, 118.6, 117.2, 68.4, 66.7, 66.6, 56.0, 55.6, 47.0, 32.3, 32.2, 23.2; HRMS (ES) Calculated for C₂₉H₃₁N₂O₈ 535.2086, found 535.2089 (M-H).

4.2.4 Synthesis of N-terminal dipeptide **68**

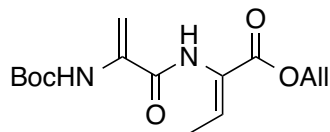
All compounds in this section were synthesized following literature procedure.⁴⁵

allyl ((*tert*-butoxycarbonyl)amino)-*L*-seryl-*L*-threoninate (66)



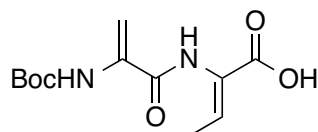
A solution of H-Thr-OAll *p*-toluenesulfonate salt (5.50 g, 16.6 mmol) was dissolved in a 5% DMF in CH₂Cl₂ solution (7.5 mL DMF, 150 mL total). Boc-L-Ser-OH (3.75 g, 18.3 mmol), HOBt (2.47 g, 18.3 mmol) and PyBOP (9.50 g, 18.3 mmol) were added to the solution and the reaction was cooled to 0 °C under Ar. After the addition of DIPEA (10.1 mL, 58.1 mmol), the reaction was stirred for 5 minutes then warmed to room temperature and stirred for 21 h. The reaction was concentrated *in vacuo*, resuspended in EtOAc (250 mL), and washed with 10% citric acid (100 mL), saturated NaHCO₃ (100 mL), water (100 mL) and brine (100 mL). The organic layer was dried over Na₂SO₄, filtered and concentrated *in vacuo*. Dipeptide **66** was purified by flash chromatography (silica gel, 50% EtOAc in hexanes) and isolated as a pale yellow oil (3.46 g, 60%). (R_f 0.6 on SiO₂, EtOAc); ¹H (CDCl₃, 400 MHz): δ 7.20 (d, *J* = 6.4 Hz, 1H, Thr N-H), 5.91 (ddt, *J* = 16.4, 10.9, 5.8 Hz, 1H, -OCH₂CH=CH₂), 5.58 (br s, 1H, Ser N-H), 5.35 (d, *J* = 17.2 Hz, 1H, -OCH₂CH=CH₂), 5.27 (d, *J* = 10.5 Hz, 1H, -OCH₂CH=CH₂), 4.68 (d, *J* = 5.8 Hz, 2H, -OCH₂CH=CH₂), 4.59 (dd, *J* = 9.1, 2.6 Hz, 1H Thr-CH_α), 4.44 – 4.36 (m, 1H, Thr-CH_β), 4.27 – 4.20 (m, 1H, Ser-CH_α), 4.10 – 4.03 (m, 1H, Ser-CH_β), 3.73 – 3.65 (m, 1H, Ser-CH_β), 3.22 (t, *J* = 6.4 Hz, 1H, Ser-OH), 2.44 (br s, 1H, Thr-OH), 1.46 (s, 9H, -C(CH₃)₃), 1.26 (dd, *J* = 9.0, 6.8 Hz, 3H, Thr-CH₃).

(Z)-allyl 2-(2-((tert-butoxycarbonyl)amino)acrylamido)but-2-enoate (67)



Methanesulfonyl chloride (3.04 mL, 39.3 mmol) was added dropwise over 5 minutes to a 0 °C solution of dipeptide **66** (3.40 g, 9.82 mmol) in dry CH₂Cl₂ (100 mL). Triethylamine (7.16 mL, 51.4 mmol) was subsequently added dropwise over 5 minutes and the reaction was warmed to room temperature and stirred for an additional 60 minutes. The solvent was removed *in vacuo* and the crude reaction mixture was dissolved in dry 1,2-dichloroethane (100 mL). DBU (6.61 mL, 44.2 mmol) was added and the reaction was refluxed at 85 °C for 18 h under an Ar atmosphere. After cooling, the mixture was washed with 10% citric acid (50 mL), saturated NaHCO₃ (50 mL), water (50 mL) and brine (50 mL). The organic layer was dried over Na₂SO₄, filtered, and concentrated *in vacuo*. Di-dehydrated dipeptide **67** was purified by flash chromatography (silica gel, 15% EtOAc in hexanes), generating a light yellow oil (1.59 g, 52%). (R_f 0.8 on SiO₂, 1:1 hexanes:EtOAc); ¹H (CDCl₃, 400 MHz): δ 7.45 (s, 1H, N-H), 7.23 (s, 1H, N-H), 6.91 (q, *J* = 7.2 Hz, 1H, =CH-CH₃), 6.14 (d, *J* = 1.9 Hz, 1H, =CH-H), 5.94 (ddt, *J* = 17.2, 10.4, 5.7 Hz, 1H, -OCH₂CH=CH₂), 5.35 (dq, *J* = 17.2, 1.5 Hz, 1H, -OCH₂CH=CH₂), 5.30 – 5.24 (m, 2H, -OCH₂CH=CH₂, =CH-H), 4.68 (dt, *J* = 5.7, 1.4 Hz, 2H, -OCH₂CH=CH₂), 1.78 (dd, *J* = 7.2, 0.7 Hz, 3H, =CH-CH₃), 1.48 (s, 9H, -C(CH₃)₃).

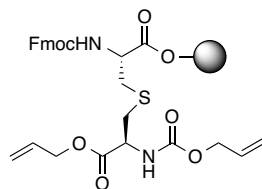
(Z)-2-(2-((tert-butoxycarbonyl)amino)acrylamido)but-2-enoic acid (68)



Phenylsilane (0.25 mL, 2.04 mmol) was added to a degassed solution of dipeptide **67** (0.317 g, 1.02 mmol) in dry CH₂Cl₂ (20 mL) under an Ar atmosphere. Pd(PPh₃)₄ (0.145 g, 0.10 mmol) was added to the reaction, which was stirred in the absence of light for 2 h. The free acid was extracted from the organic phase with saturated NaHCO₃ washes (3 x 50 mL), which were pooled and acidified to pH 3.5 by the addition of 1N HCl. The aqueous layer was washed with CH₂Cl₂ (3 x 100 mL) to recover the desired product, and pooled organic layers were dried over Na₂SO₄, filtered, and concentrated *in vacuo*. Dipeptide **68** was obtained as a light brown solid (0.101 g, 0.37 mmol) and used without further purification. (*R_f* 0.1 on SiO₂, EtOAc); IR (CHCl₃ cast) 3354, 2980, 2934, 1706, 1506 cm⁻¹; ¹H (CD₃OD, 600 MHz): δ 6.85 (q, *J* = 7.1 Hz, 1H, =CH-CH₃), 5.83 (s, 1H, =CH-H), 5.48 (s, 1H, =CH-H), 1.76 (d, *J* = 7.1 Hz, 3H, =CH-CH₃), 1.48 (s, 9H, -C(CH₃)₃); ¹³C NMR (CD₃OD, 100 MHz): δ 167.3, 165.7, 154.7, 137.2, 136.9, 128.7, 102.8, 81.5, 28.3, 14.0; HRMS (ES) Calculated for C₁₂H₁₇N₂O₅ 269.1143, found 269.1141 (M-H)⁻.

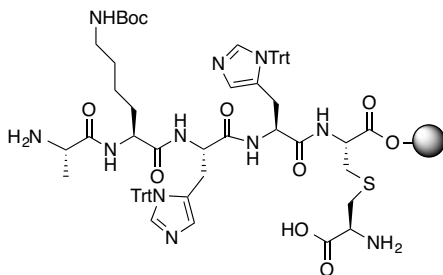
4.2.5 Synthesis of NleDAP lactocin S (47)⁶⁸

Loading orthogonally-protected lanthionine onto chlorotriyl resin (48)



2-Chlorotriyl chloride resin (2.0 g, 1.3 mmol) was pre-swelled in DCM (15 mL) without stirring for 30 min. A solution of orthogonally protected lanthionine (0.150 g, 0.27 mmol) and DIPEA (0.24 mL, 1.35 mmol) in DCM (15 mL) was added and the mixture stirred very gently for 2.5 h. The slurry was transferred to a peptide reaction vessel and the resin washed with DCM (2 × 15 mL). To cap the remaining reactive sites on the resin a solution of acetic acid (0.11 mL, 2.0 mmol) and DIPEA (1.39 mL, 8.0 mmol) in DCM (15 mL) was added to the resin and the reaction mixture was bubbled with argon for 2 h. The resin was then washed with DCM (2 × 20 mL). This yielded a resin with a reduced loading (0.14 mmol/g) of reactive sites functionalized with the C-terminal amino acid of lactocin S ready for SPPS.

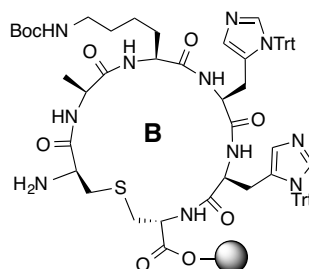
SPPS elongation to 49



The N-terminal Fmoc protecting group was removed using a solution of 20% piperidine in DMF. The resin bound peptide was coupled with Fmoc-His(Trt)-OH,

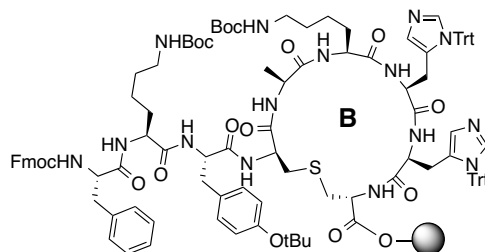
Fmoc-His(Trt)-OH, Fmoc-Lys(Boc)-OH and Fmoc-Ala-OH in the presence of PyBOP and HOBt as coupling reagents using the general elongation procedure described above. The orthogonal lanthionine Allyl/Alloc protecting groups were removed by treatment of the resin with a solution of Pd(PPh₃)₄ (0.624 g, 0.54 mmol) and PhSiH₃ (0.33 mL, 2.7 mmol) in 1:1 DMF/DCM (40 mL) in the absence of light for 2 h. The resin was then washed with DCM (40 mL) until dark brown color was removed. The resin was then washed with 0.5 % sodium diethyldithiocarbamate in DMF (3 × 20 mL) and then DMF (2 × 20 mL) to remove any remaining palladium from the resin. The N-terminal Fmoc protecting group was removed using the standard protocol of 20 % piperidine in DMF. The resin was washed with DCM (3 × 20 mL) and then DMF (3 × 20 mL).

On-resin cyclization to form lactocin S lanthionine ring B (50)



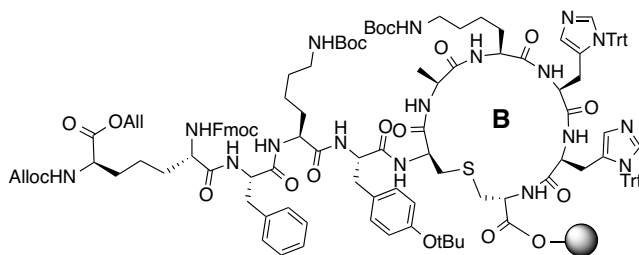
To cyclize the B ring of lactocin S a solution of PyBOP (0.688 g, 1.32 mmol), HOBt (0.182 g, 1.35 mmol) and NMM (0.30 mL, 2.70 mmol) in DMF (20 mL) was added to **49** on resin and the reaction mixture was bubbled with argon for 2 h. The resin was washed with DMF (3 × 10 mL) and then a second solution of PyBOP (0.688 g, 1.32 mmol), HOBt (0.182 g, 1.35 mmol) and NMM (0.30 mL, 2.70 mmol) in DMF (20 mL) was added to the resin and the reaction mixture was bubbled with argon for 2 h, generating the macrocyclic ring B **50**.

SPPS elongation to nonapeptide **51**



The N-terminus of **50** was elongated by Fmoc-SPPS using PyBOP and HOBt as coupling reagents to introduce residues 31-29 (Fmoc-Tyr(OtBu)-OH, Fmoc-Lys(Boc)-OH and Fmoc-Phe-OH). A small sample of the resin-bound peptide was treated with TFA/TIPS/H₂O (95/2.5/2.5) for 2 h to remove the peptide from the solid support. Following filtration the filtrate was concentrated *in vacuo* and the peptide was precipitated by addition of Et₂O at 0 °C. The resulting white solid was analyzed using MALDI-TOF MS: Calculated for C₆₆H₉₂N₁₅O₁₃S 1324.5, found 1324.8 (M+H)⁺.

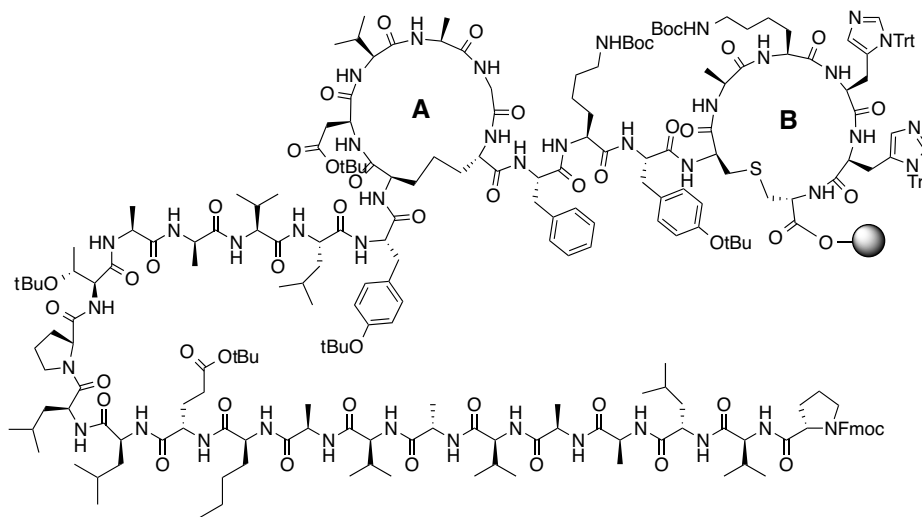
Coupling of orthogonally protected DAP (**61**) to lactocin S fragment **51** (**62**)



The N-terminus of **51** was liberated in the presence of 20% piperidine in DMF (3 x 15 mL), followed by coupling with a pre-activated solution of **61** (0.500 g, 0.93 mmol), PyBOP (0.476 g, 0.91 mmol), HOBt (0.126 g, 0.93 mmol) and NMM (0.12 mL, 1.12 mmol) for 3 h under bubbling Ar. A small sample of resin-bound peptide was treated with TFA/TIPS/H₂O (95/2.5/2.5) for 2 h to remove the peptide from the solid

support. Following analogous work up, the resulting white solid was analyzed using MALDI-TOF MS: Calculated for $C_{80}H_{101}N_{17}O_{18}S$ 1620.7, found 1621.2 ($M+H$)⁺.

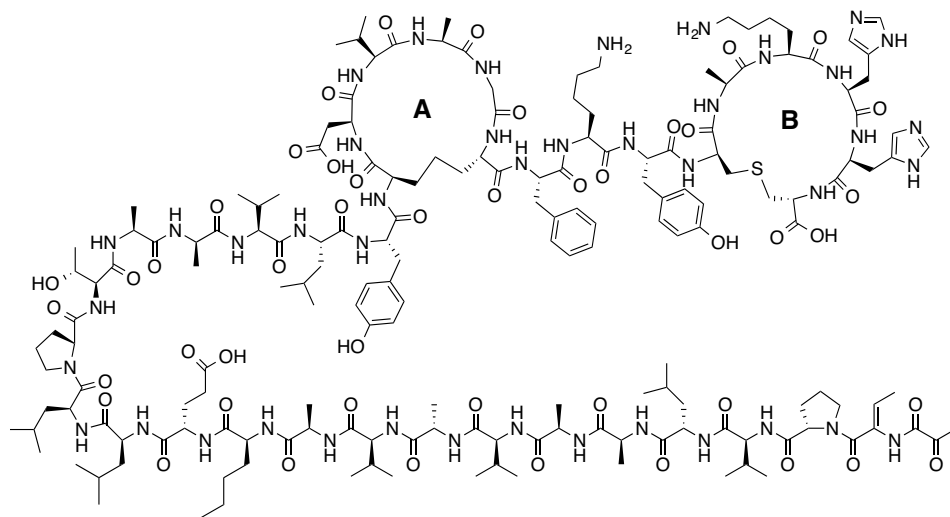
On-resin cyclization of A-DAP ring and SPPS elongation (64)



The remainder of the amino acids of ring A of lactocin S were introduced to **62** using Fmoc-SPPS in the following order - Fmoc-Gly-OH, Fmoc-Ala-OH, Fmoc-Val-OH, and Fmoc-Asp(OtBu)-OH. Removal of the Allyl/Alloc groups was carried out in an analogous fashion to that described for ring B. The N-terminal Fmoc group was deprotected using 20% piperidine in DMF and after the resin had been washed with DCM and DMF the cyclization of ring A was effected using PyBOP and HOBt as previously described. To determine the success of the cyclization reaction by MALDI-TOF MS a small sample of resin (5 mg) was coupled with the next amino acid Fmoc-Tyr(O^tBu)-OH using PyBOP and HOBt. This sample was then cleaved from the resin using TFA/TIPS/H₂O as described for ring B and analyzed by MALDI-TOF MS: Calculated for $C_{96}H_{123}N_{22}O_{23}S$ 1982.9, found 1983.2 ($M+H$)⁺. The amino acids corresponding to residues 3-22 were introduced via Fmoc-SPPS with PyBOP and HOBt as coupling reagents in the following order – Fmoc-Tyr(OtBu)-OH, Fmoc-Leu-OH,

Fmoc-Val-OH, Fmoc-D-Ala-OH, Fmoc-Ala-OH, Fmoc-Thr(OtBu)-OH, Fmoc-Pro-OH, Fmoc-Leu-OH, Fmoc-Leu-OH, Fmoc-Glu(OtBu)-OH, Fmoc-Nle-OH, Fmoc-D-Ala-OH, Fmoc-Val-OH, Fmoc-Ala-OH, Fmoc-Val-OH, Fmoc-D-Ala-OH, Fmoc-Ala-OH, Fmoc-Leu-OH, Fmoc-Val-OH and Fmoc-Pro-OH. A small sample was then cleaved from the resin using TFA/anisole/H₂O as described for rings A and B and analyzed by MALDI-TOF MS: Calculated for C₁₈₃H₂₇₂N₄₁O₄₅S 3796.0, found 3798.3 (M+H)⁺.

4.2.5.1 Coupling of dipeptide **68** and completion of NleDAP lactocin S (**47**)



Resin-bound **64** was N-terminally deprotected in the presence of 20% piperidine in DMF (4 x 15 mL), and a pre-activated solution of dipeptide **68** (147 mg, 0.54 mmol), PyBOP (230 mg, 0.53 mmol), HOBT (61 mg, 0.54 mmol), and NMM (60 μ L, 0.65 mmol) in DMF (10 mL) was added and bubbled with argon for 3 hours. After rinsing with DMF, a second 3 hour coupling was subsequently performed with a similarly pre-activated solution of the dipeptide in DMF (10 mL). The peptide was then cleaved from the resin yielding crude peptide (39.5 mg) and was purified as described previously to give 1.0 mg of product (overall yield = 1.8%) as a fluffy white solid. Monoisotopic MW

calculated for $C_{175}H_{269}N_{42}O_{46}S$ 3726.97, found *high resolution* (FTICR-ESI-MS) 3726.9716 (M+H)⁺.

4.2.6 Characterization of NleDAP lactocin S (47)⁶⁸

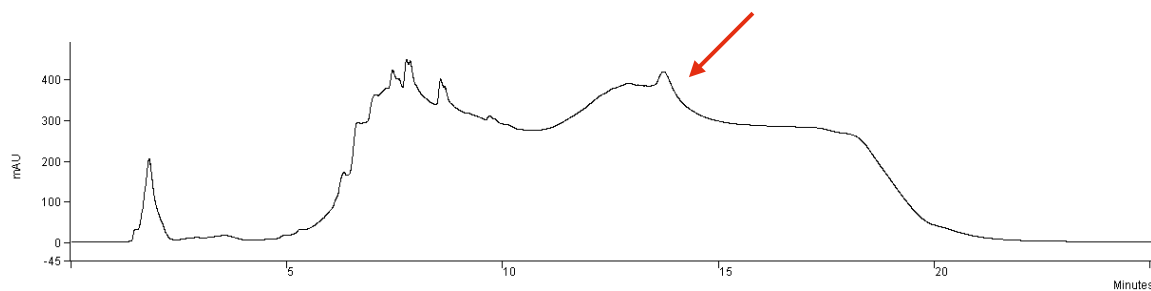


Figure 4.1 – HPLC trace of NleDAP lactocin S.

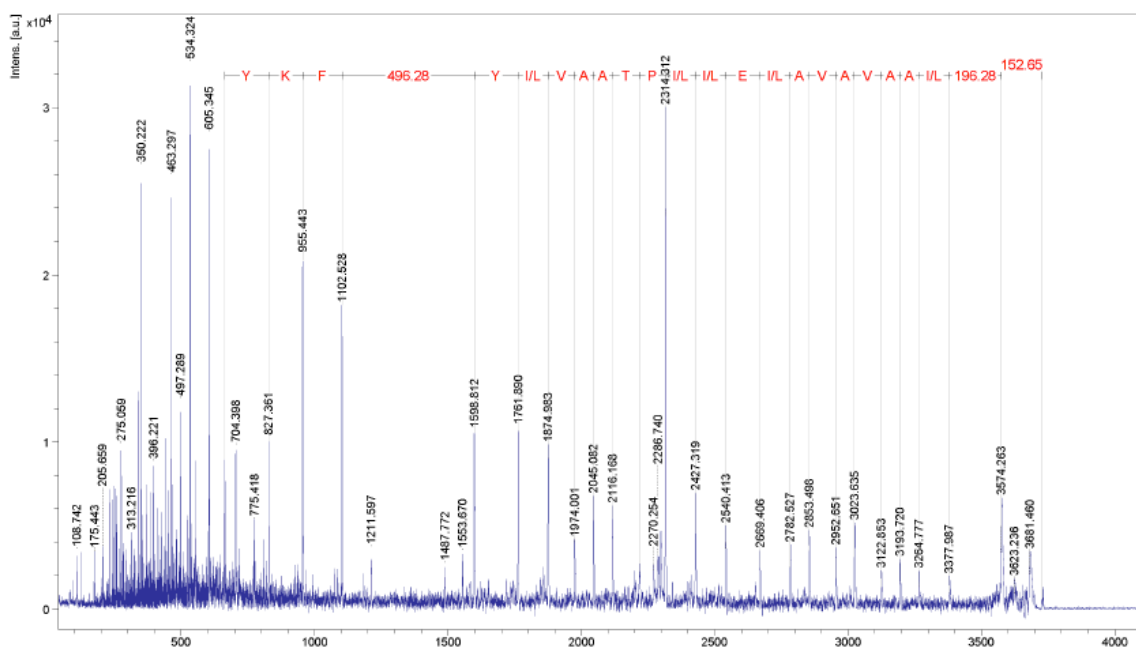


Figure 4.2 – MS/MS spectrum of NleDAP lactocin S.

4.2.7 Biological testing

4.2.7.1 Spot-on-lawn activity monitoring⁶⁸

Antibacterial activity was assayed using spot-on-lawn activity assays. Plates containing 10 mL of MRS hard agar (1.5% agar, Difco) were used for spot-on-lawn assays. MRS soft agar overlays (0.75% agar) were prepared by adding 27.5 g/L MRS broth (Difco) with 35 g/L MRS agar (Difco). Lyophilized peptide samples were dissolved in 9:1 MQ-H₂O/MeOH (0.1% TFA) for activity testing. Sample aliquots (10 µL) analyzed for activity were spotted onto a hard MRS agar plate and permitted to dry. Molten soft MRS agar (10 mL) was inoculated with 100 µL of the desired organism (1% inoculation) and poured over the hard agar plate and allowed to solidify. Plates were sealed with Parafilm and incubated overnight at the optimal temperature (30 or 37 °C) for the organism being examined (Table 4.1). Activity was measured as zones of inhibited growth. Indicator organisms that showed no zones of clearing after treatment with lactocin S or lactocin S analogues are shown in Figure 4.3.

Table 4.1 – Organisms used for activity testing

Indicator species	Strain	Growth medium	Growth temperature
<i>Lactobacillus bulgaricus</i>	11842	MRS	37 °C
<i>Lactobacillus helveticus</i>	18009	MRS	37 °C
<i>Lactobacillus sakei</i>	L45	MRS	30 °C
<i>Pediococcus acidilactici</i>	PAC1.0	MRS	30 °C
<i>Pediococcus pentosaceus</i>	FBB63	MRS	37 °C

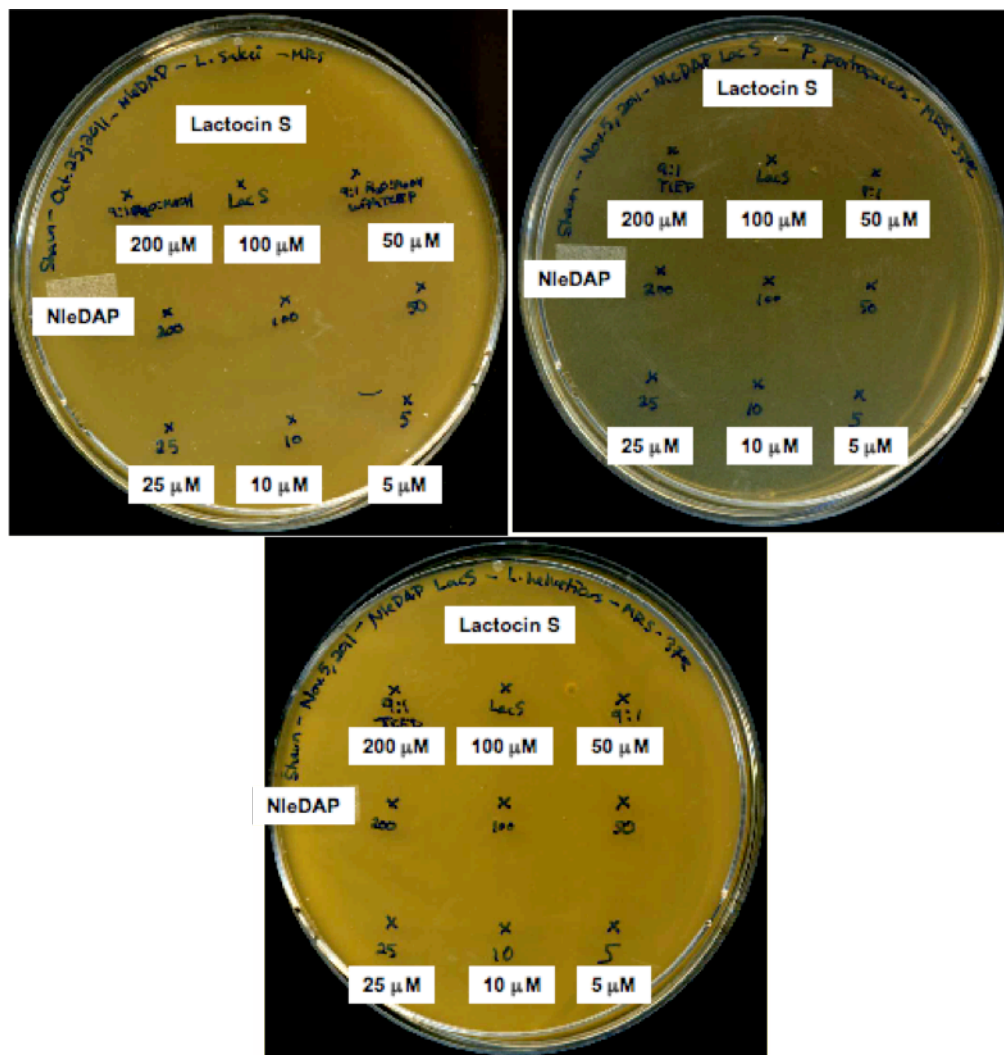


Figure 4.3 – Spot-on-lawn activity testing of 100 μM lactocin S (26) and dilutions of NleDAP lactocin S analogue (47) against producer organism *Lactobacillus sakei* L45 (top left), *Pediococcus pentosaceus* FBB63 (top right), and *Lactobacillus helveticus* 18009 (bottom).⁶⁸

4.2.7.2 Oxidative stability assay of lactocin S analogues versus lactocin S^{68,66}

Lactocin S and lactocin S analogues were prepared (100 μM solutions in 9:1 MQ-H₂O:MeOH with 0.1% TFA and 1.5 mg/L TCEP) and placed under a sealed

atmosphere of oxygen for 6 and 24 hours at room temperature (the containers were sealed to prevent evaporation of solvent from artificially concentrating samples). The activity of peptide solutions was compared to solutions maintained under an atmosphere of argon (0 h O₂ exposure) by using spot on lawn assays against sensitive bacterial strains *P. acidilactici* PAC1.0 and *L. bulgaricus* 11842.

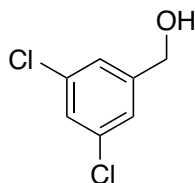
4.2.7.3 Serial dilution assay of NleDAP lactocin S⁶⁸

Solutions of peptide analogues were made in 9:1 MQ-H₂O/MeOH (0.1 % TFA) to yield initial concentrations of 200 μM. Serial dilutions were performed with 9:1 MQ-H₂O/MeOH (0.1 % TFA) to make 100 μM, 50 μM, 20 or 25 μM, 10 μM and 5 μM solutions. All solutions had 1.5 mg/L TCEP added to them to minimize oxidation of peptides due to atmospheric oxygen. Spot on lawn assays were used to test the biological activity of the diluted peptides as described above. Solutions of natural lactocin S and 9:1 MQ-H₂O/MeOH (0.1 % TFA with 1.5 mg/L TCEP added) were spotted on activity plates to serve as positive and negative controls respectively. Activity was measured as zones of inhibited growth.

4.3 Apelin analogue syntheses

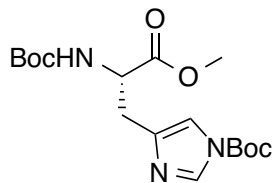
4.3.1 MLN' inhibitor synthesis

(3,5-dichlorophenyl)methanol (**85**)



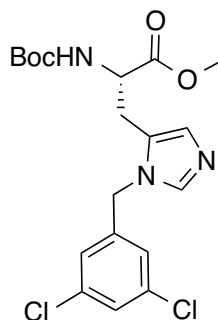
Compound **85** was synthesized based on a modified literature procedure.¹³⁴ A solution of 3,5-dichlorobenzaldehyde (0.800 g, 4.57 mmol) in dry THF (20 mL) was cooled to 0 °C. Sodium borohydride (0.208 g, 5.49 mmol) was added portionwise over 2 minutes and the reaction was slowly warmed to room temperature over 3.5 h. The solution was cooled to 0 °C and 1 N HCl (5 mL) was added to quench excess borohydride. The reaction was concentrated *in vacuo*, resuspended in EtOAc (50 mL) and washed with water (2 x 50 mL). Pooled organic layers were dried over Na₂SO₄, filtered and concentrated *in vacuo*. Alcohol **85** was purified by flash chromatography (silica gel, 25% EtOAc in hexanes), yielding a white solid (0.782 g, 97%). (*R_f* 0.7 on SiO₂, 1:1 hexanes:EtOAc); IR (CHCl₃ cast) 3241, 3086, 2927, 2887, 2854, 1595, 1574, 1431, 1206, 1104, 1057 cm⁻¹; ¹H (CDCl₃, 500 MHz): δ 7.30 – 7.27 (m, 1H, Ar-H), 7.26 – 7.25 (m, 2H, Ar-H), 4.68 (dq, *J* = 6.0, 0.7 Hz, 2H, Ar-CH₂-OH), 1.74 (t, *J* = 6.0 Hz, 1H, Ar-CH₂-OH); ¹³C (CDCl₃, 125 MHz): δ 114.2, 135.1, 127.6, 125.0, 63.9; HRMS (EI) Calculated for C₇H₆³⁵Cl₂O 175.97957, found 175.97922 (M+H)⁺.

methyl *N* α ,*N* τ -di(*tert*-butoxycarbonyl)-*L*-histidinate (88**)**



Compound **88** was synthesized following a literature procedure.¹²⁷ A solution of Boc anhydride (1.691 g, 7.75 mmol) in methanol (10 mL) was slowly added to a solution of L-His-OMe • 2 HCl (0.938 g, 3.87 mmol) and triethylamine (1.08 mL, 7.75 mmol) in methanol (10 mL) over 30 minutes. This reaction was stirred at room temperature for 24 h, and concentrated *in vacuo*. The crude residue was resuspended in CH₂Cl₂ (50 mL), washed with water (2 x 50 mL) and brine (50 mL). The organic layer was dried over Na₂SO₄, filtered and concentrated *in vacuo*. The di-Boc protected **88** was purified by trituration from cold hexanes and collected as a white solid (1.040 g, 73%). (*R*_f 0.35 on SiO₂, 1:1 hexanes:EtOAc); [α]_D²⁶ 20.3 (*c* 0.53 CHCl₃); IR (CHCl₃ cast) 3383, 3133, 2980, 1755, 1716, 1490, 1392, 1294, 1255, 1161 cm⁻¹; ¹H (CDCl₃, 500 MHz): δ 7.98 (d, *J* = 1.3 Hz, 1H, His-CH ϵ ₁), 7.13 (t, *J* = 1.1 Hz, 1H, His-CH δ ₂), 5.70 (d, *J* = 8.4 Hz, 1H, Boc-N-H), 4.57 (t, *J* = 6.8 Hz, 1H, His-CH α), 3.73 (s, 3H, -OCH₃), 3.10 – 2.98 (m, 2H, His-CH β), 1.60 (s, 9H, -C(CH₃)₃), 1.44 (s, 9H, -C(CH₃)₃); ¹³C (CDCl₃, 125 MHz): δ 172.2, 155.6, 155.2, 146.8, 136.8, 114.6, 85.6, 79.8, 53.1, 52.2, 30.3, 28.3, 27.9; HRMS (ES) Calculated for C₁₇H₂₇N₃NaO₆ 392.1792, found 392.1790 (M+Na)⁺.

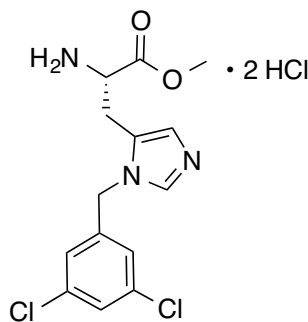
methyl *N* α -(*tert*-butoxycarbonyl)-*N* π -(3,5-dichlorobenzyl)-*L*-histidinate (89**)**



Compound **89** was synthesized following a literature procedure.¹²⁷ A solution of trifluoromethanesulfonic anhydride (0.48 mL, 2.85 mmol) in dry CH₂Cl₂ (10 mL) was cooled down to -78 °C. A second solution of **85** (0.504 g, 2.85 mmol) and DIPEA (0.50 mL, 2.85 mmol) in dry CH₂Cl₂ (10 mL) was slowly added to the -78 °C solution over 5 minutes. The reaction was stirred at -78 °C for 30 minutes, and a solution of **88** (0.957 g, 2.59 mmol) in dry CH₂Cl₂ (10 mL) was added over 5 minutes. The reaction was slowly warmed to room temperature, stirred for 20 h, and concentrated *in vacuo*. The crude product was resuspended in MeOH (20 mL) and refluxed at 65 °C for 1 h. After cooling, the reaction was concentrated *in vacuo*, resuspended in EtOAc, washed with saturated NaHCO₃ (2 x 50 mL) and brine (50 mL). The organic layer was dried over Na₂SO₄, filtered, and concentrated *in vacuo*. The product was purified by flash chromatography (silica gel, 5% MeOH in CH₂Cl₂), yielding **89** as a red-orange oil (0.702 g, 63%). (*R*_f 0.1 on SiO₂, 1:1 hexanes:EtOAc); [α]_D²⁶ 16.5 (*c* 0.88 CH₂Cl₂); IR (CH₂Cl₂ cast) 3192, 2978, 1745, 1709, 1592, 1572, 1495, 1434, 1367, 1215, 1167 cm⁻¹; ¹H (CDCl₃, 500 MHz): δ 7.48 (s, 1H, His-CH ϵ ₁), 7.34 – 7.26 (m, 1H, Ar-H), 7.00 – 6.91 (m, 2H, Ar-H), 6.89 – 6.85 (m, 1H, His-CH δ ₂), 5.20 (d, *J* = 7.4 Hz, 1H, Boc-N-H), 5.18 – 4.98 (m, 2H, Ar-CH₂), 4.44 (d, *J* = 7.2 Hz, 1H, His-CH α), 3.73 (s, 3H, -OCH₃), 3.03 – 2.88 (m, 2H, His-

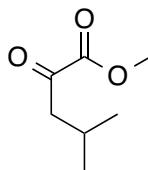
CH₂β), 1.43 (s, 9H, -C(CH₃)₃); ¹³C (CDCl₃, 125 MHz): δ 171.5, 155.1, 139.6, 138.2, 135.8, 129.3, 128.5, 126.4, 125.1, 80.5, 53.1, 52.7, 47.4, 28.3, 27.3; HRMS (ES) Calculated for C₁₉H₂₄Cl₂N₃O₄ 428.1138, found 428.1133 (M+H)⁺.

methyl *N*π-(3,5-dichlorobenzyl)-*L*-histidinate dihydrochloride (90**)**



This compound was synthesized following a literature procedure.¹²⁷ Amino acid **89** (0.549 g, 1.28 mmol) was dissolved in a 4N HCl in dioxane solution at room temperature. The reaction was stirred for 2 h, concentrated *in vacuo* and the di-HCl salt was purified by EtOAc trituration, generating **90** as a white solid (0.397 g, 77%). (R_f 0.05 on SiO₂, 9:1 CH₂Cl₂:MeOH); [α]_D²⁶ 10.6 (*c* 1.27 CH₃OH); IR (CH₃OH cast) 3394, 3100, 2954, 2878, 1751, 1593, 1572, 1436, 1297, 1230, 1104 cm⁻¹; ¹H (CD₃OD, 500 MHz): δ 9.06 (d, *J* = 1.3 Hz, 1H, His-CH_ε₁), 7.64 (s, 1H, His-CH_δ₂), 7.57 – 7.48 (m, 1H, Ar-H), 7.39 – 7.35 (m, 2H, Ar-H), 5.55 (d, *J* = 5.1 Hz, 2H, Ar-CH₂), 4.36 (t, *J* = 7.2 Hz, 1H, His-CH_α), 3.84 (s, 3H, -OCH₃), 3.39 – 3.32 (m, 1H, His-CH₂β), 3.29 – 3.22 (m, 1H, His-CH₂β); ¹³C (CDCl₃, 125 MHz): δ 169.4, 143.5, 138.4, 138.2, 137.3, 130.4, 127.8, 121.5, 54.3, 52.1, 50.5, 25.5; HRMS (ES) Calculated for C₁₄H₁₆Cl₂N₃O₂ 328.0614, found 328.0614 (M+H)⁺.

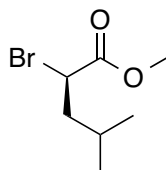
methyl 4-methyl-2-oxopentanoate (93)



α -Ketoester **93** was synthesized by following a literature procedure.¹³⁵ A suspension of H-Leu-OMe \cdot HCl (1.002 g, 5.51 mmol) in dry diethyl ether (20 mL) was neutralized by triethylamine (0.77 mL, 5.51 mmol) and cooled to 0 °C. *tert*-butyl hypochlorite (0.599 g, 5.51 mmol) was added in the absence of light and stirred for 10 minutes. The reaction was concentrated *in vacuo*, resuspended in CH₂Cl₂ (10 mL), washed with 0.1 N HCl (10 mL) and brine (2 x 10 mL). The organic layer was dried over Na₂SO₄, filtered and concentrated *in vacuo*, generating the crude N-chlorinated intermediate (0.887 g, 4.94 mmol) as a clear oil. This was immediately resuspended in diethyl ether (20 mL) and cooled to 0 °C. DBU (0.78 mL, 5.23 mmol) was added to the reaction mixture and stirred for 10 minutes. The reaction was passed through a fritted filter to remove the white solid DBU \cdot HCl precipitate and the resulting filtrate was concentrated down to ~15 mL. This solution was cooled to 0 °C, acidified with concentrated sulfuric acid (0.5 mL) and diluted by the addition of water (0.15 mL) and THF (30 mL). This reaction was heated under reflux at 60 °C for 1.5 h, then cooled and concentrated *in vacuo*. The crude α -keto ester was resuspended in CH₂Cl₂ (50 mL), washed with brine (2 x 25 mL), dried over Na₂SO₄, filtered and concentrated *in vacuo*. Crude NMR analysis indicated the presence of the desired α -keto ester with minimal impurities, and reaction was used without further purification (0.574 g, 72%). ¹H

(CDCl₃, 600 MHz) δ 3.86 (s, 3H, -OCH₃), 2.71 (d, J = 6.9 Hz, 2H, -CH₂ β), 2.27 – 2.14 (m, 1H, -CH(CH₃)₂), 0.97 (dd, J = 8.4, 6.7 Hz, 6H, -CH(CH₃)₂).

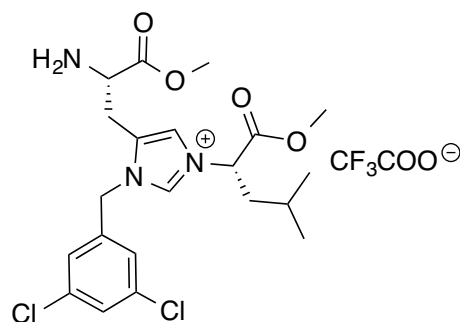
methyl (*R*)-2-bromo-4-methylpentanoate (99**)**



Compound **99** was prepared according to a literature procedure.¹³⁶ A solution of D-Leu-OH (1.030 g, 7.85 mmol) and sodium bromide (2.83 g, 27.5 mmol) in 2.5 M sulfuric acid (10 mL) was cooled down to 0 °C and stirred vigorously. Sodium nitrite (0.677 g, 9.82 mmol) was dissolved in water (10 mL) and added dropwise via addition funnel to the first solution and stirred for 1 h at 0 °C then warmed to room temperature for an additional 15 h. Organic components were extracted with EtOAc washes (3 x 50 mL) which were pooled, dried over Na₂SO₄, filtered and concentrated *in vacuo*. The yellow oil was resuspended in methanol (15 mL) and had concentrated sulfuric acid (0.25 mL) added. This solution was refluxed at 70 °C for 1 h, then cooled to room temperature and concentrated *in vacuo*. Crude residue was resuspended in diethyl ether (50 mL), washed with saturated NaHCO₃ (2 x 50 mL) and brine (50 mL). The organic layer was dried over Na₂SO₄, filtered and concentrated *in vacuo*. The desired product **99** was purified by flash chromatography (silica gel, 10% EtOAc in hexanes), generating a clear colorless liquid (0.510 g, 31%). (R_f 0.9 on SiO₂, 2:1 hexanes:EtOAc); $[\alpha]_D^{26}$ 50.1 (c 1.00 CHCl₃); IR (CHCl₃ cast) 2960, 2873, 1751, 1469, 1284, 1151 cm⁻¹; ¹H (CDCl₃, 500 MHz): δ 4.29 (dd, J = 8.1, 7.3 Hz, 1H, Br-CH α), 3.78 (s, 3H, -OCH₃), 1.97 – 1.88 (m, 2H, -CH₂ β), 1.81 – 1.72 (m, 1H, -CH(CH₃)₂), 0.96 (d, J = 6.7 Hz, 3H, -CH(CH₃)₂),

0.91 (d, $J = 6.6$ Hz, 3H, $-\text{CH}(\text{CH}_3)_2$); ^{13}C (CDCl_3 , 125 MHz): δ 170.6, 52.9, 44.4, 43.5, 26.4, 22.4, 21.6. HRMS (ES and EI) were performed but no conclusive mass was obtained due to proposed oligimerization; 231.1 ($\text{M}+\text{H}$) $^+$ observed, as well as repeating addition of 114 Da ($\text{C}_6\text{H}_{10}\text{O}_2$): 345.1, 459.1, 573.2 Da.

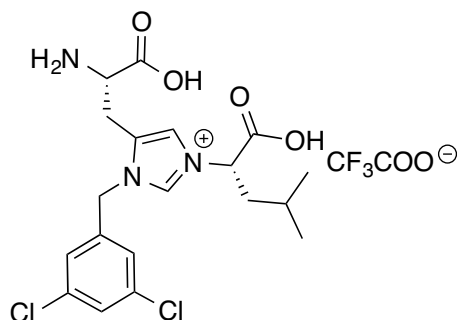
5-((*S*)-2-amino-3-methoxy-3-oxopropyl)-1-(3,5-dichlorobenzyl)-3-((*S*)-1-methoxy-4-methyl-1-oxopentan-2-yl)-1*H*-imidazol-3-ium (101)



This reaction was set up by modifying an analogous literature procedure.¹³⁷ A solution of **90** (43.5 mg, 0.108 mmol) and NaHCO_3 (29.2 mg, 0.347 mmol) in acetonitrile (10 mL) had α -bromo ester **99** (24.9 mg, 0.119 mmol) added to it. This solution was refluxed at 80 °C under an Ar atmosphere for 93 h. After cooling, the reaction was concentrated *in vacuo* and resuspended in 20 % aqueous acetonitrile. The crude reaction mixture was purified by semipreparative C_{18} RP-HPLC using the following method: 0 – 5 min 10% B, 5 – 18 min 10 – 45% B, 18 – 21 min 45 – 95% B, 21 – 24 min 95% B, 24 – 27 min 95 – 10% B, 27 – 30 min 10 % B (A = 0.1% aqueous TFA, B = 0.1% TFA in acetonitrile). Unreacted **90** was recovered at 12.7 min, and the *N*-imidazole alkylated product **101** was recovered at 16.2 min as a white powder after lyophilization (38.0 mg, 77%). (R_f 0.01 on SiO_2 , 9:1 EtOAc:MeOH); IR (CH_2Cl_2 cast) 3112, 2964, 2877, 1753, 1674, 1574, 1436, 1202, 1136 cm^{-1} ; ^1H (CD_3OD , 500 MHz): δ

9.33 (d, $J = 1.7$ Hz, 1H, His-CH ϵ_1), 7.86 (dd, $J = 7.3, 1.6$ Hz, 1H, His-CH δ_2), 7.55 (tdd, $J = 3.4, 2.0, 1.2$ Hz, 1H, Ar-H), 7.36 – 7.29 (m, 2H, Ar-H), 5.54 (s, 2H, Ar-CH $_2$), 5.29 (dd, $J = 8.8, 8.4$ Hz, 1H, N ϵ_2 -CH α), 4.41 – 4.30 (m, 1H, His-CH α), 3.83 (s, 3H, -OCH $_3$) 3.80 (s, 3H, -OCH $_3$), 3.40 – 3.25 (m, 2H, His-CH $_2\beta$), 2.17 – 2.05 (m, 2H, N ϵ_2 -CHCH $_2\beta$), 1.54 – 1.43 (m, 1H, -CH(CH $_3$) $_2$), 1.03 – 0.95 (m, 6H, -CH(CH $_3$) $_2$); ^{13}C (CD $_3$ OD, 125 MHz): δ 170.4, 169.2, 139.5, 138.2, 137.4, 130.9, 130.7, 130.5, 127.7, 127.6, 123.7, 123.5, 62.5, 54.2, 51.9, 50.7, 41.4, 26.1, 25.6, 22.9, 22.8, 21.5; HRMS (ES) Calculated for C $_{21}$ H $_{28}$ Cl $_2$ N $_3$ O $_4$ 456.1451, found 456.1454 (M+H) $^+$.

5-((*S*)-2-amino-2-carboxyethyl)-3-((*S*)-1-carboxy-3-methylbutyl)-1-(3,5-dichlorobenzyl)-1*H*-imidazol-3-ium (102)

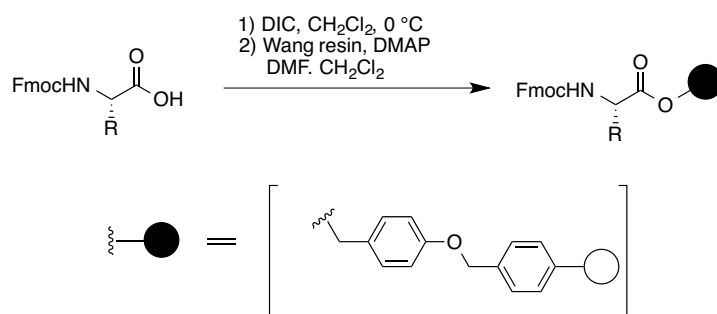


Imidazolium salt **101** (10.4 mg, 0.023 mmol) was dissolved in ethanol (2 mL) and 1N aqueous sodium hydroxide (0.137 mL, 0.137 mmol) was added. The reaction was stirred at room temperature for 18 h, concentrated by rotary evaporation and acidified by the addition of 10% aqueous TFA (0.100 mL). The material was lyophilized after C $_{18}$ RP-HPLC analysis showed one sharp peak and the di-acid **102** was obtained as a white solid (5.0 mg, 51%). (R_f 0.01 on SiO $_2$, 9:1 EtOAc:MeOH); IR (CHCl $_3$ cast) 3664, 3429, 3120, 2969, 2883, 1683, 1441, 1211, 1142 cm $^{-1}$; ^1H (CD $_3$ OD, 500 MHz): δ 9.30 (d, $J = 10.4$ Hz, 1H, His-CH ϵ_1), 7.80 (d, $J = 12.4$ Hz, 1H, His-CH δ_2), 7.52 (s, 1H,

Ar-H), 7.33 (s, 2H, Ar-H), 5.52 (d, $J = 4.3$ Hz, 2H, Ar-CH₂), 5.21 (dd, $J = 9.2, 6.4$ Hz, 1H, N ϵ_2 -CH α), 4.13 (t, $J = 6.9$ Hz, 1H, His-CH α), 3.33 (dd, $J = 16.2, 6.8$ Hz, 1H, His-CH β), 3.25 (dd, $J = 16.3, 6.8$ Hz, 1H, His-CH β), 2.11 (dd, $J = 8.6, 5.8$ Hz, 2H, N ϵ_2 -CHCH β), 1.49 (dq, $J = 13.7, 6.8$ Hz, 1H, -CH(CH₃)₂), 1.00 – 0.93 (m, 6H, -CH(CH₃)₂); ¹³C (CDCl₃, 125 MHz): δ 163.1, 162.8, 139.2, 137.3, 130.4, 127.7, 123.3, 119.4, 117.0, 63.2, 53.0, 50.7, 41.7, 26.1, 25.9, 22.9, 21.6; HRMS (ES) Calculated for C₁₉H₂₃Cl₂N₃NaO₄ 450.0959, found 450.0958 (M+Na)⁺.

4.3.2 General apelin analogue synthesis information

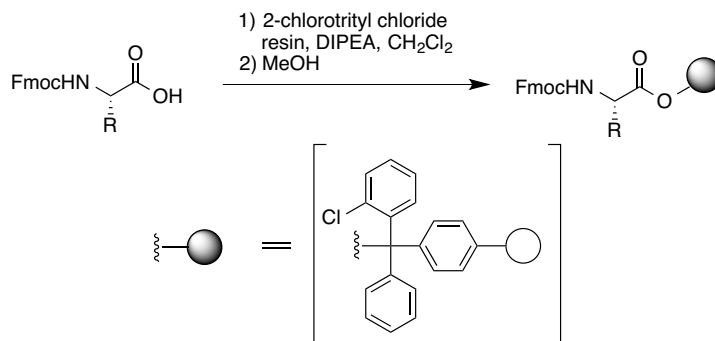
4.3.2.1 General Wang resin loading procedure



A solution of Fmoc-protected amino acid (10.0 equivalents) in dry CH₂Cl₂ was cooled to 0 °C and had diisopropylcarbodiimide (5.0 equivalents) added to generate the symmetrical anhydride. This solution was stirred for 20 minutes at 0 °C, concentrated *in vacuo* and resuspended in dry 25% CH₂Cl₂ in DMF (20 mL). Concomitantly, Wang resin (1.0 equivalent) was transferred to an SPPS vessel, washed with CH₂Cl₂ (2 x 10 mL) and DMF (2 x 10 mL), and finally suspended in DMF and bubbled under Ar gas for 1 h. The DMF solution was drained from the resin and the prepared amino acid anhydride was added along with DMAP (catalytic) and bubbled under Ar gas for 1.5 h.

The solution was drained, the resin was washed with DMF (3 x 10 mL) and unreacted sites were capped by bubbling 20% acetic anhydride in DMF (15 mL) with the resin under Ar gas for 15 min. The resin was washed with DMF (3 x 10 mL) and MeOH (10 mL) sequentially, dried thoroughly under Ar, weighed and divided into 0.1 mmol portions and stored under an Ar atmosphere at -20 °C.

4.3.2.2 General 2-chlorotrityl resin loading procedures



2-chlorotrityl chloride resin (1.05 equivalents) was transferred to a SPPS vessel and washed with CH₂Cl₂ (2 x 10 mL), DMF (2 x 10 mL), and finally suspended in DMF and bubbled under Ar gas for 10 minutes. The desired Fmoc-protected amino acid (1.0 equivalent) was suspended in dry CH₂Cl₂ (10 mL) with DIPEA (5.0 equivalents) and added to the swollen resin. This solution was bubbled under Ar gas for 2.5 h to load the desired amino acid onto the solid support, continually topping up the CH₂Cl₂ to maintain an approximately 10 mL volume. After the solution was drained, the chlorotrityl resin was washed considerably with CH₂Cl₂ (3 x 10 mL) and DMF (3 x 10 mL). Dry MeOH (5 mL) was added and bubbled under Ar gas for 45 minutes to cap unreacted sites on the resin. After draining, the resin was dried thoroughly under Ar, weighed and divided into 0.1 mmol portions, and stored under an Ar atmosphere at -20 °C.

4.3.2.3 General apelin analogue SPPS elongation method

A suspension of resin in DMF (10 mL) was bubbled under Ar gas for 15 minutes to swell. The N-terminal Fmoc group was removed by bubbling a solution of 20% piperidine in DMF (3 x 10 mL) for 3 minutes, with considerable resin washing with DMF (3 x 10 mL) after each deprotection. Fmoc-deprotection was monitored by TLC, observing the presence of the dibenzofulvene-piperidine adduct as a bright purple spot under UV. Two methods were used to pre-activate the amino acid solution:

Method A: 4-methylmorpholine (6.0 equivalents) was added to a solution of Fmoc-protected amino acid (5.0 equivalents compared to resin loading), PyBOP (4.9 equivalents), and HOBt (5.0 equivalents) in DMF (10 mL) and stirred for 5 minutes.

Method B: DIPEA (6.0 equivalents) was added to a solution of Fmoc-protected amino acid (3.0 equivalents compared to resin loading), HATU (3.0 equivalents), and HOAt (3.0 equivalents) in DMF (10 mL) and stirred for 5 minutes.

The activated amino acid solution was added to the resin and bubbled under Ar gas for 1-3 h. The resin was washed with DMF (3 x 10 mL) and the extent of coupling was assessed by either: i) cleaving a small sample of resin with a solution of 95:2.5:2.5 TFA:TIPS:H₂O for 1 h and analyzing the crude mass by MALDI-TOF or ii) performing a Kaiser test to detect the presence of any free amine. A solution of 20% acetic anhydride in DMF (10 mL) was added to the resin and bubbled under Ar gas for 10 minutes to end-cap any unreacted amines. The resin was then rinsed thoroughly with DMF (3 x 10 mL) and subjected to Fmoc-deprotection to further elongate the peptide, or rinsed with CH₂Cl₂ (3 x 10 mL) and MeOH (3 x 10 mL), dried thoroughly and stored under Ar gas at -20 °C.

4.3.2.4 Automated SPPS method

Peptides were synthesized on a CEM Liberty 1 Microwave Peptide Synthesizer. Solid phase synthesis was carried out on a 0.1 mmol scale using Fmoc chemistry. Commercially available protected amino acids were loaded on the peptide synthesizer as 0.2 M solutions in DMF. All amino acid subunits were coupled using O-benzotriazole-N,N,N',N'-tetramethyl-uronium-hexafluoro-phosphate (HBTU) as the activating agent and heated at 70 °C for a 5 minute coupling time. Fmoc residues were deprotected using a 20% solution of piperidine in DMF using UV-Vis spectroscopy to observe the dibenzofulvene-piperidine adduct absorption at $\lambda = 301$ nm.

4.3.2.5 General method for apelin analogue resin cleavage

Resin-bound apelin analogue (0.05 mmol) was suspended in 95:2.5:2.5 TFA:TIPS:H₂O with shaking under an Ar atmosphere for 2-3 h. The resin was removed via filtration through glass wool, rinsed with TFA, and the solution concentrated *in vacuo*. Cold diethyl ether (2 x 5 mL) was added to triturate the crude residue. The diethyl ether was decanted into a 15 mL Falcon tube and briefly centrifuged to pellet any residual peptide. The diethyl ether pellet and triturated crude residue were pooled together and dissolved in 10% aqueous acetonitrile, 0.1% TFA.

4.3.2.6 Apelin peptide purification methods

Peptides were purified using C₁₈ RP-HPLC using aqueous 0.1% TFA (solvent A) and 0.1 % TFA in acetonitrile (solvent B) as eluents. Three general purification methods were used:

Method A:	0 – 10 min	2% - 50% B,
	10 – 14 min	50% - 100% B,

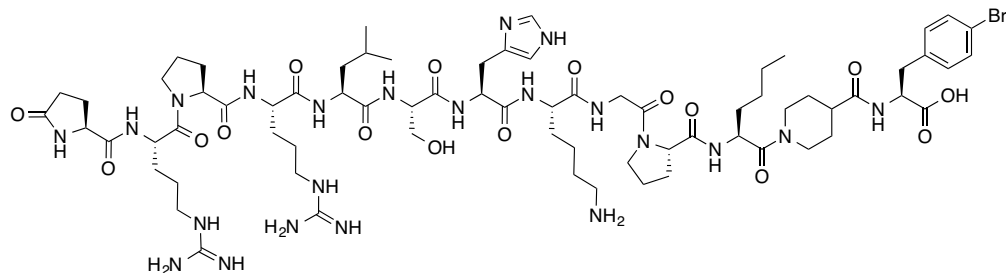
	14 – 18 min	100% B,
	18 – 22 min	100% - 2% B,
	22 – 25 min	2% B
Method B:	0 – 3 min	10% B,
	3 – 4.5 min	10 – 25% B,
	4.5 – 21.5 min	25 – 42% B,
	21.5 – 24 min	42 – 95% B,
	24 – 27 min	95% B,
	27 – 27.25 min	95 – 10% B,
	27.25 – 30 min	10% B
Method C:	0 – 3 min	10% B
	3 – 20 min	10 – 60% B
	20 – 25 min	60 – 100% B
	25 – 27 min	100% B
	27 – 27.2 min	100 – 10% B
	27.2 – 30 min	10% B

Analytical reinjections were performed to further purify analogues, using the following method:

Method D:	0 – 3 min	27% B
	3 – 13 min	27 – 35% B
	13 – 15 min	35% B
	15 – 16 min	35 – 27% B
	16 – 18 min	27% B

4.3.3 Apelin analogue SPPS

Nle11Inp12BrPhe13-pyr-1-apelin-13 – pyr-1-apelin-13 analogue 1 (**103**)¹¹⁵



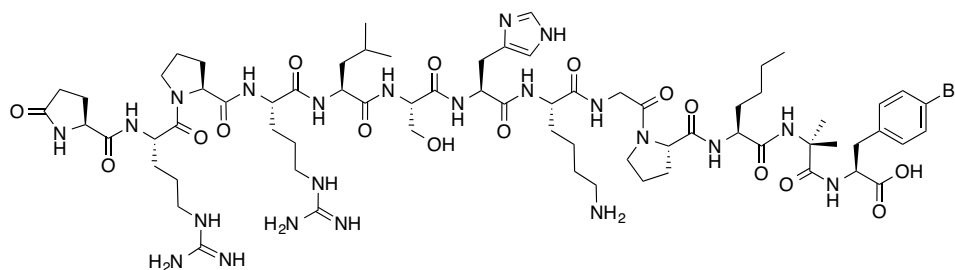
Fmoc-*p*-Br-L-Phe-OH was loaded onto Wang resin using the aforementioned procedure. 0.1 mmol of this pre-loaded resin was resuspended in DMF in an SPPS vessel and subjected to rounds of manual SPPS (method 1), introducing amino acids in the following order: Fmoc-Inp-OH, Fmoc-Nle-OH, Fmoc-Pro-OH, Fmoc-Gly-OH, Fmoc-Lys(Boc)-OH, Fmoc-His(Trt)-OH, Fmoc-Ser(*t*Bu)-OH, Fmoc-Leu-OH, Fmoc-Arg(Pmc)-OH, Fmoc-Pro-OH, Fmoc-Arg(Pmc)-OH, and pyr-Glu-OH. The peptide was cleaved as previously described and purified using a C₁₈ RP-HPLC analytical column (Method A), eluting at 12.6 minutes. The desired peptide was isolated as a white solid after lyophilization (10.5 mg, 26%). Monoisotopic MW calculated for C₇₁H₁₁₂BrN₂₂O₁₆ 1607.7805, found *high resolution* (FTICR-ESI-MS) 1607.7802 (M+H)⁺.

NMR spectroscopy was performed on a solution of **103** in 90 % H₂O 10 % D₂O at a concentration of 1 mM in a standard 5 mM NMR tube with DSS (0.01%) added for referencing. TOCSY, NOESY, and ROESY experiments were acquired at 25 °C on a Varian Inova 600 MHz spectrometer, suppressing the water signal using transmitter presaturation. Proton chemical shifts were assigned based on TOCSY and NOESY data.

Table 4.2 – ¹H-NMR chemical shifts of pyr-1-apelin-13 A1 analogue 103.¹¹⁵

	HN	H α	H β	others
pyrGlu1	7.88	4.35	2.52, 2.40	γ CH ₂ 2.02
Arg2	8.38	4.61	1.84, 1.72	γ CH ₂ 1.65 δ CH ₂ 3.20 δ NH 7.20
Pro3	-	4.39	2.28, 2.00	γ CH ₂ 1.84 δ CH ₂ 3.80, 3.61
Arg4	8.46	4.28	1.81, 1.74	γ CH ₂ 1.64 δ CH ₂ 3.18 δ NH 7.14
Leu5	8.26	4.39	1.59, 1.55	γ CH 1.52 δ CH ₃ 0.89, 0.83
Ser6	8.29	4.40	3.80	
His7	8.48	4.68	3.25, 3.15	
Lys8	8.40	4.37	1.82	γ CH ₂ 1.40 δ CH ₂ 1.69 ϵ CH ₂ 2.97
Gly9	8.26	4.11		
Pro10	-	4.43	2.26, 1.99	γ CH ₂ 1.90 δ CH ₂ 3.79, 3.61
Nle11	8.27 8.22	4.69 4.69	1.64 1.63	γ CH ₂ 1.27 δ CH ₂ 1.27 ϵ CH ₃ 0.83 γ CH ₂ 1.29 δ CH ₂ 1.23 ϵ CH ₃ 0.83 * two sets of signals due to rotamers
Inp12	-	4.27, 4.16 3.90, 3.14	2.51, 1.75 1.59, 1.38	γ CH 2.73
<i>p</i>-Br Phe13	7.89	4.55	3.21, 2.87	Ar-H 7.42, 7.10

Nle11Aib12BrPhe13-pyr-1-apelin-13 – pyr-1-apelin-13 analogue 2 (104)¹¹⁵



Fmoc-*p*-Br-L-Phe-OH was loaded onto Wang resin using the aforementioned procedure. 0.1 mmol of this pre-loaded resin was transferred to an SPPS vessel and subjected to automated SPPS (CEM Liberty One), introducing amino acids in the following order: Fmoc-Aib-OH, Fmoc-Nle-OH, Fmoc-Pro-OH, Fmoc-Gly-OH, Fmoc-Lys(Boc)-OH, Fmoc-His(Trt)-OH, Fmoc-Ser(*t*Bu)-OH, Fmoc-Leu-OH, Fmoc-Arg(Pmc)-OH, Fmoc-Pro-OH, Fmoc-Arg(Pmc)-OH, and pyr-Glu-OH. The peptide was

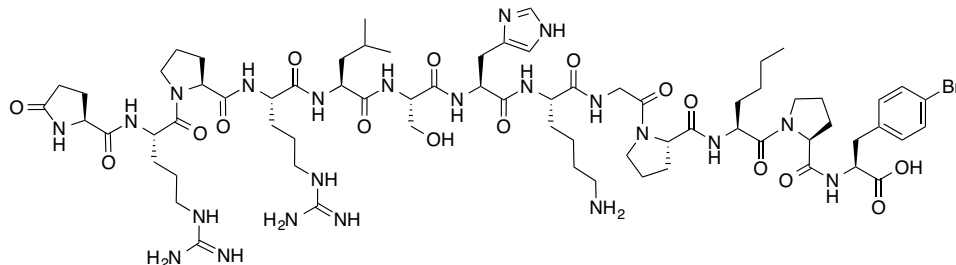
cleaved as previously described and purified using a C₁₈ RP-HPLC analytical column (Method A), eluting at 12.8 minutes. The desired peptide was isolated as a white solid after lyophilization (17.9 mg, 36%). Monoisotopic MW calculated for C₆₉H₁₁₀BrN₂₂O₁₆ 1581.7648, found *high resolution* (FTICR-ESI-MS) 1581.7666 (M+H)⁺.

NMR spectroscopy was performed on a solution of **104** in 90 % H₂O 10 % D₂O at a concentration of 1 mM in a standard 5 mM NMR tube with DSS (0.01%) added for referencing. TOCSY, NOESY, and ROESY experiments were acquired at 25 °C on a Varian VNMRS 700 MHz spectrometer, suppressing the water signal using transmitter presaturation. Proton chemical shifts were assigned based on TOCSY and NOESY data.

Table 4.3 – ¹H-NMR chemical shifts of pyr-1-apelin-13 A2 analogue 104.¹¹⁵

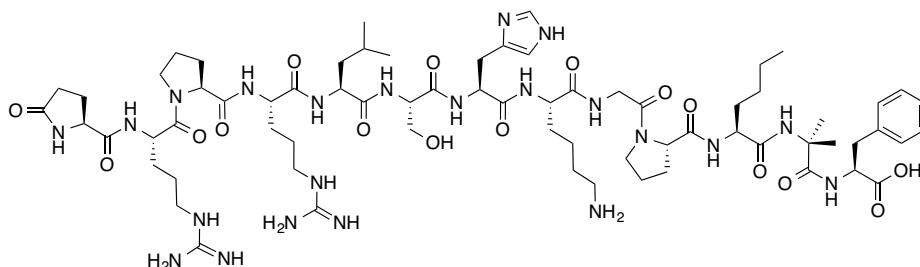
	HN	H α	H β	others
pyrGlu1	7.90	4.37	2.53, 2.38	γ CH ₂ 2.03
Arg2	8.39	4.62	1.82	γ CH ₂ 1.72 δ CH ₂ 3.21 δ NH 7.19
Pro3	-	4.41	2.29, 2.01	γ CH ₂ 1.85 δ CH ₂ 3.82, 3.61
Arg4	8.48	4.27	1.82, 1.78	γ CH ₂ 1.63 δ CH ₂ 3.26, 3.19 δ NH 7.18
Leu5	8.27	4.39	1.61, 1.58	γ CH 1.54 δ CH ₃ 0.88, 0.83
Ser6	8.31	4.41	3.81, 3.79	
His7	8.51	4.68	3.27, 3.15	
Lys8	8.39	4.36	1.81	γ CH ₂ 1.41 δ CH ₂ 1.66 ϵ CH ₂ 2.97
Gly9	8.27	4.09		
Pro10	-	4.42	2.26, 1.98	γ CH ₂ 1.90 δ CH ₂ 3.81, 3.60
Nle11	8.19	4.14	1.67, 1.59	γ CH ₂ 1.28 δ CH ₂ 1.24 ϵ CH ₃ 0.85
Aib12	8.02	-	1.38, 1.35	
p-Br Phe13	7.56	4.54	3.13, 2.99	Ar-H 7.49, 7.16

Nle11BrPhe13-pyr-1-apelin-13 – analogue 20 (105)



This peptide analogue is a literature compound.¹¹⁸ Fmoc-*p*-Br-L-Phe-OH was loaded onto Wang resin using the aforementioned procedure. 0.1 mmol of this preloaded resin was transferred to an SPPS vessel and subjected to automated SPPS (CEM Liberty One), introducing amino acids in the following order: Fmoc-Pro-OH, Fmoc-Nle-OH, Fmoc-Pro-OH, Fmoc-Gly-OH, Fmoc-Lys(Boc)-OH, Fmoc-His(Trt)-OH, Fmoc-Ser(*t*Bu)-OH, Fmoc-Leu-OH, Fmoc-Arg(Pmc)-OH, Fmoc-Pro-OH, Fmoc-Arg(Pmc)-OH, and pyr-Glu-OH. The peptide was cleaved as previously described and purified using a C₁₈ RP-HPLC analytical column (Method A). The desired peptide was isolated as a white solid after lyophilization (4.8 mg, 9%). Monoisotopic MW calculated for C₇₀H₁₁₀BrN₂₂O₁₆ 1593.7648, found *high resolution* (FTICR-ESI-MS) 1593.7689 (M+H)⁺.

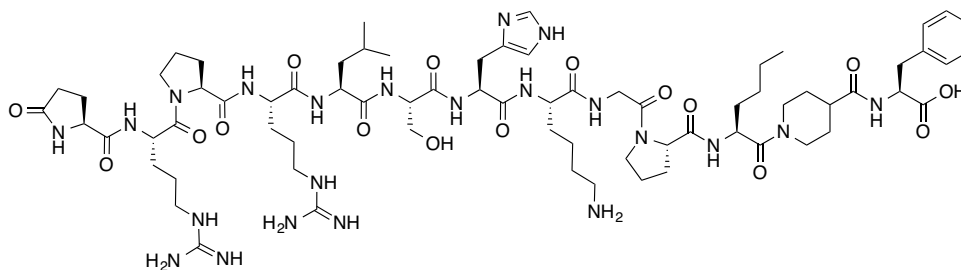
Nle11Aib12-pyr-1-apelin-13 – analogue 29 (106)



This peptide analogue is a literature compound.¹¹⁸ Preloaded Fmoc-Phe-OH on Wang resin (0.1 mmol) was transferred to an SPPS vessel and subjected to automated

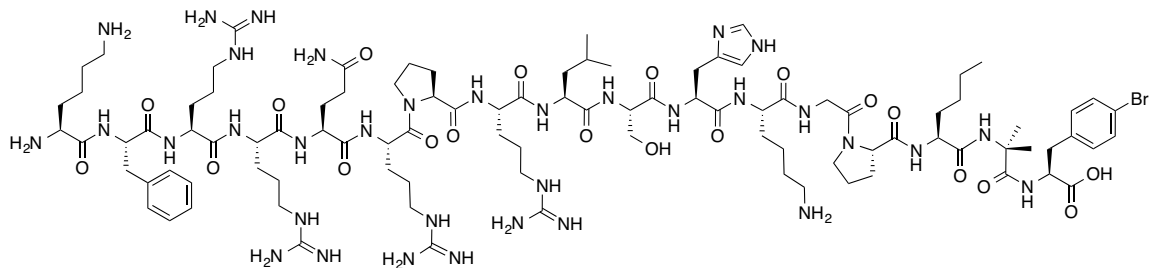
SPPS (CEM Liberty One), introducing amino acids in the following order: Fmoc-Aib-OH, Fmoc-Nle-OH, Fmoc-Pro-OH, Fmoc-Gly-OH, Fmoc-Lys(Boc)-OH, Fmoc-His(Trt)-OH, Fmoc-Ser(tBu)-OH, Fmoc-Leu-OH, Fmoc-Arg(Pmc)-OH, Fmoc-Pro-OH, Fmoc-Arg(Pmc)-OH, and pyr-Glu-OH. The peptide was cleaved as previously described and purified using a C₁₈ RP-HPLC analytical column (Method A). The desired peptide was isolated as a white solid after lyophilization (5.7 mg, 11%). Monoisotopic MW calculated for C₆₉H₁₁₂N₂₂O₁₆ 1503.8543, found *high resolution* (FTICR-ESI-MS) 1503.8577 (M+H)⁺.

Nle11Inp12-pyr-1-apelin-13 – analogue 30 (107)



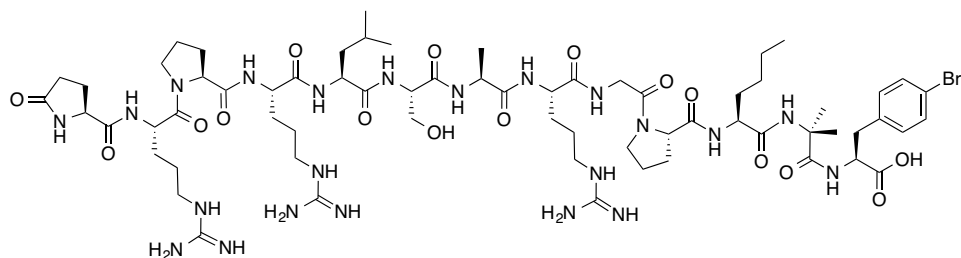
This peptide analogue is a literature compound.¹¹⁸ Preloaded Fmoc-Phe-OH on Wang resin (0.1 mmol) was transferred to an SPPS vessel and subjected to automated SPPS (CEM Liberty One), introducing amino acids in the following order: Fmoc-Inp-OH, Fmoc-Nle-OH, Fmoc-Pro-OH, Fmoc-Gly-OH, Fmoc-Lys(Boc)-OH, Fmoc-His(Trt)-OH, Fmoc-Ser(tBu)-OH, Fmoc-Leu-OH, Fmoc-Arg(Pmc)-OH, Fmoc-Pro-OH, Fmoc-Arg(Pmc)-OH, and pyr-Glu-OH. A portion of resin-bound **107** (0.033 mmol) was cleaved as previously described and purified using a C₁₈ RP-HPLC analytical column (Method A). The desired peptide was isolated as a white solid after lyophilization (4.6 mg, 9%). Monoisotopic MW calculated for C₇₁H₁₁₃N₂₂O₁₆ 1529.9, found (MALDI-TOF) 1530.3 (M+H)⁺.

Nle15Aib16BrPhe17-apelin-17 – apelin-17 A2 (108)



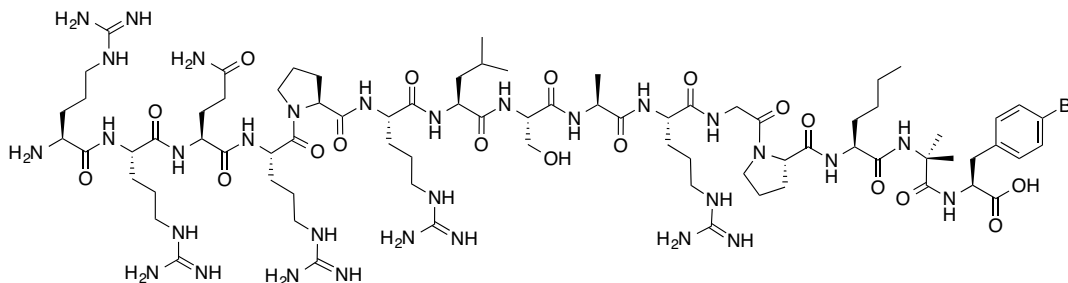
Fmoc-*p*-Br-L-Phe-OH was loaded onto 2-chlorotrityl-chloride resin using the aforementioned procedure. 0.1 mmol of this pre-loaded resin was transferred to an SPPS vessel and subjected to manual SPPS, introducing amino acids in the following order: Fmoc-Aib-OH, Fmoc-Nle-OH, Fmoc-Pro-OH, Fmoc-Gly-OH, Fmoc-Lys(Boc)-OH, Fmoc-His(Trt)-OH, Fmoc-Ser(*t*Bu)-OH, Fmoc-Leu-OH, Fmoc-Arg(Pmc)-OH, Fmoc-Pro-OH, Fmoc-Arg(Pmc)-OH, Fmoc-Gln(Trt)-OH, Fmoc-Arg(Pmc)-OH, Fmoc-Arg(Pmc)-OH, Fmoc-Phe-OH, and Fmoc-Lys(Boc)-OH. A portion (0.05 mmol) of resin-bound peptide **108** was cleaved as previously described and purified using a C₁₈ RP-HPLC analytical column (Method A). The desired peptide was isolated as a white solid after lyophilization (15.0 mg, 14%). Monoisotopic MW calculated for C₉₆H₁₆₀BrN₃₄O₂₀ 729.3905, found *high resolution* (FTICR-ESI-MS) 729.3909 (M+3H)³⁺.

Ala7Arg8-pyr-1-apelin-13 A2 – SM-6-53-A13 (109)



Fmoc-*p*-Br-L-Phe-OH was loaded onto 2-chlorotrityl-chloride resin using the aforementioned procedure. 0.1 mmol of this pre-loaded resin was transferred to an SPPS vessel and subjected to manual SPPS, introducing amino acids in the following order: Fmoc-Aib-OH, Fmoc-Nle-OH, Fmoc-Pro-OH, Fmoc-Gly-OH, Fmoc-Arg(Pmc)-OH, Fmoc-Ala-OH, Fmoc-Ser(*t*Bu)-OH, Fmoc-Leu-OH, Fmoc-Arg(Pmc)-OH, Fmoc-Pro-OH, Fmoc-Arg(Pmc)-OH, and pyr-Glu-OH. A portion (0.05 mmol) of resin-bound peptide **109** was cleaved as previously described and purified using a C₁₈ RP-HPLC analytical column (Method A), eluting at 21.4 minutes. The desired peptide was isolated as a white solid after lyophilization (9.5 mg, 12%). Monoisotopic MW calculated for C₆₆H₁₁₀BrN₂₂O₁₆ 515.2546, found *high resolution* (FTICR-ESI-MS) 515.2537 (M+3H)³⁺.

Ala9Arg10-apelin-15 A2 – SM-6-53-A15 (110)

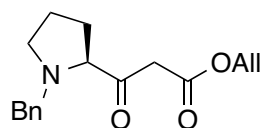


Fmoc-*p*-Br-L-Phe-OH was loaded onto 2-chlorotrityl-chloride resin using the aforementioned procedure. 0.1 mmol of this pre-loaded resin was transferred to an SPPS vessel and subjected to manual SPPS, introducing amino acids in the following order: Fmoc-Aib-OH, Fmoc-Nle-OH, Fmoc-Pro-OH, Fmoc-Gly-OH, Fmoc-Arg(Pmc)-OH, Fmoc-Ala-OH, Fmoc-Ser(*t*Bu)-OH, Fmoc-Leu-OH, Fmoc-Arg(Pmc)-OH, Fmoc-Pro-OH, Fmoc-Arg(Pmc)-OH, Fmoc-Gln(Trt)-OH, Fmoc-Arg(Pmc)-OH, and Fmoc-Arg(Pmc)-OH. A portion (0.05 mmol) of resin-bound peptide **110** was cleaved as

previously described and purified using a C₁₈ RP-HPLC analytical column (Method A), eluting at 20.2 minutes. The desired peptide was isolated as a white solid after lyophilization (9.9 mg, 11%). Monoisotopic MW calculated for C₇₈H₁₃₈BrN₃₁O₁₈ 468.9999, found *high resolution* (FTICR-ESI-MS) 468.9995 (M+4H)⁴⁺.

4.3.4 Pro12-Phe13 isostere syntheses

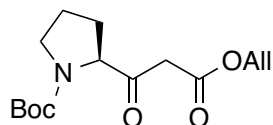
(S)-allyl 3-(1-benzylpyrrolidin-2-yl)-3-oxopropanoate (**116**)



This compound was prepared by adapting a literature protocol.¹⁴⁰ A solution of **168** (5.00 g, 20.7 mmol) in dry THF (30 mL) was neutralized with triethylamine (3.18 mL, 22.8 mmol), followed by the addition of 1,1'-carbonyldiimidazole (3.35 g, 20.7 mmol). The reaction was stirred for 4 h under Ar, and then transferred to an addition funnel. In a separate dried three-necked flask, diisopropylamine (12.2 mL, 86.9 mmol) was cooled to -78 °C and *n*-butyllithium (39.0 mL [2.23 M solution], 86.9 mmol) was slowly added over 5 minutes under Ar. Allyl acetate (5.58 mL, 51.7 mmol) was then added over 10 minutes and the reaction was stirred at -78 °C for 45 minutes. The initial reaction mixture containing **168** and 1,1'-carbonyldiimidazole was then added dropwise to the allyl acetate enolate over 20 minutes at -78 °C. The reaction was slowly warmed to room temperature and stirred for 18 h under Ar. The reaction was quenched by the addition of water (100 mL), then transferred to a separatory funnel, extracting organic components with ether (3 x 150 mL) washes. Pooled ether layers were dried over

Na₂SO₄, filtered, and concentrated *in vacuo*. Compound **116** was purified by flash chromatography (silica gel, 20% EtOAc in hexanes), obtaining the product as a light yellow oil (1.90 g, 32%). (*R_f* 0.8 on SiO₂, 1:1 hexanes:EtOAc); ¹H (CDCl₃, 500 MHz): δ 7.34 – 7.22 (m, 5H, Ar-H), 5.89 (ddt, *J* = 17.3, 10.5, 5.8 Hz, 1H, -OCH₂CH=CH₂), 5.31 (ddt, *J* = 17.2, 1.5, 1.5 Hz, 1H, -OCH₂CH=CH₂), 5.23 (ddt, *J* = 10.4, 1.3, 1.3 Hz, 1H, -OCH₂CH=CH₂), 4.60 (dt, *J* = 5.9, 1.4 Hz, 2H, -OCH₂CH=CH₂), 3.85 (d, *J* = 13.1 Hz, 1H, -CH₂Ph), 3.69 (d, *J* = 16.0 Hz, 1H, -C(O)-CH₂COOAll), 3.54 (d, *J* = 15.9 Hz, 1H, -C(O)-CH₂COOAll), 3.48 (d, *J* = 13.1 Hz, 1H, -CH₂Ph), 3.25 (dd, *J* = 9.6, 6.3 Hz, 1H, Pro-CH_α), 3.05 (dtd, *J* = 9.6, 4.2, 3.7, 2.1 Hz, 1H, Pro-CH₂δ), 2.34 (td, *J* = 9.0, 7.6 Hz, 1H, Pro-CH₂δ), 2.20 – 2.06 (m, 1H, Pro-CH₂β), 1.96 – 1.78 (m, 3H, Pro-CH₂β, 2 x Pro-CH₂γ); ¹³C (CDCl₃, 125 MHz): δ 206.1, 167.5, 138.4, 131.8, 128.9, 128.4, 127.3, 118.6, 73.2, 65.8, 59.5, 53.9, 44.3, 28.7, 23.9; HRMS (ES) Calculated for C₁₇H₂₂NO₃ 288.1594, found 288.1590 (M+H)⁺.

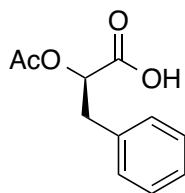
(S)-tert-butyl 2-(3-(allyloxy)-3-oxopropanoyl)pyrrolidine-1-carboxylate (117)



This compound was prepared by adapting a literature protocol.¹⁴⁰ Boc-L-Pro-OH (5.00 g, 23.2 mmol) in dry THF (30 mL) had 1,1'-carbonyldiimidazole (3.77 g, 23.2 mmol) added and was stirred for 5 h under Ar. The reaction was then transferred to an addition funnel. In a separate dried three-necked flask, diisopropylamine (10.4 mL, 74.3 mmol) was cooled to -78 °C and *n*-butyllithium (33.3 mL [2.23 M solution], 74.3 mmol) was slowly added over 5 minutes under Ar. Allyl acetate (6.26 mL, 58.1 mmol) was then added over 10 minutes and the reaction was stirred at -78 °C for 45 minutes. The

initial reaction mixture containing Boc-L-Pro-OH and 1,1'-carbonyldiimidazole was then added dropwise to the allyl acetate enolate over 20 minutes at -78 °C. The reaction was slowly warmed to room temperature and stirred for 1.5 h under Ar. The reaction was quenched by the addition of water (100 mL), then transferred to a separatory funnel, extracting organic components with diethyl ether (3 x 50 mL) washes. Pooled ether layers were washed with brine (100 mL), dried over Na₂SO₄, filtered and concentrated *in vacuo*. Compound **117** was purified by flash chromatography (silica gel, 20% EtOAc in hexanes), obtaining the product as a yellow oil (1.87 g, 27%). (*R_f* 0.8 on SiO₂, 1:1 hexanes:EtOAc); ¹H (*d*₆-DMSO, 400 MHz): δ 5.89 (ddt, *J* = 17.3, 10.6, 5.4 Hz, 1H, -OCH₂CH=CH₂), 5.32 (dt, *J* = 17.2, 1.6 Hz, 1H, -OCH₂CH=CH₂), 5.20 (dq, *J* = 10.5, 1.5 Hz, 1H, -OCH₂CH=CH₂), 4.58 (dt, *J* = 6.0, 1.9 Hz, 2H, -OCH₂CH=CH₂), 4.31 – 4.26 (m, 1H, Pro-CH_α), 3.69 – 3.58 (m, 2H, Pro-CH₂δ), 3.33 (d, *J* = 13.5 Hz, 2H, -C(O)-CH₂COOAll), 2.23 – 2.02 (m, 1H, Pro-CH₂β), 1.91 – 1.67 (m, 3H, Pro-CH₂β, 2 x Pro-CH₂γ), 1.39 (s, 3H, -C(CH₃)₃), 1.32 (s, 6H, -C(CH₃)₃); ¹³C (*d*₆-DMSO, 400 MHz, 100 °C): δ 206.5, 165.8, 152.9, 131.8, 117.3, 78.8, 64.8, 61.5, 46.1, 45.0, 27.6, 25.1, 23.0; HRMS (ES) Calculated for C₁₅H₂₃NNaO₅ 320.1468, found 320.1459 (M+Na)⁺.

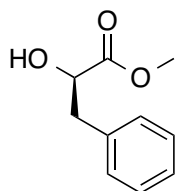
(R)-2-acetoxy-3-phenylpropanoic acid (119)



This literature compound was made following a published protocol.¹⁴¹ A vigorously stirred solution of D-phenylalanine (5.00 g, 30.3 mmol) in glacial acetic acid (100 mL) was cooled to 15 °C and had sodium nitrite (4.18 g, 60.5 mmol) added

portionwise over 3 minutes into an Ar-purged, vented round bottomed flask. The reaction was slowly warmed to room temperature and stirred for 1 h at room temperature. TLC indicated an incomplete conversion of starting material, so one additional equivalent of sodium nitrite (2.08 g, 30.3 mmol) was added and stirred for 1 h. The reaction was concentrated *in vacuo*, resuspended in water (150 mL), and organic components were extracted with diethyl ether (2 x 100 mL). Pooled organic layers were washed with water (50 mL) and brine (50 mL), dried over Na₂SO₄, filtered, and concentrated *in vacuo*. Toluene co-evaporations were used to remove residual acetic acid. Compound **119** was carried forward without further purification as a bright yellow oil (5.97 g, 95%). (*R_f* 0.95 on SiO₂, 4:1 CH₂Cl₂:MeOH, 1% AcOH); [α]_D²⁶ 7.6 (*c* 1.46 CHCl₃); IR (CH₂Cl₂ cast) 3066, 3032, 1746, 1651, 1498, 1456, 1436, 1375, 1232, 1074 cm⁻¹; ¹H (CDCl₃, 500 MHz): δ 7.76 (d, *J* = 7.5 Hz, 2H, Ar-H), ¹H (CDCl₃, 400 MHz): δ 7.40 – 7.12 (m, 5H, Ar-H), 5.27 (dd, *J* = 9.0, 4.1 Hz, 1H, AcO-CH), 3.30 – 3.18 (m, 1H, -CH₂Ph), 3.13 (dd, *J* = 14.4, 9.0 Hz, 1H, -CH₂Ph), 2.12 (s, 3H, Ac-CH₃); ¹³C (CDCl₃, 125 MHz): δ 177.9, 170.5, 135.8, 129.3, 128.6, 127.2, 72.6, 37.1, 20.5; HRMS (ES) Calculated for C₁₁H₁₁O₄ 207.0663, found 207.0662 (M-H)⁻.

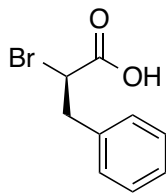
(R)-methyl 2-hydroxy-3-phenylpropanoate (120)



This literature compound was made following a published protocol.¹⁴¹ A solution of **119** (5.97 g, 28.7 mmol) in dry methanol (50 mL) was vigorously stirred and cooled to -30 °C. Thionyl chloride (2.29 mL, 31.5 mmol) was added dropwise over 5

minutes and the reaction was slowly warmed to room temperature. The reaction was stirred under an Ar atmosphere for 46 h, and then concentrated *in vacuo*. Saturated sodium bicarbonate solution was added to the reaction mixture until a pH of 9, then organic components were extracted with diethyl ether washes (4 x 50 mL). Pooled organic layers were dried over Na₂SO₄, filtered, and concentrated *in vacuo*. The product was purified by flash chromatography (silica gel, 20% EtOAc in hexanes), yielding **120** as a white solid (4.23 g, 82%). (*R_f* 0.9 on SiO₂, 4:1 CH₂Cl₂:MeOH); [α]_D²⁶ 4.7 (*c* 2.05 CHCl₃); IR (CH₂Cl₂ cast) 3457, 3064, 3030, 2954, 1741, 1648, 1497, 1455, 1439, 1276, 1220, 1097 cm⁻¹; ¹H (CDCl₃, 400 MHz): δ 7.33 – 7.21 (m, 5H, Ar-H), 4.47 (ddd, *J* = 6.5, 6.5, 4.4 Hz, 1H, HO-CH), 3.78 (s, 3H, -OCH₃), 3.13 (dd, *J* = 13.9, 4.4 Hz, 1H, -CH₂Ph), 2.98 (dd, *J* = 14.0, 6.8 Hz, 1H, -CH₂Ph), 2.70 (d, *J* = 6.2 Hz, 1H, HO-CH); ¹³C (CDCl₃, 125 MHz): δ 174.6, 136.4, 129.5, 128.5, 126.9, 71.3, 52.5, 40.6; HRMS (ES) Calculated for C₁₀H₁₂NaO₃ 203.0679, found 203.0674 (M+Na)⁺.

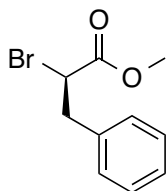
(R)-2-bromo-3-phenylpropanoic acid (121)



This compound was made following a literature protocol.¹³⁶ A vigorously stirred solution of D-phenylalanine (2.50 g, 15.1 mmol), sodium bromide (5.45 g, 53.0 mmol) in 2.5 N sulfuric acid (20 mL) was cooled to 0 °C and had a solution of sodium nitrite (1.31 g, 18.9 mmol) in water (10 mL) added dropwise via addition funnel over 10 minutes. The reaction was stirred at 0 °C for 1 h, then slowly warmed to room temperature for an additional 6 h. The reaction was transferred to a separatory funnel

and organic components were extracted with ethyl acetate (3 x 50 mL). Pooled organic layers were washed with brine (50 mL), dried over Na₂SO₄, filtered and concentrated *in vacuo*. The product was purified by flash chromatography (silica gel, 15% EtOAc in hexanes, 0.1% AcOH), yielding **121** as a pale yellow oil (2.424 g, 70%) after co-evaporation with toluene to remove residual acetic acid. (*R_f* 0.45 on SiO₂, 1:1 EtOAc:hexanes); [α]_D²⁶ 10.2 (*c* 2.00 CH₃OH); IR (CH₃OH cast) 3064, 3031, 2671, 1717, 1496, 1455, 1421, 1286, 1249, 1182 cm⁻¹; ¹H (CDCl₃, 500 MHz): δ 7.39 – 7.24 (m, 5H, Ar-H), 4.47 (dd, *J* = 8.1, 7.3 Hz, 1H, Br-CH), 3.51 (dd, *J* = 14.2, 8.2 Hz, 1H, -CH₂Ph), 3.29 (dd, *J* = 14.2, 7.2 Hz, 1H, -CH₂Ph); ¹³C (CDCl₃, 125 MHz): δ 174.5, 136.4, 129.2, 128.8, 127.5, 44.7, 40.8; HRMS (ES) Calculated for C₉H₉BrNaO₂ 250.9678, found 250.9679 (M+Na)⁺.

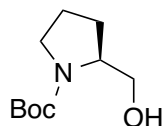
(R)-methyl 2-bromo-3-phenylpropanoate (122)



Compound **122** was made following a literature protocol.¹³⁶ A solution of **121** (2.40 g, 10.5 mmol) in methanol (30 mL) and concentrated sulfuric acid (0.31 mL) was refluxed at 69 °C for 1 h. The reaction was cooled, concentrated *in vacuo*, resuspended in diethyl ether (50 mL) and washed with saturated sodium bicarbonate (2 x 30 mL), and brine (30 mL). The organic layer was dried over Na₂SO₄, filtered and concentrated *in vacuo*. The product was purified by flash chromatography (silica gel, 15% EtOAc in hexanes), yielding **122** as a pale yellow oil (2.12 g, 83%). (*R_f* 0.8 on SiO₂, 1:3 EtOAc:hexanes); [α]_D²⁶ 18.5 (*c* 1.00 CHCl₃); IR (CHCl₃ cast) 3064, 3031, 2953, 1744,

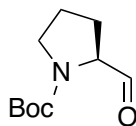
1495, 1437, 1360, 1291, 1229, 1151 cm^{-1} ; ^1H (CDCl_3 , 500 MHz): δ 7.36 – 7.24 (m, 5H, Ar-H), 4.45 (dd, $J = 8.4, 7.2$ Hz, 1H, Br-CH), 3.77 (s, 3H, -OCH₃), 3.51 (dd, $J = 14.1, 8.4$ Hz, 1H, -CH₂Ph), 3.28 (dd, $J = 14.0, 7.1$ Hz, 1H, -CH₂Ph); ^{13}C (CDCl_3 , 125 MHz): δ 169.9, 136.7, 129.2, 128.7, 127.4, 52.9, 45.1, 41.2; HRMS (ES) Calculated for $\text{C}_{10}\text{H}_{11}\text{BrNaO}_2$ 264.9835, found 264.9831 ($\text{M}+\text{Na}$)⁺.

(S)-tert-butyl 2-(hydroxymethyl)pyrrolidine-1-carboxylate (124)



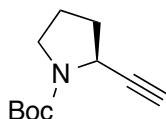
Alcohol **124** was made following a literature protocol.¹⁴³ A solution of Boc-L-Pro-OH (10.00 g, 46.5 mmol) in dry THF (100 mL) was cooled to 0 °C. $\text{BH}_3\cdot\text{SMe}_2$ (6.0 mL, 60 mmol) was added dropwise over 5 minutes and stirred for an additional 20 minutes at 0 °C until gas evolution ceased. The reaction was warmed to room temperature for 5 minutes, then heated at 75 °C for 1.5 h. After cooling, methanol (80 mL) was added to quench residual borane. The reaction was concentrated *in vacuo*, generating **124** as a white solid (9.15 g, 98%) that was carried forward without further purification. (R_f 0.55 on SiO_2 , 1:1 EtOAc:hexanes); $[\alpha]_D^{26}$ -48.1 (c 0.85 CH_2Cl_2); IR (CH_2Cl_2 cast) 3432, 2975, 2934, 2879, 1695, 1672, 1407, 1254, 1171, 1108, 1053 cm^{-1} ; ^1H (CDCl_3 , 500 MHz): δ 4.00 (br s, 1H, Pro-CH α), 3.69 – 3.59 (m, 2H, -CH₂OH), 3.45 (dt, $J = 12.6, 6.7$ Hz, 1H, Pro-CH δ), 3.30 (dt, $J = 10.8, 6.8$ Hz, 1H, Pro-CH δ), 2.04 (dq, $J = 12.5, 7.3$ Hz, 1H, Pro-CH β), 1.86 – 1.73 (m, 2H, 2 x Pro-CH γ), 1.57 – 1.50 (m, 1H, Pro-CH β), 1.47 (s, 9H, -C(CH₃)₃); ^{13}C (CDCl_3 , 125 MHz): δ 155.3, 80.2, 67.8, 60.3, 47.6, 28.8, 27.0, 24.1; HRMS (ES) Calculated for $\text{C}_{10}\text{H}_{19}\text{NNaO}_3$ 224.1257, found 224.1256 ($\text{M}+\text{Na}$)⁺.

(S)-tert-butyl 2-formylpyrrolidine-1-carboxylate (125)



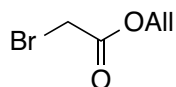
Aldehyde **125** was made following a literature protocol.¹⁴⁴ A solution of **124** (1.60 g, 7.96 mmol) in CH₂Cl₂ (20 mL) was cooled to 0 °C with vigorous stirring. TEMPO (12 mg, 0.08 mmol) and an aqueous solution (10 mL) of sodium bromide (82 mg, 0.80 mmol) were sequentially added. A solution of aqueous sodium hypochlorite (7.12 mL [10% w/v], 9.56 mmol) and sodium bicarbonate (0.356 g) was added and stirred for 10 minutes until the solution regained a yellow color. The reaction was transferred to a separatory funnel, separating the organic layer. The aqueous layers were washed with CH₂Cl₂ (3 x 30 mL) and pooled organic layers were dried over Na₂SO₄, filtered and concentrated *in vacuo*. The compound was purified by flash chromatography (silica gel, 30% EtOAc in hexanes), yielding **125** as a clear colorless oil (1.36 g, 86%). (*R_f* 0.65 on SiO₂, 1:1 EtOAc:hexanes); [α]_D²⁶ -95.6 (*c* 1.07 CH₂Cl₂); IR (CH₂Cl₂ cast) 2978, 2933, 2882, 1737, 1699, 1456, 1397, 1367, 1256, 1164, 1123 cm⁻¹; ¹H (CDCl₃, 500 MHz, as a 0.6:1 mixture of 2 rotamers): δ 9.45 (d, *J* = 3.0 Hz, 1H, Pro-CHO), 4.00 (ddd, *J* = 8.8, 6.3, 3.0 Hz, 1H, Pro-CH α), 3.58 – 3.40 (m, 2H, Pro-CH δ), 2.16 – 1.82 (m, 4H, Pro-CH β , Pro-CH γ), 1.42 (s, 9H, -C(CH₃)₃); ¹³C (CDCl₃, 125 MHz): δ 200.3, 153.8, 80.5, 65.0, 46.8, 28.3, 27.8, 24.0; HRMS (ES) Calculated for C₁₀H₁₇NNaO₃ 222.1101, found 222.1100 (M+Na)⁺.

(S)-tert-butyl 2-ethynylpyrrolidine-1-carboxylate (127)



Compound **127** was synthesized by adapting a literature protocol.¹⁴⁵ Aldehyde **125** (0.895 g, 4.49 mmol) and cesium carbonate (4.39 g, 13.5 mmol) were dissolved in THF (25 mL) and MeOH (25 mL). Dimethyl (1-diazo-2-oxopropyl)phosphonate (Bestmann-Ohira reagent, 1.35 mL, 8.98 mmol) was added over 5 minutes and the reaction was stirred for 17 h. The reaction was concentrated *in vacuo*, resuspended in EtOAc (50 mL) and washed with water (50 mL) and brine (50 mL). Aqueous layers were washed with EtOAc (2 x 50 mL), and pooled organic fractions were dried over Na₂SO₄, filtered, and concentrated *in vacuo*. **127** was purified by flash chromatography (silica gel, 15% EtOAc in hexanes), generating a clear colorless oil (0.680 g, 78%). (*R_f* 0.85 on SiO₂, 1:1 EtOAc:hexanes); [α]_D²⁶ -88.2 (*c* 1.02 CH₂Cl₂); IR (CH₂Cl₂ cast) 3293, 3247, 2978, 2933, 2881, 1699, 1394, 1255, 1168, 1122 cm⁻¹; ¹H (CDCl₃, 400 MHz): δ 4.58 – 4.38 (m, 1H, Pro-CH α), 3.47 (br s, 1H, Pro-CH δ), 3.33 (br s, 1H, Pro-CH δ), 2.22 (br s, 1H, Pro-CH β), 2.14 – 2.01 (m, 3H, Pro-CH β , -C \equiv CH, Pro-CH γ), 1.90 (br s, 1H, Pro-CH γ), 1.49 (s, 9H, -C(CH₃)₃); ¹³C (CDCl₃, 125 MHz): δ 154.0, 84.2, 79.7, 69.7, 47.9, 45.7, 33.4, 28.2, 23.2; HRMS (ES) Calculated for C₁₁H₁₇NNaO₂ 218.1151, found 218.1151 (M+Na)⁺.

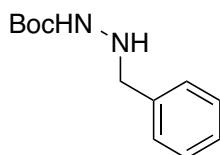
allyl 2-bromoacetate (**130**)



A solution of bromoacetic acid (5.00 g, 36.0 mmol), *p*-toluenesulfonic acid monohydrate (8.21 g, 43.2 mmol) and allyl alcohol (24.5 mL, 0.360 mol) were dissolved in toluene (100 mL) and refluxed at 130 °C under Dean Stark conditions for 6 h. After cooling, the reaction was concentrated *in vacuo*, resuspended in EtOAc (100 mL) and

washed with saturated sodium bicarbonate (2 x 100 mL) and water (100 mL). The organic layer was dried over Na₂SO₄, filtered, and concentrated *in vacuo*. Compound **130** was purified by flash chromatography (silica gel, 15% EtOAc in hexanes), generating a brown liquid (2.29 g, 36%). (*R_f* 0.80 on SiO₂, 1:3 EtOAc:hexanes); ¹H (CDCl₃, 500 MHz): δ 5.99 – 5.87 (m, 1H, -OCH₂CH=CH₂), 5.37 (dq, *J* = 17.2, 1.4 Hz, 1H, -OCH₂CH=CH₂), 5.29 (dt, *J* = 10.5, 1.2 Hz, 1H, -OCH₂CH=CH₂), 4.67 (dt, *J* = 5.8, 1.4 Hz, -OCH₂CH=CH₂), 3.86 (s, 2H, -CH₂Br); ¹³C (CDCl₃, 125 MHz): δ 166.9, 131.2, 119.2, 66.7, 25.7.

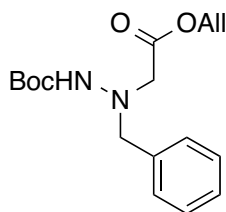
***tert*-butyl 2-benzylhydrazinecarboxylate (132)**



Compound **132** was prepared by following a literature protocol.¹⁴⁶ Boc-hydrazine (0.600 g, 4.54 mmol) and benzaldehyde (0.46 mL, 4.54 mmol) were dissolved in dry methanol (5 mL) and stirred for 3 h, precipitating the intermediate hydrazone as a flakey white powder. This material was collected by vacuum filtration assessed by NMR, then resuspended in a greater quantity of methanol (50 mL) with 10% Pd/C (50 mg) and stirred under an atmosphere of hydrogen gas for 1 h. The reaction mixture was filtered through a pad of Celite and concentrated *in vacuo*. The product was isolated as a white solid (0.807 g, 80%) and carried forward without further purification. (*R_f* 0.5 on SiO₂, 1:3 EtOAc:hexanes); ¹H (CDCl₃, 400 MHz): δ 7.40 – 7.28 (m, 5H, Ar-H), 6.12 (br s, 1H, Boc-NH), 4.24 (br s, 1H, -NHCH₂Ph), 4.02 (d, *J* = 5.0 Hz, 2H, -NHCH₂Ph), 1.50 (s, 9H, -C(CH₃)₃); ¹³C (CDCl₃, 125 MHz): δ 156.7, 137.7, 129.8, 129.0, 128.5, 127.5,

127.2, 80.6, 55.9, 28.4; HRMS (ES) Calculated for C₁₂H₁₆N₂NaO₂ 243.1104, found 243.1100 (M+Na)⁺.

***tert*-butyl 2-(2-(allyloxy)-2-oxoethyl)-2-benzylhydrazinecarboxylate (**133**)**

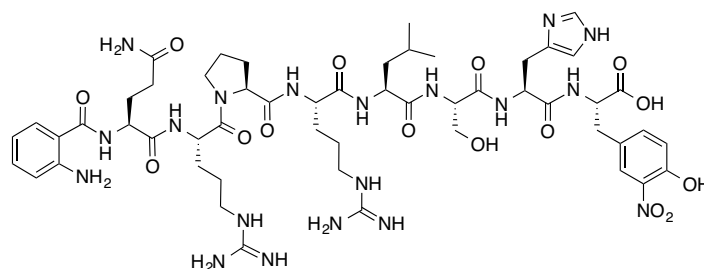


Compound **133** was prepared by modifying a literature procedure.¹⁴⁷ Hydrazine **132** (0.752 g, 3.38 mmol), **130** (1.51 g, 8.46 mmol) and potassium carbonate (0.468 g, 3.38 mmol) were suspended in toluene (20 mL) and heated under reflux (120 °C) for 18 h. After cooling, the reaction was concentrated *in vacuo*, resuspended in EtOAc (50 mL), washed with water (2 x 50 mL), dried over Na₂SO₄, filtered and concentrated *in vacuo*. The product was purified by flash chromatography (silica gel, 25% EtOAc in hexanes), isolating **133** as a orange oil (0.662 g, 61%). (*R_f* 0.8 on SiO₂, 1:1 EtOAc:hexanes); ¹H (CDCl₃, 500 MHz): δ 7.45 – 7.40 (m, 2H, Ar-H), 7.39 – 7.27 (m, 3H, Ar-H), 6.68 (br s, 1H, Boc-NH), 5.95 (ddt, *J* = 17.2, 10.4, 5.8 Hz, -OCH₂CH=CH₂), 5.36 (dq, *J* = 17.2, 1.5 Hz, 1H, -OCH₂CH=CH₂), 5.30 (dq, *J* = 10.4, 1.2 Hz, 1H, -OCH₂CH=CH₂), 4.67 (dt, *J* = 5.8, 1.4 Hz, 2H, -OCH₂CH=CH₂), 4.16 (s, 2H, -NCH₂Ph), 3.74 (s, 2H, -NCH₂COOAll), 1.43 (s, 9H, -C(CH₃)₃); ¹³C (CDCl₃, 125 MHz): δ 170.6, 136.8, 131.7, 129.4, 128.4, 127.6, 118.8, 80.1, 65.3, 60.4, 55.3, 28.3; HRMS (ES) Calculated for C₁₇H₂₄N₂NaO₄ 343.1628, found 343.1624 (M+Na)⁺.

4.3.5 Fluorescent probe SPPS

Fmoc-L-3-nitro-Tyr-OH (0.3 mmol) was loaded onto 2-chlorotrityl resin using the aforementioned procedure and used in the following syntheses:

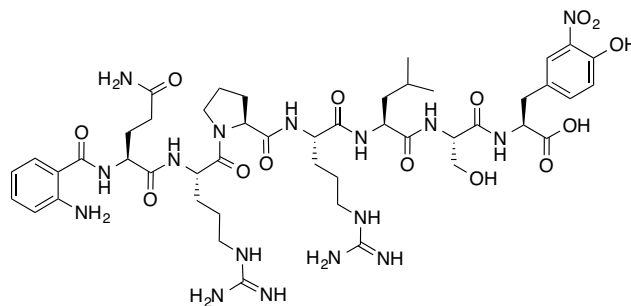
Abz-QRPRLSH-NO₂Y 9-mer (141)



Preloaded Fmoc-L-3-nitro-Tyr-OH on 2-chlorotrityl resin (0.1 mmol) was transferred to an SPPS vessel and subjected to automated SPPS, introducing amino acids in the following order: Fmoc-His(Trt)-OH, Fmoc-Ser(tBu)-OH, Fmoc-Leu-OH, Fmoc-Arg(Pmc)-OH, Fmoc-Pro-OH, Fmoc-Arg(Pmc)-OH, Fmoc-Gln(Trt)-OH, and Boc-2-Abz-OH. A portion (0.07 mmol) of resin-bound peptide **141** was cleaved as previously described and purified using a C₁₈ RP-HPLC analytical column (Method C), eluting at 8.2 minutes. The desired peptide was isolated as a yellow solid after lyophilization (3.9 mg, 5%). Monoisotopic MW calculated for C₅₃H₇₈N₁₉O₁₅ 1220.6, found (MALDI-TOF) 1220.7 (M+H)⁺.

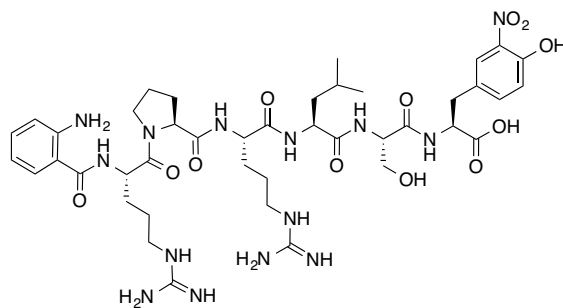
The following two analogues were synthesized by Ms. Andrea Werny (Heritage Youth Researcher Summer Student, July – August 2014)

Abz-QRPRLS-NO₂Y 8-mer (142)



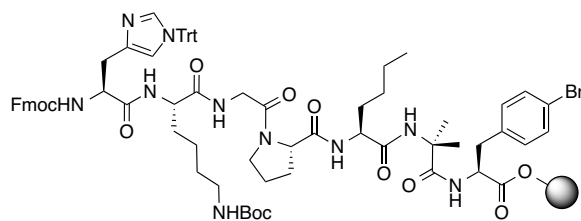
Preloaded Fmoc-L-3-nitro-Tyr-OH on 2-chlorotrityl resin (0.1 mmol) was transferred to an SPPS vessel and subjected to manual SPPS, introducing amino acids in the following order: Fmoc-Ser(tBu)-OH, Fmoc-Leu-OH, Fmoc-Arg(Pmc)-OH, Fmoc-Pro-OH, Fmoc-Arg(Pmc)-OH, Fmoc-Gln(Trt)-OH, and Boc-2-Abz-OH. A portion (0.05 mmol) of resin-bound peptide **142** was cleaved as previously described and purified using a C₁₈ RP-HPLC analytical column (Method C). The desired peptide was isolated as a yellow solid after lyophilization (1.2 mg, 2%). Monoisotopic MW calculated for C₄₇H₇₁N₁₆O₁₄ 1083.5, found (MALDI-TOF) 1083.5 (M+H)⁺.

Abz-RPRLS-NO₂Y 7-mer (143)



Preloaded Fmoc-L-3-nitro-Tyr-OH on 2-chlorotrityl resin (0.1 mmol) was transferred to an SPPS vessel and subjected to manual SPPS, introducing amino acids in the following order: Fmoc-Ser(tBu)-OH, Fmoc-Leu-OH, Fmoc-Arg(Pmc)-OH, Fmoc-Pro-OH, Fmoc-Arg(Pmc)-OH, and Boc-2-Abz-OH. A portion (0.05 mmol) of resin-bound peptide **143** was cleaved as previously described and purified using a C₁₈ RP-HPLC analytical column (Method C). The desired peptide was isolated as a yellow solid after lyophilization (0.8 mg, 2%). Monoisotopic MW calculated for C₄₂H₆₃N₁₄O₁₂ 955.5, found *high resolution* (MALDI-TOF) 955.3 (M+H)⁺.

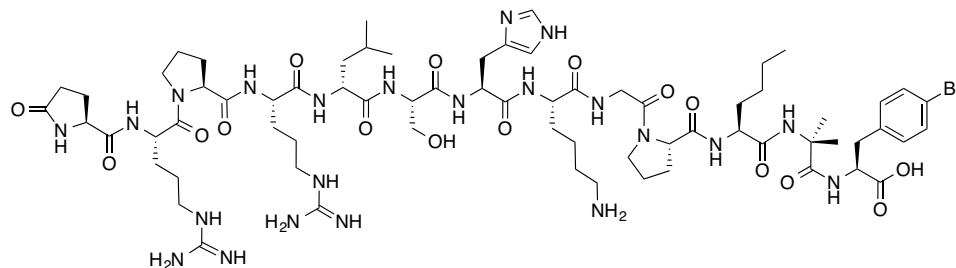
Fmoc 7-13 (153)



Fmoc-*p*-bromo-L-phenylalanine (1.0 mmol) was loaded onto 2-chlorotrityl chloride resin following the aforementioned procedure, with the following exceptions: the amino acid was mixed with the resin for 5 h, and the unreacted resin was capped with MeOH for 1 h. This resin was transferred to an SPPS vessel and subjected to manual SPPS, introducing amino acids in the following order: Fmoc-Aib-OH, Fmoc-Nle-OH, Fmoc-Pro-OH, Fmoc-Gly-OH, Fmoc-Lys(Boc)-OH, and Fmoc-His(Trt)-OH. A small sample of the resin was cleaved and analysed by MALDI-TOF: Calculated for C₅₃H₆₈BrN₁₀O₁₀ 1083.4, found 1083.0 (M+H)⁺.

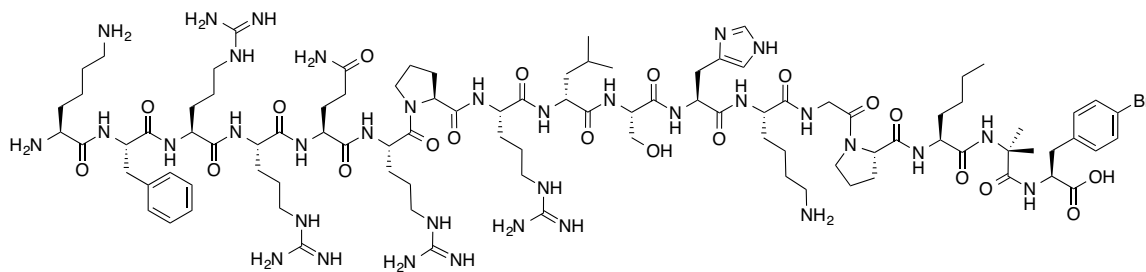
4.3.6 D-Leu analogues

D-Leu5-pyr-1-apelin-13 A2 (154)



Fmoc-*p*-Br-L-Phe-OH on 2-chlorotrityl-chloride resin (0.1 mmol) was subjected to manual SPPS, introducing amino acids in the following order: Fmoc-Aib-OH, Fmoc-Nle-OH, Fmoc-Pro-OH, Fmoc-Gly-OH, Fmoc-Arg(Pmc)-OH, Fmoc-Ala-OH, Fmoc-Ser(*t*Bu)-OH, Fmoc-D-Leu-OH, Fmoc-Arg(Pmc)-OH, Fmoc-Pro-OH, Fmoc-Arg(Pmc)-OH, and pyr-Glu-OH. A portion (0.05 mmol) of resin-bound peptide **154** was cleaved as previously described and purified using a C₁₈ RP-HPLC analytical column (Method A), eluting at 20.6 min. The desired peptide was isolated as a white solid after lyophilization (11.3 mg, 14%). Monoisotopic MW calculated for C₆₉H₁₁₁BrN₂₂O₁₆ 791.3860, found *high resolution* (FTICR-ESI-MS) 791.3846 (M+2H)²⁺.

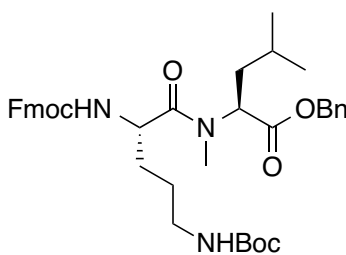
D-Leu9-apelin-17 A2 (155)



Advanced intermediate **153** (0.1 mmol) was subjected to manual SPPS, introducing amino acids in the following order: Fmoc-Ser(tBu)-OH, Fmoc-D-Leu-OH, Fmoc-Arg(Pmc)-OH, Fmoc-Pro-OH, Fmoc-Arg(Pmc)-OH, Fmoc-Gln(Trt)-OH, Fmoc-Arg(Pmc)-OH, Fmoc-Arg(Pmc)-OH, Fmoc-Phe-OH, and Fmoc-Lys(Boc)-OH. A portion (0.05 mmol) of resin-bound peptide **155** was cleaved as previously described and purified using a C₁₈ RP-HPLC analytical column (Method B), eluting at 11.2 min. The desired peptide was isolated as a white solid after lyophilization (9.9 mg, 9.1%). Monoisotopic MW calculated for C₉₆H₁₆₁BrN₃₄O₂₀ 547.2947, found *high resolution* (FTICR-ESI-MS) 547.2942 (M+4H)⁴⁺.

4.3.7 N-Methyl leucine analogues

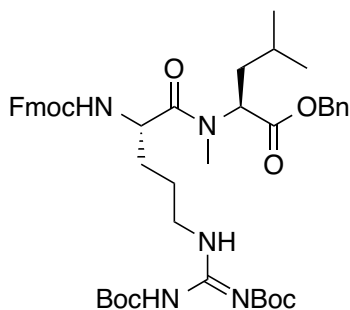
benzyl N-((S)-2-(((9H-fluoren-9-yl)methoxy)carbonyl)amino)-5-((tert-butoxycarbonyl)amino)pentanoyl)-N-methyl-L-leucinate (158)



Fmoc-Orn(Boc)-OH (1.23 g, 2.70 mmol), HATU (1.03 g, 2.70 mmol), HOAt (4.5 mL [0.6 M solution in DMF], 2.70 mmol), and DIPEA (1.28 mL, 7.36 mmol) were dissolved in dry DMF (10 mL) and stirred for 5 minutes to preactivate the amino acid. A solution of N-Me-Leu-OBn *p*-toluenesulfonate salt (1.00 g, 2.45 mmol) and DIPEA (0.43 mL, 2.45 mmol) in dry CH₂Cl₂ (10 mL) was added and the reaction was stirred for 17 h at room temperature. The reaction was washed with 10% aqueous NaHCO₃ (20

mL), 10% aqueous citric acid (20 mL) and brine (20 mL). The organic layer was dried over Na₂SO₄, filtered, and concentrated *in vacuo*. The dipeptide was purified using flash chromatography (silica gel, 25% EtOAc in hexanes), obtaining **158** as a crunchy white solid (1.25 g, 76%). (*R_f* 0.9 on SiO₂, 1:3 hexanes:EtOAc); [α]_D²⁶ -17.4 (*c* 1.0 CH₂Cl₂); IR (CH₂Cl₂ cast) 3315, 3066, 3037, 2957, 2870, 1714, 1645, 1513, 1451, 1251, 1172 cm⁻¹; ¹H (CDCl₃, 500 MHz): δ 7.76 (d, *J* = 7.5 Hz, 2H, Ar-H), 7.59 (d, *J* = 7.5 Hz, 2H, Ar-H), 7.43 – 7.27 (m, 9H, Ar-H), 5.65 (d, *J* = 8.5 Hz, 1H, Fmoc-NH), 5.35 (dd, *J* = 10.8, 5.0 Hz, 1H, Leu-CH α), 5.19 – 5.06 (m, 2H, Bn-OCH β), 4.68 (td, *J* = 7.7, 4.8 Hz, 1H, Orn-CH α), 4.51 (s, 1H, Boc-NH), 4.37 (qd, *J* = 10.6, 7.1 Hz, 2H, Fmoc-CH β), 4.21 (t, *J* = 7.1 Hz, 1H, Fmoc-CH β), 3.09 – 3.04 (m, 2H, Orn-CH β δ), 2.93 (s, 3H, N-CH β), 1.81 – 1.65 (m, 3H, 2 x Leu-CH β , Orn-CH β), 1.56 – 1.46 (m, 4H, Orn-CH β , 2 x Orn-CH β γ , Leu-CH(CH₃) β), 1.44 (s, 9H, -C(CH₃) β), 1.01 – 0.84 (m, 6H, -CH(CH₃) β); ¹³C (CDCl₃, 125 MHz): δ 172.6, 171.3, 156.0, 155.9, 143.9, 143.8, 141.3, 141.3, 135.4, 128.7, 128.5, 128.4, 127.7, 127.1, 127.1, 125.2, 120.0, 79.1, 67.1, 67.0, 54.9, 50.7, 47.2, 40.1, 36.8, 31.1, 30.0, 28.5, 25.4, 24.9, 23.2, 21.4; HRMS (ES) Calculated for C₃₉H₅₀N₃O₇ 672.3643, found 672.3642 (M+H)⁺.

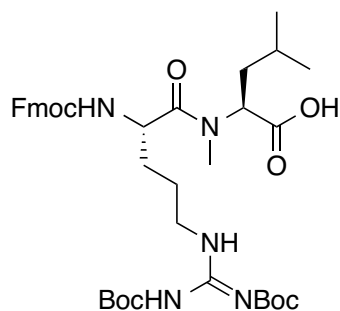
benzyl (11*S*,14*S*)-11-(((9*H*-fluoren-9-yl)methoxy)carbonyl)amino)-6-((*tert*-butoxycarbonyl)amino)-14-isobutyl-2,2,13-trimethyl-4,12-dioxo-3-oxa-5,7,13-triazapentadec-5-en-15-oate (160)



The guanidinylation reaction was adapted from a literature procedure.¹⁸⁰ Dipeptide **158** (0.701 g, 1.04 mmol) was dissolved in dry CH₂Cl₂ (10 mL) and had TFA (5 mL) added to it and stirred for 1 h. The reaction was concentrated *in vacuo*, using diethyl ether co-evaporations to remove residual TFA. The yellow oil was resuspended in dry CH₂Cl₂ (20 mL) with the addition of 1,3-di-Boc-2-(trifluoromethylsulfonyl)guanidine (0.449 g, 1.15 mmol) and triethylamine (0.32 mL, 2.30 mmol) and stirred for 80 minutes. The reaction was washed with 2 N aqueous sodium bisulfate (10 mL) and 10% NaHCO₃ (10 mL), dried over Na₂SO₄, filtered and concentrated *in vacuo*. The dipeptide was purified using flash chromatography (silica gel, 20% EtOAc in hexanes), obtaining **160** as a crunchy white solid (0.820 g, 97%). (*R_f* 0.5 on SiO₂, 3:1 hexanes:EtOAc); [α]_D²⁶ -12.5 (*c* 1.21 CHCl₃); IR (CHCl₃ cast) 3331, 2959, 2871, 1721, 1640, 1451, 1415, 1330, 1156, 1134 cm⁻¹; ¹H (CDCl₃, 500 MHz): δ 8.29 (t, *J* = 5.4 Hz, 1H, Arg-NHε), 7.76 (d, *J* = 7.6 Hz, 2H, Ar-H), 7.60 (d, *J* = 7.6 Hz, 2H, Ar-H), 7.43 – 7.27 (m, 9H, Ar-H), 5.68 (d, *J* = 8.5 Hz, 1H, Fmoc-N-H), 5.37 – 5.28 (m, 1H, Leu-CHα), 5.23 – 5.05 (m, 2H, -OCH₂Ph), 4.67 (td, *J* = 8.1, 4.3 Hz, 1H, Arg-CHα), 4.44 – 4.31 (m, 2H, Fmoc-CH₂), 4.21 (t, *J* = 6.9 Hz, 1H, Fmoc-CH), 3.36 (ddd, *J*

= 7.4, 5.0, 3.2 Hz, 2H, Arg-CH₂δ), 2.93 (s, 3H, N-CH₃), 1.82 – 1.75 (m, 1H, Leu-CH₂β), 1.75 – 1.66 (m, 2H, Leu-CH₂β, Arg-CH₂β), 1.63 – 1.55 (m, 3H, Arg-CH₂β, 2 x Arg-CH₂γ) 1.49 (m, 10H, Leu-CH(CH₃)₂, -C(CH₃)₃), 1.48 (s, 9H, -C(CH₃)₃), 0.93 (d, *J* = 6.6 Hz, 3H, Leu-CH(CH₃)₂), 0.90 (d, *J* = 6.5 Hz, 3H, Leu-CH(CH₃)₂); ¹³C (CDCl₃, 125 MHz): δ 172.5, 171.2, 163.6, 156.2, 156.0, 153.3, 143.9, 143.8, 141.3, 141.3, 135.4, 128.7, 128.6, 128.4, 127.7, 127.1, 127.1, 125.2, 125.2, 120.0, 83.1, 79.2, 67.1, 67.0, 54.9, 50.8, 47.2, 40.3, 36.8, 31.2, 29.9, 28.3, 28.1, 27.9, 27.9, 24.9, 23.2, 21.4; HRMS (ES) Calculated for C₄₅H₆₀N₅O₉ 814.4386, found 814.4378 (M+H)⁺.

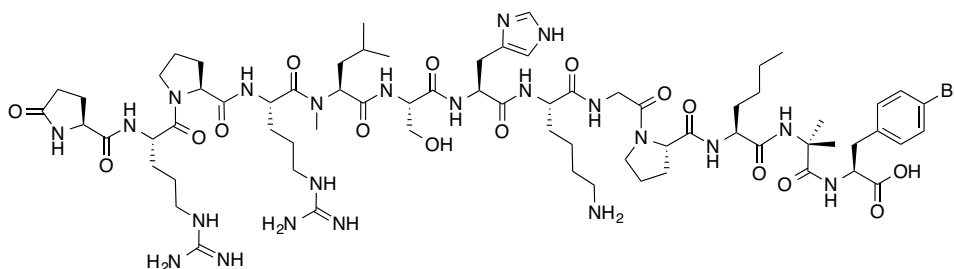
(11*S*,14*S*)-11-(((9*H*-fluoren-9-yl)methoxy)carbonyl)amino)-6-((*tert*-butoxycarbonyl)amino)-14-isobutyl-2,2,13-trimethyl-4,12-dioxo-3-oxa-5,7,13-triazapentadec-5-en-15-oic acid (161**)**



A solution of **160** (0.501 g, 0.62 mmol) was dissolved in methanol (50 mL) and had 10% Pd/C (20 mg) added. The suspension was stirred under hydrogen gas for 22 h, filtered through a pad of Celite, and concentrated *in vacuo*. The crude residue was purified using flash chromatography (silica gel, 5% MeOH in CH₂Cl₂, 0.1% AcOH), yielding **161** as a white solid (0.378 g, 85%). (*R_f* 0.2 on SiO₂, 1% AcOH in EtOAc); [α]_D²⁶ -2.8 (*c* 1.0 CH₂Cl₂); IR (CH₂Cl₂ cast) 3326, 3140, 3066, 2959, 2872, 1721, 1641, 1618, 1451, 1415, 1331, 1253, 1136 cm⁻¹; ¹H (CDCl₃, 500 MHz): δ 8.48 (s, 1H, Arg-

NH ϵ), 7.76 (d, $J = 7.5$ Hz, 2H, Ar-H), 7.61 (d, $J = 7.5$ Hz, 2H, Ar-H), 7.40 (t, $J = 7.5$ Hz, 2H, Ar-H), 7.32 (tdd, $J = 7.5, 3.4, 1.2$ Hz, 2H, Ar-H), 6.05 (d, $J = 7.6$ Hz, 1H, Fmoc-N-H), 5.37 (dd, $J = 10.7, 5.1$ Hz, 1H, Leu-CH α), 4.80 (dd, $J = 5.4, 5.3$ Hz, 1H, Arg-CH α), 4.38 (dd, $J = 10.6, 7.2$ Hz, 2H, Fmoc-CH $_2$), 4.21 (t, $J = 7.1$ Hz, 1H, Fmoc-CH), 3.55 – 3.45 (m, 1H, Arg-CH $_{2\delta}$), 3.14 – 3.05 (m, 1H, Arg-CH $_{2\delta}$), 2.98 (s, 3H, N-CH $_3$), 1.92 – 1.56 (m, 6H, 2 x Leu-CH $_{2\beta}$, 2 x Arg-CH $_{2\beta}$, 2 x Arg-CH $_{2\gamma}$), 1.52 (s, 9H, -C(CH $_3$) $_3$), 1.49 (m, 10H, Leu-CH(CH $_3$) $_2$, -C(CH $_3$) $_3$), 0.96 (d, $J = 6.6$ Hz, 3H, Leu-CH(CH $_3$) $_2$), 0.93 (d, $J = 6.5$ Hz, 3H, Leu-CH(CH $_3$) $_2$); ^{13}C (CDCl $_3$, 125 MHz): δ 172.3, 172.1, 162.8, 156.3, 155.7, 153.2, 144.9, 143.8, 141.4, 141.3, 127.7, 127.7, 127.1, 127.1, 125.2, 125.2, 120.0, 119.9, 83.1, 80.6, 66.9, 54.7, 51.1, 47.3, 40.6, 36.1, 30.7, 28.4, 28.1, 28.1, 24.8, 23.2, 21.4; HRMS (ES) Calculated for C $_{38}$ H $_{54}$ N $_5$ O $_9$ 724.3916, found 724.3924 (M+H) $^+$.

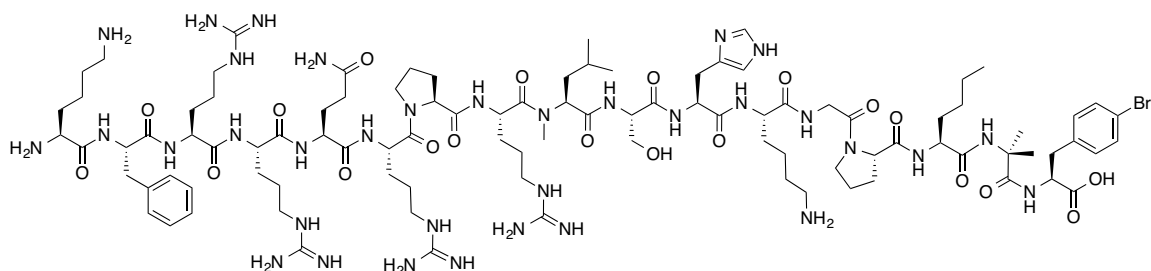
N-MeLeu5-pyr-1-apelin-13 A2 (162)



Advanced intermediate **153** (0.1 mmol) was subjected to manual SPPS, introducing amino acids in the following order: Fmoc-Ser(tBu)-OH, **161**, Fmoc-Pro-OH, Fmoc-Arg(Pmc)-OH, and pyr-Glu-OH. No endcapping was performed following addition of **161**. A portion (0.05 mmol) of resin-bound peptide **162** was cleaved as previously described and purified using a C $_{18}$ RP-HPLC analytical column (Method A), eluting at 11.2 min. The desired peptide was isolated as a white solid after lyophilization

(6.0 mg, 7%). Monoisotopic MW calculated for $C_{70}H_{114}BrN_{22}O_{16}$ 532.5983, found *high resolution* (FTICR-ESI-MS) 532.5972 ($M+3H$)³⁺.

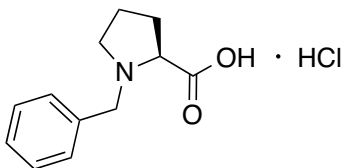
N-MeLeu-apelin-17 A2 (163)



Advanced intermediate **153** (0.1 mmol) was subjected to manual SPPS, introducing amino acids in the following order: Fmoc-Ser(tBu)-OH, **161**, Fmoc-Pro-OH, Fmoc-Arg(Pmc)-OH, Fmoc-Gln(Trt)-OH, Fmoc-Arg(Pmc)-OH, Fmoc-Arg(Pmc)-OH, Fmoc-Phe-OH, and Fmoc-Lys(Boc)-OH. No endcapping was performed following addition of **161**. A portion (0.05 mmol) of resin-bound peptide **163** was cleaved as previously described and purified using a C_{18} RP-HPLC analytical column (Method B), eluting at 11.3 min. The desired peptide was isolated as a white solid after lyophilization (23.8 mg, 22%). Monoisotopic MW calculated for $C_{97}H_{163}BrN_{34}O_{20}$ 550.7986, found *high resolution* (FTICR-ESI-MS) 550.7983 ($M+4H$)⁴⁺.

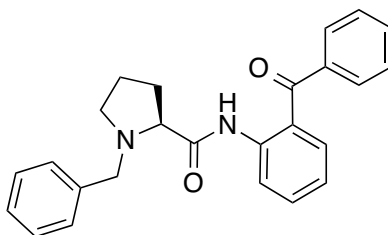
4.3.8 α -Methyl arginine analogues

benzyl-L-proline (168)



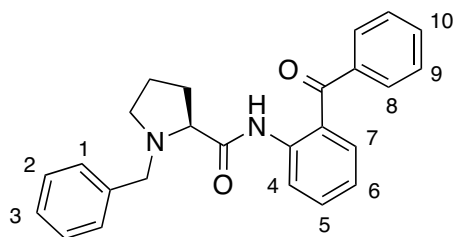
This compound was prepared according to literature procedure.¹⁶⁴ L-proline (30.0 g, 261 mmol) and KOH (55.6 g, 990 mmol) were suspended in 2-propanol (200 mL) and stirred at 40 °C until all material dissolved. Benzyl chloride (45.0 mL, 391 mmol) was added dropwise over 30 minutes to this solution, and the reaction was stirred for 20 h at 40 °C. The reaction was acidified to pH 4 with HCl, filtered through a pad of Celite to remove KCl, and concentrated *in vacuo*. The crude reaction mixture was resuspended in acetone (200 mL), cooled to -20 °C and vacuum filtered to collect the desired product, then resuspended in acetone, cooled and vacuum filtered again to further remove impurities. The product was dried in a vacuum oven overnight, obtaining **168** as a light brown solid (56.5 g, 90%) and used without further purification. IR (CH₂Cl₂ cast) 3033, 2959, 2814, 2545, 1725, 1632, 1457, 1391, 1354, 1214 cm⁻¹; ¹H (*d*₆-DMSO, 400 MHz): δ 7.50 – 7.21 (m, 5H, Ar-H), 4.30 (d, *J* = 12.8 Hz, 1H, Ph-CH₂-N), 4.08 (d, *J* = 12.9 Hz, 1H, Ph-CH₂-N), 3.87 (dd, *J* = 9.2, 6.6 Hz, 1H, Pro-CH_α), 3.32 – 3.22 (m, 1H, Pro-CH_δ), 3.02 – 2.91 (m, 1H, Pro-CH_δ), 2.33 – 2.20 (m, 1H, Pro-CH_β), 2.00 – 1.84 (m, 2H, Pro-CH_β, Pro-CH_γ), 1.85 – 1.72 (m, 1H, Pro-CH_γ); HRMS (ES) Calculated for C₁₂H₁₆NO₂ 206.1176, found 206.1175 (M+H)⁺.

(S)-N-(2-benzoylphenyl)-1-benzylpyrrolidine-2-carboxamide (169)



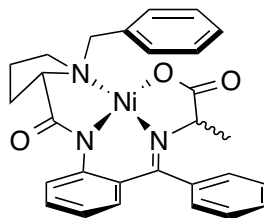
This compound was prepared according to literature procedure.¹⁶⁴ A solution of **168** (33.3 g, 162 mmol) in dry CH₂Cl₂ (200 mL) was cooled to -25 °C. Thionyl chloride

(14.7 mL, 203 mmol) was added over 15 minutes and the reaction was stirred for an additional 30 minutes before a solution of 2-aminobenzophenone (20.0 g, 101 mmol) in dry CH₂Cl₂ (50 mL) was added dropwise over 30 minutes at -25 °C. The reaction was slowly warmed to room temperature during the 15 h reaction time and was quenched by the addition of aqueous Na₂CO₃ (32.7 g, 308 mmol) at 0 °C. The organic layer was separated, dried over Na₂SO₄, filtered and concentrated *in vacuo*. Compound **169** was purified by flash chromatography (silica gel, 15% EtOAc in hexanes), yielding the desired product as a yellow solid (14.1 g, 36%). (*R_f* 0.55 on SiO₂, 2:1 hexane:EtOAc); [α]_D²⁶ -118.6 (*c* 1.05 CH₂Cl₂); IR (CH₂Cl₂ cast) 3262, 3062, 3028, 2970, 2874, 2808, 1690, 1645, 1578, 1509, 1447, 1265 cm⁻¹;

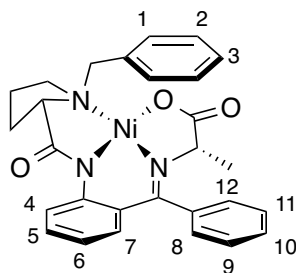


¹H (CDCl₃, 500 MHz): δ 8.57 (dd, *J* = 8.4, 1.1 Hz, 1H, Ar-H₄), 7.78 (dd, *J* = 8.2, 1.4 Hz, 2H, Ar-H₈), 7.64 – 7.56 (m, 1H Ar-H₁₀), 7.56 – 7.46 (m, 4H, Ar-H₅, Ar-H₇, Ar-H₉), 7.37 (dd, *J* = 6.6, 2.9 Hz, 2H, Ar-H₁), 7.17 – 7.05 (m, 4H, Ar-H₂, Ar-H₃, Ar-H₆), 3.92 (d, *J* = 12.9 Hz, 1H, Ph-CH₂-N), 3.59 (d, *J* = 13.0 Hz, 1H, Ph-CH₂-N), 3.32 (dd, *J* = 10.1, 4.8 Hz, 1H, Pro-CH_α), 3.22 (ddd, *J* = 9.1, 6.5, 2.5 Hz, 1H, Pro-CH_δ), 2.41 (td, *J* = 9.6, 6.7 Hz, 1H, Pro-CH_δ), 2.26 (dtd, *J* = 13.1, 9.9, 8.3 Hz, 1H, Pro-CH_β), 1.97 (ddq, *J* = 12.7, 8.2, 3.8 Hz, 1H, Pro-CH_β), 1.86 – 1.74 (m, 2H, Pro-CH_γ); ¹³C (CDCl₃, 125 MHz): δ 198.1, 174.7, 139.2, 138.6, 138.2, 133.4, 132.6, 132.5, 130.1, 129.1, 128.3, 128.2, 127.1, 125.4, 122.2, 121.6, 68.3, 59.9, 53.9, 31.0, 24.2; HRMS (ES) Calculated for C₂₅H₂₅N₂O₂ 385.1911, found 385.1913 (M+H)⁺.

alanine-Ni(II)-(S)-BPB (170)



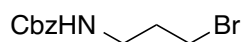
This compound was prepared according to literature procedure.¹⁶⁴ A solution of **169** (15.0 g, 39.0 mmol), L-alanine (17.4 g, 195 mmol), and Ni(NO₃)₂•6H₂O (22.7 g, 78.0 mmol) in MeOH (200 mL) was heated to 45 °C until all material dissolved. Freshly ground KOH (15.3 g, 273 mmol) was added to the reaction at 45 °C and stirred for 1 h, then stirred for 1 h at 60 °C. The deep red reaction was cooled to 0 °C and acetic acid (15.6 mL, 273 mmol) was added to quench residual KOH. The reaction was then concentrated *in vacuo*, resuspended in H₂O and the crude product was collected by vacuum filtration. Ni-complex **170** was further purified by flash chromatography (silica gel, 2.5% MeOH in EtOAc) yielding a red solid as a 12:1 mixture of diastereomers by ¹H-NMR analysis (15.5 g, 78%). Although both diastereomers were synthetically useful, characterization was performed on the isolated major diastereomer; (R_f 0.3 on SiO₂, 9:1 EtOAc:MeOH); [α]_D²⁶ 2891.6 (*c* 0.36 MeOH); IR (MeOH cast) 3453, 3059, 3028, 2977, 2923, 2869, 2819, 1679, 1640, 1591, 1546, 1471, 1441, 1356, 1333, 1260, 1166 cm⁻¹;



¹H (CDCl₃, 500 MHz): δ 8.12 – 8.04 (m, 3H, Ar-H₁, Ar-H₄), 7.55 – 7.40 (m, 3H, Ar-H₈, Ar-H₉, Ar-H₁₁), 7.36 (t, *J* = 7.7 Hz, 2H Ar-H₂), 7.28 – 7.23 (m, 1H Ar-H₁₀), 7.20 (ddt, *J* =

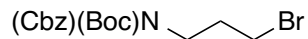
8.6, 7.3, 1.2 Hz, 1H, Ar-H₃), 7.14 (ddd, $J = 9.3, 6.7, 1.8$ Hz, 1H, Ar-H₅), 6.98 – 6.92 (m, 1H, Ar-H₁₂), 6.70 – 6.59 (m, 2H, Ar-H₆, Ar-H₇), 4.41 (d, $J = 12.6$ Hz, 1H, Ph-CH₂-N), 3.91 (q, $J = 7.0$ Hz, 1H, Ala-CH α), 3.72 (dddd, $J = 19.1, 12.4, 7.9, 4.5$ Hz, 1H, Pro-CH₂ γ), 3.59 – 3.51 (m, 2H, Ph-CH₂-N, Pro-CH₂ δ), 3.48 (dd, $J = 11.2, 5.5$ Hz, 1H, Pro-CH α), 2.79 – 2.70 (m, 1H, Pro-CH₂ β), 2.60 – 2.47 (m, 1H, Pro-CH₂ β), 2.21 (dt, $J = 13.2, 7.1$ Hz, 1H, Pro-CH₂ γ), 2.12 – 2.02 (m, 1H, Pro-CH₂ δ), 1.59 (d, $J = 6.9$ Hz, 3H, Ala-CH₃); ¹³C (CDCl₃, 125 MHz): δ 180.5, 180.4, 170.3, 142.1, 133.5, 133.3, 133.2, 132.1, 131.6, 129.7, 129.0, 128.9, 128.9, 127.5, 127.2, 126.5, 123.9, 120.8, 70.3, 66.6, 63.1, 57.3, 30.8, 24.1, 21.9; HRMS (ES) Calculated for C₂₈H₂₇N₃NaNiO₃ 534.1298, found 534.1295 (M+Na)⁺.

benzyl (3-bromopropyl)carbamate (**172**)



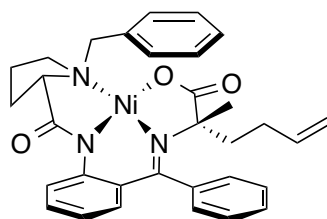
A solution of 3-bromopropylamine hydrobromide salt (5.00 g, 22.8 mmol) in water (50 mL) and CH₂Cl₂ (50 mL) was cooled to 0 °C and stirred vigorously. Sodium carbonate (5.08 g, 48.0 mmol) and benzyl chloroformate (3.21 mL, 22.8 mmol) were added to the reaction and stirred for 1.5 h at 0 °C. The reaction was separated, and the aqueous layer was washed with CH₂Cl₂ (2 x 50 mL). Pooled organic layers were dried over Na₂SO₄, filtered and concentrated *in vacuo*, producing **172** as a light yellow oil (3.86 g, 62%). (R_f 0.85 on SiO₂, 1:1 hexane:EtOAc); IR (neat film) 3413, 3332, 3065, 3033, 2946, 1698, 1534, 1454, 1260, 1134 cm⁻¹; ¹H (CDCl₃, 400 MHz): δ 7.39 – 7.28 (m, 5H, Ar-H), 5.10 (s, 2H, -OCH₂Ph), 4.96 (s, 1H, NH), 3.43 (t, $J = 6.5$ Hz, 2H, -CH₂Br), 3.35 (q, $J = 6.4$ Hz, 2H, NCH₂-), 2.07 (p, $J = 6.6$ Hz, 2H, NCH₂CH₂); HRMS (ES) Calculated for C₁₁H₁₄BrNNaO₂ 294.0100, found 294.0101 (M+Na)⁺.

benzyl *tert*-butyl (3-bromopropyl)iminodicarbonate (173)



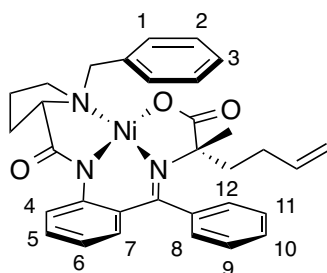
This compound was prepared according to a modified literature procedure.¹⁶⁵ A solution of **172** (3.06 g, 11.3 mmol) and DMAP (0.276 g, 2.26 mmol) was stirred in dry acetonitrile (30 mL). Boc anhydride (2.71 g, 12.4 mmol) was added in one portion and stirred for 1 h at room temperature. The reaction was concentrated *in vacuo*, resuspended in CH₂Cl₂ (50 mL) and washed with water (2 x 50 mL). The aqueous layer was washed with CH₂Cl₂ (2 x 50 mL) and pooled organic layers were dried over Na₂SO₄, filtered and concentrated *in vacuo*. Compound **173** was purified by flash chromatography (silica gel, 9:1 hexanes:EtOAc) as a colorless oil (3.43 g, 82%). (*R*_f 0.95 on SiO₂, 1:1 hexane:EtOAc); ¹H (CDCl₃, 400 MHz): δ 7.44 – 7.26 (m, 5H), 5.23 (s, 2H), 3.85 – 3.72 (m, 2H, -CH₂Br), 3.37 (t, *J* = 6.6 Hz, 2H, NCH₂-), 2.21 – 2.09 (m, 2H, NCH₂CH₂), 1.48 (s, 9H, -C(CH₃)₃); HRMS (ES) Calculated for C₁₆H₂₂BrNNaO₄ 394.0624, found 394.0630 (M+Na)⁺.

(2*S*)-2-buten-3'-yl-2-methyl-glycine-Ni(II)-(S)-BPB (174)



Nickel complex **174** was prepared according to literature procedures.¹⁶⁶ Nickel complex **170** (3.00 g, 5.86 mmol) and freshly ground sodium hydroxide (2.34 g, 58.6 mmol) were added to a flame-dried RBF and dissolved in dry DMF (50 mL) under an Ar atmosphere. This solution was stirred for 10 minutes, followed by the addition of a 1-

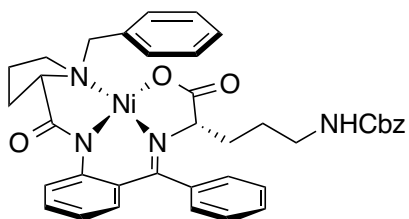
bromo-3-butene (1.78 mL, 17.6 mmol). The reaction was stirred for 90 minutes, then a second addition of 1-bromo-3-butene (1.78 mL, 17.6 mmol) was added for an additional 90 minutes. 5% aqueous acetic acid (50 mL) was added to quench the reaction, followed by extraction with benzene (3 x 50 mL). The pooled organic layers were washed with brine (2 x 50 mL), dried over Na₂SO₄, filtered and concentrated *in vacuo*. The desired diastereomer was purified by flash chromatography (silica gel; 2.5% MeOH in EtOAc), yielding **174** as a red solid (1.49 g, 45%) and recovering unreacted starting material **170** (1.01 g, 34%). (*R_f* 0.6 on SiO₂, 9:1 EtOAc:MeOH); [α]_D²⁶ 2173.0 (*c* 1.0 CH₂Cl₂); IR (CH₂Cl₂ cast) 3060, 2979, 2935, 2878, 1672, 1639, 1594, 1573, 1535, 1454, 1359, 1252, 1167 cm⁻¹;



¹H (CDCl₃, 500 MHz): δ 8.09 – 8.05 (m, 2H, Ar-H₁), 8.03 – 7.99 (m, 1H, Ar-H₄), 7.49 – 7.44 (m, 2H, Ar-H₈, Ar-H₉), 7.42 – 7.33 (m, 3H, Ar-H₂, Ar-H₁₁), 7.33 – 7.24 (m, 2H, Ar-H₃, Ar-H₁₀), 7.12 (ddd, *J* = 8.6, 6.4, 2.1 Hz, 1H, Ar-H₅), 6.98 (ddt, *J* = 7.7, 1.9, 0.9 Hz, 1H, Ar-H₁₂), 6.67 – 6.57 (m, 2H, Ar-H₆, Ar-H₇), 5.81 (dddd, *J* = 17.0, 10.2, 6.8, 6.1 Hz, 1H, -CH=CH₂), 5.10 (ddd, *J* = 17.1, 1.6, 1.6 Hz, 1H, -CH=CH₂), 5.02 (ddd, *J* = 10.2, 1.3, 1.3 Hz, 1H, -CH=CH₂), 4.48 (d, *J* = 12.7 Hz, 1H, Ph-CH₂-N), 3.72 – 3.62 (m, 2H, Ph-CH₂-N, Pro-CH₂ δ), 3.43 (dd, *J* = 10.7, 6.0 Hz, 1H, Pro-CH α), 3.31 – 3.16 (m, 1H, Pro-CH₂ γ), 3.04 – 2.95 (m, 1H, -CH₂CH=CH₂), 2.74 – 2.62 (m, 2H, -CH₂CH=CH₂, Pro-CH₂ β), 2.47 (ddt, *J* = 13.5, 10.7, 8.8 Hz, 1H, Pro-CH₂ β), 2.11 – 2.00

(m, 2H, Pro-CH₂γ, Pro-CH₂δ), 1.82 (ddd, *J* = 14.0, 12.4, 5.0 Hz, 1H, -CH₂CH₂CH=CH₂), 1.72 (ddd, *J* = 14.0, 12.5, 4.2 Hz, 1H, -CH₂CH₂CH=CH₂), 1.25 (s, 3H, CH₃); ¹³C (CDCl₃, 125 MHz): δ 182.2, 180.6, 172.6, 141.6, 137.0, 136.5, 133.4, 131.7, 131.6, 130.2, 129.5, 129.0, 128.9, 128.6, 128.0, 127.3, 127.0, 124.0, 120.8, 115.5, 77.7, 70.0, 63.4, 57.1, 39.3, 30.7, 29.9, 29.5, 23.3; HRMS (ES) Calculated for C₃₂H₃₃N₃NaNiO₃ 588.1768, found 588.1764 (M+Na)⁺.

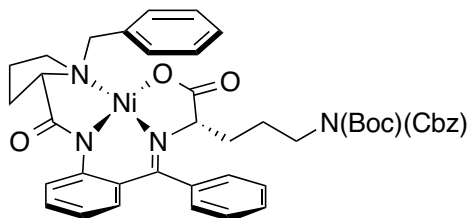
(2*S*)-2-propyl-3'-benzylcarbamate-glycine-Ni(II)-(S)-BPB (178)



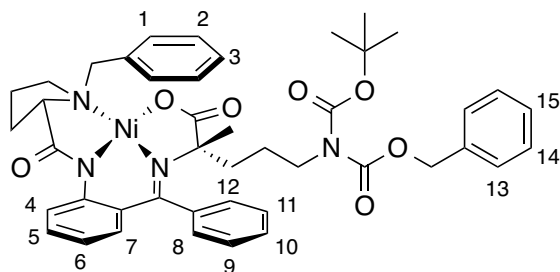
This compound was prepared by adapting a literature procedure.¹⁶⁴ A solution of **169** (0.802 g, 2.09 mmol), H-L-Orn(Cbz)-OH (2.78 g, 10.4 mmol), and Ni(NO₃)₂•6H₂O (1.21 g, 4.17 mmol) in MeOH (40 mL) was heated to 45 °C until all material dissolved. Freshly ground KOH (0.819 g, 14.6 mmol) was added to the reaction at 45 °C and then heated to 60 °C for 2 h. The deep red reaction was cooled to 0 °C and acetic acid (1.00 mL) was added to quench residual KOH. The reaction was then concentrated *in vacuo*, resuspended in cold H₂O and the crude product was collected by vacuum filtration. Due to the insolubility of unreactd H-L-Orn(Cbz)-OH, the material was dissolved in CH₂Cl₂ and filtered through Celite until all the filtrate turned clear. Ni-complex **178** was further purified by flash chromatography (silica gel, 5% MeOH in EtOAc) yielding a red solid (1.43 g, 99%). (*R_f* 0.45 on SiO₂, 9:1 EtOAc:MeOH); IR (MeOH cast) 3321, 3059, 2954, 2868, 1717, 1672, 1637, 1590, 1545, 1441, 1358, 1336, 1259 cm⁻¹; ¹H (CDCl₃, 400 MHz): δ 8.17 – 8.10 (m, 1H, Ar-H), 8.09 – 8.01 (m, 2H, Ar-

H), 7.51 – 7.45 (m, 2H, Ar-H), 7.44 – 7.28 (m, 7H, Ar-H), 7.28 – 7.10 (m, 4H, Ar-H), 6.89 (d, $J = 7.8$ Hz, 1H, Ar-H), 6.71 – 6.58 (m, 2H, Ar-H), 5.08 (s, 2H, -OCH₂Ph), 4.74 (s, 1H, Orn-NHCbz), 4.43 (d, $J = 12.7$ Hz, 1H, Ph-CH₂-N), 3.86 (dd, $J = 9.5, 3.3$ Hz, 1H, Orn-CH_α), 3.61 – 3.42 (m, 4H, Ph-CH₂-N, Pro-CH₂γ, Pro-CH₂δ, Pro-CH_α), 3.05 – 2.98 (m, 2H, Orn-CH₂δ), 2.80 – 2.70 (m, 1H, Pro-CH₂β), 2.56 – 2.42 (m, 1H, Pro-CH₂β), 2.20 – 2.00 (m, 4H, 2 x Orn-CH₂β, Pro-CH₂γ, Pro-CH₂δ), 1.68 – 1.57 (m, 2H, Orn-CH₂γ); HRMS (ES) Calculated for C₃₈H₃₉N₄NiO₅ 689.2268, found 689.2262 (M+H)⁺.

(2*S*)-2-propyl-3'-benzyl-3'-tert-butyliminodicarbonate-glycine-Ni(II)-(S)-BPB (179)

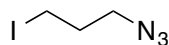


This compound was prepared by adapting a literature procedure.¹⁶⁵ A solution of **178** (0.735 g, 1.07 mmol) and DMAP (0.026 g, 0.21 mmol) was stirred in dry acetonitrile (10 mL) and CH₂Cl₂ (5 mL) to aid in Ni(II)-complex solubility. Boc anhydride (0.349 g, 1.60 mmol) was added in one portion and stirred for 18 h at room temperature. The next day, additional Boc anhydride (0.349 g, 1.60 mmol) was added and stirred for 5 h. The reaction was concentrated *in vacuo*, and then purified by flash chromatography (silica gel, 2.5% MeOH in EtOAc) yielding a red solid (0.550 g, 65%). (R_f 0.55 on SiO₂, 9:1 EtOAc:MeOH); $[\alpha]_D^{26}$ 1643.6 (c 1.0 CH₂Cl₂); IR (CH₂Cl₂ cast) 3059, 2977, 2932, 2869, 1786, 1745, 1720, 1676, 1640, 1589, 1545, 1471, 1456, 1368, 1354, 1335, 1292, 1259, 1165, 1150, 1115 cm⁻¹;



^1H (CDCl_3 , 500 MHz): δ 8.18 (dd, $J = 8.7, 1.1$ Hz, 1H, Ar- $\underline{\text{H}}_4$), 8.04 (dd, $J = 8.1, 1.3$ Hz, 2H, Ar- $\underline{\text{H}}_1$), 7.50 – 7.40 (m, 2H, Ar- $\underline{\text{H}}_8$, Ar- $\underline{\text{H}}_9$), 7.38 – 7.32 (m, 5H, Ar- $\underline{\text{H}}_2$, Ar- $\underline{\text{H}}_{11}$, Ar- $\underline{\text{H}}_{13}$), 7.29 – 7.17 (m, 5H, Ar- $\underline{\text{H}}_3$, Ar- $\underline{\text{H}}_{10}$, Ar- $\underline{\text{H}}_{14}$, Ar- $\underline{\text{H}}_{15}$), 7.15 (ddd, $J = 8.7, 6.9, 1.7$ Hz, 1H, Ar- $\underline{\text{H}}_5$), 6.75 – 6.57 (m, 3H, Ar- $\underline{\text{H}}_{12}$, Ar- $\underline{\text{H}}_6$, Ar- $\underline{\text{H}}_7$), 5.18 (s, 2H, -OCH $\underline{2}$ Ph), 4.43 (d, $J = 12.7$ Hz, 1H, Ph-CH $\underline{2}$ -N), 3.82 (dd, $J = 8.5, 3.5$ Hz, 1H, Orn-CH $\underline{\alpha}$), 3.63 – 3.41 (m, 6H, Ph-CH $\underline{2}$ -N, Pro-CH $\underline{2}\gamma$, Pro-CH $\underline{2}\delta$, Pro-CH $\underline{\alpha}$, Orn-CH $\underline{2}\delta$), 2.76 – 2.66 (m, 1H, Pro-CH $\underline{2}\beta$), 2.55 – 2.36 (m, 2H, Pro-CH $\underline{2}\beta$, Pro-CH $\underline{2}\gamma$), 2.14 – 1.91 (m, 3H, Orn-CH $\underline{2}\beta$, Pro-CH $\underline{2}\delta$, Orn-CH $\underline{2}\gamma$), 1.80 (tp, $J = 12.5, 6.5, 5.8$ Hz, 1H, Orn-CH $\underline{2}\beta$), 1.63 – 1.49 (m, 1H, Orn-CH $\underline{2}\gamma$), 1.42 (s, 9H, -C(CH $\underline{3}$) $_3$); ^{13}C (CDCl_3 , 125 MHz): δ 180.4, 179.1, 170.6, 153.8, 151.8, 142.5, 135.5, 133.7, 133.3, 133.2, 132.2, 131.6, 129.7, 129.0, 129.0, 128.9, 128.9, 128.6, 128.3, 127.5, 127.0, 126.4, 123.8, 120.7, 82.9, 70.3, 70.0, 68.4, 63.1, 57.0, 45.9, 32.6, 30.9, 28.0, 25.1, 23.6; HRMS (ES) Calculated for $\text{C}_{43}\text{H}_{47}\text{N}_4\text{NiO}_7$ 789.2793, found 789.2785 ($\text{M}+\text{Na}$) $^+$.

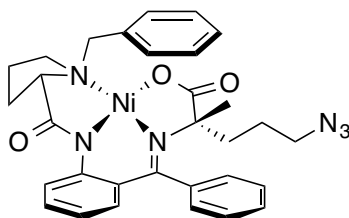
1-azido-3-iodopropane (**183**)



Compound **183** was prepared according to literature procedures.¹⁶⁷ A solution of 1-chloro-3-iodopropane (2.63 mL, 24.5 mmol) and sodium azide (1.91 g, 29.4 mmol) in dry DMF (60 mL) was stirred at room temperature for 24 h. The reaction was diluted

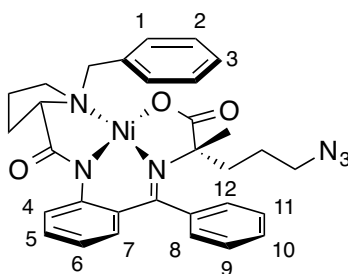
by the addition of water (100 mL) and diethyl ether washes (2 x 100 mL) were used to extract organic components. The diethyl ether fractions were dried over Na₂SO₄, filtered and concentrated *in vacuo* until a small volume (~10 mL) of ether remained. The reaction was diluted in acetone (60 mL) and following the addition of sodium iodide (5.50 g, 36.7 mmol), the reaction was heated at 60 °C for 24 h. The solution was concentrated *in vacuo* until a small volume (~10 mL) remained, then diluted with diethyl ether (100 mL) and washed with H₂O (2 x 100 mL). The organic layer was dried over Na₂SO₄, vacuum filtered through a small plug of alumina, and concentrated *in vacuo*, obtaining the desired product as a light yellow oil (3.91 g, 76%). IR (CH₂Cl₂ cast) 2927, 2869, 2098, 1449, 1428, 1347, 1290, 1224, 1173 cm⁻¹; ¹H (CDCl₃, 500 MHz): δ 3.44 (t, *J* = 6.4 Hz, 2H, -CH₂N₃), 3.25 (t, *J* = 6.6 Hz, 2H, -CH₂I), 2.04 (app pentet, *J* = 6.5 Hz, 2H, -CH₂-); ¹³C (CDCl₃, 125 MHz): δ 51.5, 32.4, 2.3.

(2*S*)-2-(3'-azidopropyl)-2-methyl-glycine-Ni(II)-(S)-BPB (184)



Complex **184** was prepared according to literature procedure.¹⁶⁷ Nickel complex **170** (6.49 g, 12.7 mmol) and potassium *tert*-butoxide (2.13 g, 19.0 mmol) were added to a flame-dried RBF and dissolved in dry DMF (50 mL) at 0 °C under an Ar atmosphere. This solution was stirred for 3 minutes, followed by the addition of a solution of **183** (5.01 g, 19.0 mmol) in dry DMF (10 mL). The reaction was stirred at 0 °C for 45 minutes, then warmed to room temperature for an additional 75 minutes. 5% aqueous acetic acid (200 mL) was added to quench the reaction, followed by extraction

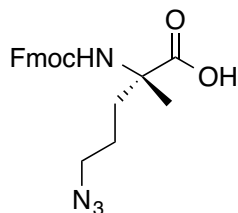
with CH₂Cl₂ (3 x 75 mL). The pooled organic layers were washed with brine (2 x 75 mL), dried over Na₂SO₄, filtered and concentrated *in vacuo*. The desired diastereomer was purified by flash chromatography (silica gel; 2.5% MeOH in EtOAc), yielding **184** as a red solid (5.18 g, 69%). Crystals of **184** were obtained after dissolution in minimal CH₂Cl₂, dilution with hexanes and slow evaporation. (*R_f* 0.6 on SiO₂, 9:1 EtOAc:MeOH); [α]_D²⁶ 1853.4 (*c* 1.0 CH₂Cl₂); IR (CH₂Cl₂ cast) 3060, 2937, 2869, 2097, 1673, 1639, 1574, 1439, 1359, 1253, 1165 cm⁻¹;



¹H (CDCl₃, 500 MHz): δ 8.12 – 8.07 (m, 2H, Ar-H₁), 8.05 (dd, *J* = 8.7, 0.9 Hz, 1H, Ar-H₄), 7.55 – 7.48 (m, 2H, Ar-H₈, Ar-H₉), 7.47 – 7.41 (m, 3H, Ar-H₂, Ar-H₁₁), 7.35 – 7.28 (m, 2H, Ar-H₃, Ar-H₁₀), 7.16 (ddd, *J* = 8.5, 5.8, 2.7 Hz, 1H, Ar-H₅), 7.08 (dt, *J* = 7.6, 1.3 Hz, 1H Ar-H₁₂), 6.69 – 6.62 (m, 2H, Ar-H₆, Ar-H₇), 4.50 (d, *J* = 12.7 Hz, 1H, Ph-CH₂-N), 3.70 (dd, *J* = 18.7, 11.8 Hz, 2H, Ph-CH₂-N, Pro-CH₂δ), 3.51 – 3.42 (m, 2H, Pro-CHα, -CH₂N₃), 3.32 – 3.20 (m, 2H, -CH₂N₃, Pro-CH₂γ), 2.71 (dddd, *J* = 12.8, 7.1, 5.8, 2.6 Hz, 1H, Pro-CH₂β), 2.58 – 2.43 (m, 2H, Pro-CH₂β, -CH₂CH₂N₃), 2.26 – 2.04 (m, 3H, -CH₂CH₂N₃, Pro-CH₂γ, Pro-CH₂δ), 1.86 (ddd, *J* = 13.8, 12.4, 4.2 Hz, 1H, -CH₂CH₂CH₂N₃), 1.76 (ddd, *J* = 13.7, 12.4, 4.6 Hz, 1H, -CH₂CH₂CH₂N₃), 1.28 (s, 3H, -CH₃); ¹³C (CDCl₃, 125 MHz): δ 182.0, 180.6, 172.8, 141.6, 136.4, 133.4, 133.4, 131.8, 131.7, 130.2, 129.6, 129.1, 129.0, 128.5, 128.1, 127.3, 127.1, 124.0, 120.8, 77.4, 70.0,

63.5, 57.2, 51.3, 37.5, 30.7, 29.4, 25.5, 23.4; HRMS (ES) Calculated for $C_{31}H_{32}N_6NaNiO_3$ 617.1782, found 617.1785 ($M+Na$)⁺.

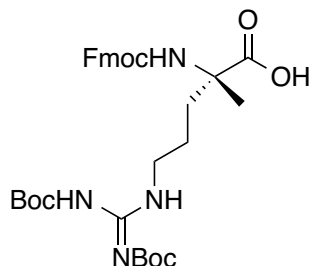
**(S)-2-(((9H-fluoren-9-yl)methoxy)carbonyl)amino)-5-azido-2-methylpentanoic acid
(185)**



Amino acid **185** was prepared according to literature procedure.¹⁶⁷ A solution of 3N HCl:MeOH (1:1, 40 mL) was heated to 70 °C and had **184** (2.60 g, 4.37 mmol) dissolved in MeOH (10 mL) added dropwise over 5 minutes. The reaction mixture was stirred for 50 minutes at 70 °C, turning from dark red to green as the reaction proceeded. The reaction was cooled to room temperature, concentrated *in vacuo* and resuspended in 10% aqueous sodium carbonate (20 mL). EDTA disodium salt (3.25 g, 8.73 mmol) was added and stirred for 0.5 h at room temperature. The reaction was cooled to 0 °C and had a solution of Fmoc-OSu (1.62 g, 4.80 mmol) dissolved in acetone (20 mL) added to it. This reaction was slowly warmed to room temperature and stirred for 16 h. The following day, the reaction was diluted with EtOAc (50 mL) and washed with 1 N HCl (3 x 20 mL). The organic layer was dried over MgSO₄, filtered, and concentrated *in vacuo*. The product was purified by flash chromatography (silica gel, 1-5% MeOH in CH₂Cl₂ gradient), yielding **185** as a white solid (1.64 g, 95%). (*R_f* 0.4 on SiO₂, 9:1 EtOAc:MeOH); ¹H (CDCl₃, 500 MHz): δ 7.77 (d, *J* = 7.5 Hz, 2H, Ar-H), 7.58 (d, *J* = 7.5 Hz, 2H, Ar-H), 7.40 (td, *J* = 7.4, 3.1 Hz, 2H, Ar-H), 7.32 (tdd, *J* = 7.4, 2.6, 1.1 Hz, 2H, Ar-H), 5.57 (br s, 1H, Fmoc-NH), 4.48 – 4.36 (m, 2H, Fmoc-CH₂), 4.21 (t, *J* = 6.2 Hz,

1H, Fmoc-CH), 3.32 – 3.19 (m, 2H, -CH₂N₃), 2.28 – 2.17 (m, 1H, Orn-CH₂γ), 2.02 – 1.90 (m, 1H, Orn-CH₂γ), 1.60 (br s, 3H, -CH₃), 1.50 – 1.39 (m, 2H, Orn-CH₂β); ¹³C (CDCl₃, 125 MHz): δ 170.1, 153.9, 143.8, 141.4, 127.7, 127.1, 125.0, 120.0, 66.6, 51.1, 47.2, 34.0, 33.4, 23.7, 23.5; HRMS (ES) Calculated for C₂₁H₂₁N₄O₄ 393.1568, found 393.1566 (M-H)⁻.

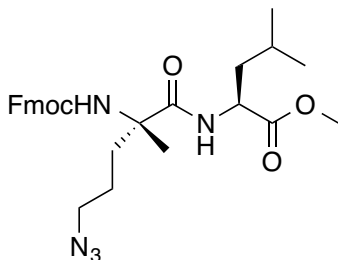
(S)-2-(((9H-fluoren-9-yl)methoxy)carbonyl)amino)-5-(2,3-bis(*tert*-butoxycarbonyl)guanidino)-2-methylpentanoic acid (175)



Amino acid **175** was prepared according to literature procedure.¹⁶⁷ Compound **185** (0.164 g, 0.42 mmol) was dissolved in 2-propanol (20 mL) and had 10% Pd/C (10 mg) added. The suspension was stirred under hydrogen gas for 12 h, filtered through a pad of Celite, and concentrated *in vacuo*. The crude residue was suspended in THF (20 mL) and *N,N'*-di-Boc-1*H*-pyrazole-1-carboximidine (0.142 g, 0.46 mmol) was added. This reaction was stirred at room temperature for 16 h, then diluted with EtOAc (50 mL) and washed with 1 N HCl (3 x 20 mL). The organic layer was dried over MgSO₄, filtered, concentrated *in vacuo* and purified using flash chromatography (silica gel, 10-50% acetone in CH₂Cl₂ gradient), yielding **175** as a white solid (0.039 g, 15%). (*R_f* 0.2 on SiO₂, 1:1 CH₂Cl₂:acetone); [α]_D²⁶ 12.6 (*c* 1.0 CH₂Cl₂); IR (CH₂Cl₂ cast) 3413, 3329, 2979, 2934, 1721, 1641, 1617, 1451, 1394, 1252, 1137 cm⁻¹; ¹H (CDCl₃, 400 MHz): δ 8.39 (br s, 1H, Arg-NHε), 7.76 (d, *J* = 7.5 Hz, 2H, Ar-H), 7.60 (d, *J* = 7.4 Hz, 2H, Ar-H),

7.39 (tt, $J = 7.5, 1.4$ Hz, 2H, Ar-H), 7.31 (tdd, $J = 7.4, 2.1, 1.2$ Hz, 2H, Ar-H), 5.89 (br s, 1H, Fmoc-NH) 4.49 – 4.30 (m, 1H, Fmoc-CH₂), 4.29 – 4.17 (m, 1H, Fmoc-CH), 3.44 – 3.24 (m, 2H, Arg-CH₂δ), 2.42 – 2.27 (m, 1H, Arg-CH₂β), 1.93 – 1.80 (m, 1H, Arg-CH₂β), 1.69 – 1.55 (m, 3H, Arg-CH₃), 1.55 – 1.40 (m, 20H, 2 x -C(CH₃)₃, Arg-CH₂γ); HRMS (ES) Calculated for C₃₂H₄₃N₄O₈ 611.3075, found 611.3065 (M+H)⁺.

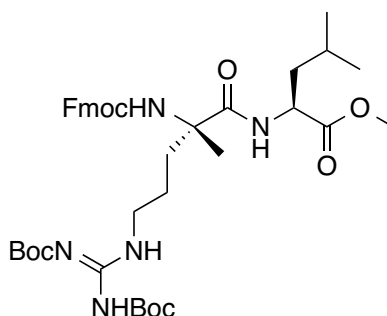
methyl ((*S*)-2-(((9*H*-fluoren-9-yl)methoxy)carbonyl)amino)-5-azido-2-methylpentanoyl)-*L*-leucinate (190**)**



Compound **185** (1.61 g, 4.09 mmol), HATU (1.55 g, 4.09 mmol), HOAt (0.68 mL [0.6 M solution in DMF], 0.41 mmol), and DIPEA (2.85 mL, 16.4 mmol) were dissolved in dry DMF (25 mL) and stirred for 5 minutes to preactivate the amino acid. A solution of H-Leu-OMe•HCl (0.780 g, 4.29 mmol) in dry CH₂Cl₂ (25 mL) was added and the reaction was stirred for 16 h at room temperature. The reaction was concentrated *in vacuo*, resuspended in EtOAc (50 mL), and washed with 10% citric acid, water, and brine (50 mL). The organic layer was dried over Na₂SO₄, filtered, and concentrated *in vacuo*. Crude **190** was purified using flash chromatography (silica gel, 33% EtOAc in hexanes), obtaining the desired dipeptide as a yellow oil (1.22 g, 57%). (R_f 0.5 on SiO₂, 2:1 hexane:EtOAc); $[\alpha]_D^{26}$ -1.2 (c 1.0 CHCl₃); IR (CHCl₃ cast) 3342, 2956, 2872, 2097, 1731, 1664, 1495, 1450, 1249, 1089 cm⁻¹; ¹H (CDCl₃, 500 MHz): δ 7.76 (dd, $J = 7.4, 1.0$ Hz, 2H, Ar-H), 7.59 (ddd, $J = 7.5, 4.0, 1.0$ Hz, 2H, Ar-H), 7.44 – 7.35 (m, 2H, Ar-H),

7.32 (dddd, $J = 7.5, 7.5, 2.2, 1.2$ Hz, 2H, Ar-H), 6.38 (br s, 1H, Leu-NH), 5.83 (br s, 1H, Fmoc-NH), 4.60 (ddd, $J = 8.6, 8.0, 4.7$ Hz, 1H, Leu-CH α), 4.49 – 4.35 (m, 2H, Fmoc-CH $_2$), 4.20 (t, $J = 6.6$ Hz, 1H, Fmoc-CH), 3.72 (s, 3H, -OCH $_3$), 3.34 – 3.18 (m, 2H, Arg-CH $_2\delta$), 2.47 – 2.23 (m, 1H, Arg-CH $_2\beta$), 1.84 – 1.76 (m, 1H, Arg-CH $_2\beta$), 1.70 – 1.40 (m, 8H, Arg-CH $_3$, 2 x Arg-CH $_2\gamma$, 2 x Leu-CH $_2\beta$, -CH(CH $_3$) $_2$), 0.93 (m, 6H, -CH(CH $_3$) $_2$); ^{13}C (CDCl $_3$, 125 MHz): δ 173.4, 173.1, 154.6, 143.9, 143.9, 141.4, 127.7, 127.1, 127.1, 125.0, 120.0, 66.5, 59.4, 52.4, 51.2, 51.1, 47.3, 41.3, 33.9, 25.0, 24.0, 23.5, 22.8, 21.9; HRMS (ES) Calculated for C $_{28}$ H $_{35}$ N $_5$ NaO $_5$ 544.2530, found 544.2527 (M+Na) $^+$.

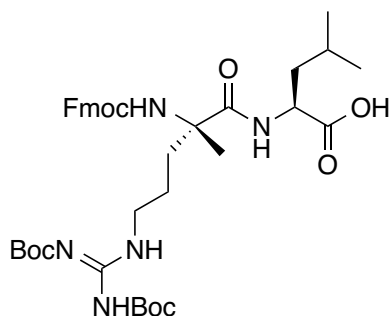
methyl ((S)-2-(((9H-fluoren-9-yl)methoxy)carbonyl)amino)-5-((Z)-2,3-bis(tert-butoxycarbonyl)guanidino)-2-methylpentanoyl)-L-leucinate (191)



The guanidinylation reaction was adapted from a literature procedure.¹⁸⁰ Dipeptide **190** (1.16 g, 2.23 mmol) was dissolved in MeOH (50 mL) and had 10% Pd/C (20 mg) added. The suspension was stirred under hydrogen gas for 2 h, filtered through a pad of Celite, and concentrated *in vacuo*. The crude residue was suspended in CH $_2$ Cl $_2$ (30 mL) and 1,3-di-Boc-2-(trifluoromethylsulfonyl)guanidine (0.961 g, 2.45 mmol) and triethylamine (0.69 mL, 4.91 mmol) were added. This reaction was stirred at room temperature under Ar for 18 h, concentrated *in vacuo*, and purified using flash chromatography (silica gel, 35% EtOAc in hexanes), yielding **191** as a white solid (1.08

g, 66%). (R_f 0.4 on SiO₂, 3:1 hexane:EtOAc); $[\alpha]_D^{26}$ 3.2 (c 1.0 CHCl₃); IR (CHCl₃ cast) 3332, 2959, 1723, 1644, 1619, 1495, 1451, 1369, 1332, 1234, 1155, 1135, 1057 cm⁻¹; ¹H (CDCl₃, 500 MHz): δ 8.28 (s, 1H, Arg-NH ϵ), 7.76 (dt, J = 7.5, 0.9 Hz, 2H, Ar-H), 7.60 (ddq, J = 7.7, 5.0, 1.0 Hz, 2H, Ar-H), 7.46 – 7.36 (m, 2H, Ar-H), 7.32 (dddd, J = 7.4, 7.4, 3.8, 1.2 Hz, 2H, Ar-H), 6.39 (br s, 1H, Leu-NH), 5.82 (br s, 1H, Fmoc-NH), 4.62 – 4.53 (m, 1H, Leu-CH α), 4.46 – 4.36 (m, 2H, Fmoc-CH $_2$), 4.21 (t, J = 6.7 Hz, 1H, Fmoc-CH $_2$), 3.71 (s, 3H, -OCH $_3$), 3.44 – 3.32 (m, 2H, Arg-CH $_2\delta$), 2.35 – 2.19 (m, 1H, Arg-CH $_2\beta$), 1.82 – 1.71 (m, 1H, Arg-CH $_2\beta$), 1.70 – 1.51 (m, 8H, Arg-CH $_3$, 2 x Arg-CH $_2\gamma$, 2 x Leu-CH $_2\beta$, -CH(CH $_3$) $_2$), 1.49 (s, 9H, -C(CH $_3$) $_3$), 1.48 (s, 9H, -C(CH $_3$) $_3$), 0.93 (d, J = 6.2 Hz, 6H, -CH(CH $_3$) $_2$); ¹³C (CDCl₃, 125 MHz): δ 173.5, 173.2, 163.5, 156.2, 153.2, 143.9, 143.9, 141.3, 127.7, 127.1, 127.1, 125.0, 120.0, 83.1, 79.3, 66.5, 59.5, 52.4, 51.1, 47.3, 41.2, 40.6, 28.3, 28.1, 25.0, 24.0, 23.7, 22.8, 21.8; HRMS (ES) Calculated for C₃₉H₅₆N₅O₉ 738.4073, found 738.4069 (M+H)⁺.

((S)-2-(((9H-fluoren-9-yl)methoxy)carbonyl)amino)-5-((Z)-2,3-bis(tert-butoxy-carbonyl)guanidino)-2-methylpentanoyl)-L-leucine (192)

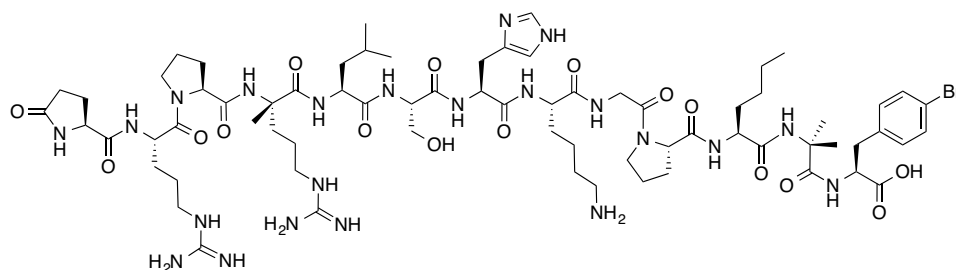


Methyl ester deprotection conditions were adapted from a literature protocol.¹⁶⁸

Dipeptide **191** (1.06 g, 1.44 mmol) was dissolved in aqueous 2-propanol (70% 2-propanol in water, 50 mL) and had CaCl₂•2H₂O (5.88 g) added to generate a 0.8 M Ca²⁺

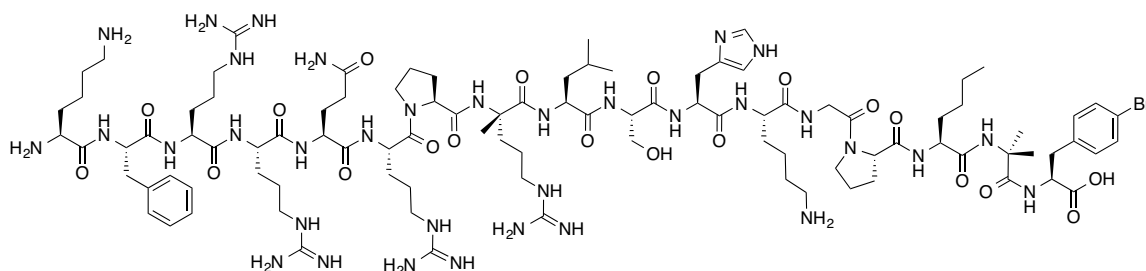
solution. Sodium hydroxide (0.115 g, 2.87 mmol) was added and the reaction was stirred for 3.5 h. Acetic acid (0.164 mL, 2.87 mmol) was added to neutralize residual base, and the reaction was concentrated *in vacuo*. The crude residue was dissolved in minimal MeOH and the dipeptide was precipitated by the addition of H₂O and collected by vacuum filtration, yielding **192** as a white solid (0.982 g, 94%). (*R_f* 0.05 on SiO₂, 1:1 hexane:EtOAc); [α]_D²⁶ -6.0 (*c* 1.0 MeOH); IR (MeOH cast) 3347, 2957, 1722, 1641, 1450, 1416, 1368, 1331, 1135 cm⁻¹; ¹H (CD₃OD, 500 MHz): δ 7.89 (s, 1H, Arg-NH ϵ), 7.78 (dt, *J* = 7.6, 0.9 Hz, 2H, Ar-H), 7.70 – 7.64 (m, 2H, Ar-H), 7.41 – 7.34 (m, 2H, Ar-H), 7.30 (td, *J* = 7.4, 1.1 Hz, 3H, Ar-H), 4.38 (d, *J* = 6.6 Hz, 2H, Fmoc-CH₂), 4.25 – 4.19 (m, 2H, Fmoc-CH, Leu-CH α), 3.33 – 3.27 (m, 2H, Arg-CH₂ δ), 2.03 – 1.94 (m, 1H, Arg-CH₂ β), 1.84 – 1.75 (m, 1H, Arg-CH₂ β), 1.68 – 1.52 (m, 4H, -CH(CH₃)₂, 2 x Leu-CH₂ β , Arg-CH₂ γ), 1.50 (d, *J* = 3.7 Hz, 10H, -C(CH₃)₃, Arg-CH₂ γ), 1.44 (s, 9H, -C(CH₃)₃), 1.40 (s, 3H, Arg-CH₃), 0.88 (d, *J* = 6.4 Hz, 3H, -CH(CH₃)₂), 0.87 (d, *J* = 6.4 Hz, 3H, -CH(CH₃)₂); ¹³C (CDCl₃, 125 MHz): δ 176.3, 172.4, 164.6, 157.5, 154.1, 145.3, 142.7, 128.9, 128.2, 126.2, 121.0, 84.5, 80.4, 79.5, 67.8, 60.6, 49.6, 49.3, 41.8, 28.6, 28.3, 26.1, 24.7, 23.7, 22.1; HRMS (ES) Calculated for C₃₈H₅₄N₅O₉ 724.3916, found 724.3913 (M+H)⁺.

α -MeArg4-pyr-1-apelin-13 A2 (193)



Advanced intermediate **153** (0.1 mmol) was subjected to manual SPPS, introducing amino acids in the following order: Fmoc-Ser(tBu)-OH, **192**, Fmoc-Pro-OH, Fmoc-Arg(Pmc)-OH, and pyr-Glu-OH. No endcapping was performed following addition of **192**. A portion (0.05 mmol) of resin-bound peptide **193** was cleaved as previously described and purified using a C₁₈ RP-HPLC analytical column (Method B), eluting at 13.4 min. The desired peptide was isolated as a white solid after lyophilization (8.5 mg, 11%). Monoisotopic MW calculated for C₇₀H₁₁₄BrN₂₂O₁₆ 532.5983, found *high resolution* (FTICR-ESI-MS) 532.5973 (M+3H)³⁺.

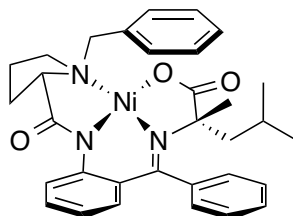
α-MeArg8-apelin-17 A2 (194)



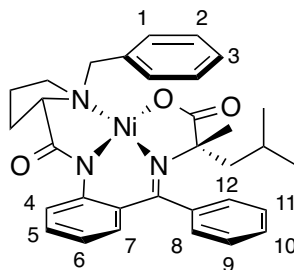
Advanced intermediate **153** (0.1 mmol) was subjected to manual SPPS, introducing amino acids in the following order: Fmoc-Ser(tBu)-OH, **192**, Fmoc-Pro-OH, Fmoc-Arg(Pmc)-OH, Fmoc-Gln(Trt)-OH, Fmoc-Arg(Pmc)-OH, Fmoc-Arg(Pmc)-OH, Fmoc-Phe-OH, and Fmoc-Lys(Boc)-OH. No endcapping was performed following addition of **192**. A portion (0.05 mmol) of resin-bound peptide **194** was cleaved as previously described and purified using a C₁₈ RP-HPLC analytical column (Method B), eluting at 13.0 min. The desired peptide was isolated as a white solid after lyophilization (12.5 mg, 11%). Monoisotopic MW calculated for C₉₇H₁₆₃BrN₃₄O₂₀ 550.7986, found *high resolution* (FTICR-ESI-MS) 550.7974 (M+4H)⁴⁺.

4.3.9 α -Methyl leucine analogues

(2*S*)-2-(2'-methylpropyl)-2-methyl-glycine-Ni(II)-(S)-BPB (**195**)



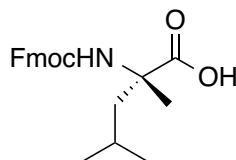
Alkylation conditions were adapted from literature protocol.¹⁶⁶ Nickel complex **170** (3.20 g, 6.25 mmol) and potassium *tert*-butoxide (1.05 g, 9.37 mmol) were added to a flame-dried RBF and dissolved in dry DMF (25 mL) at 0 °C under an Ar atmosphere. This solution was stirred for 3 minutes, followed by the addition of 1-iodo-2-methylpropane (2.16 mL, 18.7 mmol). The reaction was stirred at 0 °C for 30 minutes, then warmed to room temperature for an additional 75 minutes. 5% aqueous acetic acid (100 mL) was added to quench the reaction, followed by extraction with CH₂Cl₂ (3 x 75 mL). The pooled organic layers were washed with brine (2 x 75 mL), dried over Na₂SO₄, filtered and concentrated *in vacuo*. The desired diastereomer was purified by flash chromatography (silica gel; 2.5% MeOH in EtOAc), yielding **195** as a red solid (2.43 g, 69%). Crystals of **195** were obtained after dissolution in minimal CH₂Cl₂, dilution with hexanes and slow evaporation. (*R_f* 0.6 on SiO₂, 9:1 EtOAc:MeOH); [α]_D²⁶ 1683.7 (*c* 1.0 CHCl₃); IR (CHCl₃ cast) 2959, 2870, 1668, 1639, 1535, 1439, 1360, 1253, 1170 cm⁻¹;



^1H (CDCl_3 , 500 MHz): δ 8.12 – 8.06 (m, 3H Ar- $\underline{\text{H}}_1$, Ar- $\underline{\text{H}}_4$), 7.51 – 7.43 (m, 2H, Ar- $\underline{\text{H}}_8$, Ar- $\underline{\text{H}}_9$), 7.42 – 7.36 (m, 3H, Ar- $\underline{\text{H}}_2$, Ar- $\underline{\text{H}}_{11}$), 7.34 – 7.22 (m, 2H, Ar- $\underline{\text{H}}_3$, Ar- $\underline{\text{H}}_{10}$), 7.12 (ddd, $J = 8.6, 6.7, 1.9$ Hz, 1H, Ar- $\underline{\text{H}}_5$), 7.06 – 7.00 (m, 1H, Ar- $\underline{\text{H}}_{12}$), 6.64 – 6.53 (m, 2H, Ar- $\underline{\text{H}}_6$, Ar- $\underline{\text{H}}_7$), 4.48 (d, $J = 12.7$ Hz, 1H, Ph- $\underline{\text{C}}\underline{\text{H}}_2$ -N), 3.74 – 3.64 (m, 2H, Ph- $\underline{\text{C}}\underline{\text{H}}_2$ -N, Pro- $\underline{\text{C}}\underline{\text{H}}_2\delta$), 3.45 (dd, $J = 10.6, 6.1$ Hz, 1H, Pro- $\underline{\text{C}}\underline{\text{H}}\alpha$), 3.26 – 3.10 (m, 1H, Pro- $\underline{\text{C}}\underline{\text{H}}_2\gamma$), 2.74 – 2.65 (m, 1H, Pro- $\underline{\text{C}}\underline{\text{H}}_2\beta$), 2.56 – 2.37 (m, 2H, Pro- $\underline{\text{C}}\underline{\text{H}}_2\beta$, Leu- $\underline{\text{C}}\underline{\text{H}}\gamma$), 2.13 – 2.00 (m, 2H, Pro- $\underline{\text{C}}\underline{\text{H}}_2\gamma$, Pro- $\underline{\text{C}}\underline{\text{H}}_2\delta$), 1.73 – 1.60 (m, 2H, Leu- $\underline{\text{C}}\underline{\text{H}}_2\beta$), 1.27 (d, $J = 6.6$ Hz, 3H, Leu- $\underline{\text{C}}\underline{\text{H}}_3\delta$), 1.22 (s, 3H, Leu- $\underline{\text{C}}\underline{\text{H}}_3\beta$), 1.14 (d, $J = 6.7$ Hz, 3H, Leu- $\underline{\text{C}}\underline{\text{H}}_3\delta$); ^{13}C (CDCl_3 , 125 MHz): δ 182.9, 180.6, 172.3, 141.7, 136.8, 133.6, 133.5, 131.7, 131.6, 130.5, 129.4, 129.0, 128.9, 128.4, 127.8, 126.9, 123.8, 120.6, 77.5, 70.2, 63.6, 57.1, 48.5, 30.7, 30.7, 25.6, 24.5, 23.3, 23.3; HRMS (ES) Calculated for $\text{C}_{32}\text{H}_{36}\text{N}_3\text{NiO}_3$ 568.2105, found 568.2100 ($\text{M}+\text{H}$) $^+$.

(S)-2-(((9H-fluoren-9-yl)methoxy)carbonyl)amino)-2,4-dimethylpentanoic acid

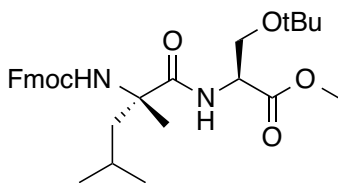
(196)



A solution of 3N HCl:MeOH (1:1, 10 mL) was heated to 70 °C and had **195** (2.36 g, 4.16 mmol) dissolved in MeOH (5 mL) added dropwise over 5 minutes. The

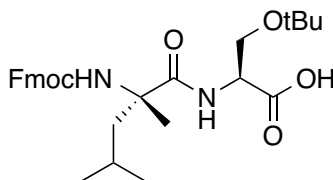
reaction mixture was stirred for 40 minutes at 70 °C, turning from dark red to green as the reaction proceeded. The reaction was cooled to room temperature, concentrated *in vacuo* and resuspended in 10% aqueous sodium carbonate (25 mL). EDTA disodium salt (3.09 g, 8.31 mmol) was added and stirred for 0.5 h at room temperature. The reaction was cooled to 0 °C and had a solution of Fmoc-OSu (1.54 g, 4.57 mmol) dissolved in acetone (25 mL) added to it. This reaction was slowly warmed to room temperature and stirred for 22 h. The following day, the reaction was diluted with EtOAc (50 mL) and washed with 1 N HCl (3 x 50 mL). The organic layer was dried over MgSO₄, filtered, and concentrated *in vacuo*. The product was purified by flash chromatography (silica gel, 1-5% MeOH in CH₂Cl₂ gradient), yielding **196** as a white solid (1.45 g, 95%). (*R_f* 0.35 on SiO₂, 7.5% MeOH in CH₂Cl₂); ¹H (CDCl₃, 500 MHz): δ 7.80 – 7.74 (m, 2H, Ar-H), 7.64 – 7.57 (m, 2H, Ar-H), 7.43 – 7.38 (m, 2H, Ar-H), 7.37 – 7.29 (m, 2H, Ar-H), 5.92 (br s, 1H, N-H), 4.46 – 4.33 (m, 2H, Fmoc-CH₂), 4.32 (t, 1H, *J* = 6.0 Hz Fmoc-CH), 2.26 – 2.19 (m, 1H, Leu-CH₂β), 1.83 – 1.73 (m, 1H, Leu-CH₂β), 1.70 – 1.55 (m, 4H, Leu-CH_γ, Leu-CH₃β), 0.96 – 0.82 (m, 6H, 2 x Leu-CH₃δ); ¹³C (CDCl₃, 125 MHz): δ 179.4, 155.2, 143.9, 141.6, 127.8, 127.1, 124.8, 120.0, 65.1, 47.3, 24.9, 24.7, 23.8, 23.0; HRMS (ES) Calculated for C₂₂H₂₄NO₄ 366.1711, found 366.1706 (M-H)⁻.

methyl *N*-((*S*)-2-(((9*H*-fluoren-9-yl)methoxy)carbonyl)amino)-2,4-dimethylpentanoyl)-*O*-(*tert*-butyl)-*L*-serinate (197**)**



Amino acid **196** (1.53 g, 4.16 mmol), HATU (1.58 g, 4.16 mmol), HOAt (0.69 mL [0.6 M solution in DMF], 0.42 mmol), and DIPEA (2.90 mL, 16.6 mmol) were dissolved in dry DMF (25 mL) and stirred for 5 minutes to preactivate the amino acid. A solution of H-Ser(tBu)-OMe•HCl (0.925 g, 4.37 mmol) in dry CH₂Cl₂ (25 mL) was added and the reaction was stirred for 20 h at room temperature. The reaction was concentrated *in vacuo*, resuspended in EtOAc (50 mL), and washed with 10% citric acid, water, and brine (50 mL). The organic layer was dried over Na₂SO₄, filtered, and concentrated *in vacuo*. Crude **190** was purified using flash chromatography (silica gel, 25% EtOAc in hexanes), obtaining the desired product as a white solid (0.872 g, 40%). (*R_f* 0.2 on SiO₂, 3:1 hexanes:EtOAc); [α]_D²⁶ 20.4 (*c* 1.0 CHCl₃); IR (CHCl₃ cast) 3440, 3384, 2973, 2956, 2872, 1730, 1669, 1493, 1364, 1241, 1099 cm⁻¹; ¹H (CDCl₃, 500 MHz): δ 7.76 (dd, *J* = 7.6, 0.9 Hz, 2H, Ar-H), 7.64 – 7.58 (m, 2H, Ar-H), 7.39 (ddd, *J* = 6.8, 6.8, 0.8 Hz, 2H, Ar-H), 7.31 (ddd, *J* = 7.4, 6.8, 1.1 Hz, 2H, Ar-H), 6.64 (br s, 1H, Ser-NH), 6.09 (s, 1H, Fmoc-NH), 4.74 – 4.68 (m, 1H, Ser-CH α), 4.43 – 4.30 (m, 2H, Fmoc-CH₂), 4.22 (t, *J* = 6.8 Hz, 1H, Fmoc-CH), 3.81 (d, *J* = 8.8 Hz, 1H, Ser-CH₂ β), 3.75 (s, 3H, -OCH₃), 3.57 (d, *J* = 8.8 Hz, 1H, Ser-CH₂ β), 2.44 – 2.31 (m, 1H, Leu-CH₂ β), 1.73 – 1.52 (m, 5H, Leu-CH₂ β , Leu-CH γ , Leu-CH₃ β), 1.13 (s, 9H, -C(CH₃)₃), 0.94 – 0.82 (m, 6H, 2 x Leu-CH₃ δ); ¹³C (CDCl₃, 125 MHz): δ 173.9, 170.7, 154.4, 144.1, 144.0, 141.3, 127.6, 127.1, 125.1, 120.0, 73.4, 66.4, 61.9, 59.6, 53.1, 52.4, 47.3, 45.1, 27.3, 25.2, 24.7, 23.7, 23.6; HRMS (ES) Calculated for C₃₀H₄₁N₂O₆ 525.2959, found 525.2956 (M+H)⁺.

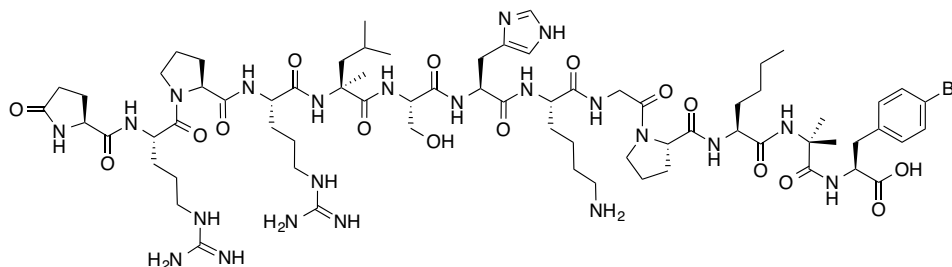
***N*-(((*S*)-2-((((9*H*-fluoren-9-yl)methoxy)carbonyl)amino)-2,4-dimethylpentanoyl)-*O*-
(*tert*-butyl)-*L*-serine (**198**)**



Methyl ester deprotection conditions were adapted from literature procedure.¹⁶⁸ Dipeptide **197** (0.853 g, 1.63 mmol) was dissolved in aqueous 2-propanol (70% 2-propanol in water, 50 mL) and had CaCl₂•2H₂O (5.88 g) added to generate a 0.8 M Ca²⁺ solution. Sodium hydroxide (0.130 g, 3.25 mmol) was added and the reaction was stirred for 4 h. Acetic acid (0.186 mL, 3.25 mmol) was added to neutralize residual base, and the reaction was concentrated *in vacuo*. The crude residue purified by flash chromatography (silica gel, 50% EtOAc in hexanes 0.1% AcOH), yielding dipeptide **198** as a white sticky solid (0.368 g, 44%). (*R*_f 0.3 on SiO₂, 0.1% AcOH in EtOAc); [α]_D²⁶ 27.0 (*c* 1.0 CHCl₃); IR (CHCl₃ cast) 3386, 3320, 3068, 3018, 2974, 2876, 1727, 1665, 1497, 1450, 1240, 1194, 1105 cm⁻¹; ¹H (CDCl₃, 500 MHz): δ 7.76 (dd, *J* = 7.7, 0.9 Hz, 2H, Ar-H), 7.59 (ddd, *J* = 7.5, 2.0, 1.0 Hz, 2H, Ar-H), 7.40 (ddd, *J* = 7.5, 7.5, 0.9 Hz, 2H, Ar-H), 7.31 (ddd, *J* = 7.7, 7.5, 1.2, Hz, 2H, Ar-H), 6.78 (br s, 1H, Ser-NH), 5.73 (s, 1H, Fmoc-NH), 4.67 – 4.56 (m, 1H, Ser-CH α), 4.48 – 4.34 (m, 2H, Fmoc-CH₂), 4.20 (t, *J* = 6.6 Hz, 1H, Fmoc-CH), 3.95 – 3.88 (m, 1H, Ser-CH₂ β), 3.54 – 3.48 (m, 1H, Ser-CH₂ β), 2.19 – 2.07 (m, 1H, Leu-CH₂ β), 1.72 – 1.59 (m, 2H, Leu-CH₂ β , Leu-CH γ), 1.54 (s, 3H, Leu-CH₃ β), 1.19 (s, 9H, -C(CH₃)₃), 0.94 – 0.82 (m, 6H, 2 x Leu-CH₃ δ); ¹³C (CDCl₃, 125 MHz): δ 174.3, 172.0, 154.9, 143.8, 141.4, 129.1, 128.2, 127.7, 127.1, 125.0, 120.0,

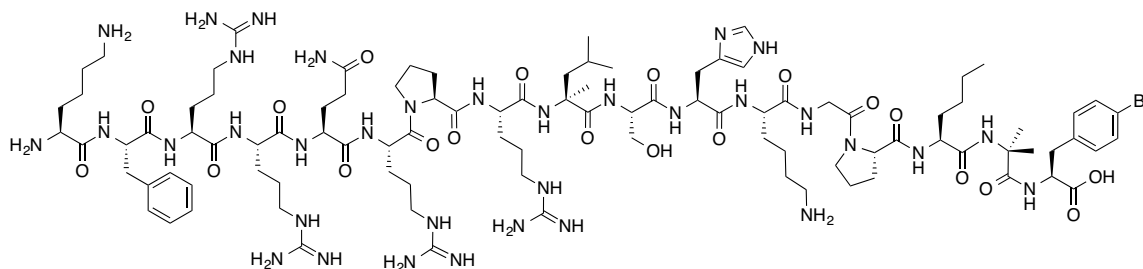
74.7, 66.6, 61.0, 59.9, 52.7, 47.2, 45.8, 27.7, 24.4, 24.0, 23.6; HRMS (ES) Calculated for $C_{29}H_{37}N_2O_6$ 509.2657, found 509.2657 (M-H)⁻.

α -MeLeu5-pyr-1-apelin-13 A2 (199)



Advanced intermediate **153** (0.2 mmol) was subjected to manual SPPS, introducing amino acids in the following order: **198**, Fmoc-Pro-OH, and Fmoc-Arg(Pmc)-OH. The resin was split into half, and Fmoc-SPPS was continued on 0.1 mmol scale, coupling pyr-Glu-OH. No endcapping was performed following addition of **192**. A portion (0.05 mmol) of resin-bound peptide **199** was cleaved as previously described and purified using a C_{18} RP-HPLC analytical column (Method B), eluting at 13.7 min. The desired peptide was isolated as a white solid after lyophilization (8.5 mg, 11%). Monoisotopic MW calculated for $C_{70}H_{114}BrN_{22}O_{16}$ 532.5983, found *high resolution* (FTICR-ESI-MS) 532.5972 (M+3H)³⁺.

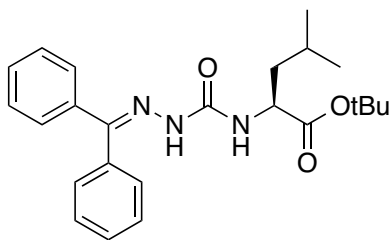
α -MeLeu9-apelin-17 A2 (200)



The remaining 0.1 mmol carried over from the synthesis of **199** was coupled with Fmoc-Gln(Trt)-OH, Fmoc-Arg(Pmc)-OH, Fmoc-Arg(Pmc)-OH, Fmoc-Phe-OH, and Fmoc-Lys(Boc)-OH. A portion (0.05 mmol) of resin-bound peptide **200** was cleaved as previously described and purified using a C₁₈ RP-HPLC analytical column (Method B), eluting at 11.5 min. The desired peptide was isolated as a white solid after lyophilization (14.3 mg, 13%). Monoisotopic MW calculated for C₉₇H₁₆₃BrN₃₄O₂₀ 550.7986, found *high resolution* (FTICR-ESI-MS) 550.7974 (M+4H)⁴⁺.

4.3.10 aza-Arginine analogues

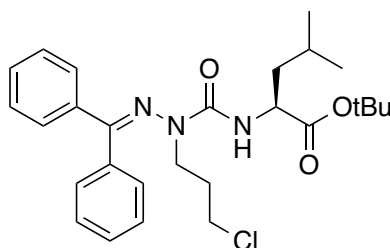
tert-butyl (2-(diphenylmethylene)hydrazine-1-carbonyl)-L-leucinate (**203**)



Semicarbazone **203** was prepared by modifying a literature procedure.¹⁸¹ A solution of benzophenone hydrazone (4.39 g, 22.4 mmol) in dry CH₂Cl₂ (50 mL) was cooled to 0 °C and cannulated into a 0 °C solution of disuccinimidyl carbonate (7.41 g [85% purity], 24.6 mmol) in dry CH₂Cl₂ (50 mL) and dry DMF (10 mL). The reaction was warmed to room temperature for 45 minutes, then cooled down to 0 °C. A 0 °C solution of H-Leu-OtBu•HCl (5.00 g, 22.4 mmol) and DIPEA (7.79 mL, 44.7 mmol) in dry CH₂Cl₂ (50 mL) was then cannulated into the reaction vessel and allowed to slowly come up to room temperature over 16 h. The reaction was concentrated *in vacuo* and purified by flash chromatography (silica gel, 20% EtOAc in hexanes), yielding a light yellow sticky solid (8.29 g, 91%). (*R*_f 0.8 on SiO₂, 1:1 hexanes:EtOAc); [*α*]_D²⁶ 36.7 (*c*

1.27 CHCl₃); IR (CHCl₃ cast) 3414, 3355, 3188, 3062, 2957, 2871, 1732, 1682, 1519, 1446, 1368, 1153, 1113 cm⁻¹; ¹H (CDCl₃, 400 MHz): δ 7.59 (s, 1H, =N-NH), 7.57 – 7.46 (m, 5H, Ar-H), 7.40 – 7.29 (m, 3H, Ar-H), 7.29 – 7.22 (m, 2H, Ar-H), 6.68 (d, *J* = 9.0 Hz, 1H, Leu-NH), 4.52 (ddd, *J* = 8.8, 8.8, 5.6 Hz, 1H, Leu-CH_α), 1.85 – 1.74 (m, 1H, Leu-CH_γ), 1.74 – 1.60 (m, 2H, Leu-CH_{2β}), 1.50 (s, 9H, -C(CH₃)₃), 1.00 (d, *J* = 6.5 Hz, 6H, 2 x Leu-CH_{3δ}); ¹³C (CDCl₃, 125 MHz): δ 172.6, 154.9, 148.2, 137.0, 131.9, 129.8, 129.7, 129.4, 129.3, 128.8, 128.5, 128.3, 128.1, 127.2, 126.5, 81.7, 51.9, 42.4, 28.1, 25.0, 23.0, 22.1; HRMS (ES) Calculated for C₂₄H₃₂N₃O₃ 410.2438, found 410.2438 (M+H)⁺.

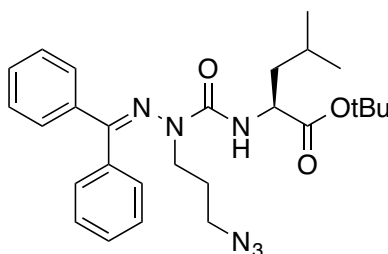
***tert*-butyl (1-(3-chloropropyl)-2-(diphenylmethylene)hydrazine-1-carbonyl)-*L*-leucinate (204)**



Alkylation conditions were initially adapted from a literature procedure.¹⁷⁴ Semicarbazone **203** (2.47 g, 6.03 mmol) was dissolved in THF (50 mL) and cooled to 0 °C. Aqueous tetraethylammonium hydroxide (22.2 mL [20% solution], 30.1 mmol) was added and stirred for 30 minutes, followed by the addition of 1-bromo-3-chloropropane (4.47 mL, 45.2 mmol) at 0 °C. The reaction was slowly warmed to room temperature and was quenched after 72 h by the addition of 10% citric acid (20 mL) followed by brine (20 mL). Organic components were extracted with EtOAc (3 x 100 mL), dried over Na₂SO₄, filtered and concentrated *in vacuo*. Alkylated semicarbazone **204** was purified by flash chromatography (silica gel, 15% EtOAc in hexanes) and was isolated as

a yellow oil (2.16 g, 74%). (R_f 0.85 on SiO₂, 2:1 hexanes:EtOAc); $[\alpha]_D^{26}$ 67.5 (c 1.42 CHCl₃); IR (CHCl₃ cast) 3414, 3061, 2959, 2870, 1734, 1682, 1499, 1446, 1368, 1154 cm⁻¹; ¹H (CDCl₃, 500 MHz): δ 7.55 – 7.41 (m, 6H, Ar-H), 7.41 – 7.30 (m, 4H, Ar-H), 6.69 (d, J = 8.7 Hz, 1H, Leu-NH), 4.47 (ddd, J = 8.8, 8.7, 5.6 Hz, 1H, Leu-CH α), 3.46 (dt, J = 14.7, 6.8 Hz, 1H, N-CH β), 3.38 – 3.27 (m, 3H, N-CH β , 2 x N-CH γ), 1.80 – 1.72 (m, 3H, 2 x -CH γ Cl, Leu-CH γ), 1.66 (ddd, J = 13.6, 8.0, 5.6 Hz, 1H, Leu-CH β), 1.61 – 1.51 (m, 1H, Leu-CH β), 1.48 (s, 9H, -C(CH β)₃), 0.98 (d, J = 6.6 Hz, 6H, 2 x Leu-CH δ); ¹³C (CDCl₃, 125 MHz): δ 172.8, 159.4, 158.3, 138.6, 135.7, 130.2, 129.8, 128.9, 128.8, 128.6, 128.2, 81.3, 52.7, 44.1, 42.4, 42.1, 30.0, 28.1, 25.1, 22.9, 22.2; HRMS (ES) Calculated for C₂₇H₃₇ClN₃O₃ 486.2518, found 486.2518 (M+H)⁺.

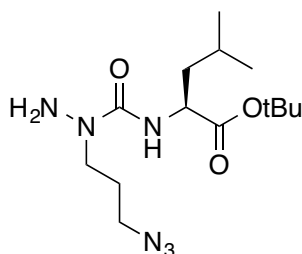
***tert*-butyl (1-(3-azidopropyl)-2-(diphenylmethylene)hydrazine-1-carbonyl)-*L*-leucinate (205)**



This reaction was adapted from a literature procedure.¹⁷⁴ Chloroalkylated semicarbazone **204** (2.08 g, 4.27 mmol) and sodium azide (0.833 g, 12.8 mmol) were dissolved in DMF (50 mL) and heated at 60 °C for 20 h. The reaction was cooled and had H₂O (150 mL) added to it, followed by EtOAc (3 x 150 mL) washes to extract organic components. Pooled EtOAc layers were dried over Na₂SO₄, filtered, and concentrated *in vacuo*. The product was purified using flash chromatography (silica gel, 10% EtOAc in hexanes), generating azide **205** as a yellow oil (1.90 g, 90%). (R_f 0.2 on

SiO₂, 9:1 hexanes:EtOAc); $[\alpha]_D^{26}$ 53.8 (*c* 1.00 CHCl₃); IR (CHCl₃ cast) 3411, 3061, 2958, 2871, 2097, 1734, 1683, 1499, 1446, 1368, 1257, 1154 cm⁻¹; ¹H (CDCl₃, 500 MHz): δ 7.54 – 7.40 (m, 6H, Ar-H), 7.40 – 7.26 (m, 4H, Ar-H), 6.74 (d, *J* = 8.7 Hz, 1H, Leu-NH), 4.47 (ddd, *J* = 8.8, 8.7, 5.6 Hz, 1H, Leu-CH α), 3.42 (dt, *J* = 14.7, 7.0 Hz, 1H, N-CH β), 3.27 (dt, *J* = 14.7, 6.8 Hz, 1H, N-CH β), 3.05 (t, *J* = 7.1 Hz, 2H, -CH β N₃), 1.76 (ddsept, *J* = 12.9, 7.8, 6.5 Hz, 1H, Leu-CH γ), 1.70 – 1.62 (m, 1H, Leu-CH β), 1.61 – 1.55 (m, 1H, Leu-CH β), 1.56 – 1.49 (m, 2H, -CH β CH β N₃), 1.48 (s, 9H, -C(CH β)₃), 0.99 (d, *J* = 6.6 Hz, 3H, Leu-CH δ), 0.98 (d, *J* = 6.6 Hz, 3H, Leu-CH δ); ¹³C (CDCl₃, 125 MHz): δ 172.8, 158.5, 158.4, 138.6, 135.8, 130.2, 129.8, 128.9, 128.8, 128.5, 128.3, 81.3, 52.7, 48.9, 43.4, 42.1, 28.1, 26.2, 25.1, 22.9, 22.2; HRMS (ES) Calculated for C₂₇H₃₇N₆O₃ 493.2922, found 493.2922 (M+H)⁺.

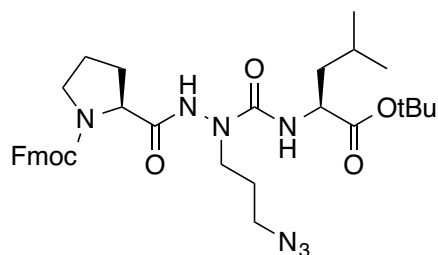
***tert*-butyl (1-(3-azidopropyl)hydrazine-1-carbonyl)-L-leucinate (206)**



This procedure was adapted from literature protocols.^{178,181} Azide **205** (1.89 g, 3.84 mmol) was dissolved in a solution of hydroxylamine hydrochloride (1.07 g, 15.4 mmol) in pyridine (75 mL) and heated to 60 °C for 22 h. The reaction was cooled to room temperature, then concentrated *in vacuo*, using CH₂Cl₂ and EtOAc co-evaporations to remove residual pyridine. The product was purified using flash chromatography (silica gel, 60% EtOAc in hexanes, 0.1% DIPEA) yielding semicarbazide **206** as a yellow oil (1.19 g, 94%). (*R_f* 0.5 on SiO₂, 1:1 hexanes:EtOAc); $[\alpha]_D^{26}$ 5.0 (*c* 0.92

CHCl₃); IR (CHCl₃ cast) 3406, 3335, 3216, 2958, 2934, 2871, 2098, 1732, 1654, 1510, 1368, 1257, 1155 cm⁻¹; ¹H (CDCl₃, 500 MHz): δ 6.67 (d, *J* = 8.8 Hz, 1H, Leu-NH), 4.33 (ddd, *J* = 8.9, 8.8, 5.5 Hz, 1H, Leu-CH_α), 3.64 (s, 2H, H₂N-N), 3.62 – 3.51 (m, 2H, N-CH₂), 3.36 (t, *J* = 6.7 Hz, 2H, -CH₂N₃), 1.84 (app p, *J* = 6.8 Hz, 2H, -CH₂CH₂N₃), 1.71 (ddsept, *J* = 8.2, 8.0, 6.5 Hz, 1H, Leu-CH_γ), 1.59 (ddd, *J* = 13.6, 8.1, 5.5 Hz, 1H, Leu-CH₂β), 1.53 – 1.47 (m, 1H, Leu-CH₂β), 1.45 (s, 9H, -C(CH₃)₃), 0.95 (d, *J* = 6.6 Hz, 6H, 2 x Leu-CH₃δ); ¹³C (CDCl₃, 125 MHz): δ 173.5, 158.7, 81.3, 52.3, 49.2, 48.0, 42.4, 28.1, 26.3, 25.0, 22.9, 22.1; HRMS (ES) Calculated for C₁₄H₂₉N₆O₃ 329.2296, found 329.2290 (M+H)⁺.

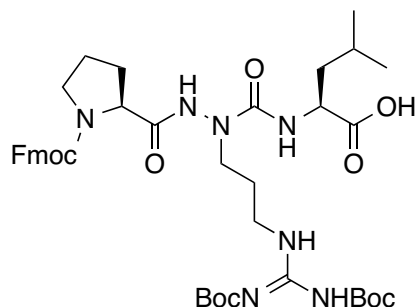
(9H-fluoren-9-yl)methyl (S)-2-(2-(3-azidopropyl)-2-(((S)-1-(tert-butoxy)-4-methyl-1-oxopentan-2-yl)carbamoyl)hydrazine-1-carbonyl)pyrrolidine-1-carboxylate (208)



A solution of Fmoc-Pro-OH (1.65 g, 4.88 mmol), HATU (1.86 g, 4.88 mmol), HOAt (0.81 mL [0.6 M solution], 0.49 mmol) and DIPEA (2.13 mL, 12.2 mmol) were dissolved in dry DMF (20 mL) and preactivated for 5 minutes before the addition of a solution of semicarbazide **206** (1.34 g, 4.07 mmol) in dry DCM (20 mL). The reaction mixture was stirred under Ar gas for 18 h then concentrated *in vacuo*. The crude reaction mixture was resuspended in EtOAc (75 mL) and washed with 10% citric acid (50 mL), water (50 mL) and brine (50 mL). Pooled aqueous layers were washed with EtOAc (2 x 75 mL), and pooled organic fractions were dried over Na₂SO₄, filtered and concentrated

in vacuo. The product was purified by flash chromatography (silica gel, 50% EtOAc in hexanes) yielding azatripeptide **208** as a white solid (1.74 g, 66%). (R_f 0.4 on SiO₂, 1:1 hexanes:EtOAc); $[\alpha]_D^{26}$ -7.2 (c 0.83 CHCl₃); IR (CHCl₃ cast) 3357, 3229, 2957, 2872, 2097, 1690, 1529, 1452, 1424, 1367, 1257, 1155 cm⁻¹; ¹H (CDCl₃, 500 MHz): δ 8.20 (s, 1H, C(O)NH-N), 7.80 – 7.74 (m, 2H, Ar-H), 7.61 – 7.54 (m, 2H, Ar-H), 7.47 – 7.37 (m, 2H, Ar-H), 7.31 (t, J = 7.5 Hz, 2H, Ar-H), 6.04 (d, J = 8.2 Hz, 1H, Leu-NH), 4.47 (dd, J = 10.5, 7.1 Hz, 1H, Fmoc-CH₂), 4.42 – 4.29 (m, 2H, Fmoc-CH₂, Leu-CH₂ α), 4.25 (t, J = 6.8 Hz, 1H, Fmoc-CH), 4.19 (dd, J = 7.4, 4.5 Hz, 1H, Pro-CH₂ α), 3.67 – 3.54 (m, 3H, 2 x N-CH₂, Pro-CH₂ δ), 3.55 – 3.46 (m, 1H, Pro-CH₂ δ), 3.44 – 3.33 (m, 2H, -CH₂N₃), 2.27 (ddd, J = 11.5, 5.3, 4.9 Hz, 1H, Pro-CH₂ β), 2.17 – 2.06 (m, 2H, Pro-CH₂ β , Pro-CH₂ γ), 2.01 – 1.93 (m, 1H, Pro-CH₂ γ), 1.82 – 1.72 (m, 2H, -CH₂CH₂N₃), 1.63 (ddd, J = 13.4, 6.7, 6.5 Hz, 1H, Leu-CH γ), 1.54 (ddd, J = 7.1, 6.7, 6.7 Hz, 1H, Leu-CH₂ β), 1.48 – 1.38 (m, 10H, Leu-CH₂ β , -C(CH₃)₃), 0.84 (d, J = 6.5, 3H, Leu-CH₃ δ), 0.83 (d, J = 6.5, 3H, Leu-CH₃ δ); ¹³C (CDCl₃, 125 MHz): δ 173.5, 170.9, 156.8, 156.0, 143.7, 141.4, 127.9, 127.1, 125.0, 120.1, 81.3, 68.0, 59.2, 52.6, 49.2, 47.2, 47.1, 46.2, 41.9, 28.8, 28.0, 27.2, 25.0, 24.7, 22.8, 22.1; HRMS (ES) Calculated for C₃₄H₄₆N₇O₆ 648.3504, found 648.3503 (M+H)⁺.

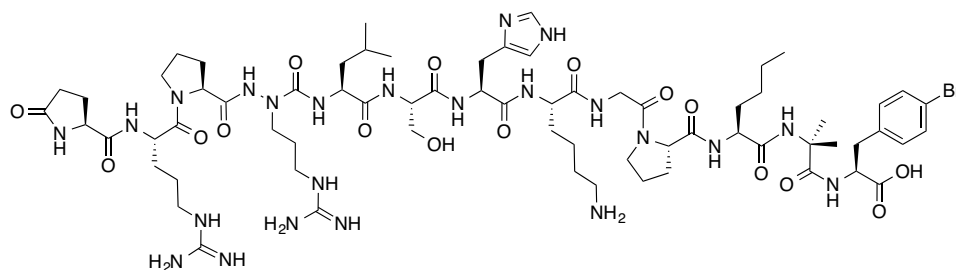
(2-((S)-1-(((9H-fluoren-9-yl)methoxy)carbonyl)pyrrolidine-2-carboxamido)-7-((tert-butoxycarbonyl)amino)-11,11-dimethyl-9-oxo-10-oxa-2,6,8-triazadodec-7-enoyl)-L-leucine (209)



A solution of azatripeptide **208** (0.803 g, 1.24 mmol) in dry CH₂Cl₂ (20 mL) was cooled to 0 °C and had TFA (10 mL) added and stirred for 15 minutes. The reaction was warmed to room temperature for 90 minutes and concentrated *in vacuo*, using toluene co-evaporations to remove residual TFA. The product was resuspended in MeOH (20 mL), 10% Pd/C (25 mg) was added, and the reaction was stirred under an atmosphere of hydrogen gas for 75 minutes. The reaction mixture was filtered through a pad of Celite, concentrated *in vacuo* to dryness, and resuspended in dry CH₂Cl₂ (20 mL) with triethylamine (0.76 mL, 5.45 mmol) and 1,3-di-Boc-2-(trifluoromethylsulfonyl)guanidine (0.801 g, 2.05 mmol) for 40 h. Solvents were removed *in vacuo* and **209** was purified using flash chromatography (silica gel, 90% EtOAc in hexanes, 0.1 % AcOH), yielding a white solid (0.413 g, 41%). (*R*_f 0.05 on SiO₂, 0.1% AcOH in EtOAc); [α]_D²⁶ -42.4 (*c* 1.00 CH₃OH); IR (CH₃OH cast) 3328, 2959, 1721, 1688, 1642, 1530, 1419, 1335, 1156, 1136 cm⁻¹; ¹H (CDCl₃, 500 MHz): δ 9.47 (br s, 1H, Arg-NH ϵ), 8.53 (s, 1H, C(O)NH-N), 7.75 (d, *J* = 7.5 Hz, 2H, Ar-H), 7.56 (d, *J* = 7.5 Hz, 1H, Ar-H), 7.54 (d, *J* = 7.5 Hz, 1H, Ar-H), 7.39 (app t, *J* = 7.4 Hz, 2H, Ar-H), 7.30 (app t, *J* = 7.5 Hz, 2H, Ar-H), 6.47 (br s, 1H, Leu-NH), 4.39 (dd, *J* = 10.4, 7.1 Hz, 1H, Fmoc-CH₂), 4.30 – 4.23 (m,

2H, Fmoc-CH₂, Leu-CH_α), 4.23 – 4.17 (m, 2H, Fmoc-CH, Pro-CH_α), 3.84 – 3.69 (m, 1H, Arg-N-CH₂β), 3.64 – 3.57 (m, 1H, Pro-CH₂δ), 3.56 – 3.48 (m, 2H, Pro-CH₂δ, Arg-CH₂δN), 3.46 – 3.38 (m, 1H, Pro-CH₂δ), 3.35 – 3.26 (m, 1H, Arg-CH₂δN), 2.21 – 2.09 (m, 2H, Pro-CH₂β, Arg-CH₂γ), 2.09 – 2.01 (m, 1H, Arg-CH₂γ), 1.93 – 1.86 (m, 1H, Pro-CH₂β), 1.84 – 1.72 (m, 2H, Pro-CH₂γ), 1.70 – 1.54 (m, 3H, Leu-CH_γ, 2 x Leu-CH₂β), 1.49 (m, 9H, -C(CH₃)₃), 1.46 (s, 9H, -C(CH₃)₃), 0.95 – 0.77 (m, 6H, 2 x Leu-CH₃δ); ¹³C (CDCl₃, 125 MHz): δ 171.8, 163.1, 158.7, 156.5, 155.3, 153.1, 143.7, 141.3, 129.0, 128.2, 127.8, 127.1, 127.1, 125.3, 125.0, 120.0, 83.4, 79.8, 67.8, 58.7, 53.1, 47.1, 44.9, 39.9, 37.9, 29.7, 28.3, 28.1, 27.2, 24.9, 24.5, 22.8, 21.8; HRMS (ES) Calculated for C₄₁H₅₆N₇O₁₀ 806.4094, found 806.4088 (M-H)⁻.

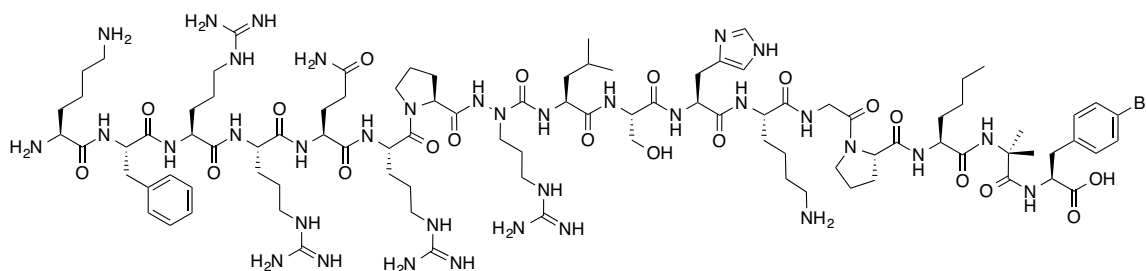
azaArg4-pyr-1-apelin-13 A2 (210)



Advanced intermediate **153** (0.2 mmol) was subjected to manual SPPS, introducing amino acids in the following order: Fmoc-Ser(tBu)-OH, **209**, and Fmoc-Arg(Pmc)-OH. The resin was split into half, and Fmoc-SPPS was continued on 0.1 mmol scale, coupling pyr-Glu-OH. No endcapping was performed following addition of **209**. A portion (0.05 mmol) of resin-bound peptide **210** was cleaved as previously described and purified using a C₁₈ RP-HPLC analytical column (Method B), eluting at 13.5 min. The desired peptide was isolated as a white solid after lyophilization (5.5 mg,

7%). Monoisotopic MW calculated for $C_{68}H_{111}BrN_{23}O_{16}$ 528.2582, found *high resolution* (FTICR-ESI-MS) 528.2571 ($M+3H$)³⁺.

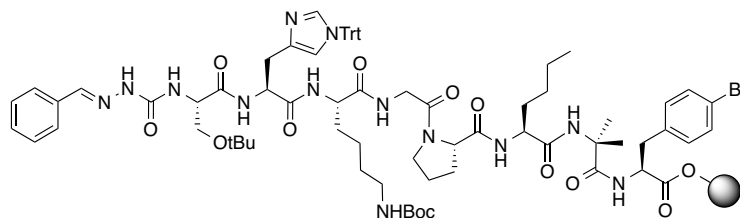
azaArg8-apelin-17 A2 (211)



The remaining 0.1 mmol carried over from the synthesis of **210** was coupled with Fmoc-Gln(Trt)-OH, Fmoc-Arg(Pmc)-OH, Fmoc-Arg(Pmc)-OH, Fmoc-Phe-OH, and Fmoc-Lys(Boc)-OH. A portion (0.05 mmol) of resin-bound peptide **211** was cleaved as previously described and purified using a C_{18} RP-HPLC analytical column (Method B), eluting at 11.1 min. The desired peptide was isolated as a white solid after lyophilization (15.6 mg, 14%). Monoisotopic MW calculated for $C_{95}H_{160}BrN_{35}O_{20}$ 547.5435, found *high resolution* (FTICR-ESI-MS) 547.5430 ($M+4H$)⁴⁺.

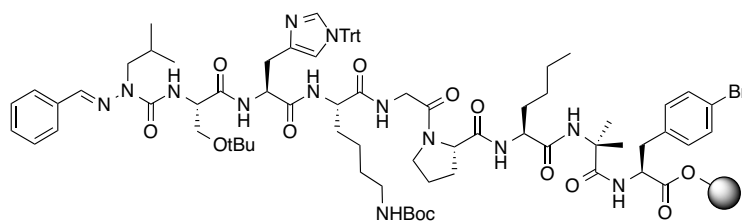
4.3.11 aza-Leucine analogues

On-resin semicarbazone formation (216)



This procedure was adapted from a literature protocol.¹⁷⁴ Advanced intermediate **153** (0.1 mmol) was Fmoc deprotected with 20% piperidine in DMF, coupled with Fmoc-Ser(tBu)-OH and Fmoc deprotected one additional time. In a separate flask, benzaldehyde (0.051 mL, 0.5 mmol) was added slowly to a solution of hydrazine monohydrate (0.073 mL, 1.5 mmol) in CH₂Cl₂ (1 mL) at 0 °C and stirred for 1 h. This solution was transferred to an addition funnel and added dropwise to a solution of *p*-nitrophenyl chloroformate (0.101 g, 0.5 mmol) and DIPEA (0.174 mL, 1.0 mmol) in CH₂Cl₂ (2 mL) at 0 °C over 10 minutes. The mixture was stirred at 0 °C for 30 minutes, then brought to room temperature for an additional 90 minutes. This mixture was added to the Fmoc-deprotected octapeptide on resin and shaken at room temperature for 18 h. The bright yellow solution was filtered through a fritted filter to collect the resin, then washed with DMF (3 x 5 mL), MeOH (3 x 5 mL), THF (3 x 5 mL) and CH₂Cl₂ (3 x 5 mL). The resin was dried under vacuum and a small sample was taken and cleaved as previously described. Monoisotopic MW calculated for for C₄₉H₆₉BrN₁₃O₁₁ 1094.4, found (MALDI-TOF) 1094.2 (M+H)⁺.

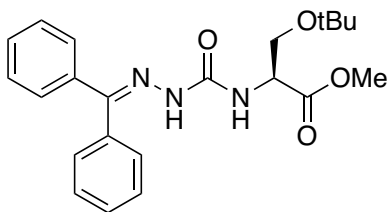
On-resin semicarbazone alkylation (**218**)



This procedure was adapted from a literature protocol.¹⁷⁴ Compound **216** on resin was swollen in THF (3 mL) for 15 minutes with shaking, then aqueous tetraethylammonium hydroxide (20% v/v solution, 0.22 mL, 0.3 mmol) was added to the solution and shaken at room temperature for 30 minutes. The resin turned a darker

yellow color consistent with the deprotonation of the benzylidene azaGly hydrogen as previously observed. 1-iodo-2-methylpropane (0.037 mL, 0.32 mmol) was added to the reaction mixture and shaken at room temperature for 3 hours. After cleaving a small sample, and analysis by MALDI-TOF, the desired product was not observed. The semicarbazone alkylation reaction was set up again and shaken for 48 h at room temperature. After this extended reaction time, the desired product was observed by MALDI-TOF. Monoisotopic MW calculated for C₅₃H₇₈BrN₁₃O₁₁ 1150.5, found (MALDI-TOF) 1151.3 (M+H)⁺.

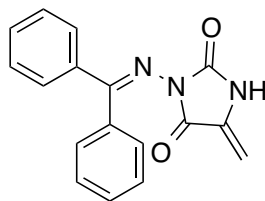
methyl *O*-(*tert*-butyl)-*N*-(2-(diphenylmethylene)hydrazine-1-carbonyl)-*L*-serinate
(220)



This molecule was prepared by adapting a literature procedure.¹⁸¹ A solution of benzophenone hydrazone (1.85 g, 9.45 mmol) in dry CH₂Cl₂ (40 mL) was cooled to 0 °C and cannulated into a 0 °C solution of disuccinimidyl carbonate (3.13 g [85% purity], 10.4 mmol) in dry CH₂Cl₂ (40 mL) and dry DMF (5 mL). The reaction was warmed to room temperature for 1 h, then cooled down to 0 °C. A 0 °C solution of H-Ser(*t*Bu)-OMe•HCl (2.00 g, 9.45 mmol) and DIPEA (3.29 mL, 18.9 mmol) in dry CH₂Cl₂ (20 mL) was then cannulated into the reaction vessel and allowed to slowly come up to room temperature over 17 h. The reaction was concentrated *in vacuo* and purified by flash chromatography (silica gel, 25% EtOAc in hexanes), yielding a light yellow sticky solid (3.13 g, 83%). (R_f 0.3 on SiO₂, 1:1 hexanes:EtOAc); [α]_D²⁶ -35.5 (*c* 1.00 CH₂Cl₂); IR

(CH₂Cl₂ cast) 3428, 3355, 3184, 3084, 3062, 2974, 2878, 1740, 1681, 1517, 1446, 1363, 1195, 1116, 1102 cm⁻¹; ¹H (CDCl₃, 500 MHz): δ 7.67 (s, 1H, =N-NH), 7.60 – 7.48 (m, 5H, Ar-H), 7.41 – 7.31 (m, 3H, Ar-H), 7.31 – 7.27 (m, 2H, Ar-H), 7.24 (d, *J* = 8.8 Hz, 1H, Ser-NH) 4.68 (ddd, *J* = 8.8, 3.1, 3.1 Hz, 1H, Ser-CH_α), 3.95 (dd, *J* = 8.9, 2.9 Hz, 1H, Ser-CH_{2β}), 3.80 (s, 3H, -OCH₃), 3.70 (dd, *J* = 8.9, 3.5 Hz, 1H, Ser-CH_{2β}), 1.25 (s, 9H, -C(CH₃)₃); ¹³C (CDCl₃, 125 MHz): δ 171.5, 155.1, 148.1, 137.0, 131.8, 129.8, 129.8, 129.3, 128.5, 128.3, 127.1, 73.5, 62.3, 53.3, 52.4, 27.4; HRMS (ES) Calculated for C₂₂H₂₈N₃O₄ 398.2074, found 398.2067 (M+H)⁺.

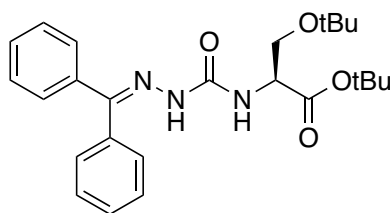
3-((diphenylmethylene)amino)-5-methyleneimidazolidine-2,4-dione (**222**)



Alkylation conditions were attempted following literature procedure.¹⁷⁸ A solution of semicarbazone **220** (0.500 g, 1.26 mmol) in dry THF (5 mL) was cooled to 0 °C prior to the addition of potassium *tert*-butoxide (1.38 mL [1.0 M solution in THF], 1.38 mmol). After 15 minutes, 1-iodo-2-methylpropane (0.159 mL, 1.38 mmol) was added at 0 °C dropwise over 2 minutes, and the reaction was stirred for 16 h in the absence of light. The product was concentrated *in vacuo* and purified by flash chromatography (silica gel, 50% EtOAc in hexanes). The unexpected hydantoin product **222** was isolated as a clear oil (0.222 g, 61%). (*R*_f 0.5 on SiO₂, 1:1 hexanes:EtOAc); ¹H (CDCl₃, 500 MHz): δ 7.74 – 7.66 (m, 2H, Ar-H), 7.57 – 7.48 (m, 1H, Ar-H), 7.48 – 7.38 (m, 4H, Ar-H), 7.38 – 7.28 (m, 3H, Ar-H), 7.05 (s, 1H, NH), 5.36 – 5.28 (m, 1H, =CHH), 4.83 (d, *J* = 2.2 Hz, 1H, =CHH); ¹³C (CDCl₃, 125 MHz): δ 180.3, 157.4, 150.7,

135.7, 134.5, 132.6, 132.3, 130.1, 130.0, 128.3, 128.3, 128.2, 127.9, 96.9; HRMS (ES)
Calculated for C₁₇H₁₄N₃NaO₄ 314.0900, found 314.0895 (M+Na)⁺.

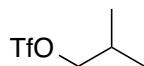
***tert*-butyl *O*-(*tert*-butyl)-*N*-(2-(diphenylmethylene)hydrazine-1-carbonyl)-*L*-serinate
(223)**



This molecule was prepared by adapting a literature procedure.¹⁸¹ A solution of benzophenone hydrazone (1.55 g, 7.88 mmol) in dry CH₂Cl₂ (30 mL) was cooled to 0 °C and cannulated into a 0 °C solution of disuccinimidyl carbonate (2.61 g [85% purity], 8.67 mmol) in dry CH₂Cl₂ (30 mL) and dry DMF (5 mL). The reaction was warmed to room temperature for 45 min, then cooled down to 0 °C. A 0 °C solution of H-Ser(tBu)-OtBu•HCl (2.00 g, 7.88 mmol) and DIPEA (2.75 mL, 15.8 mmol) in dry CH₂Cl₂ (20 mL) was then cannulated into the reaction vessel and allowed to slowly come up to room temperature over 24 h. The reaction was concentrated *in vacuo* and purified by flash chromatography (silica gel, 25% EtOAc in hexanes), yielding a light yellow sticky solid (2.94 g, 83%). (R_f 0.4 on SiO₂, 1:1 hexanes:EtOAc); [α]_D²⁶ 28.0 (*c* 1.0 CH₂Cl₂); IR (CH₂Cl₂ cast) 3425, 3173, 3059, 2975, 2932, 1751, 1743, 1693, 1518, 1367, 1161 cm⁻¹; ¹H (CDCl₃, 500 MHz): δ 7.61 (s, 1H, =N-NH), 7.58 – 7.45 (m, 5H, Ar-H), 7.38 – 7.29 (m, 3H, Ar-H), 7.29 – 7.23 (m, 2H, Ar-H), 7.17 (d, *J* = 8.9 Hz, 1H, Ser-NH), 4.55 (ddd, *J* = 8.9, 3.3, 2.9 Hz, 1H, Ser-CH_α), 3.88 (dd, *J* = 8.6, 2.9 Hz, 1H, Ser-CH₂β), 3.64 (dd, *J* = 8.6, 3.3 Hz, 1H, Ser-CH₂β), 1.50 (s, 9H, C(O)OC(CH₃)₃), 1.22 (s, 9H, -CH₂OC(CH₃)₃); ¹³C (CDCl₃, 125 MHz): δ 169.9, 155.2, 147.9, 137.1, 131.9, 129.7, 129.2, 128.5, 128.2,

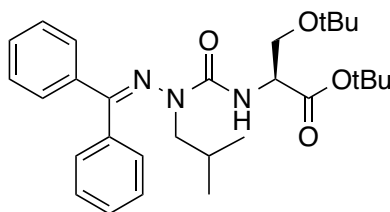
127.1, 81.6, 73.1, 62.7, 53.8, 28.1, 27.5; HRMS (ES) Calculated for C₂₅H₃₄N₃O₄ 440.2544, found 440.2549 (M+H)⁺.

2-methylpropyl trifluoromethanesulfonate (**226**)



Triflate **226** was prepared by a literature procedure.¹⁸² Isobutanol (0.14 mL, 1.49 mmol) and pyridine (0.14 mL, 1.78 mmol) were added to dry CH₂Cl₂ (5 mL) and cooled to -78 °C. Trifluoromethanesulfonic anhydride (0.25 mL, 1.50 mmol) was added dropwise over 1 minute, stirred for 5 minutes at -78 °C, then warmed to 0 °C for 25 minutes. The reaction was diluted with *n*-pentane (10 mL) and cold 1 M sulfuric acid (10 mL), the organic layer was separated, dried over Na₂SO₄, filtered and concentrated *in vacuo*. Colorless liquid **226** was used without further purification (0.195 g, 64%). ¹H (CDCl₃, 500 MHz): δ 4.31 (d, *J* = 6.4 Hz, 2H, -OCH₂), 2.12 (tsept, *J* = 6.7, 6.6 Hz, 1H, -CH(CH₃)₂), 1.03 (d, *J* = 6.8 Hz, 6H, CH(CH₃)₂); ¹³C (CDCl₃, 125 MHz): δ 118.7 (q, *J* = 319 Hz), 82.8, 28.5, 18.2; ¹⁹F (CDCl₃, 375 MHz): δ -74.8.

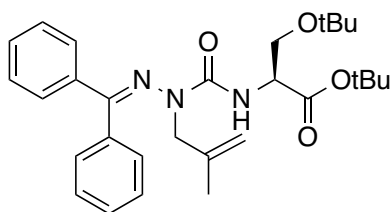
tert-butyl *O*-(*tert*-butyl)-*N*-(2-(diphenylmethylene)-1-isobutylhydrazine-1-carbonyl)-*L*-serinate (**228**)



Alkylation conditions were adapted from a literature procedure.¹⁷⁴ A solution of semicarbazone **223** (0.218 g, 0.496 mmol) in dry THF (5 mL) was cooled to 0 °C. Sodium hydride (0.021 g [60% dispersion in mineral oil], 0.52 mmol) was added and

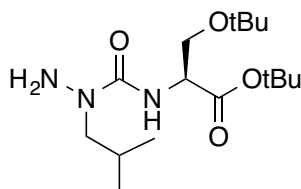
stirred for 30 minutes, after which a solution of **226** (0.153 g, 0.744 mmol) in dry THF was added and stirred at 0 °C for 6 h. The reaction was quenched by the addition of 10% citric acid (10 mL) followed by brine (10 mL). Organic components were extracted with EtOAc (3 x 30 mL), dried over Na₂SO₄, filtered and concentrated *in vacuo*. Alkylated semicarbazone **228** was purified by flash chromatography (silica gel, 15% EtOAc in hexanes) and isolated as a clear, colorless oil (0.083 g, 34%). (*R_f* 0.6 on SiO₂, 3:1 hexanes:EtOAc); [α]_D²⁶ 1.8 (*c* 1.13 CH₂Cl₂); IR (CH₂Cl₂ cast) 3423, 3060, 2973, 2934, 2873, 1746, 1687, 1496, 1367, 1154, 1055 cm⁻¹; ¹H (CDCl₃, 500 MHz): δ 7.53 (dt, *J* = 7.2, 1.4 Hz, 2H, Ar-H), 7.48 – 7.42 (m, 3H, Ar-H), 7.41 – 7.36 (m, 1H, Ar-H), 7.35 – 7.29 (m, 5H, 4 x Ar-H, Ser-NH), 4.55 (ddd, *J* = 8.7, 3.2, 3.2 Hz, 1H, Ser-CH_α), 3.83 (dd, *J* = 8.6, 3.1 Hz, 1H, Ser-CH_{2β}), 3.60 (dd, *J* = 8.6, 3.4 Hz, 1H, Ser-CH_{2β}), 3.16 (dd, *J* = 14.5, 7.7 Hz, 1H, Leu-NCH_{2β}), 3.02 (dd, *J* = 14.5, 7.2 Hz, 1H, Leu-NCH_{2β}), 1.69 (ddsept, *J* = 7.7, 7.5, 6.9 Hz, 1H, Leu-CH_γ), 1.47 (s, 9H, C(O)OC(CH₃)₃), 1.15 (s, 9H, -CH₂OC(CH₃)₃), 0.64 (d, *J* = 6.7 Hz, 6H, Leu-CH(CH₃)₂); ¹³C (CDCl₃, 125 MHz): δ 170.3, 158.7, 155.5, 138.8, 136.1, 129.7, 129.4, 128.9, 128.6, 128.3, 128.1, 81.6, 72.9, 62.8, 54.6, 51.8, 28.1, 27.4, 25.1, 19.3, 19.2; HRMS (ES) Calculated for C₂₉H₄₂N₃O₄ 496.3170, found 496.3164 (M+H)⁺.

***tert*-butyl *O*-(*tert*-butyl)-*N*-(2-(diphenylmethylene)-1-(2-methylallyl)hydrazine-1-carbonyl)-*L*-serinate (**229**)**



Alkylation conditions were adapted from a literature procedure.¹⁷⁴ Semicarbazone **223** (0.945 g, 2.15 mmol) was dissolved in THF (10 mL) and cooled to 0 °C. Aqueous tetraethylammonium hydroxide (7.91 mL [20% solution], 10.8 mmol) was added and stirred for 30 minutes, followed by the addition of 3-bromo-2-methylpropene (1.63 mL, 16.1 mmol) at 0 °C. The reaction was slowly warmed to room temperature and was quenched after 60 h by the addition of 10% citric acid (15 mL) followed by brine (15 mL). Organic components were extracted with EtOAc (3 x 75 mL), dried over Na₂SO₄, filtered and concentrated *in vacuo*. Alkylated semicarbazone **229** was purified by flash chromatography (silica gel, 20% EtOAc in hexanes) and was isolated as a yellow oil (1.06 g, 99%). (*R_f* 0.6 on SiO₂, 3:1 hexanes:EtOAc); [α]_D²⁶ 6.1 (*c* 0.75 CH₂Cl₂); IR (CH₂Cl₂ cast) 3421, 3062, 2974, 2935, 2877, 1745, 1687, 1496, 1366, 1154, 1098 cm⁻¹; ¹H (CDCl₃, 500 MHz): δ 7.50 – 7.39 (m, 6H, Ar-H, Ser-NH), 7.39 – 7.34 (m, 1H, Ar-H), 7.32 – 7.27 (m, 4H, Ar-H), 4.71 (dq, *J* = 1.4, 1.1 Hz, 1H, =CHH), 4.58 (ddd, *J* = 8.9, 3.2, 3.2 Hz, 1H, Ser-CH α), 4.48 – 4.43 (m, 1H, =CHH), 3.98 (d, *J* = 17.0 Hz, 1H, Leu-NCH β), 3.88 – 3.79 (m, 2H, Ser-CH β , Leu-NCH β), 3.62 (dd, *J* = 8.6, 3.3 Hz, 1H, Ser-CH β), 1.48 (s, 9H, C(O)OC(CH₃)₃), 1.41 – 1.32 (m, 3H, -CH₃), 1.17 (s, 9H, -CH₂OC(CH₃)₃); ¹³C (CDCl₃, 125 MHz): δ 170.2, 158.5, 154.1, 139.8, 139.2, 135.9, 129.5, 129.4, 128.3, 128.2, 128.0, 111.8, 81.3, 72.9, 62.8, 54.7, 50.6, 28.1, 27.4 19.5; HRMS (ES) Calculated for C₂₉H₄₀N₃O₄ 494.3013, found 494.3010 (M+H)⁺.

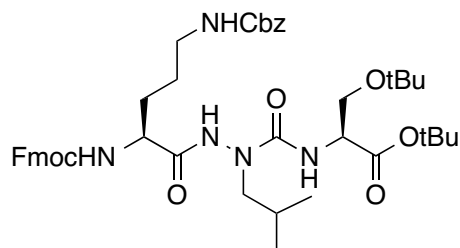
***tert*-butyl *O*-(*tert*-butyl)-*N*-(1-isobutylhydrazine-1-carbonyl)-*L*-serinate (230)**



Procedure A:¹⁷⁸ Alkylated semicarbazone **228** (0.056 g, 0.113 mmol) was dissolved in a solution of hydroxylamine hydrochloride (0.031 g, 0.452 mmol) in pyridine (15 mL) and heated to 60 °C for 18 h. The reaction was cooled to room temperature, then concentrated *in vacuo*, using CH₂Cl₂ and EtOAc co-evaporations to remove residual pyridine. The reaction was purified using flash chromatography (silica gel, 50% EtOAc in hexanes, 0.1 % DIPEA) yielding semicarbazide **230** as a yellow oil (0.010 g, 27%).

Procedure B: Alkylated semicarbazone **229** (2.19 g, 4.43 mmol) was dissolved in MeOH (50 mL) and had 10% Pd/C (20 mg) added. The suspension was stirred under hydrogen gas for 20 h, filtered through a pad of Celite, and concentrated *in vacuo*. The crude residue purified using flash chromatography (silica gel, 50% EtOAc in hexanes), yielding semicarbazide **230** as a yellow oil (1.37 g, 93%). (*R_f* 0.6 on SiO₂, 3:1 hexanes:EtOAc); [α]_D²⁶ 20.8 (*c* 0.45 CH₂Cl₂); IR (CH₂Cl₂ cast) 3420, 3331, 3217, 2974, 2934, 2873, 1741, 1656, 1509, 1366, 1232, 1157, 1100 cm⁻¹; ¹H (CDCl₃, 500 MHz): δ 7.04 (d, *J* = 9.0 Hz, 1H, Ser-NH), 4.45 (ddd, *J* = 9.0, 3.1, 3.0 Hz, 1H, Ser-CH α), 3.78 (dd, *J* = 8.6, 3.1 Hz, 1H, Ser-CH β), 3.56 (s, 2H, H₂N-N), 3.52 (dd, *J* = 8.6, 3.2 Hz, 1H, Ser-CH β), 3.36 (dd, *J* = 13.9, 7.7 Hz, 1H, Leu-NCH β), 3.26 (dd, *J* = 13.9, 7.4 Hz, 1H, Leu-NCH β), 2.01 – 1.89 (m, 1H, Leu-CH γ), 1.46 (s, 9H, C(O)OC(CH₃)₃), 1.14 (s, 9H, -CH₂OC(CH₃)₃), 0.92 (d, *J* = 6.7Hz, 3H, Leu-CH δ), 0.91 (d, *J* = 6.7Hz, 3H, Leu-CH δ); ¹³C (CDCl₃, 125 MHz): δ 170.8, 159.1, 81.1, 72.8, 63.1, 57.4, 54.4, 28.1, 27.4, 26.1, 19.9; HRMS (ES) Calculated for C₁₆H₃₄N₃O₄ 332.2544, found 332.2539 (M+H)⁺.

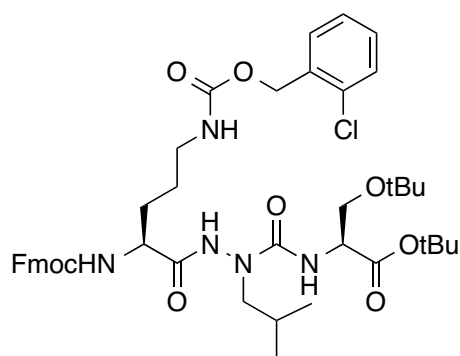
***tert*-butyl *N*-(2-((*S*)-2-(((9*H*-fluoren-9-yl)methoxy)carbonyl)amino)-5-(((benzyloxy)carbonyl)amino)pentanoyl)-1-isobutylhydrazine-1-carbonyl)-*O*-(*tert*-butyl)-*L*-serinate (**233**)**



A solution of Fmoc-Orn(Cbz)-OH (0.990 g, 2.03 mmol), HATU (0.771 g, 2.03 mmol), HOAt (3.4 mL [0.6 M solution], 2.03 mmol) and DIPEA (1.18 mL, 6.79 mmol) were dissolved in dry DMF (15 mL) and preactivated for 5 minutes before the addition of a solution of semicarbazide **230** (0.560 g, 1.69 mmol) in dry DCM (15 mL). This reaction was stirred under Ar for 24 h then concentrated *in vacuo*. The crude reaction was resuspended in EtOAc (50 mL) and washed with saturated aqueous NaHCO₃ (50 mL), water (50 mL) and brine (50 mL). Pooled aqueous layers were washed with EtOAc (2 x 50 mL), and pooled organic fractions were dried over Na₂SO₄, filtered and concentrated *in vacuo*. The reaction was purified by flash chromatography (silica gel, 50% EtOAc in hexanes) yielding azatripeptide **233** as a white solid (0.620 g, 46%), with a 29% recovery of **230** starting material. (*R*_f 0.2 on SiO₂, 1:1 hexanes:EtOAc); [α]_D²⁶ 8.9 (*c* 0.36 CH₂Cl₂); IR (CH₂Cl₂ cast) 3315, 3035, 2973, 2933, 2873, 1696, 1655, 1523, 1367, 1247, 1157, 1102, 1027 cm⁻¹; ¹H (CDCl₃, 500 MHz): δ 8.42 (s, 1H, C(O)NH-N), 7.76 (dd, *J* = 7.6, 1.0 Hz, 2H, Fmoc-Ar-H), 7.59 (d, *J* = 7.5 Hz, 2H, Fmoc-Ar-H), 7.40 (t, *J* = 7.5 Hz, 2H, Fmoc-Ar-H), 7.37 – 7.28 (m, 7H, 2 x Fmoc-Ar-H, 5 x Cbz-Ar-H), 5.83 (d, *J* = 8.2 Hz, 1H, Ser-NH), 5.61 – 5.56 (m, 1H, Orn-NH α), 5.25 – 5.18 (m, 1H, Orn-

NH ϵ), 5.13 (d, $J = 12.2$ Hz, 1H, -OCH $_2$ Ph), 5.03 (d, $J = 12.3$ Hz, 1H, -OCH $_2$ Ph), 4.49 – 4.38 (m, 3H, Ser-CH α , Orn-CH α , Fmoc-CH $_2$), 4.37 – 4.31 (m, 1H, Fmoc-CH $_2$), 4.20 (t, $J = 7.0$ Hz, 1H, Fmoc-CH), 3.71 (dd, $J = 8.7, 2.9$ Hz, 1H, Ser-CH $_2\beta$), 3.59 – 3.36 (m, 3H, Ser-CH $_2\beta$, Orn-CH $_2\delta$, Leu-NCH $_2\beta$), 3.34 – 3.25 (m, 1H, Leu-NCH $_2\beta$), 3.22 – 3.14 (m, 1H, Orn-CH $_2\delta$), 1.99 – 1.90 (m, 1H, Orn-CH $_2\beta$), 1.88 – 1.77 (m, 1H, Leu-CH γ), 1.74 – 1.55 (m, 3H, Orn-CH $_2\beta$, 2 x Orn-CH $_2\gamma$), 1.41 (s, 9H, C(O)OC(CH $_3$) $_3$), 1.08 (s, 9H, -CH $_2$ OC(CH $_3$) $_3$), 0.94 – 0.86 (m, 6H, 2 x Leu-CH $_3\delta$); ^{13}C (CDCl $_3$, 125 MHz): δ 171.1, 170.3, 157.3, 156.9, 156.4, 143.7, 143.7, 141.3, 136.4, 128.6, 128.5, 128.5, 128.2, 128.1, 127.8, 127.1, 125.1, 120.0, 81.6, 72.9, 67.3, 66.9, 62.6, 55.5, 54.5, 52.1, 47.1, 39.6, 29.9, 28.3, 28.1, 27.4, 26.9, 26.3, 25.7, 20.0; HRMS (ES) Calculated for C $_{44}$ H $_{60}$ N $_5$ NaO $_9$ 824.4205, found 824.4204 (M+H) $^+$.

***tert*-butyl *N*-(2-((*S*)-2-(((9*H*-fluoren-9-yl)methoxy)carbonyl)amino)-5-(((2-chlorobenzyl)oxy)carbonyl)amino)pentanoyl)-1-isobutylhydrazine-1-carbonyl)-*O*-(*tert*-butyl)-*L*-serinate (234)**

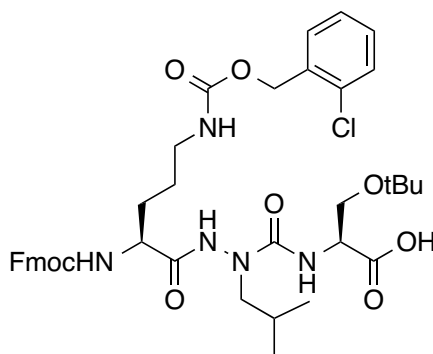


A solution of Fmoc-Orn(2-Cl-Cbz)-OH (2.59 g, 4.91 mmol), HATU (1.87 g, 4.91 mmol), HOAt (0.82 mL [0.6 M solution], 0.49 mmol) and DIPEA (2.14 mL, 12.3 mmol) were dissolved in dry DMF (20 mL) and preactivated for 5 minutes before the

addition of a solution of semicarbazide **230** (1.36 g, 4.09 mmol) in dry DCM (20 mL). This reaction was stirred under Ar for 30 h then concentrated *in vacuo*. The crude reaction was resuspended in EtOAc (100 mL) and washed with 10% citric acid (2 x 100 mL) and brine (100 mL). Pooled aqueous layers were washed with EtOAc (2 x 100 mL), and pooled organic fractions were dried over Na₂SO₄, filtered and concentrated *in vacuo*. The reaction was purified by flash chromatography (silica gel, 40% EtOAc in hexanes) yielding azatripeptide **233** as a white solid (2.64 g, 77%), with a 17% recovery of **230** starting material. (*R_f* 0.2 on SiO₂, 1:1 hexanes:EtOAc); [α]_D²⁶ 11.8 (*c* 1.00 CHCl₃); IR (CHCl₃ cast) 3321, 3007, 2974, 2934, 2873, 1700, 1657, 1523, 1450, 1367, 1247, 1157 cm⁻¹; ¹H (CDCl₃, 500 MHz): δ 8.31 (s, 1H, C(O)NH-N), 7.79 – 7.74 (m, 2H, Fmoc-Ar-H), 7.59 (d, *J* = 7.5 Hz, 2H, Fmoc-Ar-H), 7.39 (m, 4H, 2 x Fmoc-Ar-H, 2 x 2-Cl-Ar-H), 7.34 – 7.28 (m, 2H, Fmoc-Ar-H), 7.27 – 7.23 (m, 2H, 2 x 2-Cl-Ar-H), 5.82 (d, *J* = 8.2 Hz, 1H, Ser-NH), 5.53 (d, *J* = 7.8 Hz, 1H, Orn-NH α), 5.27 – 5.20 (m, 2H, -OCH₂(2-Cl)Ph, Orn-NH ϵ), 5.16 (d, *J* = 13.0 Hz, 1H, -OCH₂(2-Cl)Ph), 4.48 – 4.38 (m, 3H, Ser-CH α , Orn-CH α , Fmoc-CH₂), 4.38 – 4.32 (m, 1H, Fmoc-CH₂), 4.21 (t, *J* = 7.0 Hz, 1H, Fmoc-CH), 3.71 (dd, *J* = 8.8, 2.8 Hz, 1H, Ser-CH₂ β), 3.54 – 3.45 (m, 2H, Ser-CH₂ β , Orn-CH₂ δ), 3.44 – 3.36 (m, 1H, Leu-NCH₂ β), 3.33 – 3.24 (m, 1H, Leu-NCH₂ β), 3.24 – 3.15 (m, 1H, Orn-CH₂ δ), 2.00 – 1.90 (m, 1H, Orn-CH₂ β), 1.86 – 1.77 (m, 1H, Leu-CH γ), 1.75 – 1.56 (m, 3H, Orn-CH₂ β , 2 x Orn-CH₂ γ), 1.41 (s, 9H, C(O)OC(CH₃)₃), 1.08 (s, 9H, -CH₂OC(CH₃)₃), 0.89 (d, *J* = 6.6 Hz, 6H, 2 x Leu-CH₃ δ); ¹³C (CDCl₃, 125 MHz): δ 173.7, 170.2, 157.1, 156.7, 156.4, 143.6, 141.3, 134.1, 133.5, 129.7, 129.5, 129.4, 127.8, 127.1, 126.8, 125.1, 120.0, 81.6, 72.9, 67.3, 64.1, 62.6, 55.4, 54.5, 52.1, 47.1, 39.7, 29.8,

28.0, 27.3, 26.9, 26.2, 20.0, 20.0; HRMS (ES) Calculated for C₄₄H₅₉ClN₅O₉ 836.3996, found 836.4008 (M+H)⁺.

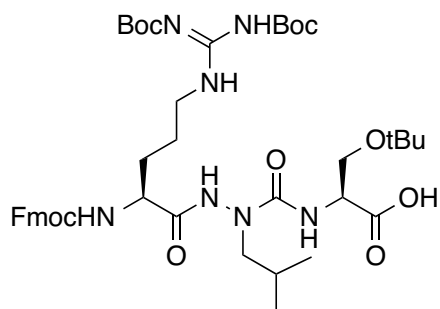
N-***(2-(((S)***-***2-(((9H***-fluoren-9-yl)methoxy)carbonyl)amino)-5-(((2-chlorobenzyl)oxy)carbonyl)amino)pentanoyl)-1-isobutylhydrazine-1-carbonyl)-*O*-(*tert*-butyl)-*L*-serine (237)



Azatripeptide **234** (1.21 g, 1.44 mmol) was dissolved in toluene (100 mL) and had flash-grade silica (25.0 g) added. This suspension was refluxed at 115 °C for 95 minutes, checking TLC and LC-MS every 30 minutes. The reaction was cooled to room temperature and a 10% MeOH in CH₂Cl₂ solution (100 mL) was added, then filtered through a pad of Celite. The reaction was concentrated *in vacuo*, and purified by flash chromatography (silica gel, 0-2% MeOH in EtOAc, 0.1% AcOH). The desired product was obtained as a sticky white solid (0.770 g, 69%). (*R*_f 0.3 on SiO₂, 1:4 hexanes:EtOAc, 0.1% AcOH); [α]_D²⁶ 14.5 (*c* 1.00 CHCl₃); IR (CHCl₃ cast) 3313, 3018, 2971, 2874, 1697, 1528, 1450, 1249, 1193, 1104 cm⁻¹; ¹H (CDCl₃, 500 MHz): δ 8.10 (s, 1H, C(O)NH-N), 7.71 (d, *J* = 7.6 Hz, 2H, Fmoc-Ar-H), 7.54 (d, *J* = 7.5 Hz, 2H, Fmoc-Ar-H), 7.40 – 7.29 (m, 4H, 2 x Fmoc-Ar-H, 2 x 2-Cl-Ar-H), 7.29 – 7.16 (m, 4H, 2 x Fmoc-Ar-H, 2 x 2-Cl-Ar-H), 6.05 (br s, 1H, Ser-NH), 5.53 (br s, 1H, Orn-NHα), 5.22 – 5.11 (m, 2H, -OCH₂(2-Cl)Ph), 4.42 – 4.37 (m, 2H, Ser-CHα, Fmoc-CH₂), 4.35 – 4.27

(m, 1H, Orn-CH α), 4.25 – 4.17 (dd, $J = 10.1, 8.7$ Hz, 1H, Fmoc-CH $_2$), 4.14 (t, $J = 8.3$ Hz, 1H, Fmoc-CH), 3.76 – 3.68 (m, 1H, Ser-CH $_2\beta$), 3.52 – 3.46 (m, 1H, Ser-CH $_2\beta$), 3.33 – 3.13 (m, 4H, 2 x Orn-CH $_2\delta$, 2 x Leu-NCH $_2\beta$), 1.89 – 1.80 (m, 1H, Orn-CH $_2\beta$), 1.79 – 1.65 (m, 2H, Orn-CH $_2\beta$, Leu-CH γ), 1.62 – 1.54 (m, 2H, Orn-CH $_2\gamma$), 1.02 (s, 9H, -CH $_2$ OC(CH $_3$) $_3$), 0.83 (d, $J = 6.5$ Hz, 3H, Leu-CH $_3\delta$), 0.81 (d, $J = 6.5$ Hz, 3H, Leu-CH $_3\delta$); ^{13}C (CDCl $_3$, 125 MHz): δ 171.8, 170.4, 159.7, 158.3, 156.6, 143.6, 141.2, 134.2, 133.4, 129.6, 129.5, 129.3, 127.8, 127.1, 126.9, 125.1, 120.0, 73.6, 67.3, 63.9, 62.1, 55.7, 55.2, 52.5, 47.0, 39.9, 29.7, 27.3, 27.0, 25.9, 20.0; HRMS (ES) Calculated for C $_{40}$ H $_{49}$ ClN $_5$ O $_9$ 778.3224, found 778.3208 (M-H) $^-$.

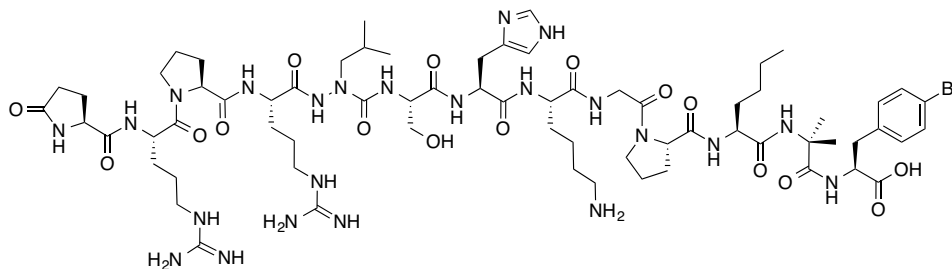
***N*-((*S*)-5-(((9*H*-fluoren-9-yl)methoxy)carbonyl)amino)-10-((*tert*-butoxycarbonyl)amino)-2-isobutyl-14,14-dimethyl-4,12-dioxo-13-oxa-2,3,9,11-tetraazapentadec-10-enoyl)-*O*-((*tert*-butyl)-*L*-serine (238)**



A solution of **237** (0.730 g, 0.94 mmol) in MeOH (50 mL) had 10% Pd/C (25 mg) added, and the suspension was stirred under an atmosphere of hydrogen gas for 135 minutes. The reaction mixture was filtered through a pad of Celite, concentrated *in vacuo* to dryness, and resuspended in dry CH $_2$ Cl $_2$ (30 mL) with triethylamine (0.59 mL, 4.21 mmol) and 1,3-di-Boc-2-(trifluoromethylsulfonyl)guanidine (0.549 g, 1.40 mmol) for 30 h. Solvents were removed *in vacuo* and the azatripeptide product was purified

using flash chromatography (silica gel, 90% EtOAc in hexanes, 0.1 % AcOH), yielding white solid **238** (0.161 g, 20%). (R_f 0.1 on SiO₂, 1:4 hexanes:EtOAc, 0.1% AcOH); $[\alpha]_D^{26}$ 2.3 (c 0.85 CHCl₃); IR (CHCl₃ cast) 3326, 2978, 2934, 1722, 1644, 1531, 1368, 1331, 1136, 1054 cm⁻¹; ¹H (CDCl₃, 500 MHz): δ 8.94 (br s, 1H, C(O)NH-N), 8.46 (br s, 1H, Arg-NH ϵ), 7.75 (d, J = 7.6 Hz, 2H, Ar-H), 7.58 (d, J = 7.6 Hz, 2H, Ar-H), 7.39 (t, J = 7.5 Hz, Ar-H), 7.30 (t, J = 7.5 Hz, 2H, Ar-H), 6.16 (br s, 1H, Arg-NH α), 6.08 (s, 1H, Ser-NH), 4.49 – 4.40 (m, 3H, Arg-CH α , Ser-CH α , Fmoc-CH₂), 4.34 – 4.28 (m, 1H, Fmoc-CH₂), 4.18 (t, J = 7.0 Hz, 1H, Fmoc-CH), 3.81 – 3.75 (m, 1H, Ser-CH₂ β), 3.61 – 3.49 (m, 1H, Ser-CH₂ β), 3.49 – 3.24 (m, 4H, 2 x Arg-CH₂ δ , 2 x Leu-NCH₂ β), 1.92 – 1.83 (m, 1H, Arg-CH₂ β), 1.81 – 1.60 (m, 4H, Arg-CH₂ β , 2 x Arg-CH₂ γ , Leu-CH γ), 1.50 (s, 9H, Arg-C(CH₃)₃), 1.47 (s, 9H, Arg-C(CH₃)₃), 1.12 (s, 9H, -CH₂OC(CH₃)₃), 0.91 – 0.85 (m, 6H, 2 x Leu-CH₃ δ); ¹³C (CDCl₃, 125 MHz): δ 171.1, 170.2, 163.3, 162.4, 157.7, 156.5, 153.2, 143.7, 141.3, 127.8, 127.1, 125.0, 120.0, 83.6, 79.9, 74.7, 67.3, 61.5, 55.8, 54.0, 53.1, 47.1, 40.4, 29.4, 28.3, 28.0, 27.3, 27.0, 25.5, 20.2, 20.1; HRMS (ES) Calculated for C₄₃H₆₄N₇O₁₁ 854.4658, found 854.4654 (M+H)⁺.

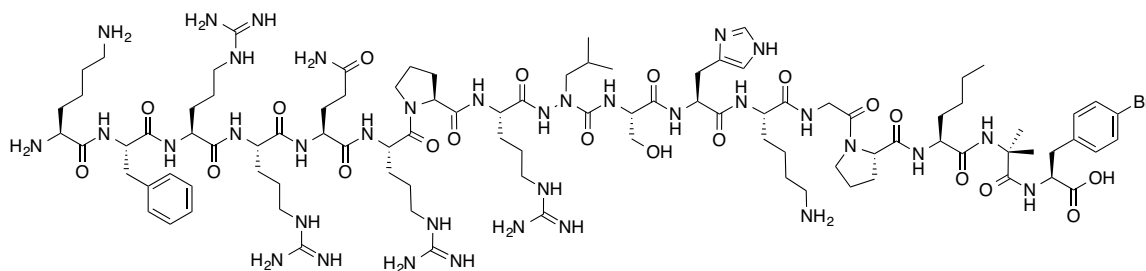
azaLeu5-pyr-1-apelin-13 A2 (**239**)



Advanced intermediate **153** (0.2 mmol) was subjected to manual SPPS, introducing amino acids in the following order: **238**, Fmoc-Pro-OH, and Fmoc-Arg(Pmc)-OH. The resin was split into half, and Fmoc-SPPS was continued on 0.1

mmol scale, coupling pyr-Glu-OH. No endcapping was performed following addition of **238**. A portion (0.05 mmol) of resin-bound peptide **239** was cleaved as previously described and purified using a C₁₈ RP-HPLC analytical column (Method B), eluting at 13.3 min. The desired peptide was isolated as a white solid after lyophilization (4.8 mg, 6%). Monoisotopic MW calculated for C₆₈H₁₁₁BrN₂₃O₁₆ 528.2582, found *high resolution* (FTICR-ESI-MS) 528.2576 (M+3H)³⁺.

azaLeu9-pyr-1-apelin-13 A2 (240)



The remaining 0.1 mmol carried over from the synthesis of **239** was coupled with Fmoc-Gln(Trt)-OH, Fmoc-Arg(Pmc)-OH, Fmoc-Arg(Pmc)-OH, Fmoc-Phe-OH, and Fmoc-Lys(Boc)-OH. A portion (0.05 mmol) of resin-bound peptide **240** was cleaved as previously described and purified using a C₁₈ RP-HPLC analytical column (Method B), eluting at 11.3 min. The desired peptide was isolated as a white solid after lyophilization (4.4 mg, 4%). Monoisotopic MW calculated for C₉₅H₁₆₀BrN₃₅O₂₀ 547.5435, found *high resolution* (FTICR-ESI-MS) 547.5420 (M+4H)⁴⁺.

4.3.12 Apelin biological experiments

4.3.12.1 rhACE2 *in vitro* assay

ACE2 assays were performed according to literature procedure.¹²⁴ Apelin peptides (pyr-1-apelin-13 and apelin-17, Tocris Bioscience) were diluted to 400 μM in

Milli-Q water. Recombinant human ACE2 (rhACE2) was diluted to 40 nM in MES buffer (50 mM MES, 300 mM NaCl, 10 μ M ZnCl₂, 0.01% Brij-35 pH 6.5). Apelin (5 μ L) was diluted in MES buffer (45 μ L) and had 50 μ L of rhACE2 added and incubated at 37 °C for a defined period of time (final [apelin] = 20 μ M, [rhACE2] 20 nM). Assays were quenched by the addition of 100 μ L of EDTA (100 mM, pH 7.0) and 5 μ L of 1 mM Fmoc-Asp-OH was added as an internal standard. Assays were diluted with Milli-Q water up to 1 mL and analyzed by C₁₈ RP-HPLC (Vydac Protein-Peptide Column 300 Å, 5 μ m, 4.6 mm x 250 mm). Peptides were separated using the following method:

0 – 3 min	10% B
3 – 23 min	10 – 45% B
23 – 25 min	45 – 100% B
25 – 26 min	100% B
26 – 27.25 min	100 – 10% B
27.25 – 30 min	10% B

where (A = 0.1% aqueous TFA; B = 0.1% TFA in acetonitrile). The extent of proteolysis was done by comparing the areas of substrate and product peaks (area of product peak/(area of product peak + area of substrate peak)).

4.3.12.2 ACE2 kinetic determination of apelin peptides

ACE2 assays were set up as previously outlined, varying the concentration of apelin peptides (5, 20, 50 and 100 μ M). The percentages of apelin degradation products were converted to micromoles of product formed and used to calculate the initial velocities of apelin substrate degradation. These initial velocities were graphed against substrate concentration and analyzed using GraphPad PRISM version 4.0 software to

determined kinetic parameters. A calculated ACE2 molecular mass of 85 kDa was used to determine the turnover number (k_{cat}) analogous to that previously reported.¹²⁴

4.3.12.3 Isolation and quantification of apelin peptides from plasma

20 μ L of plasma was portioned into microfuge tubes and pre-warmed to 37 °C. 5 μ L of apelin peptide (400 μ M) was added and incubated at 37 °C for varying lengths of time. Experiments were quenched by the addition of 20 μ L of 10% aqueous TFA. 5 μ L of internal standard (mouse plasma: 1 mM Fmoc-Asp-OH; human plasma: 1 mM dansyl-Tyr-Val-Gly-OH) was added and experiments were diluted up to 100 μ L with 0.1% aqueous TFA. These assays were loaded onto a pre-equilibrated C₁₈ spin column (Harvard Apparatus), which had previously been wet with 2 x 300 μ L 50% acetonitrile in 0.1% aqueous TFA and 2 x 300 μ L 0.1 % aqueous TFA respectively, centrifuging at 300 x *g* for 2 minutes between each 300 μ L aliquot. Quenched plasma assays were centrifuged at 300 x *g* until the sample was loaded. The resultant filtrate was reloaded onto the column along with 100 μ L 0.1% aqueous TFA and centrifuged at 300 x *g* two additional times. The desired plasma peptides were washed by the addition of 2 x 300 μ L 0.1% aqueous TFA and centrifuged at 300 x *g* for 2 min, discarding the filtrate after each wash. Desired peptides were eluted by the addition of 300 μ L of either 75% acetonitrile (mouse plasma) or 40% acetonitrile (human plasma) in 0.1% aqueous TFA and centrifugation at 300 x *g* for 2 minutes. Eluted samples were diluted with 0.1 % aqueous trifluoroacetic acid prior to analysis by C₁₈ RP-HPLC. To analyze the remaining percentage of apelin peptides in plasma, incubations of pyr-1-apelin-13 or apelin-17 in plasma were immediately quenched, worked up and analyzed by C₁₈ RP-HPLC as previously described, and the ratio of apelin peptide to internal standard was calculated

based on the area under the peaks. This 0 minute incubation ratio was used to compare the apelin peptide:internal standard ratios for the time experiments.

4.3.12.4 LC MS/MS protocol to identify initial sites of apelin degradation in plasma

A C18 solid phase extraction column (Phenomenex, Strata C18-E) was opened and 100 mg portions of silica were measured into glass pipettes stoppered by a glass wool plug. The silica was washed with 1 mL ethanol (100%) and then 1 mL Milli-Q water. 100 μ L aliquots of plasma (mouse or human) were warmed to 37 °C prior to the addition of 5 μ L of pyr-1-apelin-13 A1 (**103**) or A2 (**104**) analogue (1 mM) for a defined period of time. After the time point was complete, samples were immediately put on ice and acidified by the addition of 300 μ L 1% aqueous acetonitrile, 0.1% TFA. Samples were loaded onto the C18 silica and washed twice with 300 μ L 1% aqueous acetonitrile, 0.1% TFA. The resin-bound peptides were washed with 1 mL of Milli-Q water, then 1 mL of 4 : 6 (H₂O saturated *n*-butanol : diisopropylether), and finally eluted with 1 mL of 90% aqueous methanol. Samples were concentrated *in vacuo* to approximately 100 μ L and analyzed by C18 RP-HPLC, MALDI-TOF, and submitted to Jing Zheng for LC-MS/MS.

4.3.12.5 FRET assay protocol

These protocols were modified from a literature procedure.¹⁵⁰ Briefly, a 1 mM solution of fluorescent probe **141** (10 μ L) and additional additives (10 μ L each) were dissolved in sodium phosphate buffer (67 mM, pH 7.6; 100 μ L total volume) and incubated for a defined period of time. Solutions were analyzed by fluorometry using a 1 nm bandwidth diffraction filter for both the excitation and emission filters. A negative

control (10 μ L of **141** in 90 μ L of buffer) was used to determine the excitation and emission maxima ($\lambda_{\text{ex}} = 325$ nm, $\lambda_{\text{em}} = 420$ nm). Fluorescent counts at 420 nm were used to characterize the liberation of the unquenched 2-Abz fluorophore-containing peptide fragments.

4.3.12.6 Plasma protease isolation

Ammonium sulfate precipitation – An aliquot of human blood plasma (200 μ L) was diluted by the addition of Milli-Q water (800 μ L). Ammonium sulfate (0.200 g) was added to the solution and shaken at 4 $^{\circ}$ C for 15 minutes. Precipitated proteins were pelleted by centrifugation (10000 \times g, 15 minutes, 4 $^{\circ}$ C), the supernatant was decanted into a fresh tube and the 20% ammonium sulfate precipitation (20% ASP) was resuspended in 1 mL of sodium phosphate buffer (67 mM, pH 7.6). The decanted supernatant had additional ammonium sulfate (0.200 g) added, shaken at 4 $^{\circ}$ C for 15 minutes and the resultant 40% ammonium sulfate precipitation (40% ASP) was collected and resuspended in an analogous manner to the 20% ASP. The remaining 40% ammonium sulfate supernatant was spin concentrated using a 10 kDa MWCO Amicon filter centrifugation tube, using sodium phosphate buffer (67 mM, pH 7.6) to exchange the buffer to a final volume of 1 mL. FRET assays were performed as described above.

Size exclusion chromatography – Sephadex G-100 (Sigma-Aldrich, 4.3 g) was suspended in 100 mL of sodium phosphate buffer (67 mM, pH 7.6) and occasionally mixed over 3 hours. The resin was loaded onto a biological column and 1 mL of the 40% ASP was loaded onto the top of the column. The column was run at 0.2 mL/min using a BIORAD collector with UV monitoring, collecting fractions every 5 minutes. A large UV peak was observed from 120-210 minutes, with the maximum at 180 minutes.

Every second fraction within this region was assayed by FRET, using 50 μL of the size exclusion fraction, 10 μL of **141** (1mM), and 40 μL of sodium phosphate buffer (67 mM, pH 7.6).

Trypsin digestion – 20 μL aliquots of active size exclusion fractions, and a solution of bovine serum albumin (10 mg/mL, Sigma-Aldrich) used to serve as a positive control for trypsin activity, were individually mixed with 100 μL ammonium bicarbonate (100 mM). 10 μL of freshly prepared DTT (100 mM) was added and incubated at 50 °C for 30 minutes. After cooling, 10 μL of freshly prepared iodoacetamide (200 mM) was added and incubated at room temperature for 20 minutes in the dark to alkylate cysteines. 5 μL of Trypsin Gold (0.5 mg/mL) was added and the reactions were held at 37 °C for 3 hours, followed by a room temperature incubation for an additional 3 hours. Samples were diluted by the addition of 500 μL of 0.1% aqueous TFA, and peptide components were isolated through the use of C18 ZipTip (Millipore), eluting with 50% aqueous acetonitrile, 0.1% TFA. LC-MS/MS determination was subsequently performed on peptide samples.

4.3.12.7 pI approximation

9 x 250 μL aliquots of ion exchange resin (Q Sepharose, Pharmacia; SP-sepharose, Sigma-Aldrich) were partitioned into individual Eppendorf tubes and centrifuged (1 min, 1000 x g) to precipitate the resin. The storage buffer was decanted off the top, and 750 μL of Tris buffer (20 mM) ranging from pH 5.0 – 9.0 (0.5 pH increments) was added to each Eppendorf tube and vortexed. The resin was pelleted via centrifugation (1 min, 100 x g), the supernatant was decanted, and the resin was

resuspended in the same pH Tris buffer. This procedure was repeated an additional 3 times to pre-equilibrate the resin. After equilibration, the resin was shaken overnight at 4 °C in the appropriate pH Tris buffer, then centrifuged and decanted as previously described.

Simultaneously, 1 mL of the 40% ASP, in sodium phosphate buffer (67 mM, pH 7.6) was spin concentrated in a 10000 MWCO tube (Amicon) and rinsed three times with Milli-Q water to remove salts and neutralize the pH, concentrating after each rinse. After concentration, the 40% ASP was diluted up to 1 mL with Milli-Q water and 9 x 50 µL aliquots were portioned into Eppendorf tubes. These tubes were individually diluted with 450 µL of Tris buffer (20 mM) of pHs ranging from 5.0 – 9.0 (0.5 pH increments) and incubated overnight at their respective pHs at 4 °C, giving a ‘pH-adjusted 40% ASP fraction.’

After overnight incubations, 450 µL of the pH 5.0 incubated 40% ASP fraction was added to the pH 5.0 incubated ion exchange resin, performing a similar technique for the 8 other pH fractions. The remaining 50 µL of ‘pH-adjusted 40% ASP fraction’ were saved for control experiments. These fractions were incubated at room temperature for 30 minutes with shaking. The resin was pelleted by centrifugation (1 min, 1000 x g) and the supernatant was pipetted off the top. Assays were set up by incubating 50 µL of ion exchange resin incubated supernatant with 10 µL **141** (1 mM) and 40 µL of 20 mM Tris buffer, and compared to the negative control (10 µL **141** (1 mM) and 90 µL of 20 mM Tris buffer) and positive control (50 µL pH-adjusted 40% ASP fraction, 10 µL **141** (1 mM) and 40 µL of 20 mM Tris buffer) at the equivalent pH. Assays were incubated at

room temperature for equivalent amounts of time to the controls (4 h for Q-sepharose binding, 6 h for SP-sepharose binding) and assayed via fluorimetry (Table 4.4).

Table 4.4 – Ion exchange binding experiments of pH adjusted 40% ASP fractions (n = 1), with all data in counts x 10⁵ at 420 nm.

pH	Q-Sepharose			SP-Sepharose		
	neg. cont.	pos. cont.	Q-seph	neg. cont.	pos. cont.	SP-seph
5.0	7.6	7.4	7.1	7.6	6.2	5.9
5.5	6.8	9.4	7.4	6.8	7.1	6.1
6.0	6.5	11.4	5.8	6.5	8.5	7.8
6.5	5.9	14.4	5.8	5.9	8.8	7.4
7.0	5.0	13.0	4.7	5.0	8.2	7.2
7.5	3.4	11.4	3.5	3.4	7.2	6.2
8.0	2.6	11.2	2.7	2.6	6.2	5.5
8.5	2.3	9.9	2.3	2.3	5.5	4.5
9.0	2.15	7.0	2.15	2.15	4.8	4.0

4.3.12.8 Inhibition experiments

Aqueous solutions (10 mM) of AEBSF (4-(2-aminoethyl)benzenesulfonyl fluoride), IA (iodoacetamide), EDTA (ethylenediaminetetraacetic acid), and TCEP (tris (2-carboxyethyl)phosphine)) were prepared alongside a 10 mM solution of PMSF (phenylmethylsulfonyl fluoride) in 2-propanol. Assays were set up as follows: 10 µL of 40% ASP in 70 µL of Tris buffer (20 mM, pH 6.0) had 10 µL of inhibitor solution (10 mM) added and preincubated for 5 minutes prior to the addition of 10 µL of **141** (1 mM). These were compared to negative control experiments (10 µL of 40% ASP in 80 µL of Tris buffer (20 mM, pH 6.0) with 10 µL of **141** (1 mM)) by fluorimetry assays (Table 4.5).

Table 4.5 – Inhibition experiments of 40% ASP fractions, with all data in fluorescent counts x 10⁵ at 420 nm.

Inhibitor	neg. cont.	Inhibitor exp. 1	Inhibitor exp. 2
AEBSF	5.1	8.6	9.2
PMSF	6.6	7.6	8.1
EDTA	4.9	5.0	5.1
IA	5.3	10.1	11.3
TCEP	6.1	5.7	5.6

4.3.12.9 Mouse endoproteinase ArgC assays

Murine endoproteinase ArgC from submaxillaris glands (Boehringer Mannheim GmbH) was thawed from -20 °C and 10 µL were aliquoted into 80 µL Tris buffer (100 mM, pH 8.0). 10 µL of apelin peptide (400 µM) was added to this solution and incubated at 37 °C for varying lengths of time (90 minutes, 24 hours) prior to analysis by C18 RP-HPLC.

4.3.12.10 Plasma kallikrein activation

This protocol was modeled after that proposed by the commercial supplier of the kallikrein proteins. Briefly, recombinant human plasma kallikrein (rhKLKB1, 10 µg, R&D systems) was suspended in kallikrein storage buffer (25 mM MES, 150 mM NaCl, pH 5.5) at a concentration of 500 µg/mL and stored at -20 °C. To activate this zymogen, a portion of the rhKLKB1 solution was diluted to 200 µg/mL in activation buffer (50 mM Tris, 10 mM CaCl₂, 150 mM NaCl, pH 7.5). A separate solution of thermolysin (880 µg/mL, R&D systems) was prepared by diluting the stock solution to 20 µg/mL in activation buffer. Equivalent volumes of the 200 µg/mL rhKLKB1 solution and the 20

$\mu\text{g/mL}$ thermolysin solution were mixed together and incubated at $37\text{ }^{\circ}\text{C}$ for 30 minutes. The thermolysin was inactivated by the addition of an equivalent volume of EDTA (100 mM, pH 7.0) to the reaction mixture. The activated kallikrein solution was diluted to a working concentration of $0.5\text{ }\mu\text{g/mL}$ by the addition of Tris assay buffer (50 mM Tris, 250 mM NaCl, pH 7.5).

4.3.12.11 Tissue kallikrein activation

The activation protocols were modeled after those proposed by the commercial supplier of the kallikrein proteins. Recombinant human tissue kallikrein (rhKLK1, 10 μg , R&D systems) was provided in a storage buffer (25 mM Tris, 5 mM CaCl_2 , 150 mM NaCl, pH 7.5) at a concentration of 459 $\mu\text{g/mL}$ and stored at $-20\text{ }^{\circ}\text{C}$. To activate this zymogen, a portion of the rhKLK1 solution was diluted to 200 $\mu\text{g/mL}$ in activation buffer (50 mM Tris, 10 mM CaCl_2 , 150 mM NaCl, pH 7.5). Two procedures were employed to prepare this activated rhKLK1 solution:

Protocol A – The literature protocol involved the preparation of a 2 $\mu\text{g/mL}$ solution of thermolysin (880 $\mu\text{g/mL}$, R&D systems) in activation buffer. Equivalent volumes of the 200 $\mu\text{g/mL}$ rhKLKB1 solution and the 2 $\mu\text{g/mL}$ thermolysin solution were mixed together and incubated at $37\text{ }^{\circ}\text{C}$ for 60 minutes. The thermolysin was inactivated by the addition of an equivalent volume of freshly prepared aqueous 1,10-phenanthroline (20 mM, prepared from a 0.6 M DMSO stock) to the reaction mixture. The activated kallikrein solution was diluted to a working concentration of $0.4\text{ }\mu\text{g/mL}$ by the addition of CHES assay buffer (50 mM CHES, 250 mM NaCl, pH 10.0).

Protocol B – An aliquot of the 200 $\mu\text{g}/\text{mL}$ rhKLK1 solution was mixed with an equivalent volume of a 20 $\mu\text{g}/\text{mL}$ thermolysin solution and incubated at 37 °C for 60 minutes. The thermolysin was inactivated by the addition of a freshly prepared aqueous 1,10-phenanthroline solution (20 mM, prepared from a 0.6 M DMSO stock), adding 10 times the reaction volume to compensate for the additional thermolysin. The activated kallikrein solution was diluted to a working concentration of 0.4 $\mu\text{g}/\text{mL}$ by the addition of Tris assay buffer (50 mM Tris, 250 mM NaCl, pH 7.5).

4.3.12.12 Kallikrein FRET experiments

An aqueous 200 μM solution of H-Pro-Phe-Arg-AMC acetate salt (PFR-AMC, Bachem) was prepared in assay buffer (CHES buffer for rhKLK1-**Protocol A**, Tris buffer for rhKLKB1 and rhKLK1-**Protocol B**). This PFR-AMC solution (50 μL) was added to a solution of activated kallikrein enzyme (10 μL) diluted in assay buffer (40 μL) and was immediately analyzed by fluorescence ($\lambda_{\text{ex}} = 380 \text{ nm}$, $\lambda_{\text{em}} = 460 \text{ nm}$, 1 nm slit bandwidth). Fluorescent counts were read every 1 s over 300 s to determine the relative extent of activation.

4.3.12.13 Kallikrein MALDI assays

A solution of activated kallikrein enzyme (10 μL) in assay buffer (85 μL) had a 400 μM solution of apelin peptide (5 μL) added to it and incubated at 37 °C. At desired time points, 1 μL aliquots of the reaction mixture were removed, mixed with 9 μL of 10% TFA, then 1 μL of this dilution was mixed with 1 μL of HCCA layer 2 and MALDI analysis was performed as previously described.

4.3.12.14 Plasma quantification procedure

80 μL of human plasma was portioned into an Eppendorf tube and pre-warmed to 37 $^{\circ}\text{C}$. 20 μL of apelin peptide (400 μM) was added and thoroughly mixed by pipetting. 20 μL of the mixture was immediately removed and quenched into 20 μL of 10% aqueous TFA ($t = 0$ min). 20 μL aliquots were removed every ten minutes and quenched in an analogous manner, generating 10, 20 and 30-minute time experiments. 5 μL of internal standard (1 mM dansyl-Tyr-Val-Gly-OH) were added, isolating peptide components by C_{18} spin columns (Harvard Apparatus) as previously described. After sample elution, samples were concentrated via spin concentration, resolubilized in 15 μL of water and 1.5 μL of acetonitrile and submitted to Mr. Bela Reiz for HPLC-UV-MS analysis.

RP-HPLC-UV-MS was performed using an Agilent 1200 SL HPLC System with a Phenomenex, C8, 300A, 2.1x50mm column with guard, thermostated at 40 $^{\circ}\text{C}$ and a buffer gradient system composed of 0.1% formic acid in water as mobile phase A and 0.1% formic acid in acetonitrile as mobile phase B.

For the detection of peptides samples were resolubilized in 15 μL of water and 1.5 μL of ACN and loaded onto the column at a flow rate of 0.50 mL/min and an initial buffer composition of 98% mobile phase A and 2% mobile phase B. After injection, the following method was used to resolve peptide components:

0 – 2 min	2% B
2 – 30 min	2 – 30% B
30 – 40 min	30 – 65% B
40 – 44 min	65 – 95% B

44 – 45 min 95 – 2% B

Blank runs were run between sample runs to ensure peptide components were not artificially retained on the column. UV absorbance was monitored at 214, 220, 254 and 280 nm. Mass spectra were acquired in positive mode ionization using an Agilent 6220 Accurate-Mass TOF HPLC/MS system (Santa Clara, CA, USA) equipped with a dual sprayer electrospray ionization source with the second sprayer providing a reference mass solution. Mass spectrometric conditions were drying gas 10 L/min at 325°C, nebulizer 20 psi, mass range 100-3200 Da, acquisition rate of ~1.03 spectra/sec, fragmentor 175V, skimmer 65V, capillary 4000V, instrument state 4GHz High Resolution. Mass correction was performed for every individual spectrum using peaks at m/z 121.0509 and 922.0098 from the reference solution. Data acquisition was performed using the Mass Hunter software package (ver. B.04.00) Analysis of the HPLC-UV-MS data was done using the Agilent Mass Hunter Qualitative Analysis software (ver. B.07.00).

5 References

1. Nilsson, B. L.; Soellner, M. B.; Raines, R. T., Chemical synthesis of proteins. *Annu. Rev. Biophys. Biomol. Struct.* **2005**, *34*, 91-118.
2. Finking, R.; Marahiel, M. A., Biosynthesis of nonribosomal peptides. *Annu. Rev. Microbiol.* **2004**, *58*, 453-488.
3. Cahn, R. S.; Ingold, C.; Prelog, V., Specification of molecular chirality. *Angew. Chem. Int. Ed.* **1966**, *5*, 385-415.
4. Merrifield, R. B., Solid Phase Peptide Synthesis. I. The synthesis of a tetrapeptide. *J. Am. Chem. Soc.* **1963**, *85*, 2149-2154.
5. Kaiser, E.; Colescott, R. L.; Bossinger, C. D.; Cook, P. I., Color test for detection of free terminal amino groups in the solid-phase synthesis of peptides. *Anal. Biochem.* **1970**, *34*, 595-598.
6. Dawson, P. E.; Muir, T. W.; Clark-Lewis, I.; Kent, S. B. H., Synthesis of proteins by native chemical ligation. *Science* **1994**, *266*, 776-779.
7. McCaldon, P.; Argos, P., Oligopeptide biases in protein sequences and their use in predicting protein coding regions in nucleotide sequences. *Proteins* **1988**, *4*, 99-122.
8. Kochendoerfer, G. G.; Chen, S.-Y.; Mao, F.; Cressman, S.; Traviglia, S.; Shao, H.; Hunter, C.; Low, D.; Cagle, N.; Carnevali, M.; Gueriguian, V.; Keogh, P.; Porter, H.; Stratton, S. M.; Wiedeke, M. C.; Wilken, J.; Tang, T.; Levy, J. J.; Miranda, L. P.; Crnogorac, M.; Kalbag, S.; Botti, P.; Schindler-Horvath, J.; Savatski, L.; Adamson, J. W.; Kung, A.; Kent, S. B.; Bradburne, J. A., Design and chemical synthesis of a homogenous polymer-modified erythropoiesis protein. *Science* **2003**, *299*, 884-887.
9. Pattabiraman, V. R.; Ogunkoya, A. O.; Bode, J. W., Chemical protein synthesis by chemoselective alpha-ketoacid-hydroxylamine (KAHA) ligations with 5-oxaproline. *Angew. Chem. Int. Ed.* **2012**, *51*, 5114-5118.
10. Pusterla, I.; Bode, J. W., An oxazetidino amino acid for chemical protein synthesis by rapid, serine-forming ligations. *Nat. Chem.* **2015**, *7*, 668-672.

11. He, C.; Kulkarni, S. S.; Thuaud, F.; Bode, J. W., Chemical synthesis of the 20 kDa heme protein nitrophorin 4 by alpha-ketoacid-hydroxylamine (KAHA) ligation. *Angew. Chem. Int. Ed.* **2015**, *54*, DOI: 10.1002/anie.201505379.
12. Kent, S. B., Total chemical synthesis of proteins. *Chem. Soc. Rev.* **2009**, *38*, 338-351.
13. Goodwin, D.; Simerska, P.; Toth, I., Peptides as therapeutics with enhanced bioactivity. *Curr. Med. Chem.* **2012**, *19*, 4451-4461.
14. Albericio, F.; Kruger, H. G., Therapeutic peptides. *Future Med. Chem.* **2012**, *4*, 1527-1531.
15. Prothiwa, M.; Syed, I.; Huising, M. O.; van der Meulen, T.; Donaldson, C. J.; Trauger, S. A.; Kahn, B. B.; Saghatelian, A., Data-driven synthesis of proteolysis-resistant peptide hormones. *J. Am. Chem. Soc.* **2014**, *136*, 17710-17713.
16. Cohen, M. A.; Ellis, S. M.; Le Roux, C. W.; Batterham, R. L.; Park, A.; Patterson, M.; Frost, G. S.; Ghatei, M. A.; Bloom, S. R., Oxyntomodulin suppresses appetite and reduces food intake in humans. *J. Clin. Endocrinol. Metab.* **2003**, *88*, 4696-4701.
17. Jorgensen, R.; Kubale, V.; Vrecl, M.; Schwartz, T. W.; Elling, C. E., Oxyntomodulin differentially affects glucagon-like peptide-1 receptor β -arrestin recruitment and signaling through $G\alpha(s)$. *J. Pharmacol. Exp. Ther.* **2007**, *322*, 148-154.
18. Knudsen, L. B., Glucagon-like peptide-1: The basis of a new class of treatment for type 2 diabetes. *J. Med. Chem.* **2004**, *47*, 4128-4134.
19. Johnson, L. M.; Barrick, S.; Hager, M. V.; McFedries, A.; Homan, E. A.; Rabaglia, M. E.; Keller, M. P.; Attie, A. D.; Saghatelian, A.; Bisello, A.; Gellman, S. H., A potent α/β -peptide analogue of GLP-1 with prolonged action in vivo. *J. Am. Chem. Soc.* **2014**, *136*, 12848-12851.
20. Stymiest, J. L.; Mitchell, B. F.; Wong, S.; Vederas, J. C., Synthesis of biologically active dicarba analogues of the peptide hormone oxytocin using ring-closing metathesis. *Org. Lett.* **2003**, *5*, 47-49.

21. Wipf, P.; Xiao, J.; Stephenson, C. R., Peptide-like molecules (PLMs): A journey from peptide bond isosteres to gramicidin S mimetics and mitochondrial targeting agents. *Chimia* **2009**, *63*, 764-775.
22. Choudhary, A.; Raines, R. T., An evaluation of peptide-bond isosteres. *ChemBioChem* **2011**, *12*, 1801-1807.
23. Xiao, J.; Weisblum, B.; Wipf, P., Electrostatic versus steric effects in peptidomimicry: Synthesis and secondary structure analysis of gramicidin S analogues with (*E*)-alkene peptide isosteres. *J. Am. Chem. Soc.* **2005**, *127*, 5742-5743.
24. Chatterjee, C.; Paul, M.; Xie, L.; van der Donk, W. A., Biosynthesis and mode of action of lantibiotics. *Chem. Rev.* **2005**, *105*, 633-683.
25. Arnison, P. G.; Bibb, M. J.; Bierbaum, G.; Bowers, A. A.; Bugni, T. S.; Bulaj, G.; Camarero, J. A.; Campopiano, D. J.; Challis, G. L.; Clardy, J.; Cotter, P. D.; Craik, D. J.; Dawson, M.; Dittmann, E.; Donadio, S.; Dorrestein, P. C.; Entian, K. D.; Fischbach, M. A.; Garavelli, J. S.; Goransson, U.; Gruber, C. W.; Haft, D. H.; Hemscheidt, T. K.; Hertweck, C.; Hill, C.; Horswill, A. R.; Jaspars, M.; Kelly, W. L.; Klinman, J. P.; Kuipers, O. P.; Link, A. J.; Liu, W.; Marahiel, M. A.; Mitchell, D. A.; Moll, G. N.; Moore, B. S.; Muller, R.; Nair, S. K.; Nes, I. F.; Norris, G. E.; Olivera, B. M.; Onaka, H.; Patchett, M. L.; Piel, J.; Reaney, M. J.; Rebuffat, S.; Ross, R. P.; Sahl, H. G.; Schmidt, E. W.; Selsted, M. E.; Severinov, K.; Shen, B.; Sivonen, K.; Smith, L.; Stein, T.; Sussmuth, R. D.; Tagg, J. R.; Tang, G. L.; Truman, A. W.; Vederas, J. C.; Walsh, C. T.; Walton, J. D.; Wenzel, S. C.; Willey, J. M.; van der Donk, W. A., Ribosomally synthesized and post-translationally modified peptide natural products: overview and recommendations for a universal nomenclature. *Nat. Prod. Rep.* **2013**, *30*, 108-160.
26. Escano, J.; Smith, L., Multipronged approach for engineering novel peptide analogues of existing lantibiotics. *Expert Opin. Drug Discovery* **2015**, *10*, 857-870.
27. Schnell, N.; Entian, K. D.; Schneider, U.; Götz, F.; Zahner, H.; Kellner, R.; Jung, G., Prepeptide sequence of epidermin, a ribosomally synthesized antibiotic with four sulphide-rings. *Nature* **1988**, *333*, 276-278.
28. Bauer, R.; Dicks, L. M., Mode of action of lipid II-targeting lantibiotics. *Int. J. Food Microbiol.* **2005**, *101*, 201-216.

29. Kruszewska, D.; Sahl, H. G.; Bierbaum, G.; Pag, U.; Hynes, S. O.; Ljungh, A., Mersacidin eradicates methicillin-resistant *Staphylococcus aureus* (MRSA) in a mouse rhinitis model. *J. Antimicrob. Chemother.* **2004**, *54*, 648-653.
30. Ghobrial, O. G.; Derendorf, H.; Hillman, J. D., Pharmacodynamic activity of the lantibiotic MU1140. *Int. J. Antimicrob. Agents* **2009**, *33*, 70-74.
31. Sass, P.; Jansen, A.; Szekat, C.; Sass, V.; Sahl, H. G.; Bierbaum, G., The lantibiotic mersacidin is a strong inducer of the cell wall stress response of *Staphylococcus aureus*. *BMC Microbiol.* **2008**, *8*, 186.
32. Jabes, D.; Brunati, C.; Candiani, G.; Riva, S.; Romano, G.; Donadio, S., Efficacy of the new lantibiotic NAI-107 in experimental infections induced by multidrug-resistant Gram-positive pathogens. *Antimicrob. Agents Chemother.* **2011**, *55*, 1671-1676.
33. Delves-Broughton, J.; Blackburn, P.; Evans, R. J.; Hugenholtz, J., Applications of the bacteriocin, nisin. *Antonie van Leeuwenhoek* **1996**, *69*, 193-202.
34. You, Y. O.; van der Donk, W. A., Mechanistic investigations of the dehydration reaction of lactacin 481 synthetase using site-directed mutagenesis. *Biochemistry* **2007**, *46*, 5991-6000.
35. Garg, N.; Salazar-Ocampo, L. M. A.; van der Donk, W. A., In vitro activity of the nisin dehydratase NisB. *Proc. Natl. Acad. Sci. U.S.A.* **2013**, *110*, 7258-7263.
36. van der Donk, W. A.; Nair, S. K., Structure and mechanism of lanthipeptide biosynthetic enzymes. *Curr. Opin. Struct. Biol.* **2014**, *29*, 58-66.
37. Oman, T. J.; van der Donk, W. A., Follow the leader: the use of leader peptides to guide natural product biosynthesis. *Nat. Chem. Biol.* **2010**, *6*, 9-18.
38. Tang, W.; Jimenez-Oses, G.; Houk, K. N.; van der Donk, W. A., Substrate control in stereoselective lanthionine biosynthesis. *Nat. Chem.* **2015**, *7*, 57-64.
39. Tang, W.; van der Donk, W. A., The sequence of the enterococcal cytolysin imparts unusual lanthionine stereochemistry. *Nat. Chem. Biol.* **2013**, *9*, 157-159.

40. Lohans, C. T.; Li, J. L.; Vederas, J. C., Structure and biosynthesis of carnolysin, a homologue of enterococcal cytolyisin with D-amino acids. *J. Am. Chem. Soc.* **2014**, *136*, 13150-13153.
41. Knerr, P. J.; van der Donk, W. A., Chemical synthesis of the lantibiotic lactacin 481 reveals the importance of lanthionine stereochemistry. *J. Am. Chem. Soc.* **2013**, *135*, 7094-7097.
42. Velasquez, J. E.; Zhang, X.; van der Donk, W. A., Biosynthesis of the antimicrobial peptide epilancin 15X and its N-terminal lactate. *Chem. Biol.* **2011**, *18*, 857-867.
43. Skaugen, M.; Nissen-Meyer, J.; Jung, G.; Stevanovic, S.; Sletten, K.; Abildgaard, C. I. M.; Nes, I. F., *In vivo* conversion of L-serine to D-alanine in a ribosomally synthesized polypeptide. *J. Biol. Chem.* **1994**, *269*, 27183-27185.
44. Abildgaard, C. I. M.; Nissen-Meyer, J.; Sletten, K.; Nes, I. F., Purification and amino acid sequence of lactocin S, a bacteriocin produced by *Lactobacillus sake* L45. *Appl. Environ. Microbiol.* **1991**, *57*, 1829-1834.
45. Ross, A. C.; Liu, H.; Pattabiraman, V. R.; Vederas, J. C., Synthesis of the lantibiotic lactocin S using peptide cyclizations on solid phase. *J. Am. Chem. Soc.* **2010**, *132*, 462-463.
46. Skaugen, M.; Abildgaard, C. I. M.; Nes, I. F., Organization and expression of a gene cluster involved in the biosynthesis of the lantibiotic lactocin S. *Mol. Gen. Genet.* **1997**, *253*, 674-686.
47. Cotter, P. D.; O'Connor, P. M.; Draper, L. A.; Lawton, E. M.; Deegan, L. H.; Hill, C.; Ross, R. P., Posttranslational conversion of L-serines to D-alanines is vital for optimal production and activity of the lantibiotic lactacin 3147. *Proc. Natl. Acad. Sci. U.S.A.* **2005**, *102*, 18584-18589.
48. Fukase, K.; Kitazawa, M.; Sano, A.; Shimbo, K.; Fujita, H.; Horimoto, S.; Wakamiya, T.; Shiba, T., Total synthesis of peptide antibiotic nisin. *Tetrahedron Lett.* **1988**, *29*, 795-798.
49. Bregant, S.; Tabor, A. B., Orthogonally protected lanthionines: synthesis and use for the solid-phase synthesis of an analogue of nisin ring C. *J. Org. Chem.* **2005**, *70*, 2430-2438.

50. Mothia, B.; Appleyard, A. N.; Wadman, S.; Tabor, A. B., Synthesis of peptides containing overlapping lanthionine bridges on the solid phase: an analogue of rings D and E of the lantibiotic nisin. *Org. Lett.* **2011**, *13*, 4216-4219.
51. Liu, W.; Chan, A. S.; Liu, H.; Cochrane, S. A.; Vederas, J. C., Solid supported chemical syntheses of both components of the lantibiotic lactacin 3147. *J. Am. Chem. Soc.* **2011**, *133*, 14216-14219.
52. Knerr, P. J.; van der Donk, W. A., Chemical synthesis and biological activity of analogues of the lantibiotic epilancin 15X. *J. Am. Chem. Soc.* **2012**, *134*, 7648-7651.
53. Wilson-Stanford, S.; Kalli, A.; Hakansson, K.; Kastrantas, J.; Orugunty, R. S.; Smith, L., Oxidation of lanthionines renders the lantibiotic nisin inactive. *Appl. Environ. Microbiol.* **2009**, *75*, 1381-1387.
54. Boakes, S.; Cortes, J.; Appleyard, A. N.; Rudd, B. A.; Dawson, M. J., Organization of the genes encoding the biosynthesis of actagardine and engineering of a variant generation system. *Mol. Microbiol.* **2009**, *72*, 1126-1136.
55. Ross, A. C.; Vederas, J. C., Fundamental functionality: recent developments in understanding the structure-activity relationships of lantibiotic peptides. *J. Antibiot.* **2011**, *64*, 27-34.
56. Pattabiraman, V. R.; McKinnie, S. M.; Vederas, J. C., Solid-supported synthesis and biological evaluation of the lantibiotic peptide bis(desmethyl) lactacin 3147 A2. *Angew. Chem. Int. Ed.* **2008**, *47*, 9472-9475.
57. Pattabiraman, V. R.; Stymiest, J. L.; Derksen, D. J.; Martin, N. I.; Vederas, J. C., Multiple on-resin olefin metathesis to form ring-expanded analogues of the lantibiotic peptide, lactacin 3147 A2. *Org. Lett.* **2007**, *9*, 699-702.
58. Liu, H.; Pattabiraman, V. R.; Vederas, J. C., Synthesis and biological activity of oxa-lactacin A2, a lantibiotic analogue with sulfur replaced by oxygen. *Org. Lett.* **2009**, *11*, 5574-5577.
59. Ghalit, N.; Poot, A. J.; Furstner, A.; Rijkers, D. T.; Liskamp, R. M., Ring-closing alkyne metathesis approach toward the synthesis of alkyne mimics of thioether A-, B-, C-, and DE-ring systems of the lantibiotic nisin. *Z. Org. Chem.* **2005**, *7*, 2961-2964.

60. Ghalit, N.; Rijkers, D. T.; Kemmink, J.; Versluis, C.; Liskamp, R. M., Pre-organization induced synthesis of a crossed alkene-bridged nisin Z DE-ring mimic by ring-closing metathesis. *Chem. Commun. (Cambridge, U.K.)* **2005**, 192-194.
61. Ghalit, N.; Reichwein, J. F.; Hilbers, H. W.; Breukink, E.; Rijkers, D. T.; Liskamp, R. M., Synthesis of bicyclic alkene-/alkane-bridged nisin mimics by ring-closing metathesis and their biochemical evaluation as lipid II binders: toward the design of potential novel antibiotics. *ChemBioChem* **2007**, *8*, 1540-1554.
62. Ghalit, N.; Kemmink, J.; Hilbers, H. W.; Versluis, C.; Rijkers, D. T.; Liskamp, R. M., Step-wise and pre-organization induced synthesis of a crossed alkene-bridged nisin Z DE-ring mimic by ring-closing metathesis. *Org. Biomol. Chem.* **2007**, *5*, 924-934.
63. Slootweg, J. C.; Peters, N.; Quarles van Ufford, H. L.; Breukink, E.; Liskamp, R. M.; Rijkers, D. T., Semi-synthesis of biologically active nisin hybrids composed of the native lanthionine ABC-fragment and a cross-stapled synthetic DE-fragment. *Bioorg. Med. Chem.* **2014**, *22*, 5345-5353.
64. de Araujo, A. D.; Mobli, M.; King, G. F.; Alewood, P. F., Cyclization of peptides by using selenolanthionine bridges. *Angew. Chem. Int. Ed.* **2012**, *51*, 10298-10302.
65. O'Brien, K.; ó Proinsias, K.; Kelleher, F., Synthesis of orthogonally protected azalanthionines (lanazanines) by sequential ring-opening of N-substituted aziridine 2-carboxylates. *Tetrahedron Lett.* **2013**, *54*, 2395-2397.
66. Ross, A. C.; McKinnie, S. M.; Vederas, J. C., The synthesis of active and stable diaminopimelate analogues of the lantibiotic peptide lactocin S. *J. Am. Chem. Soc.* **2012**, *134*, 2008-2011.
67. Ross, A. C. Synthesis and biological evaluation of the lantibiotic peptide lactocin S and its analogues. *Ph.D. Thesis, University of Alberta*, **2012**.
68. McKinnie, S. M. K.; Ross, A. C.; Little, M. J.; Vederas, J. C., The solid phase supported peptide synthesis of analogues of the lantibiotic lactocin S. *Med. Chem. Commun.* **2012**, *3*, 971-974.

69. Spantulescu, M. D.; Jain, R. P.; Derksen, D. J.; Vederas, J. C., Photolysis of diacyl peroxides: A radical-based approach for the synthesis of functionalized amino acids. *Org. Lett.* **2003**, *5*, 2963-2965.
70. Lebar, M. D.; Lupoli, T. J.; Tsukamoto, H.; May, J. M.; Walker, S.; Kahne, D., Forming cross-linked peptidoglycan from synthetic gram-negative lipid II. *J. Am. Chem. Soc.* **2013**, *135*, 4632-4635.
71. Tatemoto, K.; Hosoya, M.; Habata, Y.; Fujii, R.; Kakegawa, T.; Zou, M.-X.; Kawamata, Y.; Fukusumi, S.; Hinuma, S.; Kitada, C.; Kurokawa, T.; Onda, H.; Fujino, M., Isolation and characterization of a novel endogenous peptide ligand for the human APJ receptor. *Biochem. Biophys. Res. Commun.* **1998**, *251*, 471-476.
72. Pitkin, S. L.; Maguire, J. J.; Bonner, T. I.; Davenport, A. P., International Union of Basic and Clinical Pharmacology. LXXIV. Apelin receptor nomenclature, distribution, pharmacology, and function. *Pharmacol. Rev.* **2010**, *62*, 331-342.
73. Narayanan, S.; Harris, D. L.; Maitra, R.; Runyon, S. P., Regulation of the apelinergic system and its potential in cardiovascular disease: Peptides and small molecules as tools for discovery. *J. Med. Chem.* **2015**, *Article ASAP*, DOI: 10.1021/acs.jmedchem.1025b00527.
74. Maguire, J. J.; Kleinz, M. J.; Pitkin, S. L.; Davenport, A. P., [Pyr1]apelin-13 identified as the predominant apelin isoform in the human heart: vasoactive mechanisms and inotropic action in disease. *Hypertension* **2009**, *54*, 598-604.
75. Shin, K.; Pandey, A.; Liu, X. Q.; Anini, Y.; Rainey, J. K., Preferential apelin-13 production by the proprotein convertase PCSK3 is implicated in obesity. *FEBS Open Bio* **2013**, *3*, 328-333.
76. Habata, Y.; Fujii, R.; Hosoya, M.; Fukusumi, S.; Kawamata, Y.; Hinuma, S.; Kitada, C.; Nishizawa, N.; Murosaki, S.; Kurokawa, T.; Onda, H.; Tatemoto, K.; Fujino, M., Apelin, the natural ligand of the orphan receptor APJ, is abundantly secreted in the colostrum. *Biochim. Biophys. Acta.* **1999**, *1452*, 25-35.
77. Langelaan, D. N.; Bebbington, E. M.; Reddy, T.; Rainey, J. K., Structural Insight into G-protein coupled receptor binding by apelin. *Biochemistry* **2009**, *48*, 537-548.

78. O'Dowd, B. F.; Heiber, M.; Chan, A.; Heng, H. H. Q.; Tsui, L.-C.; Kennedy, J. L.; Shi, X.; Petronis, A.; George, S. R.; Nguyen, T., A human gene that shows identity with the gene encoding the angiotensin receptor is located on chromosome 11. *Gene* **1993**, *136*, 355-360.
79. Masri, B.; Morin, N.; Pedebornade, L.; Knibiehler, B.; Audigier, Y., The apelin receptor is coupled to Gi1 or Gi2 protein and is differentially desensitized by apelin fragments. *J. Biol. Chem.* **2006**, *281*, 18317-18326.
80. Szokodi, I.; Tavi, P.; Földes, G.; Voutilainen-Myllylä, S.; Ilves, M.; Tokola, H.; Pikkarainen, S.; Piuhola, J.; Rysä, H.; Tóth, M.; Ruskoaho, H., Apelin, the novel endogenous ligand of the orphan receptor APJ, regulates cardiac contractility. *Circ. Res.* **2002**, *91*, 434-440.
81. Fleming, I.; Busse, R., Molecular mechanisms involved in the regulation of the endothelial nitric oxide synthase. *Am. J. Physiol.: Regul., Integr. Comp. Physiol.* **2003**, *284*, R1-R12.
82. Tatemoto, K.; Takayama, K.; Zou, M.-X.; Kumaki, I.; Zhang, W.; Kumano, K.; Fujimiya, M., The novel peptide apelin lowers blood pressure via a nitric oxide-dependent mechanism. *Regul. Pept.* **2001**, *99*, 87-92.
83. Evans, N. A.; Groarke, D. A.; Warrack, J.; Greenwood, C. J.; Dodgson, K.; Milligan, G.; Wilson, S., Visualizing differences in ligand-induced beta-arrestin-GFP interactions and trafficking between three recently characterized G protein-coupled receptors. *J. Neurochem.* **2001**, *77*, 476-485.
84. Lee, D. K.; Ferguson, S. S.; George, S. R.; O'Dowd, B. F., The fate of the internalized apelin receptor is determined by different isoforms of apelin mediating differential interaction with beta-arrestin. *Biochem. Biophys. Res. Commun.* **2010**, *395*, 185-189.
85. Kalea, A. Z.; Batlle, D., Apelin and ACE2 in cardiovascular disease. *Curr. Opin. Investig. Drugs* **2010**, *11*, 273-282.
86. El Messari, S.; Iturrioz, X.; Fassot, C.; De Mota, N.; Roesch, D.; Llorens-Cortes, C., Functional dissociation of apelin receptor signaling and endocytosis: implications for the effects of apelin on arterial blood pressure. *J. Neurochem.* **2004**, *90*, 1290-1301.

87. Luttrell, L. M.; Lefkowitz, R. J., The role of β -arrestins in the termination and transduction of G-protein-coupled receptor signals. *J. Cell. Sci.* **2002**, *115*, 455-465.
88. Kenakin, T., Functional selectivity and biased receptor signaling. *J. Pharmacol. Exp. Ther.* **2011**, *336*, 296-302.
89. Chapman, N. A.; Dupre, D. J.; Rainey, J. K., The apelin receptor: physiology, pathology, cell signalling, and ligand modulation of a peptide-activated class A GPCR. *Biochem. Cell. Biol.* **2014**, *92*, 431-440.
90. Gerbier, R.; Leroux, V.; Couvineau, P.; Alvear-Perez, R.; Maigret, B.; Llorens-Cortes, C.; Iturrioz, X., New structural insights into the apelin receptor: identification of key residues for apelin binding. *FASEB J.* **2015**, *29*, 314-322.
91. Langelaan, D. N.; Reddy, T.; Banks, A. W.; Dellaire, G.; Dupre, D. J.; Rainey, J. K., Structural features of the apelin receptor N-terminal tail and first transmembrane segment implicated in ligand binding and receptor trafficking. *Biochim. Biophys. Acta.* **2013**, *1828*, 1471-1483.
92. Iturrioz, X.; Gerbier, R.; Leroux, V.; Alvear-Perez, R.; Maigret, B.; Llorens-Cortes, C., By interacting with the C-terminal Phe of apelin, Phe255 and Trp259 in helix VI of the apelin receptor are critical for internalization. *J. Biol. Chem.* **2010**, *285*, 32627-32637.
93. Han, H. M.; Shimuta, S. I.; Kanashiro, C. A.; Oliveira, L.; Han, S. W.; Paiva, A. C., Residues Val254, His256, and Phe259 of the angiotensin II AT1 receptor are not involved in ligand binding but participate in signal transduction. *Mol. Endocrinol.* **1998**, *12*, 810-814.
94. Lee, D. K.; Saldivia, V. R.; Nguyen, T.; Cheng, R.; George, S. R.; O'Dowd, B. F., Modification of the terminal residue of apelin-13 antagonizes its hypotensive action. *Endocrinology* **2005**, *146*, 231-236.
95. Clark-Lewis, I.; Kim, K. S.; Rajarathnam, K.; Gong, J. H.; Dewald, B.; Moser, B.; Baggiolini, M.; Sykes, B. D., Structure-activity relationships of chemokines. *J. Leukocyte Biol.* **1995**, *57*, 703-711.
96. Hoare, S., Mechanisms of peptide and nonpeptide ligand binding to class B G-protein-coupled receptors. *Drug Discovery Today* **2005**, *10*, 417-427.

97. Kleinz, M. J.; Davenport, A. P., Emerging roles of apelin in biology and medicine. *Pharmacol. Ther.* **2005**, *107*, 198-211.
98. Medhurst, A. D.; Jennings, C. A.; Robbins, M. J.; Davis, R. P.; Ellis, C.; Winborn, K. Y.; Lawrie, K. W. M.; Hervieu, G.; Riley, G.; Bolaky, J. E.; Herrity, N. C.; Murdock, P.; Darker, J. G., Pharmacological and immunohistochemical characterization of the APJ receptor and its endogenous ligand apelin. *J. Neurochem.* **2003**, *84*, 1162-1172.
99. Reaux-Le Goazigo, A.; Alvear-Perez, R.; Zizzari, P.; Epelbaum, J.; Bluet-Pajot, M. T.; Llorens-Cortes, C., Cellular localization of apelin and its receptor in the anterior pituitary: evidence for a direct stimulatory action of apelin on ACTH release. *Am. J. Physiol.: Endocrinol. Metab.* **2007**, *292*, E7-E15.
100. Yokomori, H.; Oda, M.; Yoshimura, K.; Machida, S.; Kaneko, F.; Hibi, T., Overexpression of apelin receptor (APJ/AGTRL1) on hepatic stellate cells and sinusoidal angiogenesis in human cirrhotic liver. *J. Gastroenterol.* **2011**, *46*, 222-231.
101. Reaux-Le Goazigo, A.; De Mota, N.; Skultetyova, I.; Lenkei, Z.; El Messari, S.; Gallatz, K.; Corvol, P.; Palkovits, M.; Llorens-Cortes, C., Physiological role of a novel neuropeptide, apelin, and its receptor in the rat brain. *J. Neurochem.* **2001**, *77*, 1085-1096.
102. De Mota, N.; Reaux-Le Goazigo, A.; El Messari, S.; Chartrel, N.; Roesch, D.; Dujardin, C.; Kordon, C.; Vaudry, H.; Moos, F.; Llorens-Cortes, C., Apelin, a potent diuretic neuropeptide counteracting vasopressin actions through inhibition of vasopressin neuron activity and vasopressin release. *Proc. Natl. Acad. Sci. U.S.A.* **2004**, *101*, 10464-10469.
103. Boucher, J.; Masri, B.; Daviaud, D.; Gesta, S.; Guigne, C.; Mazzucotelli, A.; Castan-Laurell, I.; Tack, I.; Knibiehler, B.; Carpene, C.; Audigier, Y.; Saulnier-Blache, J. S.; Valet, P., Apelin, a newly identified adipokine up-regulated by insulin and obesity. *Endocrinology* **2005**, *146*, 1764-1771.
104. Heinonen, M. V.; Purhonen, A. K.; Miettinen, P.; Paakkonen, M.; Pirinen, E.; Alhava, E.; Akerman, K.; Herzig, K. H., Apelin, orexin-A and leptin plasma levels in morbid obesity and effect of gastric banding. *Regul. Pept.* **2005**, *130*, 7-13.

105. Yue, P.; Jin, H.; Aillaud, M.; Deng, A. C.; Azuma, J.; Asagami, T.; Kundu, R. K.; Reaven, G. M.; Quertermous, T.; Tsao, P. S., Apelin is necessary for the maintenance of insulin sensitivity. *Am. J. Physiol.: Endocrinol. Metab.* **2010**, *298*, E59-E67.
106. Chen, H.; Zheng, C.; Zhang, X.; Li, J.; Li, J.; Zheng, L.; Huang, K., Apelin alleviates diabetes-associated endoplasmic reticulum stress in the pancreas of Akita mice. *Peptides* **2011**, *32*, 1634-1639.
107. Attané, C.; Foussal, C.; Le Gonidec, S.; Benani, A.; Daviaud, D.; Wanecq, E.; Guzmán-Ruiz, R.; Dray, C.; Bezaire, V.; Rancoule, C.; Kuba, K.; Ruiz-Gayo, M.; Levade, T.; Penninger, J. M.; Burcelin, R.; Pénicaud, L.; Valet, P.; Castan-Laurell, I., Apelin treatment increases complete fatty acid oxidation, mitochondrial oxidative capacity, and biogenesis in muscle of insulin-resistant mice. *Diabetes* **2012**, *61*, 310-320.
108. Choe, H.; Farzan, M.; Konkel, M.; Martin, K.; Sun, Y.; Marcon, L.; Cayabyab, M.; Berman, M.; Dorf, M. E.; Gerard, N.; Gerard, C.; Sodroski, J., The orphan seven-transmembrane receptor Apj supports the entry of primary T-cell-line-tropic and dualtropic human immunodeficiency virus type 1. *J. Virol.* **1998**, *72*, 6113-6118.
109. Fan, X.; Zhou, N.; Zhang, X.; Mukhtar, M.; Lu, Z.; Fang, J.; DuBois, G. C.; Pomerantz, R. J., Structural and functional study of the apelin-13 peptide, an endogenous ligand of the HIV-1 coreceptor, APJ. *Biochemistry* **2003**, *42*, 10163-10168.
110. Lee, D. K.; Cheng, R.; Nguyen, T.; Fan, T.; Kariyawasam, A. P.; Liu, Y.; Osmond, D. H.; George, S. R.; O'Dowd, B. F., Characterization of apelin, the ligand for the APJ receptor. *J. Neurochem.* **2000**, *74*, 34-41.
111. Japp, A. G.; Cruden, N. L.; Amer, D. A.; Li, V. K.; Goudie, E. B.; Johnston, N. R.; Sharma, S.; Neilson, I.; Webb, D. J.; Megson, I. L.; Flapan, A. D.; Newby, D. E., Vascular effects of apelin in vivo in man. *J. Am. Coll. Cardiol.* **2008**, *52*, 908-913.
112. Japp, A. G.; Cruden, N. L.; Barnes, G.; van Gemeren, N.; Mathews, J.; Adamson, J.; Johnston, N. R.; Denvir, M. A.; Megson, I. L.; Flapan, A. D.; Newby, D. E., Acute cardiovascular effects of apelin in humans: potential role in patients with chronic heart failure. *Circulation* **2010**, *121*, 1818-1827.

113. Barnes, G. D.; Alam, S.; Carter, G.; Pedersen, C. M.; Lee, K. M.; Hubbard, T. J.; Veitch, S.; Jeong, H.; White, A.; Cruden, N. L.; Huson, L.; Japp, A. G.; Newby, D. E., Sustained cardiovascular actions of APJ agonism during renin-angiotensin system activation and in patients with heart failure. *Circ.: Heart Failure* **2013**, *6*, 482-491.
114. Zhang, Z.; Yu, B.; Tao, G.-z., Apelin protects against cardiomyocyte apoptosis induced by glucose deprivation. *Chin. Med. J.* **2009**, *122*, 2360-2365.
115. Wang, W.; McKinnie, S. M.; Patel, V. B.; Haddad, G.; Wang, Z.; Zhabyeyev, P.; Das, S. K.; Basu, R.; McLean, B.; Kandalam, V.; Penninger, J. M.; Kassiri, Z.; Vederas, J. C.; Murray, A. G.; Oudit, G. Y., Loss of apelin exacerbates myocardial infarction adverse remodeling and ischemia-reperfusion injury: therapeutic potential of synthetic apelin analogues. *J. Am. Heart Assoc.* **2013**, *2*, e000249.
116. Kidoya, H.; Ueno, M.; Yamada, Y.; Mochizuki, N.; Nakata, M.; Yano, T.; Fujii, R.; Takakura, N., Spatial and temporal role of the apelin/APJ system in the caliber size regulation of blood vessels during angiogenesis. *EMBO J.* **2008**, *27*, 522-534.
117. Picault, F. X.; Chaves-Almagro, C.; Progetti, F.; Prats, H.; Masri, B.; Audigier, Y., Tumour co-expression of apelin and its receptor is the basis of an autocrine loop involved in the growth of colon adenocarcinomas. *Eur. J. Cancer* **2014**, *50*, 663-674.
118. Murza, A.; Parent, A.; Besserer-Offroy, E.; Tremblay, H.; Karadereye, F.; Beaudet, N.; Leduc, R.; Sarret, P.; Marsault, E., Elucidation of the structure-activity relationships of apelin: influence of unnatural amino acids on binding, signaling, and plasma stability. *ChemMedChem* **2012**, *7*, 318-325.
119. Hamada, J.; Kimura, J.; Ishida, J.; Kohda, T.; Morishita, S.; Ichihara, S.; Fukamizu, A., Evaluation of novel cyclic analogues of apelin. *Int. J. Mol. Med.* **1998**, *22*, 547-552.
120. Brame, A. L.; Maguire, J. J.; Yang, P.; Dyson, A.; Torella, R.; Cheriyan, J.; Singer, M.; Glen, R. C.; Wilkinson, I. B.; Davenport, A. P., Design, characterization, and first-in-human study of the vascular actions of a novel biased apelin receptor agonist. *Hypertension* **2015**, *65*, 834-840.

121. Zecri, F.; Golosov, A.; Grosche, P.; Yasoshima, K.; Zhao, H.; Hu, Q. Y.; Imase, H.; Parker, D. T. Synthetic apelin mimetics for the treatment of heart failure. US 20130196899 A1, Aug. 1, 2013.
122. Macaluso, N. J.; Pitkin, S. L.; Maguire, J. J.; Davenport, A. P.; Glen, R. C., Discovery of a competitive apelin receptor (APJ) antagonist. *ChemMedChem* **2011**, *6*, 1017-1023.
123. Murza, A.; Besserer-Offroy, E.; Cote, J.; Berube, P.; Longpre, J. M.; Dumaine, R.; Lesur, O.; Auger-Messier, M.; Leduc, R.; Sarret, P.; Marsault, E., C-Terminal modifications of apelin-13 significantly change ligand binding, receptor signaling, and hypotensive action. *J. Med. Chem.* **2015**, *58*, 2431-2440.
124. Vickers, C.; Hales, P.; Kaushik, V.; Dick, L.; Gavin, J.; Tang, J.; Godbout, K.; Parsons, T.; Baronas, E.; Hsieh, F.; Acton, S.; Patane, M.; Nichols, A.; Tummino, P., Hydrolysis of biological peptides by human angiotensin-converting enzyme-related carboxypeptidase. *J. Biol. Chem.* **2002**, *277*, 14838-14843.
125. Crackower, M. A.; Sarao, R.; Oudit, G. Y.; Yagil, C.; Koziaradzki, I.; Scanga, S. E.; Oliveira-dos-Santos, A. J.; da Costa, J.; Zhang, L.; Pei, Y.; Scholey, J.; Ferrario, C. M.; Manoukian, A. S.; Chappell, M. C.; Backx, P. H.; Yagil, Y.; Penninger, J. M., Angiotensin-converting enzyme 2 is an essential regulator of heart function. *Nature* **2002**, *417*, 822-828.
126. Towler, P.; Staker, B.; Prasad, S. G.; Menon, S.; Tang, J.; Parsons, T.; Ryan, D.; Fisher, M.; Williams, D.; Dales, N. A.; Patane, M. A.; Pantoliano, M. W., ACE2 X-ray structures reveal a large hinge-bending motion important for inhibitor binding and catalysis. *J. Biol. Chem.* **2004**, *279*, 17996-18007.
127. Dales, N. A.; Gould, A. E.; Brown, J. A.; Calderwood, E. F.; Guan, B.; Minor, C. A.; Gavin, J. M.; Hales, P.; Kaushik, V. K.; Stewart, M.; Tummino, P. J.; Vickers, C. S.; Ocain, T. D.; Patane, M. A., Substrate-based design of the first class of angiotensin-converting enzyme-related carboxypeptidase (ACE2) inhibitors. *J. Am. Chem. Soc.* **2002**, *124*, 11852-11853.
128. Zhong, J.; Basu, R.; Guo, D.; Chow, F. L.; Byrns, S.; Schuster, M.; Loibner, H.; Wang, X. H.; Penninger, J. M.; Kassiri, Z.; Oudit, G. Y., Angiotensin-converting enzyme 2 suppresses pathological hypertrophy, myocardial fibrosis, and cardiac dysfunction. *Circulation* **2010**, *122*, 717-728.

129. Masri, B.; Lahlou, H.; Mazarguil, H.; Knibiehler, B.; Audigier, Y., Apelin (65-77) activates extracellular signal-regulated kinases via a PTX-sensitive G protein. *Biochem. Biophys. Res. Commun.* **2002**, *290*, 539-545.
130. Wang, W.; McKinnie, S. M.; Farhan, M.; Paul, M.; McDonald, T.; McLean, B.; Hazra, S.; Murray, A. G.; Vederas, J. C.; Oudit, G. Y., Angiotensin converting enzyme 2 metabolizes and partially inactivates pyr-apelin-13 and apelin-17: Physiological effects in the cardiovascular system. *J. Biol. Chem.* **2015**, *in submission*.
131. Huang, L.; Sexton, D. J.; Skogerson, K.; Devlin, M.; Smith, R.; Sanyal, I.; Parry, T.; Kent, R.; Enright, J.; Wu, Q. L.; Conley, G.; DeOliveira, D.; Morganelli, L.; Ducar, M.; Wescott, C. R.; Ladner, R. C., Novel peptide inhibitors of angiotensin-converting enzyme 2. *J. Biol. Chem.* **2003**, *278*, 15532-15540.
132. Ye, M.; Wysocki, J.; Gonzalez-Pacheco, F. R.; Salem, M.; Evora, K.; Garcia-Halpin, L.; Poglitsch, M.; Schuster, M.; Battle, D., Murine recombinant angiotensin-converting enzyme 2: effect on angiotensin II-dependent hypertension and distinctive angiotensin-converting enzyme 2 inhibitor characteristics on rodent and human angiotensin-converting enzyme 2. *Hypertension* **2012**, *60*, 730-740.
133. Pedersen, K. B.; Sriramula, S.; Chhabra, K. H.; Xia, H.; Lazartigues, E., Species-specific inhibitor sensitivity of angiotensin-converting enzyme 2 (ACE2) and its implication for ACE2 activity assays. *Am. J. Physiol.: Regul., Integr. Comp. Physiol.* **2011**, *301*, R1293-R1299.
134. Moorthy, J. N.; Mandal, S.; Venugopalan, P., Hydrogen-bonded helical self-assembly of sterically-hindered benzyl alcohols: Rare isostructurality and synthon equivalence between alcohols and acids. *Cryst. Growth Des.* **2012**, *12*, 2942-2947.
135. Poisel, H., α -Ketoester aus α -aminosäureestern. *Chem. Ber.* **1978**, *111*, 3136-3139.
136. Moumné, R.; Denise, B.; Guitot, K.; Rudler, H.; Lavielle, S.; Karoyan, P., New scalable asymmetric aminomethylation reaction for the synthesis of β 2-amino acids. *Eur. J. Org. Chem.* **2007**, 1912-1920.

137. Harfenist, M.; Hoerr, D. C.; Crouch, R., Enantiospecific synthesis of the trans-9-[3-(3,5-dimethyl-1-piperazinyl)propyl]carbazoles. *J. Org. Chem.* **1985**, *50*, 1356-1359.
138. Nishizawa, N.; Hosoya, M.; Kitada, C.; Hinuma, S.; Onda, H.; Nishimura, O.; Fujino, M., High Potency Analogs of Apelin, A Ligand of Orphan GPCR APJ, *37th Japanese Peptide Symposium*, Shiori, T., Ed. Nagoya, Japan, **2001**, 151-154.
139. Zucker, I. H., Angiotensin-converting enzyme 2: a new player in central sympathetic regulation? *Circ. Res.* **2008**, *102*, 628-629.
140. Hoffman, R. V.; Tao, J., A stereocontrolled synthesis of monofluoro ketomethylene dipeptide isosteres. *J. Org. Chem.* **1999**, *64*, 126-132.
141. Poterała, M.; Plenkiewicz, J., Synthesis of new chiral ionic liquids from α -hydroxycarboxylic acids. *Tetrahedron: Asymmetry* **2011**, *22*, 294-299.
142. Wolfe, M. S.; Lee, Y.; Bartlett, W. J.; Borcharding, D. R.; Borchardt, R. T., Synthesis of 4'-modified analogues of aristeromycin and neplanocin A from intermediate ketones. *J. Med. Chem.* **1992**, *35*, 1782-1791.
143. Trybulski, E. J.; Kramss, R. H.; Mangano, R. M.; Rusinko, A., Chemical and biochemical Studies of 2-propynylpyrrolidine derivatives. Restricted-rotation analogues of *N*-Methyl-*N*-(1-methyl-4-pyrrolidino-2-butynyl)acetamide (BM-5). *J. Med. Chem.* **1990**, *33*, 3190-3198.
144. Anelli, P. L.; Biffi, C.; Montanari, F.; Quici, S., Fast and selective oxidation of primary alcohols to aldehydes or to carboxylic acids and of secondary alcohols to ketones mediated by oxoammonium salts under two-phase conditions. *J. Org. Chem.* **1987**, *52*, 2559-2562.
145. Quesada, E.; Taylor, R. J. K., One-pot conversion of activated alcohols into terminal alkynes using manganese dioxide in combination with the Bestmann–Ohira reagent. *Tetrahedron Lett.* **2005**, *46*, 6473-6476.
146. Melendez, R. E.; Lubell, W. D., Aza-amino acid scan for rapid identification of secondary structure based on the application of *N*-Boc-aza1-dipeptides in peptide synthesis. *J. Am. Chem. Soc.* **2004**, *126*, 6759-6764.

147. Cheguillaume, A.; Salaün, A.; Sinbandhit, S.; Potel, M.; Gall, P.; Baudy-Floc'h, M.; Le Grel, P., Solution synthesis and characterization of aza- β 3-peptides (N α -substituted hydrazino acetic acid oligomers). *J. Org. Chem.* **2001**, *66*, 4923-4929.
148. Murza, A.; Belleville, K.; Longpre, J. M.; Sarret, P.; Marsault, E., Stability and degradation patterns of chemically modified analogs of apelin-13 in plasma and cerebrospinal fluid. *Biopolymers* **2014**, *101*, 297-303.
149. Zhang, Y.; Maitra, R.; Harris, D. L.; Dhungana, S.; Snyder, R.; Runyon, S. P., Identifying structural determinants of potency for analogs of apelin-13: integration of C-terminal truncation with structure-activity. *Bioorg. Med. Chem.* **2014**, *22*, 2992-2997.
150. Blanchard, J. E.; Elowe, N. H.; Huitema, C.; Fortin, P. D.; Cechetto, J. D.; Eltis, L. D.; Brown, E. D., High-throughput screening identifies inhibitors of the SARS coronavirus main proteinase. *Chem. Biol.* **2004**, *11*, 1445-1453.
151. Meldal, M.; Breddam, K., Anthranilamide and nitrotyrosine as a donor-acceptor pair in internally quenched fluorescent substrates for endopeptidases: Multicolumn peptide synthesis of enzyme substrates for subtilisin Carlsberg and pepsin. *Anal. Biochem.* **1991**, *195*, 141-147.
152. Fujimoto, Y.; Suzuki, C.; Watanabe, Y.; Matsuda, Y.; Akihama, S., Purification and characterization of a kallikrein from human submaxillary glands. *Biochem. Med. Metab. Biol.* **1990**, *44*, 218-227.
153. Goettig, P.; Magdolen, V.; Brandstetter, H., Natural and synthetic inhibitors of kallikrein-related peptidases (KLKs). *Biochimie* **2010**, *92*, 1546-1567.
154. Weber, W.; Buck, F.; Meyer, A.; Hilz, H., Prostate specific antigen: one out of five disulfide bridges determines inactivation by reduction. *Biochem. Biophys. Res. Commun.* **2009**, *379*, 1101-1106.
155. Lieberthal, W.; Oza, N. B.; Bernard, D., B.; Levinsky, N. G., The effect of cations on the activity of human urinary kallikrein. *J. Biol. Chem.* **1982**, *257*, 10827-10830.
156. Lundwall, A.; Band, V.; Blaber, M.; Clements, J. A.; Courty, Y.; Diamandis, E. P.; Fritz, H.; Lilja, H.; Malm, J.; Maltais, L. J.; Olsson, A. Y.; Petraki, C.; Scorilas, A.; Sotiropoulou, G.; Stenman, U. H.; Stephan, C.; Talieri, M.; Yousef,

- G. M., A comprehensive nomenclature for serine proteases with homology to tissue kallikreins. *Biol. Chem.* **2006**, *387*, 637-641.
157. Chun, H. J.; Ali, Z. A.; Kojima, Y.; Kundu, R. K.; Sheikh, A. Y.; Agrawal, R.; Zheng, L.; Leeper, N. J.; Pearl, N. E.; Patterson, A. J.; Anderson, J. P.; Tsao, P. S.; Lenardo, M. J.; Ashley, E. A.; Quertermous, T., Apelin signaling antagonizes Ang II effects in mouse models of atherosclerosis. *J. Clin. Invest.* **2008**, *118*, 3343-3354.
158. Bai, B.; Liu, L.; Zhang, N.; Wang, C.; Jiang, Y.; Chen, J., Heterodimerization of human apelin and bradykinin 1 receptors: novel signal transduction characteristics. *Cell. Signalling* **2014**, *26*, 1549-1559.
159. Siddiquee, K.; Hampton, J.; McAnally, D.; May, L. T.; Smith, L., The apelin receptor inhibits the angiotensin II type 1 receptor via allosteric trans-inhibition. *Br. J. Pharmacol.* **2013**, *168*, 1104-1117.
160. Freidinger, R. M.; Perlow, D. S.; Veber, D. F., Protected lactam-bridged dipeptides for use as conformational constraints in peptides. *J. Org. Chem.* **1982**, *47*, 104-109.
161. van Ameijde, J.; Poot, A. J.; van Wandelen, L. T.; Wammes, A. E.; Ruijtenbeek, R.; Rijkers, D. T.; Liskamp, R. M., Preparation of novel alkylated arginine derivatives suitable for click-cycloaddition chemistry and their incorporation into pseudosubstrate- and bisubstrate-based kinase inhibitors. *Org. Biomol. Chem.* **2010**, *8*, 1629-1639.
162. Williams, R. M.; Sinclair, P. J.; Zhai, D.; Chen, D., Practical asymmetric syntheses of α -amino acids through carbon-carbon bond constructions on electrophilic glycine templates. *J. Am. Chem. Soc.* **1988**, *110*, 1547-1557.
163. Schöllkopf, U.; Groth, U.; Deng, C., Enantioselective synthesis of (*R*)-amino acids using L-Valine as chiral agent. *Angew. Chem. Int. Ed.* **1981**, *20*, 798-799.
164. Belokon', Y. N.; Tararov, V. I.; Maleev, V. I.; Savel'eva, T. F.; Ryzhov, M. G., Improved procedures for the synthesis of (*S*)-2-[*N*-(*N'*-benzyl-propyl)amino]benzophenone (BPB) and Ni(II) complexes of Schiff's bases derived from BPB and amino acids. *Tetrahedron: Asymmetry* **1998**, *9*, 4249-4252.

165. Almeida, M. L. S.; Grehn, L.; Ragnarsson, U., Selective protection of polyamines: Synthesis of model compounds and spermidine derivatives. *J. Chem. Soc., Perkin Trans. I* **1988**, 1905-1911.
166. Gu, X.; Ndungu, J. M.; Qiu, W.; Ying, J.; Carducci, M. D.; Wooden, H.; Hruby, V. J., Large scale enantiomeric synthesis, purification, and characterization of ω -unsaturated amino acids via a Gly-Ni(II)-BPB-complex. *Tetrahedron* **2004**, *60*, 8233-8243.
167. Nash, H. M.; Annis, D. A.; Guerlavais, V.; Licklider, L. Improved peptidomimetic macrocycles. WO 2011047215, April 21, 2011.
168. Pascal, R.; Sola, R., Preservation of the Fmoc protective group under alkaline conditions by using CaCl₂. Applications in peptide synthesis. *Tetrahedron Lett.* **1998**, *39*, 5031-5034.
169. Proulx, C.; Sabatino, D.; Hopewell, R.; Spiegel, J.; Garcia-Ramos, Y.; Lubell, W. D., Azapeptides and their therapeutic potential. *Future Med. Chem.* **2011**, *3*, 1139-1164.
170. Hess, H.-J.; Moreland, W. T.; Laubach, G. D., N-[2-Isopropyl-3-(L-aspartyl-L-arginyl)-carbazoyl]-L-tyrosyl-L-valyl-L-histidyl-L-prolyl-L-phenylalanine, an isostere of bovine angiotensin II. *J. Am. Chem. Soc.* **1963**, *85*, 4040-4041.
171. Gante, J., Azapeptides. *Synthesis* **1989**, *6*, 405-413.
172. André, F.; Vicherat, A.; Boussard, G.; Aubry, A.; Marraud, M., Aza peptides. III. Experimental structural analysis of aza-alanine and aza-asparagine-containing peptides. *J. Peptide Res.* **1997**, *50*, 372-381.
173. Reynolds, C. H.; Hormann, R. E., Theoretical study of the structure and rotational flexibility of diacylhydrazines: Implications for the structure of nonsteroidal ecdysone agonists and azapeptides. *J. Am. Chem. Soc.* **1996**, *118*, 9395-9401.
174. Traore, M.; Doan, N. D.; Lubell, W. D., Diversity-oriented synthesis of azapeptides with basic amino acid residues: aza-lysine, aza-ornithine, and aza-arginine. *Org. Lett.* **2014**, *16*, 3588-3591.

175. Zhang, J.; Proulx, C.; Tomberg, A.; Lubell, W. D., Multicomponent diversity-oriented synthesis of aza-lysine-peptide mimics. *Org. Lett.* **2014**, *16*, 298-301.
176. Sabatino, D.; Proulx, C.; Pohankova, P.; Ong, H.; Lubell, W. D., Structure-activity relationships of GHRP-6 azapeptide ligands of the CD36 scavenger receptor by solid-phase submonomer azapeptide synthesis. *J. Am. Chem. Soc.* **2011**, *133*, 12493-12506.
177. Proulx, C.; Picard, E.; Boeglin, D.; Pohankova, P.; Chemtob, S.; Ong, H.; Lubell, W. D., Azapeptide analogues of the growth hormone releasing peptide 6 as cluster of differentiation 36 receptor ligands with reduced affinity for the growth hormone secretagogue receptor 1a. *J. Med. Chem.* **2012**, *55*, 6502-6511.
178. Bourguet, C. B.; Proulx, C.; Klocek, S.; Sabatino, D.; Lubell, W. D., Solution-phase submonomer diversification of aza-dipeptide building blocks and their application in aza-peptide and aza-DKP synthesis. *J. Pept. Sci.* **2010**, *16*, 284-296.
179. Jackson, R. W., A mild and selective method for the cleavage of *tert*-butyl esters. *Tetrahedron Lett.* **2001**, *42*, 5163-5165.
180. Preparation and use of N,N'-di-Boc-N''-triflylguanidine. *Org. Synth.* **2002**, *78*, 91.
181. Garcia-Ramos, Y.; Lubell, W. D., Synthesis and alkylation of aza-glycinyll dipeptide building blocks. *J. Pept. Sci.* **2013**, *19*, 725-729.
182. Hugelshofer, C. L.; Mellem, K. T.; Myers, A. G., Synthesis of quaternary α -methyl α -amino acids by asymmetric alkylation of pseudo-ephedrine alaninamide pivaldimine. *Org. Lett.* **2013**, *15*, 3134-3137.